Metatech

Meta-R-319

Geomagnetic Storms and Their Impacts on the U.S. Power Grid

John Kappenman

Metatech Corporation
358 S. Fairview Ave., Suite E
Goleta, CA 93117

January 2010

Prepared for

Oak Ridge National Laboratory
Attn: Dr. Ben McConnell
1 Bethel Valley Road
P.O. Box 2008
Oak Ridge, Tennessee 37831
Subcontract 6400009137

FOREWORD

This report describes the threat of geomagnetic storms on the Earth caused by solar activity and further discusses their impacts (past and future) on the U.S. power grid. The intention is to describe the seriousness of the threat through a description of past geomagnetic storms and their impacts. In addition, the ability to model the interactions of the geomagnetic field with power grids allows an understanding of past events and the ability to predict the effects of future geomagnetic storms. This report provides the baseline for determining the future recommendations for protecting the U.S. power grid from this threat in the future.

This report is organized to provide in Section 1 a detailed overview of how geomagnetic storms affect the power grid through past experience and through the development of validated computer models at Metatech over many years. Section 2 focuses more directly on the power system impacts caused by the March 13, 1989 Great Geomagnetic Storm in Canada and the United States. Section 3 looks to the future and examines several possible geomagnetic storm scenarios and their effects on the U.S. power grid. Section 4 provides more details on the specific impacts to at-risk EHV transformers in the United States. Appendices A1 through A4 provide additional information to support the analyses and conclusions reached in the body of the report.

Table of Contents

Appendix **Page**

List of Figures

Figure **Page**

Figure **Page**

Figure **Page**

Figure **Page**

Figure **Page**

Figure **Page**

Figure **Page**

List of Tables

Section 1
An Overview of the U.S. Power Grid Model for the Geomagnetic Storm Threat Environments

The ability to comprehensively assess the vulnerability of the U.S. power grid to the geomagnetic storm environment produced by solar activity stems from the parallel investigations that have been underway to understand the problems of power system vulnerability from high altitude nuclear-burst (HEMP) events. Power system impacts from geomagnetic storms were first observed in 1940 and have been growing in importance as the power system has grown over the intervening years.

Geomagnetic storms are created when the Earth's magnetic field captures ionized particles carried by the solar wind due to coronal mass ejections or coronal holes at the Sun. Although there are different types of disturbances noted at the Earth surface, the disturbances can be characterized as a very slowly varying magnetic field, with rise times as fast as a few seconds, and pulse widths of up to an hour. The rate of change of the magnetic field is a major factor in creating electric fields in the Earth and thereby inducing quasi-dc current flow in the power transmission network. Unlike the HEMP threats, geomagnetic storms are a much more frequent occurrence, which also allows for extensive opportunities to fully benchmark each component of the simulation models and therefore provide greater confidence in the analysis of plausible severe threats, such as the threat posed by an extreme geomagnetic storm scenario.

The context of the evolution of power system discoveries of vulnerability can be further understood by an overview of the geomagnetic storm phenomena, which is closely associated with the more familiar variability of the sunspot cycle. Figure 1-1 provides a plot of the sunspot count as well as large geomagnetic storms over the last 70 years. Because each sunspot cycle is typically ~11 years in duration, this plot provides the status of the current solar cycle (Cycle 23) back to Cycle 17, which began in ~1932. As can be seen, not all sunspot cycles are of equal intensity and Cycle 19 (late 1950's-early 1960's) is in fact the largest sunspot cycle of human-record. The most recent cycle, Cycle 23, exhibits a profile similar to that of Cycle 17. As noted in this figure, at the time of Cycle 19, much of the present U.S. power grid high-voltage transmission system of today did not exist. To further explore the importance of the evolution of the power grid and its growing vulnerability, it is necessary to look at specific large geomagnetic storms, as the sunspot count does not provide sufficient correlations to impacts observed at the Earth. In classification of the intensity of geomagnetic storms an index called the Ap index is used, which provides a planetary measure of storm activity. Many of these storms caused notable impacts to various terrestrial technology systems of their respective eras. The storms of March 1989 and several in 1991 produced large and unprecedented operational impacts to power grids in the U.S. and at other world locations. Also noteworthy is that large geomagnetic storms generally have not occurred around the peaks of sunspot activity. For example, a storm in February 1986 caused power system problems all across the eastern U.S. but actually occurred at the absolute minimum between Solar Cycle 21 and 22. Because sunspots only provide a gross measure of overall solar activity, it does not accurately reflect the discrete eruptive events from violent solar

active regions that, when Earth-directed, can trigger large geomagnetic storms. Rather, it is clear from this comparison that large and threatening geomagnetic storms can occur at any time during the sunspot cycle, and pose a near continuous threat probability.

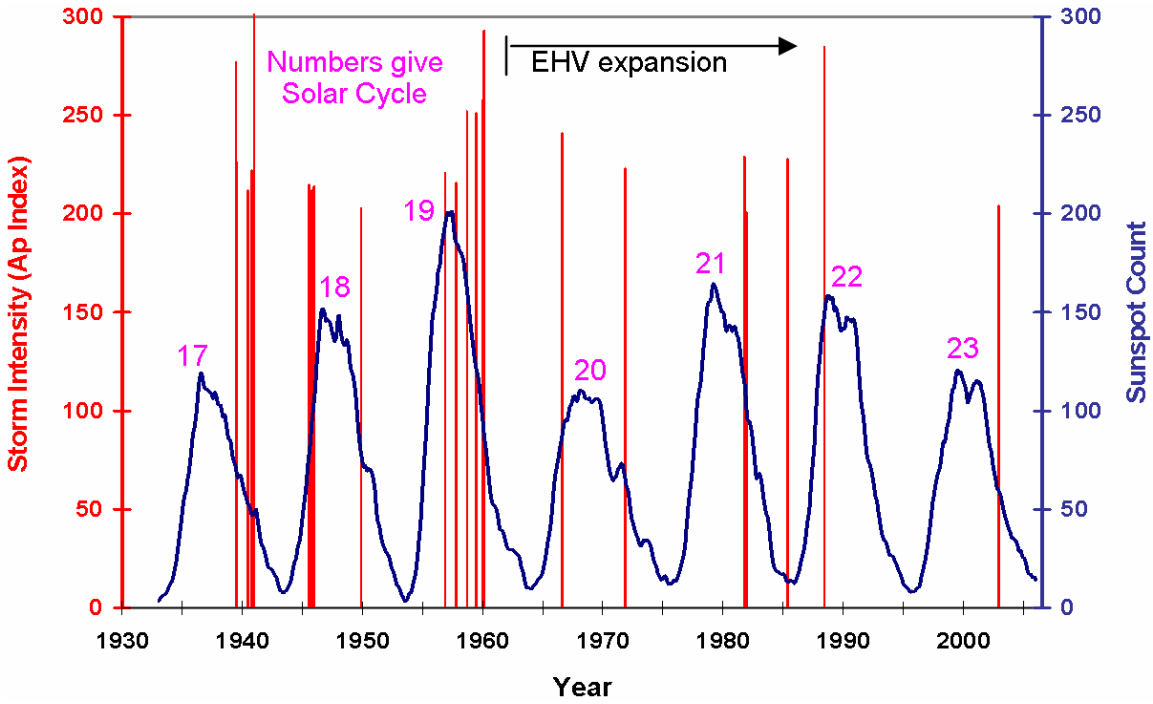

Figure 1-1. Sunspot cycles and the occurrence and intensity (using Ap index) of large geomagnetic storms.

When reviewing the occurrence of large storms, it is important to recognize that the problem of power system impacts is compounded by growing vulnerability of this infrastructure to geomagnetic disturbances. The extent of the growth in vulnerability over time is due to factors stemming from the growth of the high-voltage transmission grid in the U.S., as well as changes within the grid that introduce new or enhance existing impact problems to the power grid. Figure 1-2 shows the growth of the U.S. high voltage transmission grid over the last 50 years. This geographically widespread infrastructure readily couples through multiple ground points to the geo-electric field produced by disturbances in the geomagnetic field. As shown, from Cycle 19 through Cycle 22, the high voltage grid grew nearly tenfold. In essence, the antenna that is sensitive to disturbances has grown dramatically over time. As this network has grown in size, it has also grown in complexity. As will be discussed in later sections, one of the more important changes in the technology base for the U.S. power grid that can increase impacts to geomagnetic storms is the evolution to higher operating voltages of the network. The operating levels of the high voltage network has increased from the 115-230kV levels of the 1950's to networks that operate from 345kV, 500kV and 765 kV across the continent.

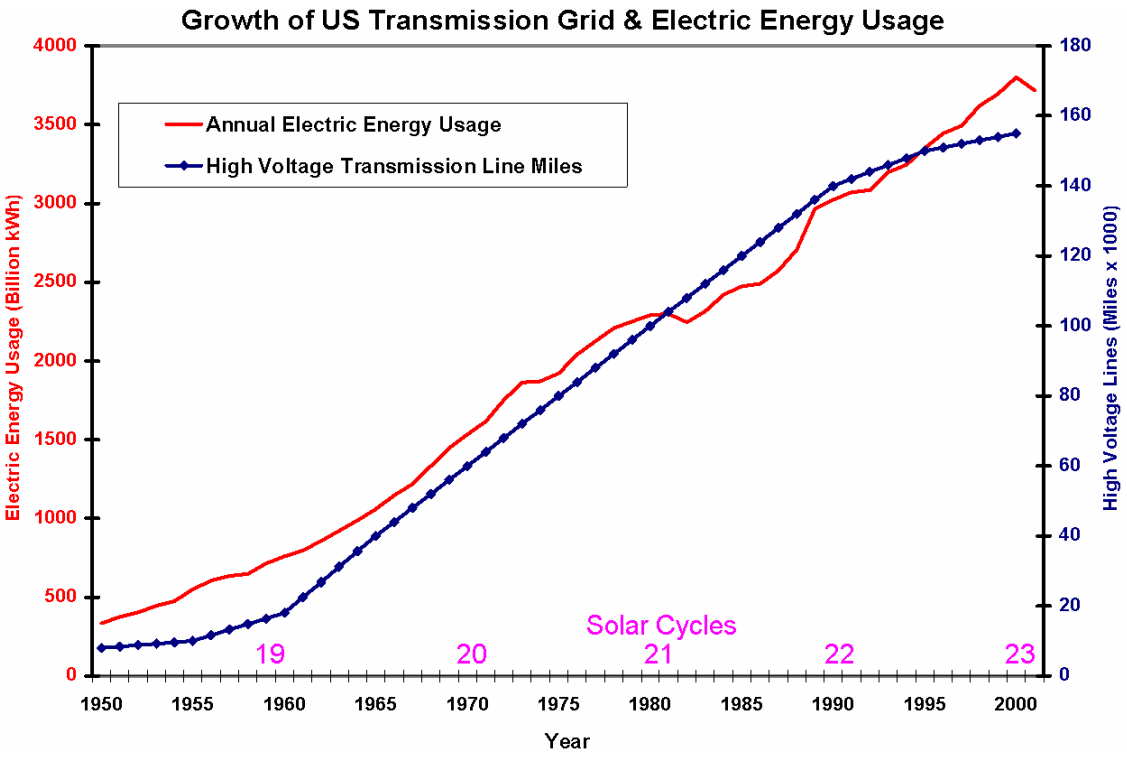

Figure 1-2. Growth of the U.S. high voltage transmission network and the annual electric energy usage over the past 50 years. In addition to increasing total network size, the network has grown in complexity with introduction of higher kV rated lines that subsequently also tend to carry larger GIC flows. (Grid size derived from data in EHV Transmission Line Reference Book and NERC Electricity Supply and Demand Database; energy usage statistics from U.S. Dept of Energy – Energy Information Agency.)

In order to quantify the impacts of the severe geomagnetic storm threats to the U.S. power grid is it necessary to develop a series of models that translate the disturbed space environment, or geomagnetic field environment, into specific impacts to the operation of the electric power grid. This requires the following steps:

- Modeling in detail the geographically wide-spread disturbances to the geomagnetic field from natural geomagnetic storm processes.
- Modeling the electromagnetic coupling between the disturbed space environment and the deep-earth ground conductivity that produces a geo-electric field across the surface of the Earth.
- Modeling the interaction between the geo-electric field and the complex power grid topology to calculate the flow of geomagnetically induced current (GIC) throughout the exposed power grid infrastructure.
- Modeling of the operational impacts in the U.S. power grid due to GIC flows caused by either E3 threats or severe geomagnetic storm conditions.

While each of these models and associated environments are complex, these modeling efforts have been highly successful in accurately replicating geomagnetic storm events and performing detailed forensic analysis of geomagnetic storm impacts to electric power systems. This capability has also been successfully applied towards providing predictive geomagnetic storm forecasting services to the electric power industry. To further

describe the methodology used in this analysis, a brief overview is provided for each of the key modeling steps that were undertaken.

1.1 Geomagnetic Storm Environment Model

An important facet of this investigation requires the simulation of geomagnetic storm events and the impacts that these storms caused to electric power grid operation, and to also investigate the potential impacts of very large storm events that have not recently been experienced by today's power systems. Electric power system operators realize that large and severe geomagnetic storms (such as the March 1989 storm) have the potential to cause important power system impacts. However, the U.S. power industry in general have not developed comprehensive simulation models such as being developed in this effort to better quantify the nature of the threat environment. The power industry also has a very limited perspective on the extremes of storm intensity due to the flaws of the K Index rating of storms. While some past storms have severely threatened the U.S. grid, these storms do not represent the most severe storm events that are plausible. Therefore, comprehensive models allow the development of improved understandings of the extremes of the geomagnetic environment and consequential impacts that future severe storms may pose to the integrity of this important infrastructure. The forensic analysis of prior storm events provides two benefits: 1.) it allows for validation of the overall U.S. Power Grid Model accuracy by reproducing past observations of storm impacts on the infrastructure, 2.) the simulation allows for more detailed assessment of past critical storm events and levels of reactive power and voltage regulation stress that occurred across the U.S. power grid.

Geomagnetic disturbances are caused by interactions of the solar wind with the Earth's magnetic field. There are a number of ways that a geomagnetic storm can produce a ground-level geomagnetic field disturbance that could have the potential to impact power system operations. One of the most important geomagnetic storm processes involves the intensification and flow of ionospheric currents known as electrojets. These electrojets are formed around the north and south magnetic poles at altitudes of about 100km and can have magnitudes of ~1 million amps, which is sufficient in intensity to cause wide-spread disturbances to the geomagnetic field. Because of the large geographic scale of the U.S. power grid, it would not be suitable to assume the application of a simple plane-wave model for the disturbance conditions. Therefore, to simulate the geomagnetic storm environment, it is necessary to develop a geographically gridded specification of the complex spatial and temporal dynamics of the disturbances as they propagate across North American locations that are to be modeled. Electrons injected into the ionosphere along geomagnetic field lines produce the ionospheric current systems and resulting electrojet current. Geomagnetic storms can propagate geographically rapidly and in complex and wide-spread disturbance patterns. In order to accurately model the ground-level geomagnetic variations from these disturbance events, a data assimilation model has been developed utilizing a wide-spread array of ground-based geomagnetic observatories. In the calculation of power system impacts, it is primarily the horizontal components of the magnetic field disturbance that are of concern (the north-south and east-west

variations). Figure 1-3 shows the vector description of a disturbance of the geomagnetic field simultaneously observed at a number of locations across North America at time 9:10 UT May 10, 1992.

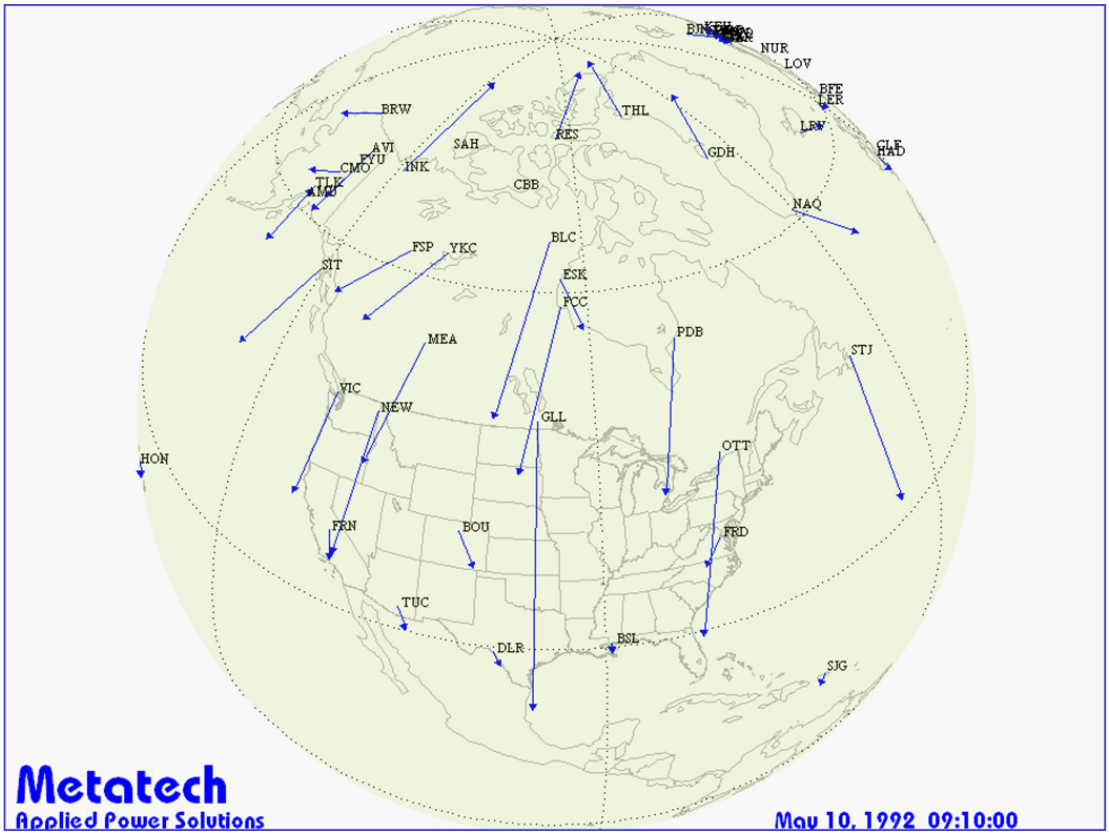

Figure 1-3. Vector intensity of geomagnetic field disturbances at numerous magnetic observatories.

As shown in this example, many of the North American observatories are seeing a large and coherent southward-oriented vector disturbance in the locally observed geomagnetic field. This pattern describes the physical attributes expected from a westward electrojet current system extending across the region. The intensity of the vector also describes an observation point that is located with a relatively closer proximity to the ionospheric current source as well. Using this data, an assimilative model can be developed to provide a more detailed definition to the disturbance environment that would be suitable for application on the U.S. Power Grid Model. Figure 1-4 provides a depiction of this model's results for the same 9:10 UT time step. This graphic more clearly defines the complex spatial disturbance pattern of the westward electrojet intensification that is occurring at this time. By assimilating other simultaneous observation data it is possible to also accurately characterize the temporal dynamics of the storm event as well. This modeling approach provides an averaging between inter-observatory intensities. It is possible that there could be small regions of higher intensity between observation locations, but this was not assumed for modeling purposes. In many of the storms that

have been selected for evaluation, this uncertainty has been minimized by using as many observatories as possible and avoiding sparse data conditions.

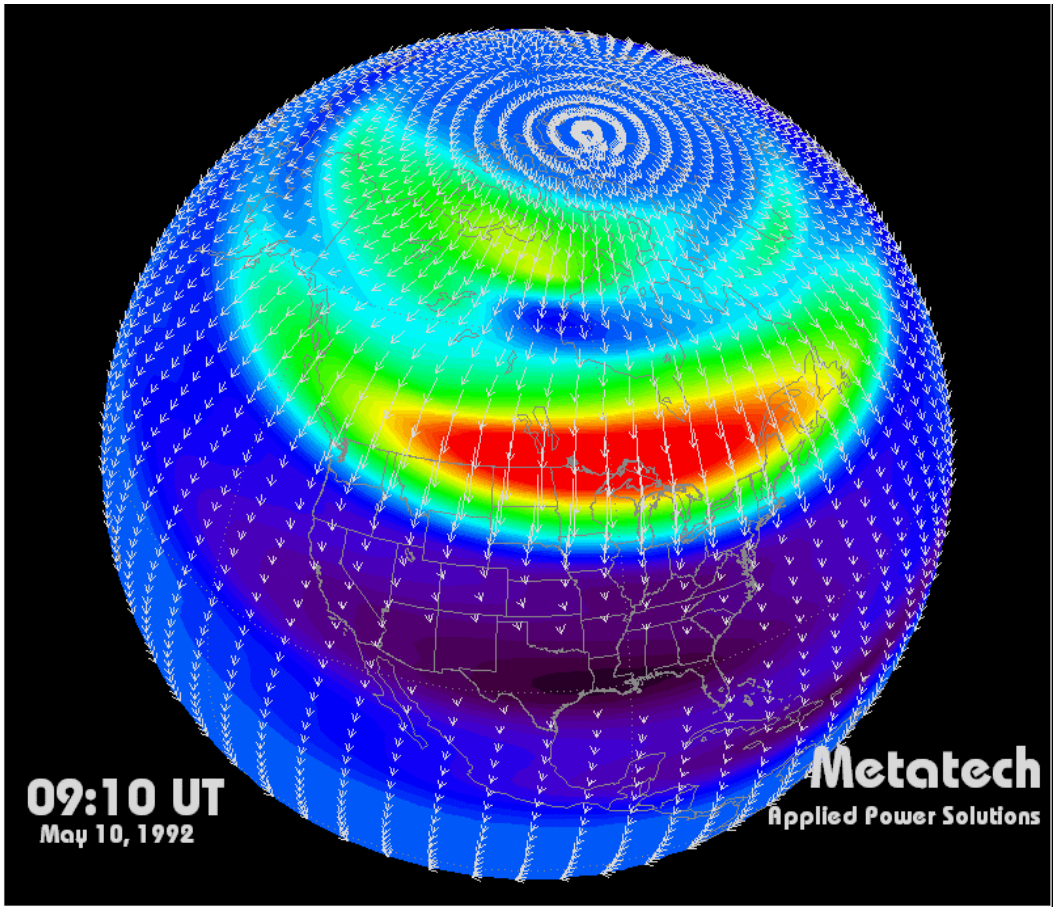

Figure 1-4. Environment model using the vector data from Figure 1-3.

For all the geomagnetic storm simulations, discrete magnetic observatory data is used and depicted at the highest available data cadence available. This is usually one-minute cadence, however some limited availability of 1 and 3-second data is also available for storm events. In addition to important benchmark storms, this same storm environment modeling capability is also used to develop the storm environments and a detailed understanding of the climatology concerns for large and historically important storm threat conditions such as the Great Geomagnetic Storm of March 13-14, 1989 and possible larger storm threats to the U.S. power grid.

1.2 Ground Models and Electric Field Calculation

In order to compute the induced currents flowing in a power network, it is necessary to be able to establish the electric fields induced in the Earth by variations in the geomagnetic field. Numerical models developed by Metatech require knowledge of the layered Earth conductivity to depths greater than 300 km. Past experience has indicated that 1-D Earth conductivity models are sufficient to compute the local electric fields. Because there is considerable heterogeneity in conductivity over North America, multiple 1-D models can be used where the conductivity variations are extremely large.

Four different techniques are used to develop ground conductivity models.

- Measurements of the conductivity versus depth for the top 10s of km.
- Descriptions of the local geology, which can be used to infer an average conductivity versus depth.
- Measurements of the deep conductivity for the region of interest (although continental data exists for most of the world).
- Actual measurements of geomagnetic and electric fields along with resultant geomagnetically-induced currents (GIC) at locations and frequencies of interest.

In general across the U.S., information is available in each category, although the last technique is the most useful.

Ground conductivity models need to accurately reproduce geo-electric field variations that are caused by the very low frequency ranges of geomagnetic storms. These electromagnetic disturbances require models accurate over a frequency range from 0.3 Hz to as low as 0.00001 Hz. Because of the low-frequency content of the disturbance environments, it is necessary to take into consideration ground conductivities to appropriate depths. Numerous studies confirm that depths required are more than several hundred kilometers, although the exact depth is a function of the layers of conductivities present in a specific region. In most locations, ground conductivity varies substantially at the surface. These conductivity variations with depth can range 3 to 5 orders of magnitude. While surface conductivity can exhibit considerable lateral heterogeneity across the U.S., conductivity at depth is more uniform. Because of this, models of ground conductivity can be successfully applied over meso-scale distances and can be accurately represented by use of layered conductivity profiles or models. Frequent occurrences of geomagnetic storm events and subsequent measurement of these storm environments and associated impacts have provided opportunities to use this information to develop and validate models of the ground conductivity for the U.S. Power Grid Model.

A severe electrojet disturbance can produce a rate-of-change intensity profile (or dB/dt) of 2400 nT/min or greater. This disturbance is a very severe disturbance that could be possible at high to mid latitude locations throughout the U.S. A waveform of this intensity was used to evaluate differing ground model responses in terms of the peak geo-electric field that would be produced by such a disturbance. The comparative results of this evaluation for 18 differing ground models is shown in Figure 1-5. In the case of peak magnitude alone, the difference between the most responsive and the least responsive

ground model can be more than a factor of 7. For the most responsive ground model, the peak geo-electric field exceeded 15 volts/km in intensity.

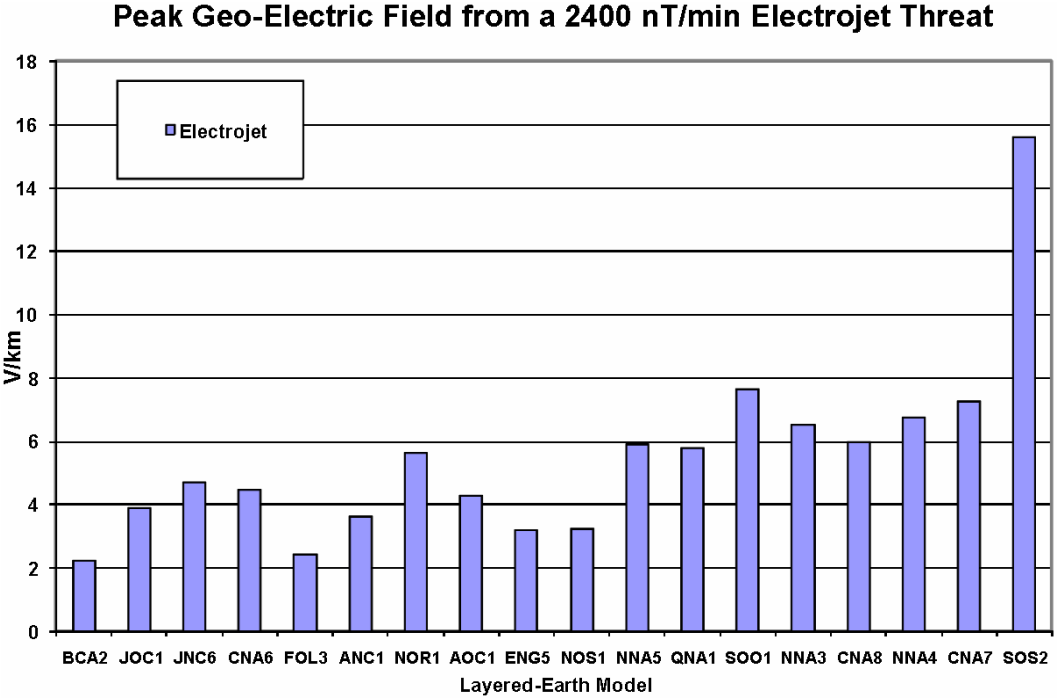

Figure 1-5. Peak geo-electric field from a 2400 nT/min electrojet threat.

Figure 1-6 provides an overview map of the ground models selected for each color-coded region in the U.S. As shown, these models are applied in meso-scale dimensions throughout the U.S. The specific models were assigned based upon selecting a group of ground conductivity models that were appropriate to the known geological profiles of the region. The geological profiles provided were used to narrow the search to several candidate ground models for various regions. Further refinements to select the most appropriate ground model were done through a series of simulations where the best model was selected by validation against local observations through the use of monitored data from prior geomagnetic storms (see Appendix 3).

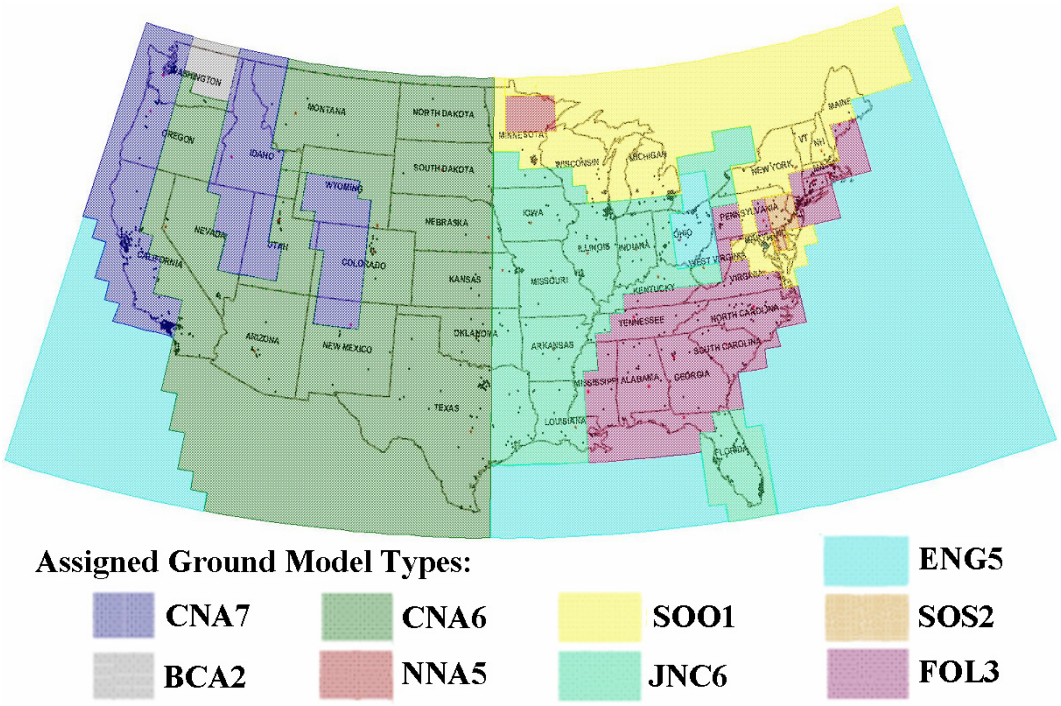

Figure 1-6. Multiple 1-D ground models for the U.S. grid.

Because of the wide range of magnitude, as well as spectral response characteristics of the impulsive geomagnetic field disturbance environment, it is critical to select appropriate ground models for each region in order to produce valid simulation results. Validation of the ground models against forensic data provides the best means to assure that appropriate responses are being observed and to provide assurance that correct responses will result when simulations of more severe disturbances are undertaken. Several examples of model response versus actual observations are provided in this overview.

Figure 1-7 provides an example of the validation of a ground model. This figure shows a comparison of the observed North-South and East-West geo-electric field during a minor geomagnetic storm on Nov 4, 1993 in northern Minnesota (from Kappenman, Zanetti, Radasky, EOS Transactions of AGU, Jan. 28, 1997, pg 37-45). Also provided are the results of the simulation, which indicate good agreement in magnitudes as well as wave shape. These observations and simulations were conducted using a 1-second data cadence. The ability to replicate over a broad frequency range provides for good overall fit between observed and simulated electric fields. This example illustrates the ability to validate the ground model separately from the Power Grid Model.

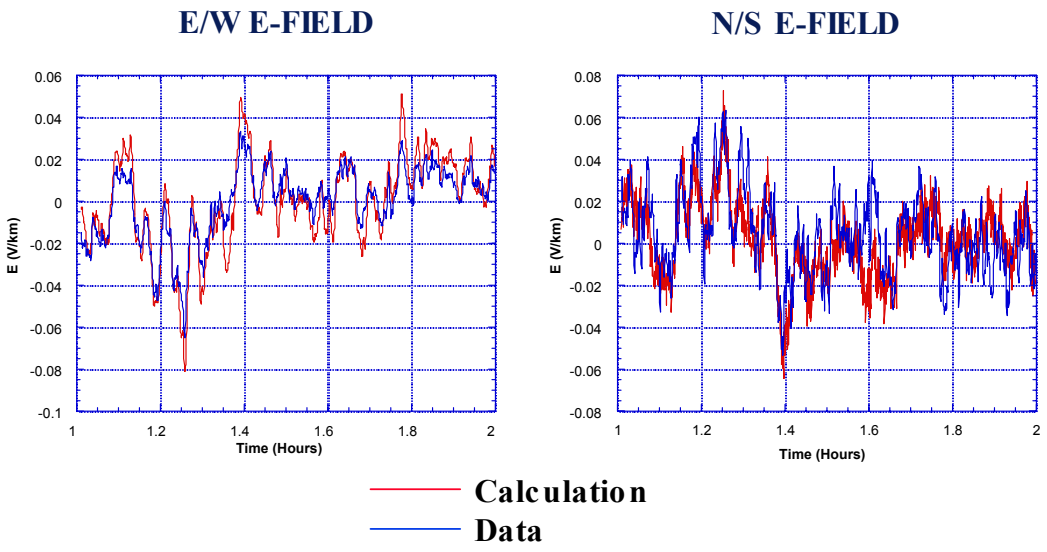

Figure 1-7. Comparison of calculated and measured electric fields for 4 Nov 1993.

It is also possible to demonstrate the validation using measurements of GIC with the combined ground model and Power Grid Model. An example of this is provided in Figure 1-8 for GIC measurements made in northern Maine during a storm on May 4, 1998. In this case, the measured data was observed at a 10 second cadence, while the calculation was limited to a one-minute cadence due to availability of regional geomagnetic field disturbance data. This will also limit the frequency response of the simulation and reduce some of the ability to replicate minor high frequency variations. In spite of the data limitation for simulations, the close agreement between observed GIC and calculated GIC indicates that both the ground model and the Power Grid Model are accurately replicating the storm impacts.

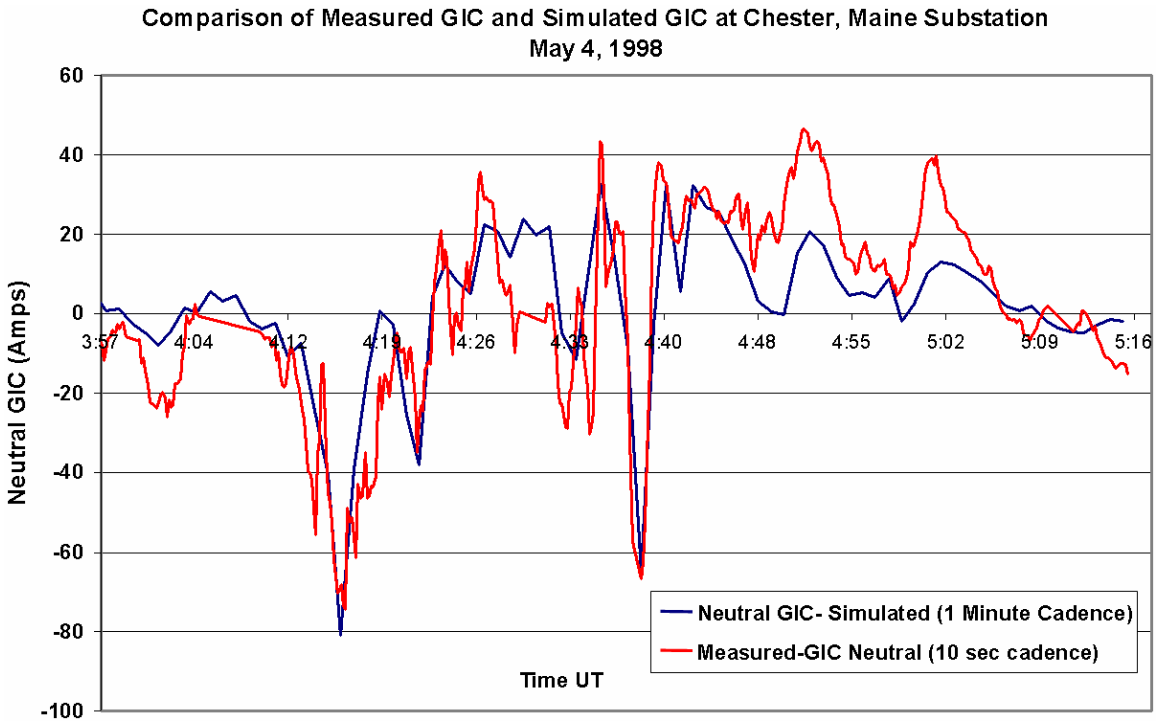

Figure 1-8. Comparison of measured and calculated GIC at Chester Maine.

1.3 U.S. Electric Power Grid Circuit Model

As one of the four component models that are necessary to calculate GIC flows and the impacts on power system reliability due to GIC flows, the Power Grid Model is important for two reasons in determining the simulation results. This portion of the model in particular defines the complex topology of the network circuit, as this topology couples with the equally complex geo-electric field environment that occurs from natural geomagnetic storm processes. The other important aspect of the power grid circuit model is contained in the resistive impedance of the network circuit elements (primarily the transmission lines, transformers, and substation-to-ground resistance). The values of these circuit resistances combined with the resultant geo-electric fields across the network define the pattern and magnitude of GIC flows.

Because of the mature nature of this data and the many years of power industry experience in modeling AC flows in the network, it is expected that this portion of the U.S. Power Grid Model will be less uncertain than other portions of the overall model. The U.S. Power Grid Model was assembled by using publicly available load flow model data and available transmission asset maps to define approximate locations. In order to calculate the flow of GIC, the model needs to define not only the impedance of all circuit elements, but also their locations. The definition of locations allows for proper determination of coupling with the complex 2D geo-electric field patterns that will occur due to various threat conditions that are to be examined. In the estimation of substation position accuracy, in most cases, the position is accurate to within +/- 1 mile. This accuracy will be sufficient given the large-scale nature of the overall U.S. simulation model that is being developed. Due to the expedited nature of the investigation, the model for the CONUS region of the U.S. was limited to transmission network portions that are 345kV or higher in voltage. As will be shown in subsequent analysis, the majority of all GIC flows will occur in the highest voltage portions of the network, hence this limitation accounts for most of the GIC flows and resulting impacts from those flows.

Figure 1-9 provides a map of the overall transmission network included in the CONUS region model of the U.S. grid. The major transmission voltages are color highlighted by operating voltage with the three operating voltages of 345kV, 500kV and 765kV (there are also several lines in the Washington state region that are operated at 300kV which are included in the model, and in the figure are combined with 345kV lines). Figure 1-10 provides the mileage statistics for each of these three voltage classes that are represented in the U.S. model for the CONUS region. As shown, the most common transmission voltage is the 345kV, which makes up about 64% of total transmission line miles. The highest operating voltage is the 765kV and is primarily located in the Illinois, Ohio, Indiana, West Virginia and upstate New York regions of the U.S. Both the 345kV and 500kV portions of the network are more widely distributed across the U.S.

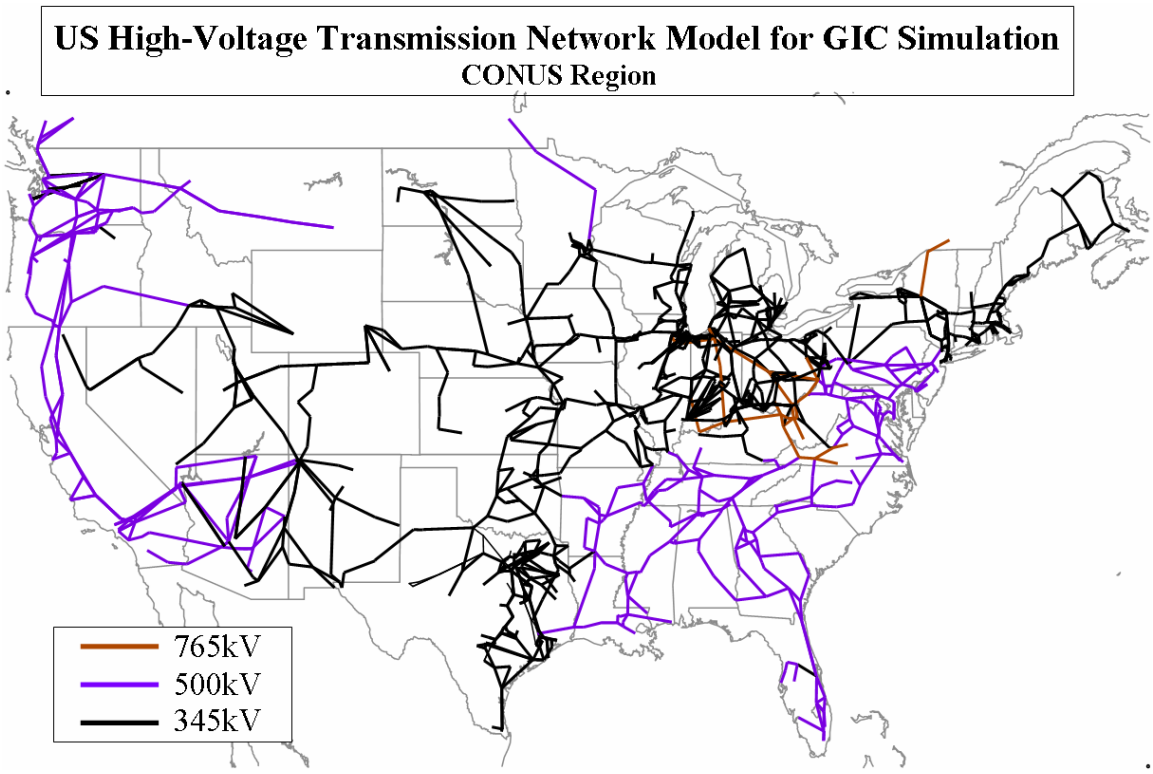

Figure 1-9. Map of 345kV, 500kV and 765kV substations and transmission network in U.S. grid model.

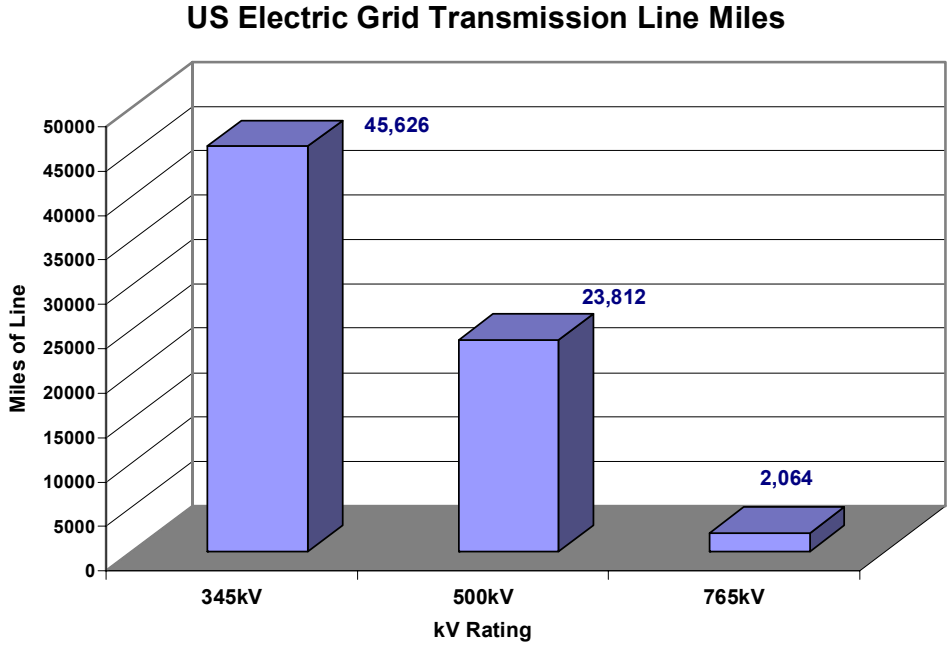

Figure 1-10. Miles of 345kV, 500kV and 765kV transmission lines in U.S. grid model.

A total of 2146 high-voltage transformers will be modeled in the CONUS Region for the U.S. Power Grid Model. The population of transformers by kV rating is shown in Figure 1-11. The population of transformers by kV rating generally follows the population of transmission line miles as previously shown. The simulation model will be able to calculate and estimate the flow of GIC in each of these transformers and provide estimates of the degree of half-cycle saturation and system impacts this saturation could cause to operation of the U.S. Power Grid.

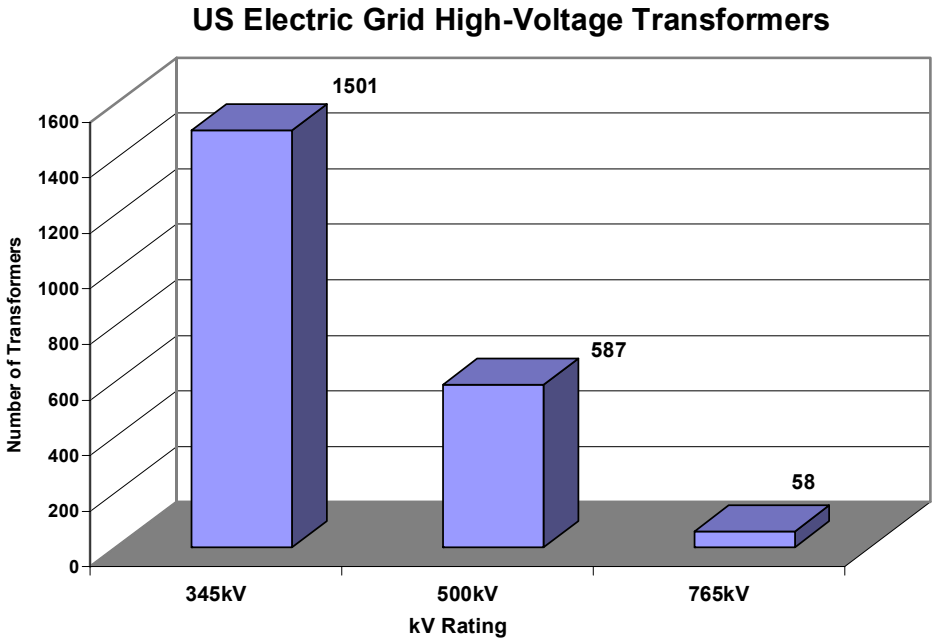

Figure 1-11. Number of 345kV, 500kV, and 765kV transformers in U.S. grid model.

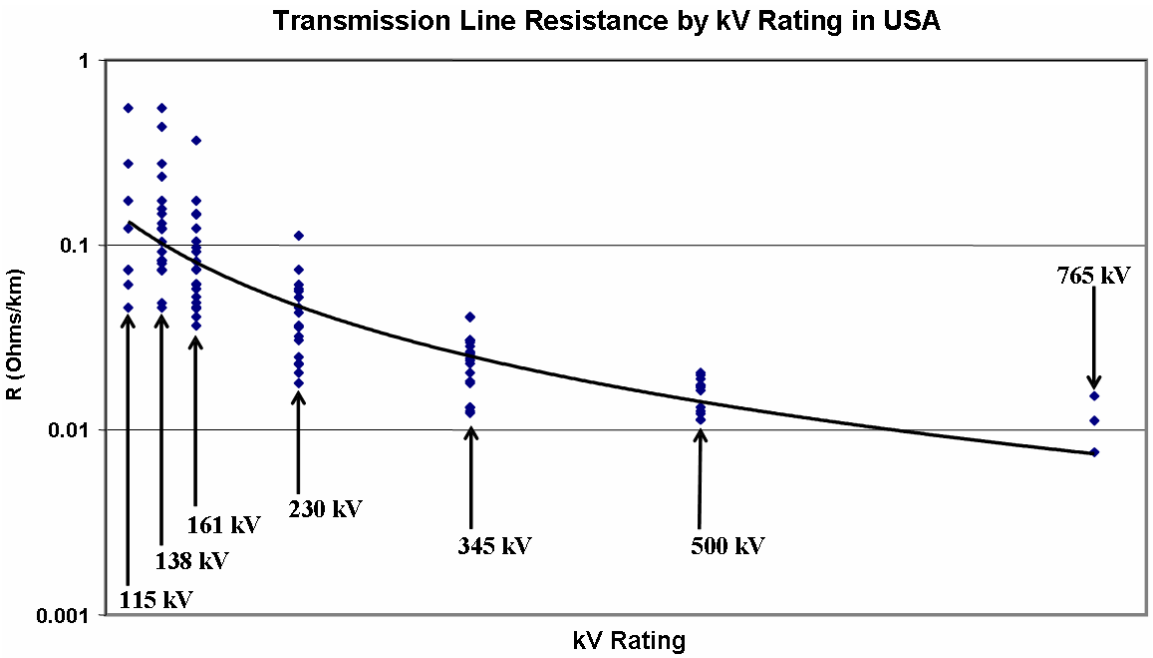

Figure 1-12. Range of transmission line resistance for the major kV rating classes for transmission lines in the U.S. electric power grid infrastructure population. Also shown is a trend line of resistance weighted to population averages. The lower R for the higher voltage lines will also cause proportionately larger GIC flows in this portion of the power grid (Derived from data in EHV Transmission Line Reference Book and from U.S. Dept of Energy-Energy Information Agency and FERC Form 1 Database.)

The operating voltage of the transmission network is an important factor in determining the level of GIC flow that will occur on each part of the U.S. power grid. At the higher operating voltages, there are pronounced trends that: the average length of each line increases and the average circuit resistance decreases. These trends result in larger GIC flows in the higher voltage portions of the network, given the same geo-electric field conditions. To better illustrate the impact of kV rating and associated design factors that affect circuit resistance, a statistical analysis was performed on the network data that was available. This analysis also reviewed some of the lower voltage transmission elements as well. For example, when looking at the resistance per mile of transmission lines in the U.S., the resistance generally declines as larger and lower resistance conductors are used for the higher kV-rated facilities. Figure 1-12 provides a summary of the average line resistance in the U.S. versus the kV rating of the transmission line. This summary extends from the 115kV to the 765kV transmission voltages. As shown in this figure, the per mile resistance decreases on average by approximately a factor of 10 as you increase from the 69kV line to the 765kV line. It is also generally shown that for operating voltages of 345kV and above the resistances are generally very small (less than 0.1 ohms per mile). There is some diversity in the overall population due to variation in conductors that are used on specific transmission lines. The actual line resistance was used from the system model data that was available, reflecting actual conditions for each specific facility in the overall model.

Transformers also exhibit a general characteristic of lower resistance as kV rating increases. However, the trend in transformer design is even more pronounced as a function of MVA or current rating of the transformer. It is generally consistent that the higher MVA rated transformers are also the highest kV rated transformers, though there can be a few exceptions. Figure 1-13 provides a plot of the transformer winding resistance versus the current rating of the transformers in the U.S. population. The blue scatter plot points illustrate specific transformers from the data available, while the red line shows the general best-estimate trend of this data. As illustrated, there is also more than a factor of 10 reduction in transformer winding resistance as the current rating or MVA size of transformers increases. Since these very large transformers generally tend to be located on the higher kV rated portions of the network, this will again result in significantly larger GIC flows in these portions of the network given the same geo-electric field exposures. In the available transformer data, nearly 29% of all transformers modeled did not have available winding resistance data. Therefore, in order to fill in this missing data, estimated data was used that conformed with the trend line of the population statistics shown.

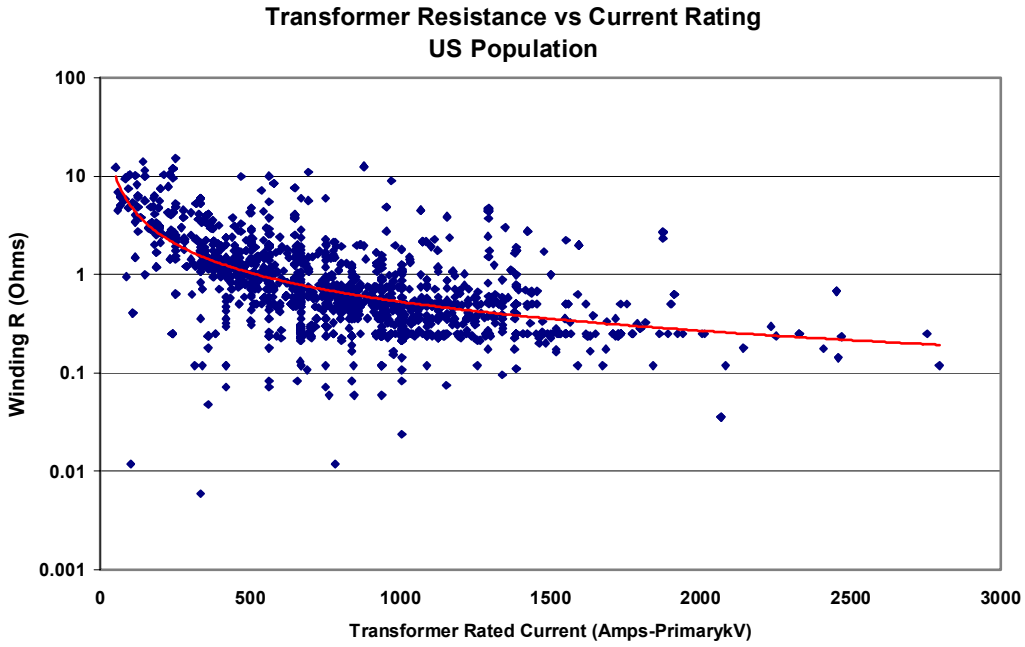

Figure 1-13. Decrease in transformer DC resistance versus MVA rating for transformers in U.S. grid model.

In addition to the lower resistances at the higher kV rating lines on the network, average length of these lines also introduces a higher overall risk of GIC flows as well. Figure 1-14 provides a summary of average transmission line lengths in the U.S. by kV rating. As illustrated, the average length of transmission lines also increases significantly with increased kV ratings. The 765kV lines average over 60 miles in length while the 115kV lines are less than 15 miles in average length. While predicting GIC flows, it is necessary to take into consideration the network topology as a integrated whole. It is evident that on an individual line basis a combination of longer average length (and increased geo-electric potential between end points of the line) combined with lower average resistances will produce substantially larger GICs on average in the higher voltage portions of the power grid.

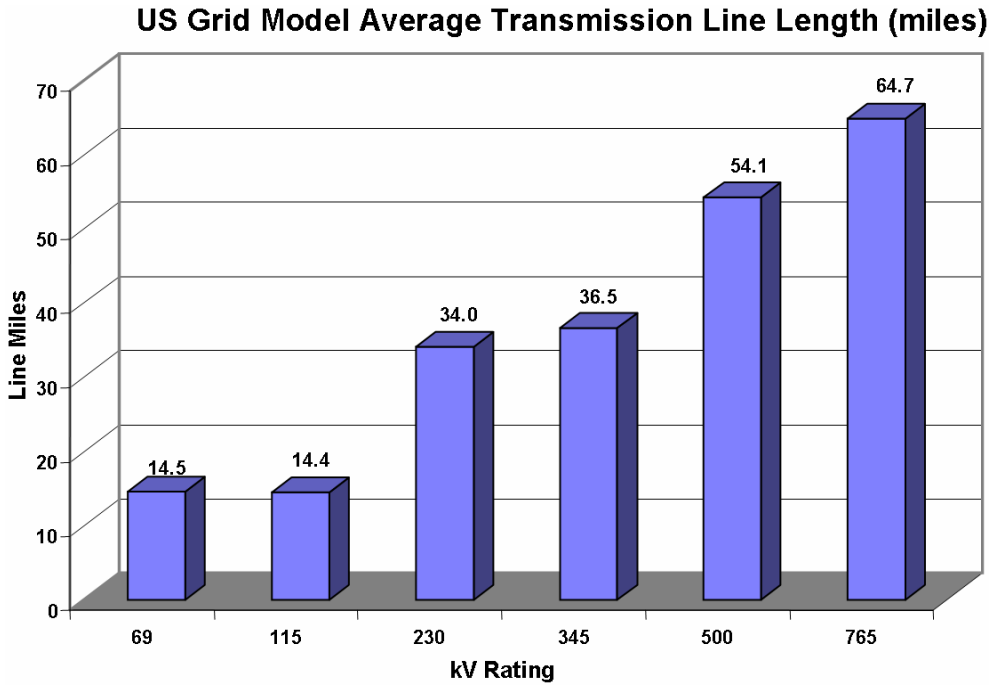

Figure 1-14. Average length of transmission lines in U.S. by kV rating.

The application of series capacitors on transmission lines will block the flow of GIC. In the entire eastern U.S. grid only two lines have series capacitors, however in the western grid a significant number of the lines are series compensated. Figure 1-15 shows the extensive application of series capacitors on the transmission lines in the U.S. portion of the WECC pool, and is further described in the chart in Figure 1-16. There are near equal total miles of both 500kV and 345kV transmission in the WECC pool. Of the 500kV transmission, approximately 55% of these lines have series capacitors while for the 345kV only ~25% of these lines are series compensated.

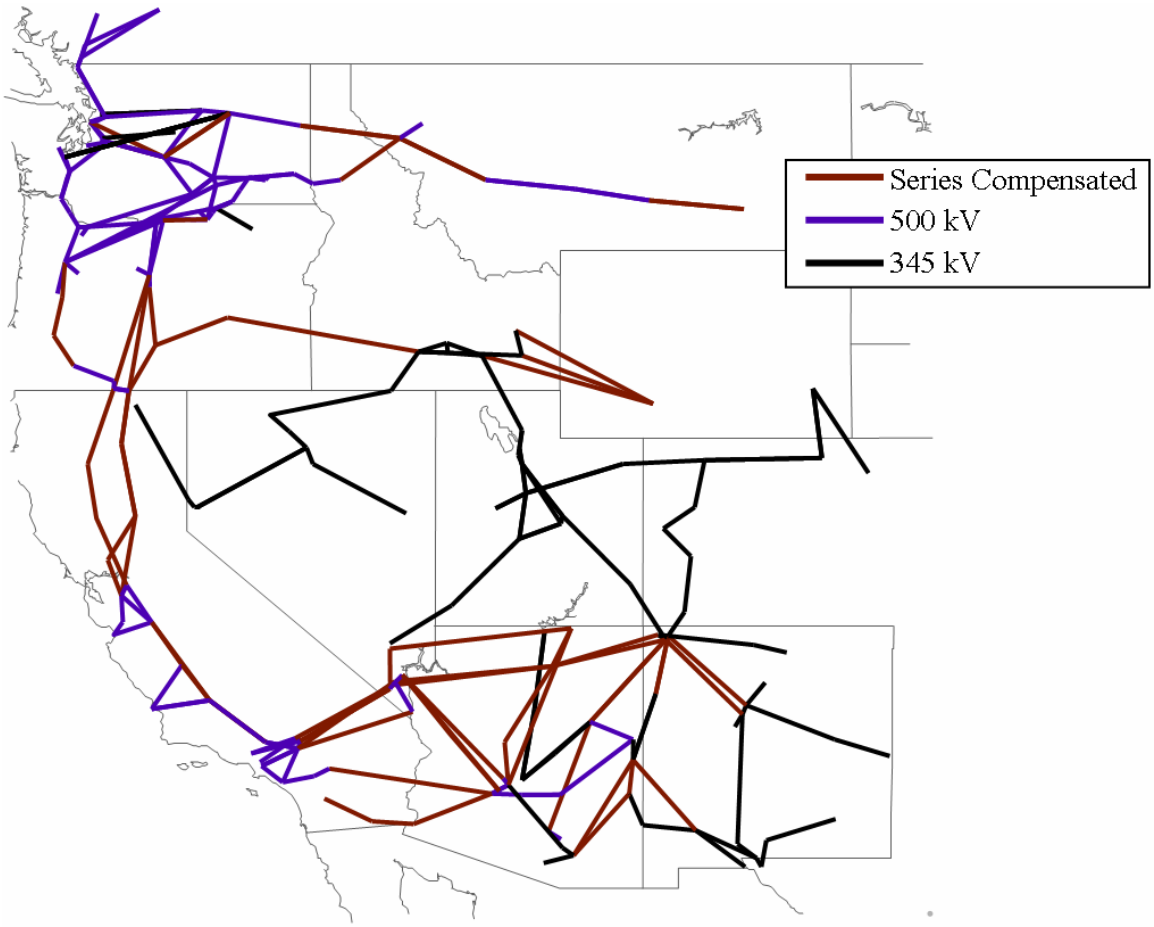

Figure 1-15. WECC 345kV and 500kV transmission lines that are uncompensated and series compensated.

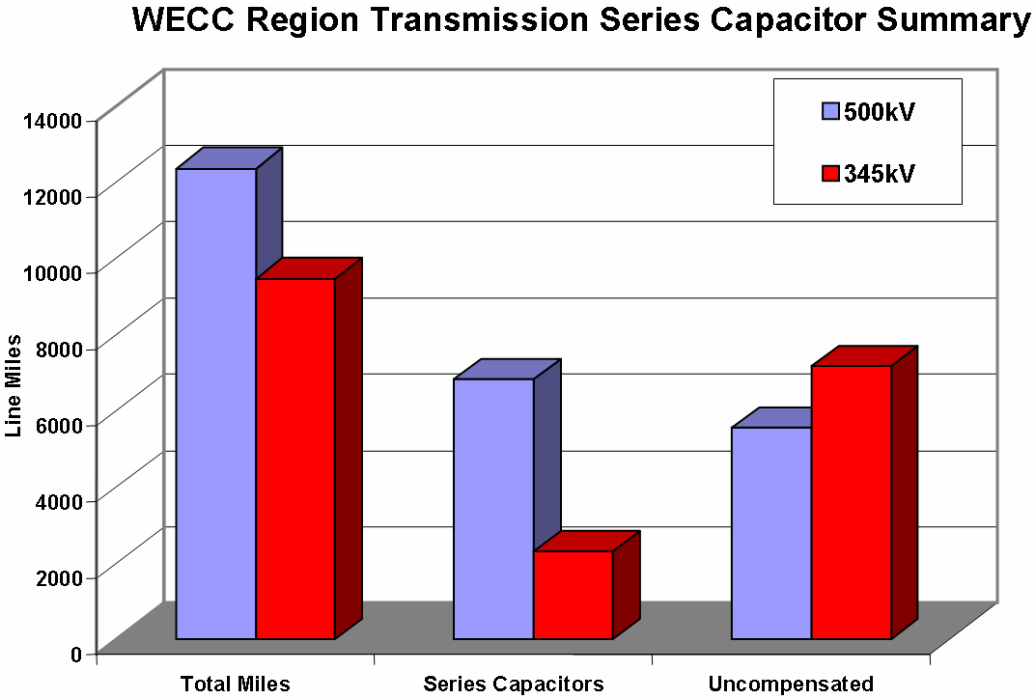

Figure 1-16. Miles of 345kV and 500kV series compensated and uncompensated transmission lines in WECC.

1.4 Transformer and AC Power Grid Performance Model

The flow of GIC in transformers is the root cause of all power system problems, as the GIC causes half-cycle saturation to occur in the exposed transformers. While the extremes of the threat environment, the conductivity of the deep-earth ground, and the kV rating and topology of the power grid can all cause significant enhancements of the total GIC flows, the most significant enhancement of impacts due to GIC is how that GIC interacts within the transformer. Only a few amps of GIC can result an amplification of impacts in the operation of AC current flows in the transformer. In some cases the amplification effect can cause normal AC excitation current in a transformer to increase from less than 1 amp to nearly 300 amps, due to the flow of only 25 amps/phase of GIC.

Transformer design is an important consideration. In particular, single-phase core design transformers are much more responsive to influence from GIC than most standard 3 phase designs. Also, the higher the kV rating of the transformer, the higher the total reactive power increase will be that occurs due to GIC. Figure 1-17 provides a comparison plot of the reactive demand increase that occurs in both a single-phase and three-phase 500 kV transformer for various levels of GIC per phase. As shown, the simple difference between three-phase design and single-phase design causes a factor of four increase in total reactive power demand over the range of GIC flow levels.

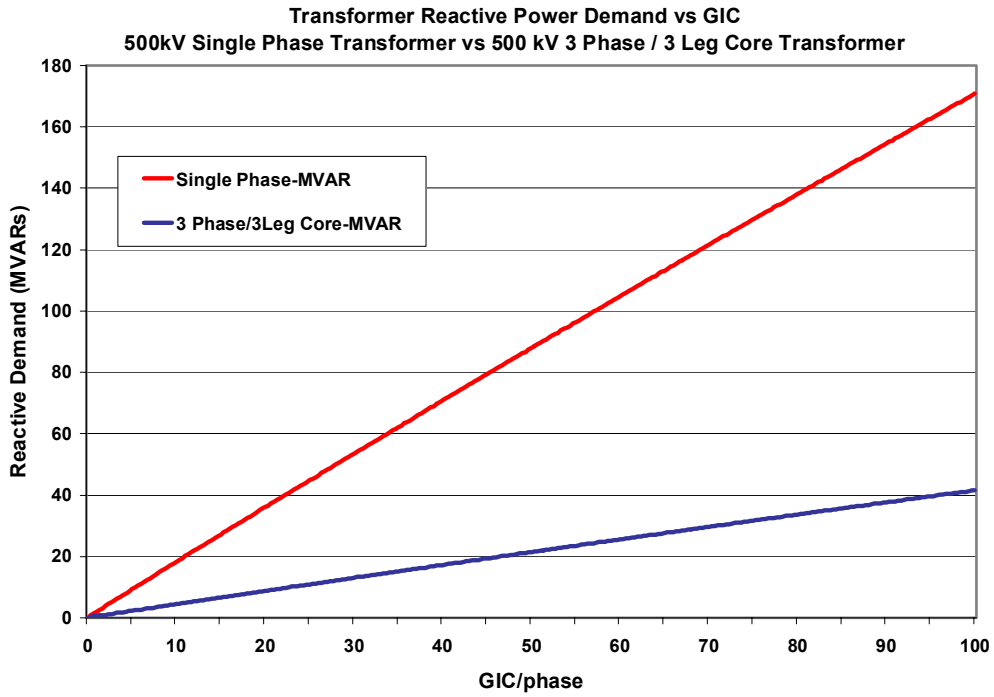

Figure 1-17. Transformer MVAR increase versus GIC for 500kV single-phase and 3-phase, 3-legged core form.

A similar increase in the impacts of GIC flows on transformer reactive power demands occurs for increases in transformer kV rating. Figure 1-18 provides a comparison for a single-phase 345kV, 500kV and 765kV transformer. As shown in this comparison, for the same level of GIC flow, the 765kV transformer will have nearly two times higher reactive power demands than the 345kV transformer. A similar ratio of reactive power demand versus kV rating would also occur for three-phase transformers, though total reactive power levels will be smaller than those in comparable single-phase design transformers.

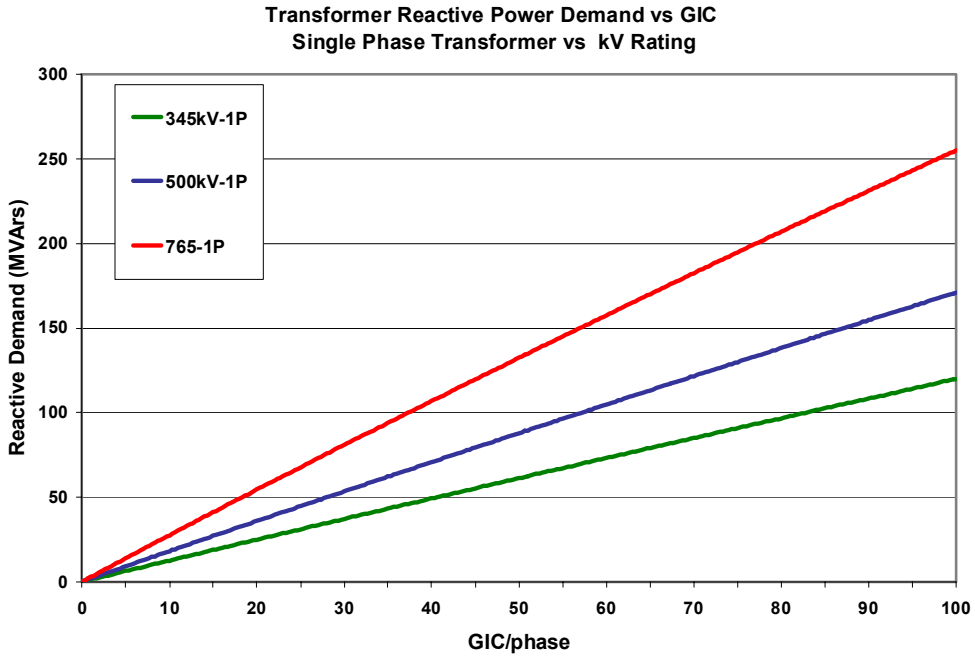

Figure 1-18. Transformer MVAR increase versus GIC for 345kV, 500kV and 765kV transformers.

As evident from these behavior characteristics, transformer design factors can be an important determinant in system behavior. While transformer kV rating is fully defined for all transformers included in the U.S. Power Grid Model, there is some uncertainty about the context of the ratio of single phase and three-phase transformers in the overall transformer population. Because the design of transformers were not readily available in all cases, estimates of single-phase/three-phase populations were therefore based upon MVA rating, in that transformers of 600MVA or larger in size were assumed to be single-phase design. Based upon these estimates, it is estimated that 85% of the 345kV transformers will be three-phase (Figure 1-19). For the 500kV population, only 34% of these transformers are three-phase (Figure 1-20) while the bulk of the population is the more susceptible single-phase design. At the 765kV level, nearly all of these transformers are expected to be of single-phase design (Figure 1-21).

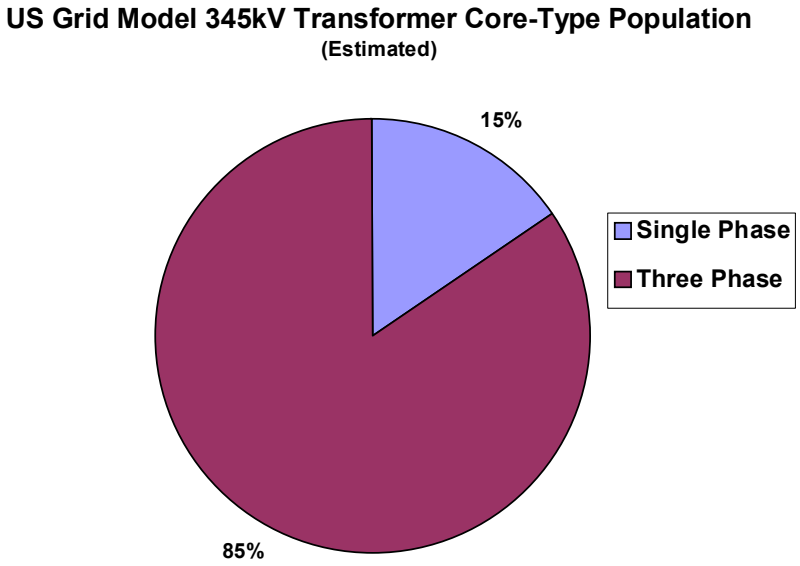

Figure 1-19. Demographic estimates of 345kV transformers – single-phase vs. 3-phase.

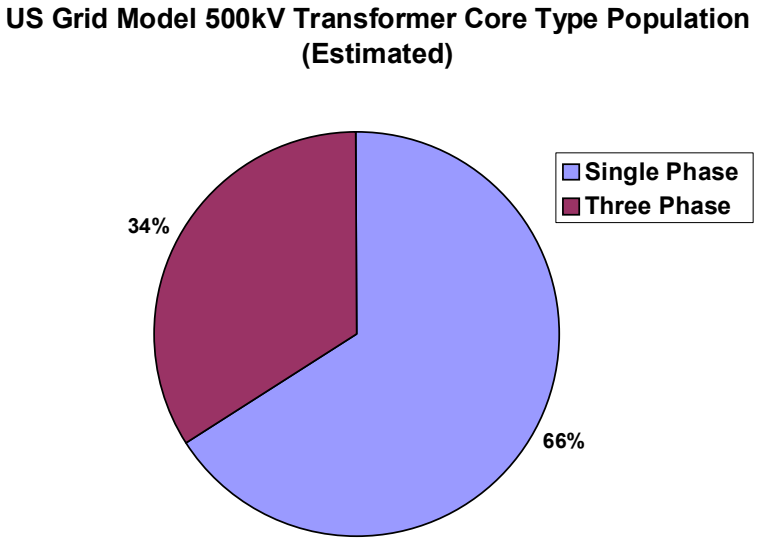

Figure 1-20. Demographic estimates of 500kV transformers – single-phase vs. 3-phase.

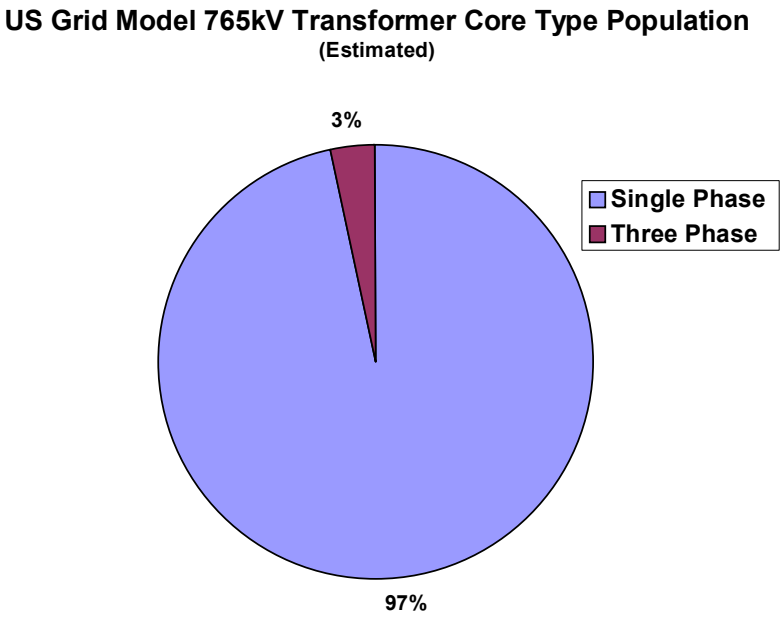

Figure 1-21. Demographic estimates of 765kV transformers – single-phase vs. 3-phase.

Using this method of allocating transformer design is a possible source of uncertainty and one goal for this analysis is to not produce overly pessimistic results, which might occur if population estimates of single-phase transformer design in the U.S. grid are over-estimated. In order to test the assumptions applied to the U.S. grid as a whole regarding the transformer design population, a comparison was made with available transformer data from the BPA power grid in the Pacific Northwest region. The BPA system is predominantly a 500kV and 230kV transmission system with a small number of 345kV facilities. BPA has ~6% of the U.S. ownership of all 500kV transformers included in the Power Grid Model. The population statistics on single-phase and three-phase design for their 500kV transformer is shown in Figure 1-22. The transformer nameplate data confirms that the population is indeed heavily single-phase design, with 97% of all 500kV transformers in this region being single-phase units. This population ratio is actually much higher than the U.S. 500kV population as a whole, which is modeled as being only 66% single-phase design. BPA also has a large population of 230kV transformers, therefore population ratios of these transformers can be a somewhat relevant comparison for the estimated populations for the 345kV transformers estimated for the U.S. model. As shown in Figure 1-23, the ratio of single-phase design in the BPA 230kv transformers is 25%. This is also a higher ratio of single-phase units than assumed for the entire U.S. 345kV population, which is estimated to be only 15%. This comparison suggests that the estimated 345kV population of single-phase design transformers may actually be larger than currently represented in the U.S. model.

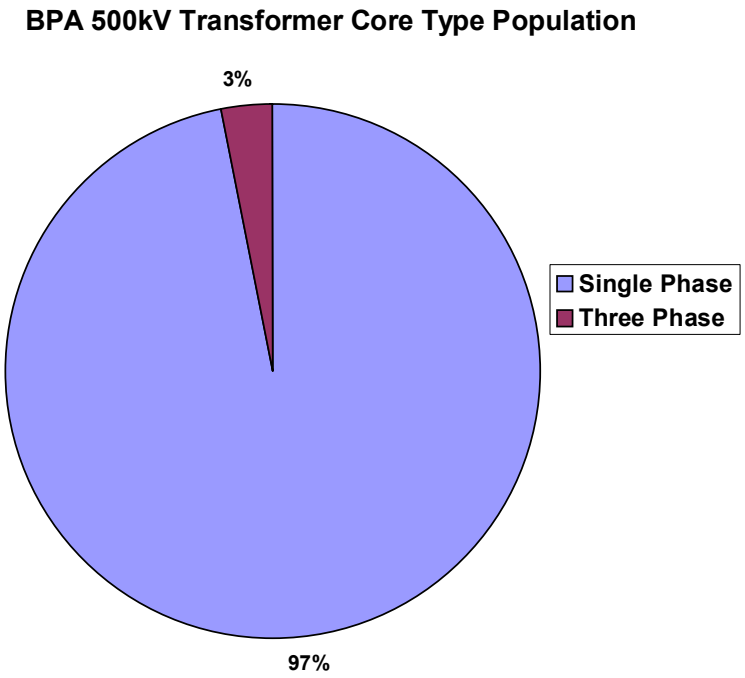

Figure 1-22. BPA 500kV transformer demographics – single-phase vs. 3-phase.

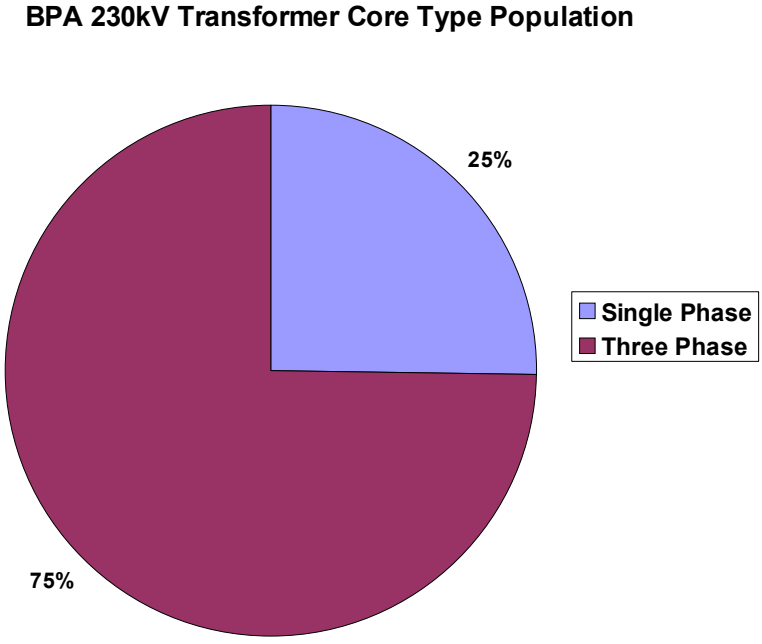

Figure 1-23. BPA 230kV transformer demographics – single-phase vs. 3-phase.

Publicly available data from the ECAR pool was also used to confirm the very high population of 765kv single-phase design transformers. The ECAR power pool contains nearly all the 765kV transformers in the U.S., with the exception of a handful of 765kV transformers operating in upstate New York. These verifications provide a level of confidence that simulation results, which are in part based upon population estimates of transformer design, will generally not be overly pessimistic and may in actuality be somewhat optimistic for this review.

Transformers under half-cycle saturation pose a dual threat to system reliability; system-wide voltage collapse by increase in reactive power in each exposed transformer, and the increase of the disruptive effects of harmonics and AC waveform distortion on relay and protective systems. Accurate estimates of both reactive power demand and AC waveform distortions are therefore necessary in models of transformer behavior. Figures 1-17 and 1-18 (previously discussed) provided an overview of reactive power demand behavior of transformers. The AC waveform distortions are more difficult to estimate and need to be considered on a case-by-case basis. Some general examples can be provided to illustrate the nature of impacts that can occur on a wide-scale during disturbance threats. Figure 1-24 provides a plot of the normal AC excitation current that would be observed in the high-side of a 500kV transformer, while Figures 1-25, 1-26, and 1-27 show the significant increases and distortion of transformer excitation current for 5 amps/phase of GIC (Figure 1-25) and also for 25 amp (Figure 1-26) and 100 amp GIC events (Figure 1-27). These examples illustrate that AC peak excitation currents drawn from the power system by a transformer under various levels of GIC excitation can increase from less than 1 amp to over 800 amps. These increased transformer excitation currents are highly distorted and rich in both even and odd harmonics and they combine with the normal load current on the transformer and propagate distortions throughout the power grid. To illustrate the potential impact of these distortions, the primary current (including a load of 300 amps under normal conditions) can be synthesized during several severe GIC exposures. Figure 1-28 shows the normal AC load current for a 500kV transformer (blue waveform) and the resulting AC currents under three different GIC conditions. It is evident that not only are large distortions occurring, but also a significant peak of over-current will result. Total waveform distortions of over 200% are expected to occur. These simulations do not take into account additional waveform distortions that could occur due to simultaneous saturation of adjacent transformers and local resonance's, which could increase distortions further.

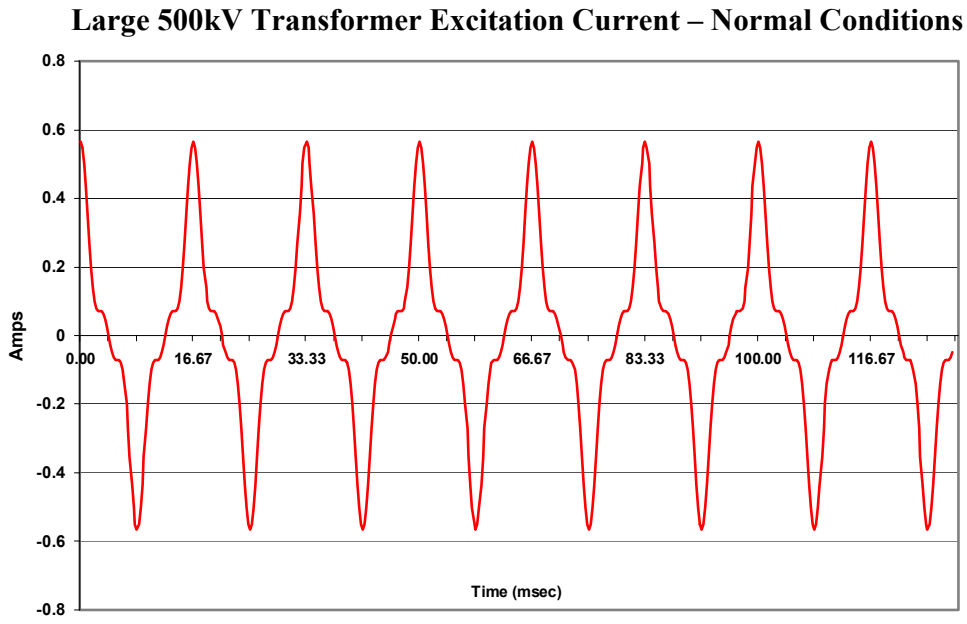

Figure 1-24. Normal excitation current in 500kV transformer.

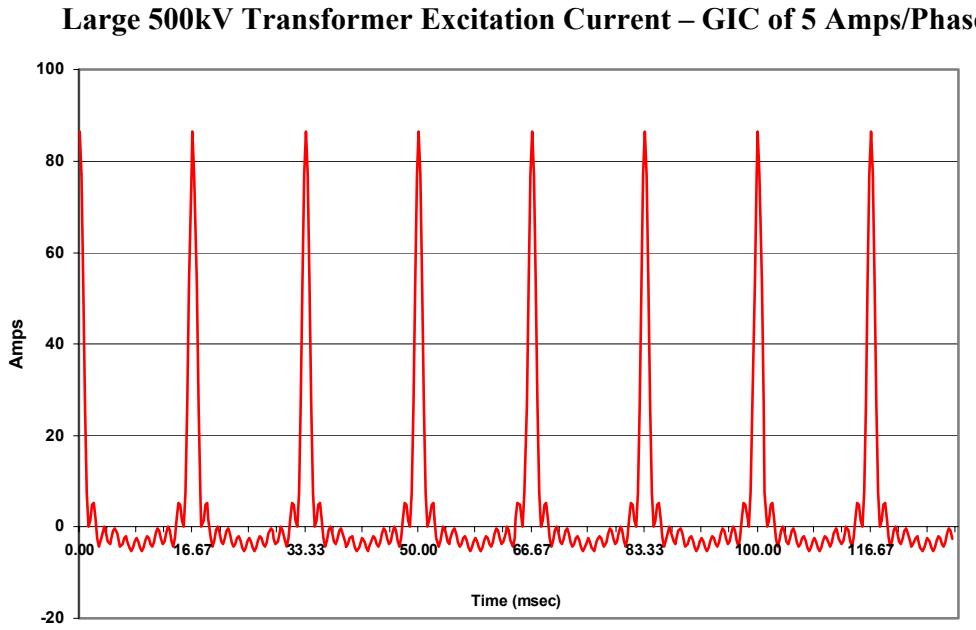

Figure 1-25. Distorted excitation current with 5 amps/phase of GIC.

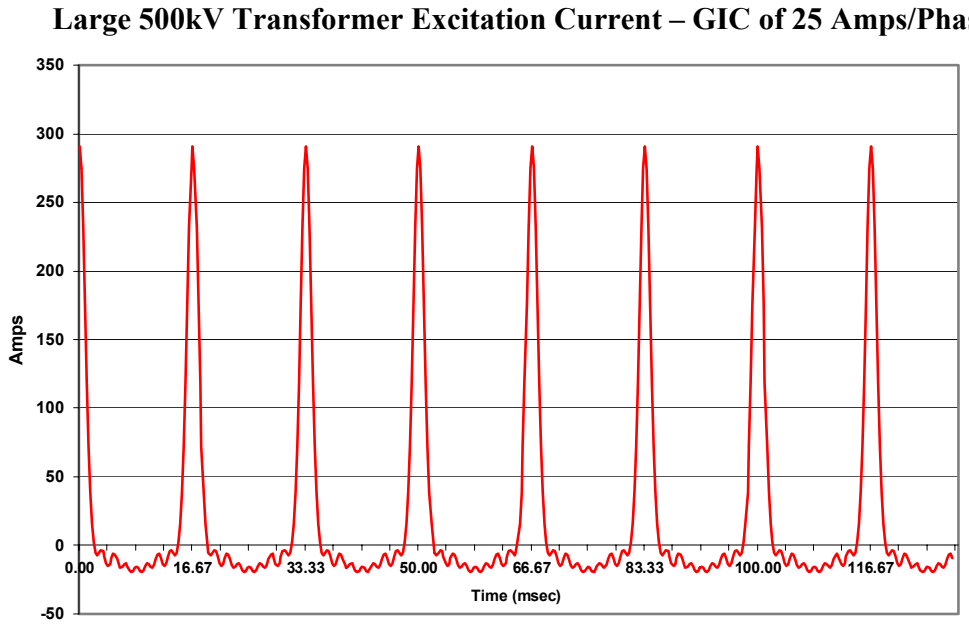

Figure 1-26. Distorted excitation current with 25 amps/phase of GIC.

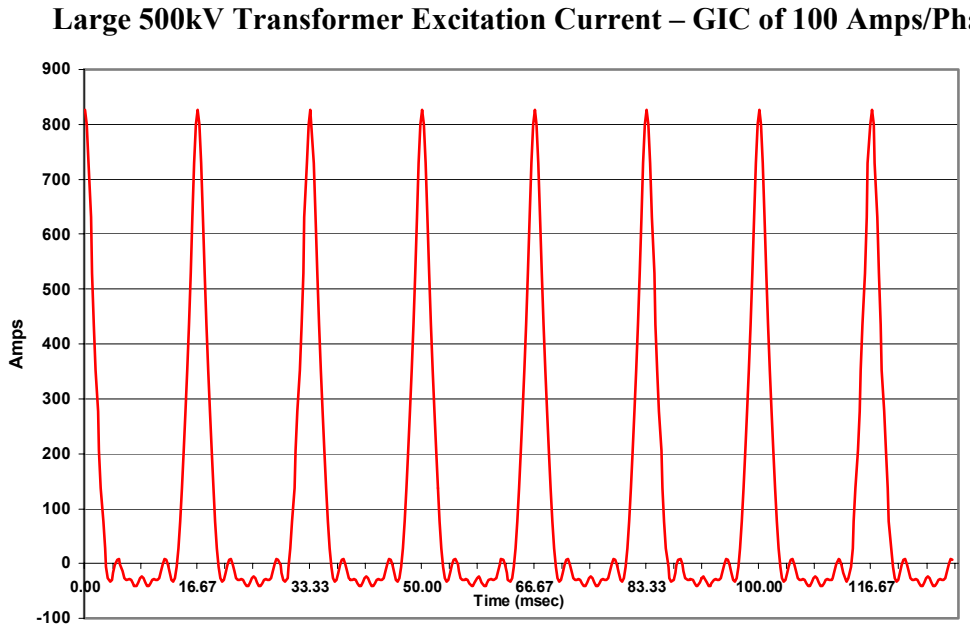

Figure 1-27. Distorted excitation current with 100 amps/phase of GIC.

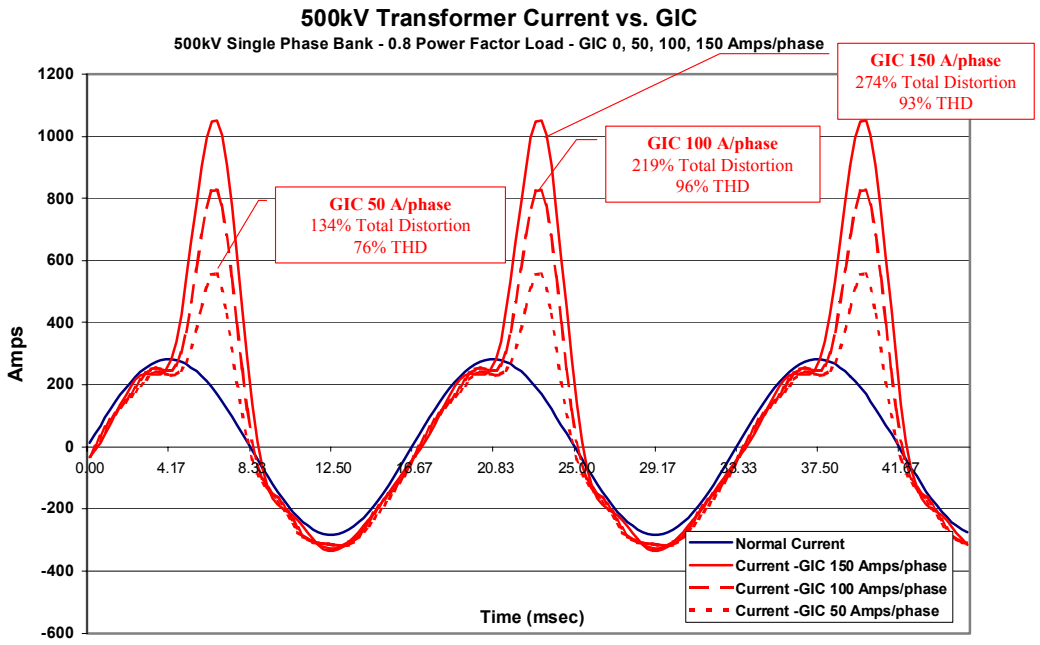

Figure 1-28. Transformer total load current – normal conditions and with 50, 100 and 150 amps/phase of GIC.

In addition to the details of behavior by individual transformers on the power grid, the disturbance conditions can be summarized for the network as a whole, which provides a descriptive overview of the disturbance impact regions. Figure 1-29 provides a summary of geomagnetic storm conditions for the mid-Atlantic through New England region of the U.S. for a storm event on May 4, 1998 at time 4:18 UT. This graphic shows the geographic location of all transmission lines and stations across the region. Also shown are the storm conditions and GIC flows at this moment in time. The storm conditions in this example are illustrated by the blue vectors that depict the spatial complexity of the geo-electric field across the region. These vectors depict both the orientation of the field as well as relative intensity. As shown in this figure there is a strong southeasterly oriented geo-electric field over the New England region and this field rapidly diminishes in intensity and changes in orientation over mid-Atlantic locations. The relative levels of GIC flows are shown at each substation by red or green colored dots. The colors indicate polarity of GIC flow in transformers located at each of these stations. Red means a flow of current into the transformer from ground while green indicates a flow of GIC from the transformer to ground. The polarity of the GIC flow does not have any particular significance on the impact of that GIC to individual transformers, as either polarity of GIC will produce half-cycle saturation effects in a transformer. The sizes of the colored dots also change in proportion to the magnitude of the GIC flow at each location. Therefore, the size of dots indicates the relative level of regional impacts.

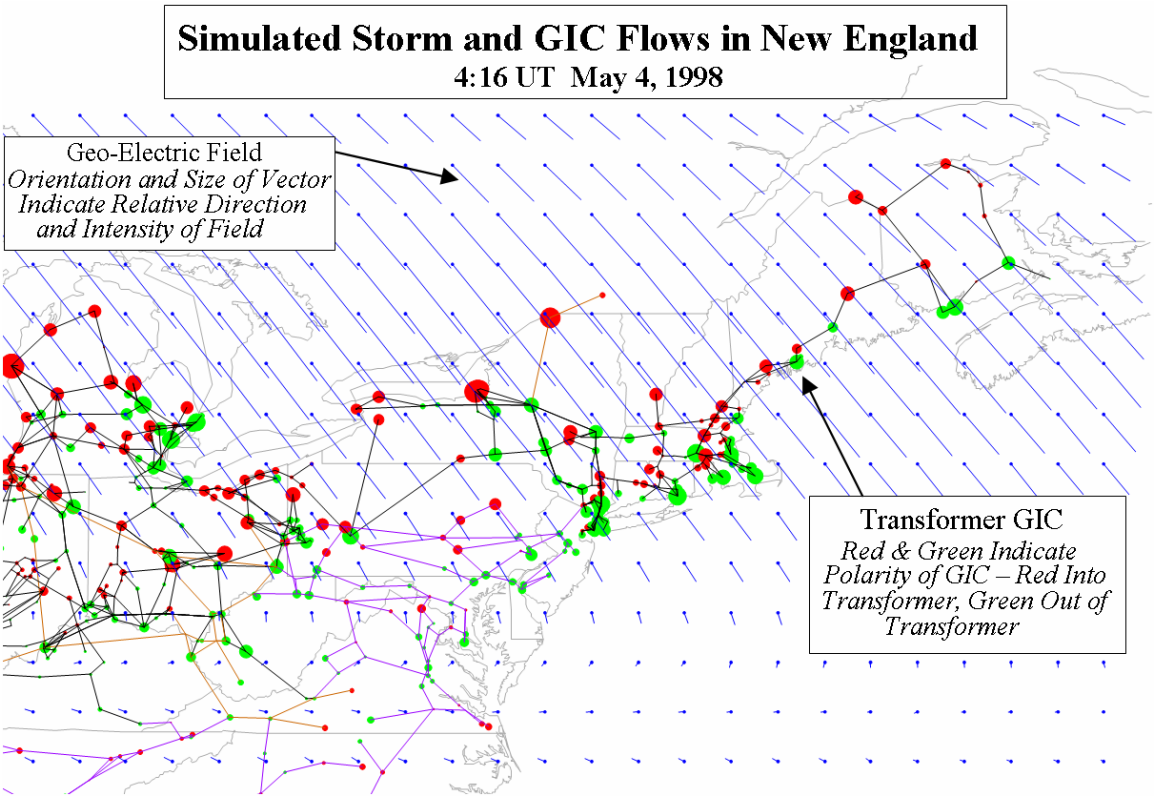

Figure 1-29. Pattern of geo-electric field and GIC flows in New England region of Power Grid Model for May 4, 1998 storm at 4:16 UT.

1.5 The Evolving Vulnerability of Electric Power Grids and Implications for Historically Large Storms

A simple way to summarize much of the discussion in this overview of the Power Grid Model is the interpretation that today's sprawling, high-voltage power grids are more susceptible to space weather impacts than ever before. While almost all research into space weather impacts on technology systems has focused upon the dynamics of the space environment, the role of the design and operation of the technology system in introducing or enhancing vulnerabilities to space weather is often overlooked. In the case of electric power grids, both the manner in which systems are operated and the accumulated design decisions engineered into present-day networks around the world have tended to significantly enhance geomagnetic storm impacts. The result is to increase the vulnerability of this critical infrastructure to space weather disturbances.

The space weather community and the power industry have not fully understood these operation and design implications. The application of detailed simulation models has provided tools for forensic analysis of recent storm activity, and when adequately validated, can be readily applied to examine impacts due to historically large storms, as will be described in subsequent sections of this report. However, even simple empirical extrapolations provide some perspective on the level of threat and the possible consequences of storms on present day infrastructures.

Historical records of geomagnetic disturbance conditions, and more importantly, geo-electric field measurements, provide a perspective on the ultimate driving force that can produce large GIC flows in power grids. Because geo-electric fields and resulting GIC are caused by the rate of change of the geomagnetic field, one of the most meaningful methods to measure the severity of impulsive geomagnetic field disturbances is by the magnitude of the geomagnetic field change per minute, measured in nanoteslas per minute (nT/min). For example, the regional disturbance intensity that triggered the Hydro Quebec collapse during the 13 March 1989 storm only reached an intensity of ~480 nT/min. Large numbers of power system impacts in the United States were also observed for intensities that ranged from 300 to 600 nT/min during this storm. However, the most severe rate of change in the geomagnetic field observed during this storm reached a level of ~2000 nT/min over the lower Baltic. The last such disturbance with an intensity of ~2000 nT/min over North America was observed during a storm on 4 August 1972 when the power grid infrastructure was less than half its current size.

An analysis of the AT&T telecom cable (L4) failure in northern Illinois in a region of ~800 nT/min indicated the disturbance intensity caused a geo-electric field of at least 7 V/km. A dB/dt disturbance of >2000 nT/min was observed over central and southern Sweden on 13-14 July 1982. A coincident peak geo-electric field of 9.1 V/km was observed in central Sweden during this storm on railroad communication circuits. Similar observations from that region of 20 V/km occurred for a storm in May 1921, suggesting that a peak rate of change of ~5000 nT/min is possible. This disturbance level is nearly 10 times larger than the levels that precipitated the North American power system impacts of 13 March 1989. While the magnetospheric drivers and deep-Earth conductivities that shape the geo-electric field response have not changed significantly over this period of time, power system infrastructures have experienced dramatic changes in size and complexity. A recurrence of historically large storms, even like the recent 1982 storm, could have entirely different outcomes in terms of impacts on today's power systems.

For any natural hazard, prudence requires that design and operational adjustments be made to mitigate such risks to infrastructures. Power system designers and operators expect these systems to be challenged by the elements, and where those challenges were fully understood in the past, the system design has worked extraordinarily well. Most of these challenges have been terrestrial weather related. In cases of understood threats, system designers usually applied design and operational standards to harden or mitigate the consequences of these environments on the reliability of the power system. Indeed, investments in arresters and transmission line shield wires to mitigate against lightning alone can be measured in the several billion-dollar range. This has generally confined problems and usually limited the spread of outages that do occur to small regions at any one time. In contrast, the awareness of the geomagnetic storm environments and their potential impacts are much less understood and have aspects that are inherently more threatening than more familiar hazards such as earthquakes and extreme terrestrial weather events (including hurricanes). Geomagnetic storm environments can develop almost instantaneously over large geographic footprints. They have the ability to essentially blanket the continent with an intense threat environment and have the

capability to produce significant collateral damage to critical infrastructures. Power networks are operated using what is termed an "N-1" operation criterion. That is, the system must always be operated to withstand the next credible disturbance contingency without causing a cascading collapse of the system as a whole. This criterion normally works very well for the well-understood terrestrial environment challenges, which usually propagate more slowly and are more geographically confined. When a routine weather-related single-point failure occurs, the power system needs to be rapidly adjusted (10 minutes being the allowed time limit) and positioned to survive the next possible contingency. Both EMP and space weather disturbances, however, can have a sudden onset and cover large geographic regions. They therefore cause near-simultaneous, correlated, multipoint failures in power system infrastructures, allowing little or no time for meaningful human interventions. In contrast to well-conceived design standards that have been successfully applied for more conventional threats, no comprehensive design criteria have ever been considered to check the impact of the geomagnetic storm environments. Further, as this analysis demonstrates, the design actions that have occurred over many decades have greatly escalated the dangers posed by these storm threats for this critical infrastructure.

Section 2
An Analysis of the Impacts of the March 13-14, 1989 Great Geomagnetic Storm on the U.S. and Quebec Power Grids

The events that led to the collapse of the Hydro Quebec system in the early morning hours of March 13, 1989 illustrate the challenges that lie ahead in managing the risk of GIC flows in contemporary electric power grids. Starting at 2:44 AM (EST), all operations on the Hydro Quebec power grid (which serves the entire Quebec province) were normal. At that time a large impulse in the Earth's geomagnetic field erupted along the U.S./Canada border (Figure 2-1). This started a chain of power system disturbance events that only 92 seconds later resulted in a complete collapse to the entire power grid in Quebec. The rapid manifestation of the storm and impacts to the Quebec power grid allowed no time to even assess what was happening to the power system, let alone provide any meaningful human intervention. The rest of the North American power grid also reeled from this great geomagnetic storm. Over the course of the next 24 hours, additional large disturbances propagated across the continent, the only difference being that they extended much further south and came, at times, arguably close to toppling power systems from the New England and Mid-Atlantic regions of the U.S. to the Midwest. The NERC (North American Electric Reliability Council) in their post analysis (Reference 2-1) attributed ~200 significant anomalies in the power grids across the continent to this one storm (Appendix 2).

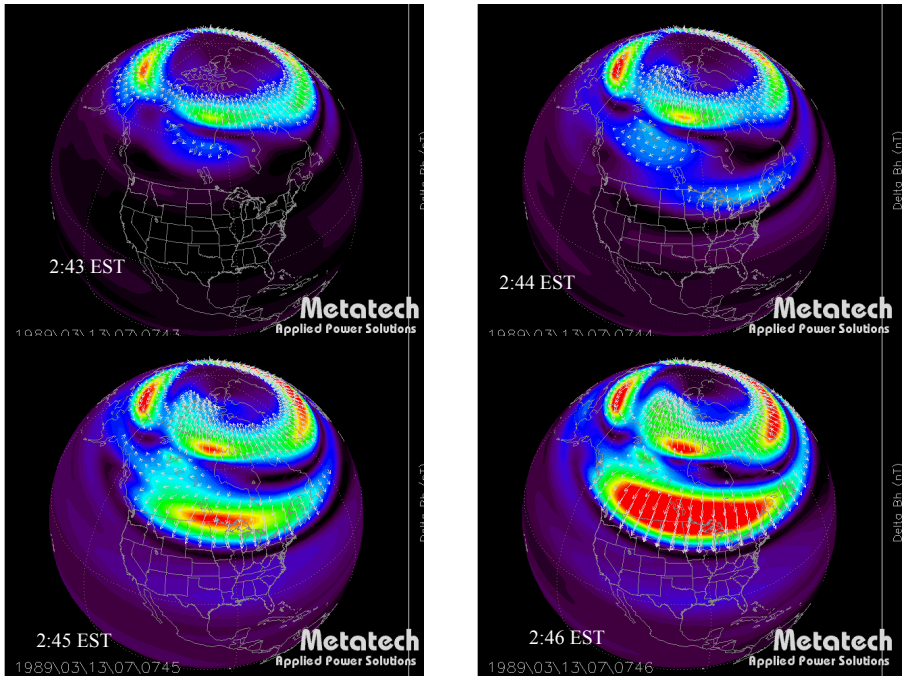

Figure 2-1. Rapid development of electrojet conditions over North America and principally along U.S./Canada border lead to Hydro Quebec collapse and other reported problems in Minnesota, Manitoba and Ontario at these times. These images depict the ground level geomagnetic intensification for over 4 minutes from 2:43 – 2:46 EST.

From the observations and reports available on this storm, the most intense storm activity across North America was observed principally in the broad areas highlighted in Figure 2-2. While the discussion of this section will provide the details of GIC flows and impacts to the North American power grid, a brief overview of the storm conditions can provide a quick perspective. One of the most meaningful ways to describe geomagnetic storm intensity from a perspective of GIC flows in exposed power grids is to consider the rate-of-change of the disturbed magnetic field. GIC levels are primarily driven by rate-of-change (or dB/dt in units of nT/min) of local geomagnetic fields. The higher the dB/dt, the higher the relative levels of GIC. Predicting exact levels of GIC requires extensive models of power grid and deep-earth conditions. But by knowing impulsive geomagnetic disturbance levels across regions, relative intensity comparisons can be provided between storms to classify size. For purposes of this summary, the dB/dt information will be referred to as the RGI (regional GIC index). Figure 2-3 provides a summary of the RGI intensity observed each minute over a 48 hour period between March 12-14, 1989 as observed at the Ottawa Canada observatory, which also provides a proxy for nearby regions in the New York, New England and Canada. As noted in this figure, the Hydro Quebec system collapsed due to an impulse that was slightly greater than 400 nT/min at 2:45 EST. More energetic disturbances exceeding 550 nT/min occurred even later at this site during this storm, many of which precipitated significant problems in portions of the U.S. grid. The ~400 nT/min disturbance level that caused the Quebec collapse provides a useful threshold for analysis. In Figure 2-4, the peak RGI observed at other locations during this storm in North America is noted, along with the time of the peak disturbance. The observations indicated that the largest RGI in North America was actually observed in southern Manitoba/northern Minnesota from the same westward electrojet intensification that triggered the Hydro Quebec collapse. It is also evident that RGI levels of ~400 nT/min were observed as far south as Bay St Louis, Mississippi and from Colorado to Washington State. The later incident times of the more southerly located peak RGI's are due to growth and equator-ward expansion during periods of intensification (i.e. sub storms) as large auroral electrojet currents extended well down into mid-latitude locations of the U.S. To further evaluate the impacts of this storm on the U.S. grid, four specific periods of intense sub storm activity were selected over the time intervals shown in Figure 2-5. For the Hydro Quebec system, since the collapse occurs during the first storm, only that interval is of concern. Each of these four will be evaluated in Subsection 2.2.

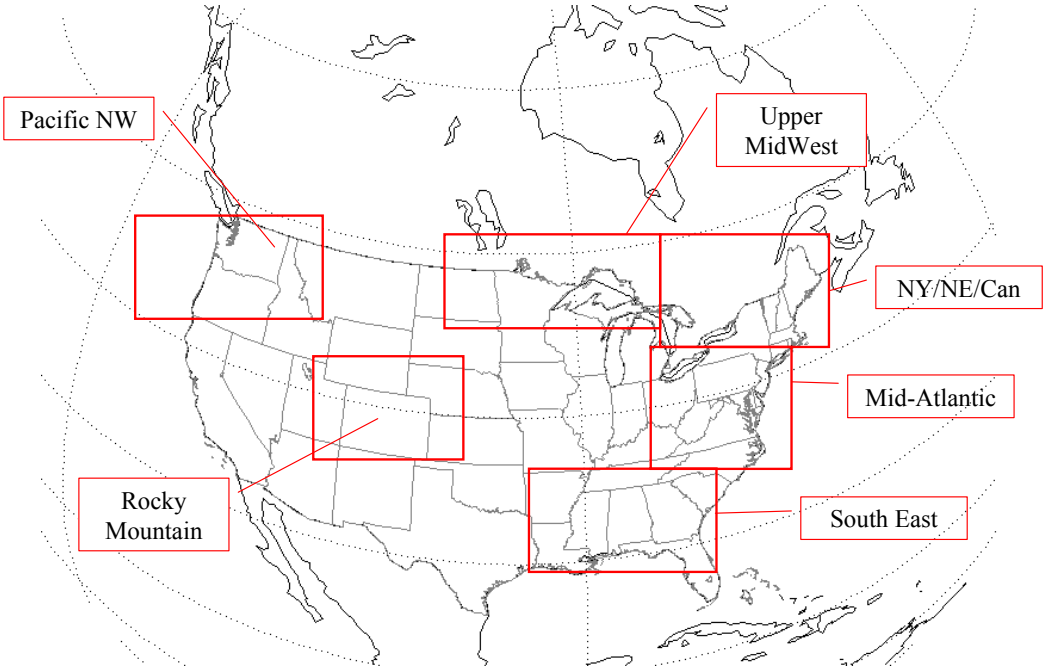

Figure 2-2. Regions with the most disturbed geomagnetic field environments on March 13-14, 1989.

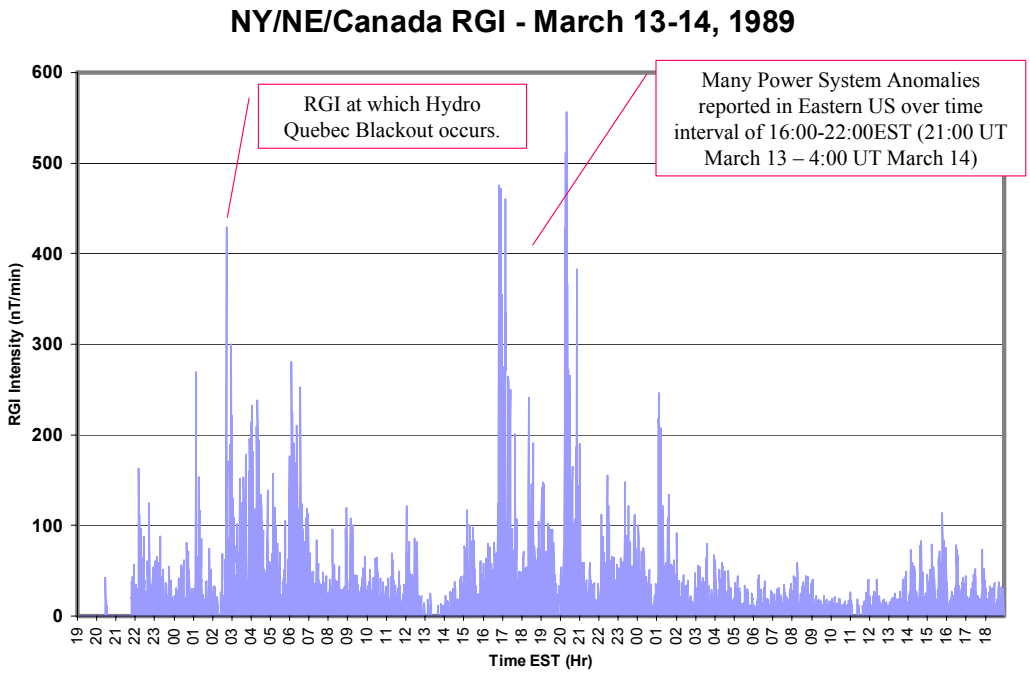

Figure 2-3. Regional GIC Index (RGI) on March 13-14, 1989.

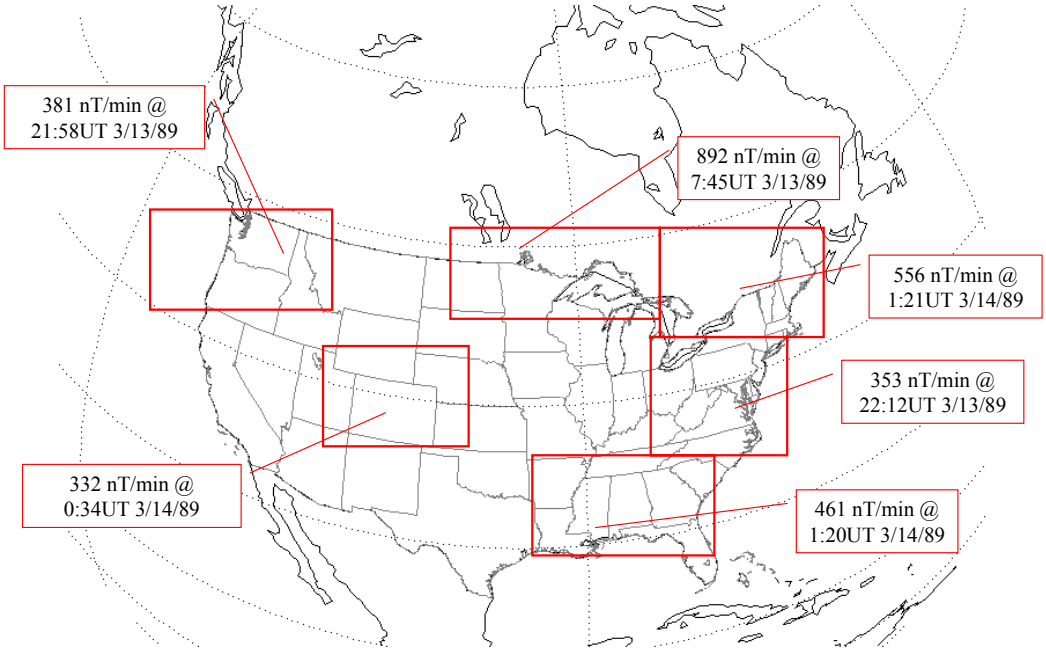

Figure 2-4. Peak RGI observed by region on March 13-14, 1989.

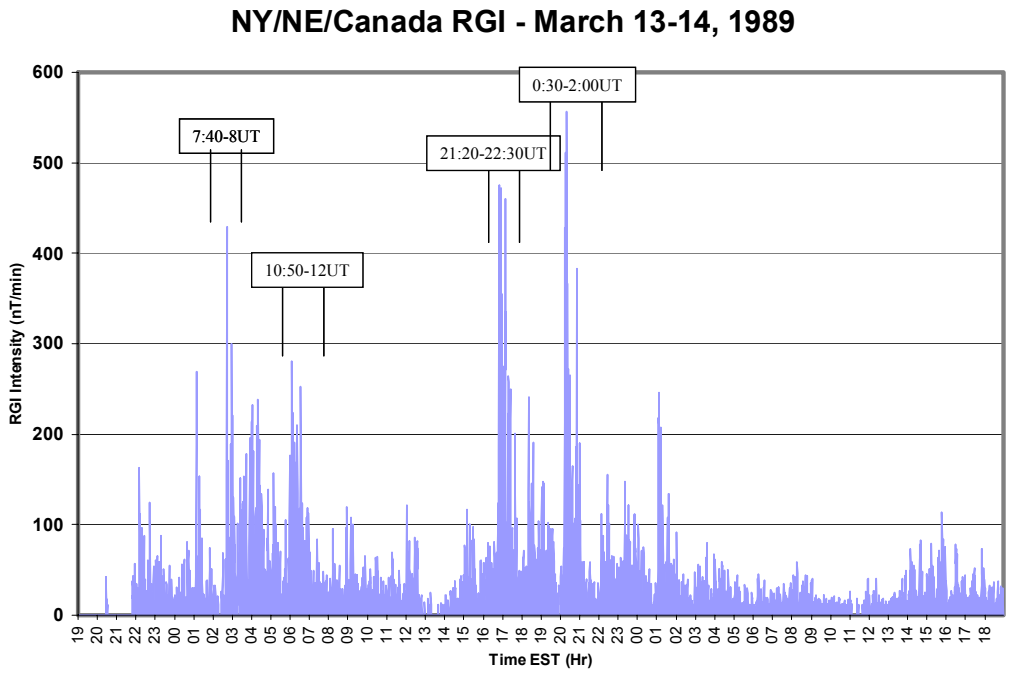

Figure 2-5. Specific storm intervals on March 13-14, 1989 selected for forensic analysis.

2.1 Simulations and Review of the Quebec Power System Collapse

Virtually all power equipment operation and protection problems due to GIC are traceable to two direct effects. They are the half-cycle saturation of power transformers and the half-cycle saturation of current transformers used with protective relay systems. Of the two, the former, with its numerous secondary effects, has been the more serious. Large power transformer half-cycle saturation can lead to four serious problems:

- The transformer suffers high values of exciting current, with extreme peaks on the saturated half-cycle, overheating the unit and greatly increasing internal losses.
- The transformer begins injecting even and odd harmonics of exceptional magnitude into the power system, which can overload capacitor banks, SVC's, and cause malfunction of protective relays.
- The transformer draws a tremendous increase in reactive power from the grid, which, when combined with many other transformers doing the same, can lead to voltage regulation problems and voltage collapse of the network as a whole.
- The transformer suffers stray flux leakage effects, such as damage from localized overheating.

One or more of these effects occurred, and as a result, triggered hundreds of incidents across many regions of the North American continent during the March 13-14, 1989 geomagnetic storm. The effects on the Hydro Quebec system, in particular, are a prime example of how impacts can accumulate and compound upon themselves to a level that is sufficient to precipitate collapse of an entire modern power grid.

Other sections of this report provide an overview of geological and design factors and influences that can introduce higher levels of susceptibility for power grids to geomagnetic disturbances. The Hydro Quebec system has all the elements that contribute to susceptibility:

- It is located in the northern latitudes, near the frequent location of the auroral electrojet current.
- It is in an area of relatively high resistive igneous rock.
- It operates a very high voltage 735kV transmission network and, as a result, experiences higher relative magnitudes of GIC flow than lower voltage networks.
- It has a population of 735kV transformers that are predominantly single-phase units, which readily saturate and, because of the high voltage rating, consume proportionately higher reactive power demands.
- It has a transmission transfer capability that is highly dependent upon intermediate shunt capacitive compensation devices (in this case, multiple SVCs) to maintain proper voltage regulation at all times.

In the aftermath of the March 1989 storm, Hydro Quebec has provided information via papers on the chain of events that caused their system to collapse during this storm (Reference 2-2). They have also undertaken extensive efforts to install both hardware

and operational procedures to prevent recurrences of such a collapse (Reference 2-3). However, there were very few direct measurements anywhere in the world of GIC levels during this important storm event. The Hydro Quebec collapse was triggered by a dB/dt observed in the region that reached a peak of ~480 nT/min. Climatology evidence also suggests that much higher levels of dB/dt are possible in the future, throughout much of the high latitude regions of the U.S. and southern Canada (Reference 2-4). Prior to Metatech's analysis, no detailed forensic analysis modeling the geospace environment of the Quebec power grid was ever undertaken to more fully and accurately assess the conditions that precipitated the network collapse. In addition, it is also evident that reliability of the U.S. grid is also closely tied to reliability of the interconnected power systems in Canada. In March 1989, the Hydro Quebec grid had interconnection capacity capable of exporting ~2000 MW of generation to U.S. markets in the New York and New England regions. Today, the export capability from Quebec has more than doubled, which suggests that collapse of the Quebec system under current conditions would cause a larger loss to the U.S. grid, presenting an even larger threat than before. The development of a model and analysis of the failure of the Quebec power grid presents an opportunity for both understanding of how geomagnetic disturbances can trigger grid failures, as well as quantification of future risks that the Quebec network may imply for U.S. power grid reliability.

As previously shown in Figure 2-1, the southern Quebec region was subjected to a sudden intensification of a westward electrojet which produced ground level geomagnetic disturbance intensities that exceeded 400 nT/min. This created a geo-electric field across the surface of the Earth that lead to GIC flows predominantly in the southern portions of the Quebec grid. The GIC began to flow into transformers across the network, which caused an increase in reactive power demands due to half-cycle saturation effects. At this time the SVCs (static var compensators) on the network began to turn themselves on to supply the increased reactive demand due to the storm. However, the GIC also created harmonics. These harmonics flowed into the SVCs, whose capacitive legs act as a sink to these higher frequencies, to such an extent that protective systems rapidly tripped the devices offline. This left the entire system without the support of these voltage regulation devices, leading to rapid erosion of system integrity and ultimately complete collapse. At the time of the disturbance, the Quebec operating posture can be summarized as shown in Figure 2-6. The load demand of ~22,000MW is primarily concentrated in the greater Montreal region. A large part of the load was supplied by remote hydrogeneration, ~10,000MW from the James Bay and another ~5100MW from the Manicougan and Churchill Falls complexes.

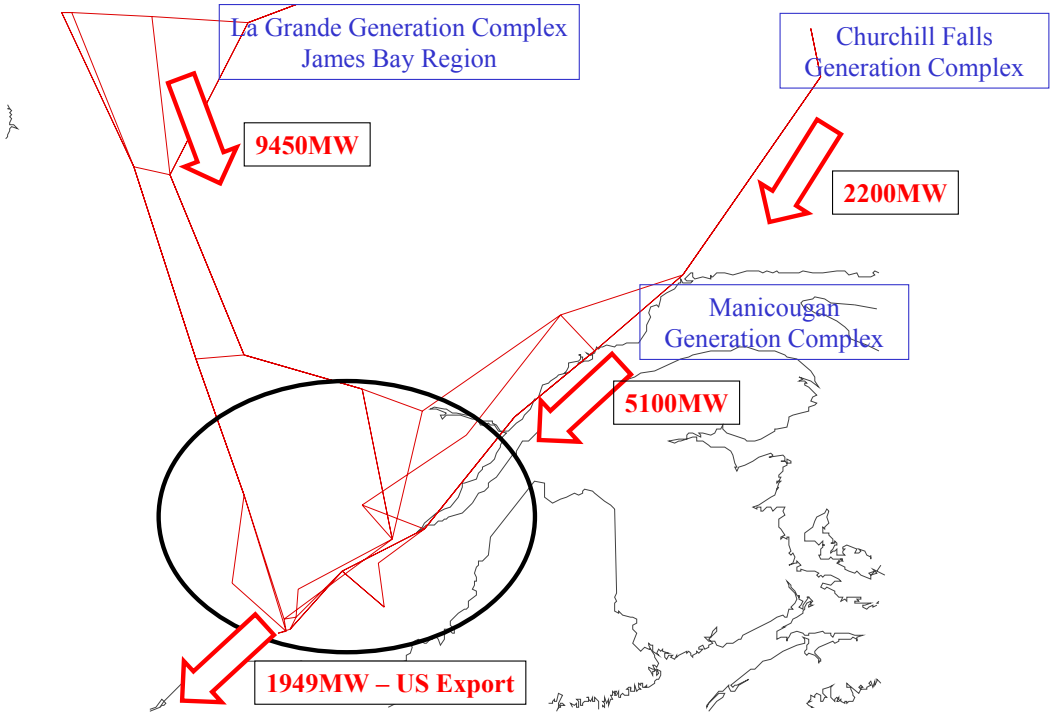

Figure 2-6. Hydro Quebec – 1989 735kV transmission network.

The progression of the storm impacts in the minutes leading up to the network collapse, as measured by total system reactive demand and average GIC flow per transformer, is shown in Figure 2-7, as estimated from the simulation model developed for the Quebec grid. Low levels of GIC were occurring until the intensity of the storm began accelerating at time 7:43 UT (2:43EST). By the time of the system collapse at 7:45:49 UT, the system reactive demand increase due to the storm was approximately 1600 MVARs, while the average GIC flow in each of the Quebec 735kV transformers was ~12 amps/phase. In addition to these substantial increases in reactive demands, the rapid collapse of the Hydro Quebec grid was accelerated by a harmonic interaction/relay malfunction chain of events that literally pulled the legs out from under the voltage regulation infrastructure of the network, just as these voltage regulating SVCs were most needed to counter the reactive demand increases brought on by the storm. Figures 2-8 shows the four minutes of GIC flows and geo-electric field conditions from 7:42-7:45 UT that depict the overall conditions and pattern of GIC flows leading up to the collapse. The important chain of relay malfunction events are reviewed in more detail in Figures 2-9 and 2-10, which show the simulation model results in more detail, with annotations of the relay actions. Figure 2-9 shows the first 6 relay actions, which resulted in tripping 6 of the 7 SVCs on the Quebec grid, with the first trip initiating at 7:44:16 UT. All of these SVCs provide voltage support for the heavy transfers on the 5 lines that tie the Montreal load region to the James Bay generation complex. Figure 2-10 show the remaining relay actions leading up to the collapse. By 7:45:16 UT, the seventh relay action in the chain

was also the tripping of the seventh and final SVC on the James Bay transmission lines. All of these key devices were lost in an elapsed time of only 1 minute. The loss of these devices in concert with storm impacts set up angular swing conditions between the load and generation regions, which progressed to the point that by time 7:45:25 UT, all five 735kV tie lines between Montreal and James Bay tripped by out-of-step relay action (relay actions #8-12). Given the prior loss of the SVCs, this relay action is likely to be proper, however it sealed the fate of the Quebec grid in that nearly half of the generation capacity supplying the network was now lost. Load shedding triggered by frequency decay is designed to equalize the level of load with available generation in order to preserve the network as a whole. All levels of shedding operated, but were not designed to shed enough load fast enough to make up for this large loss of generation. This problem was further compounded by similar out-of-step tripping of lines that tied to the 2200 MW of Churchill Falls generation. By 7:45:49 UT, frequency in the remaining system had decayed, causing complete system collapse.

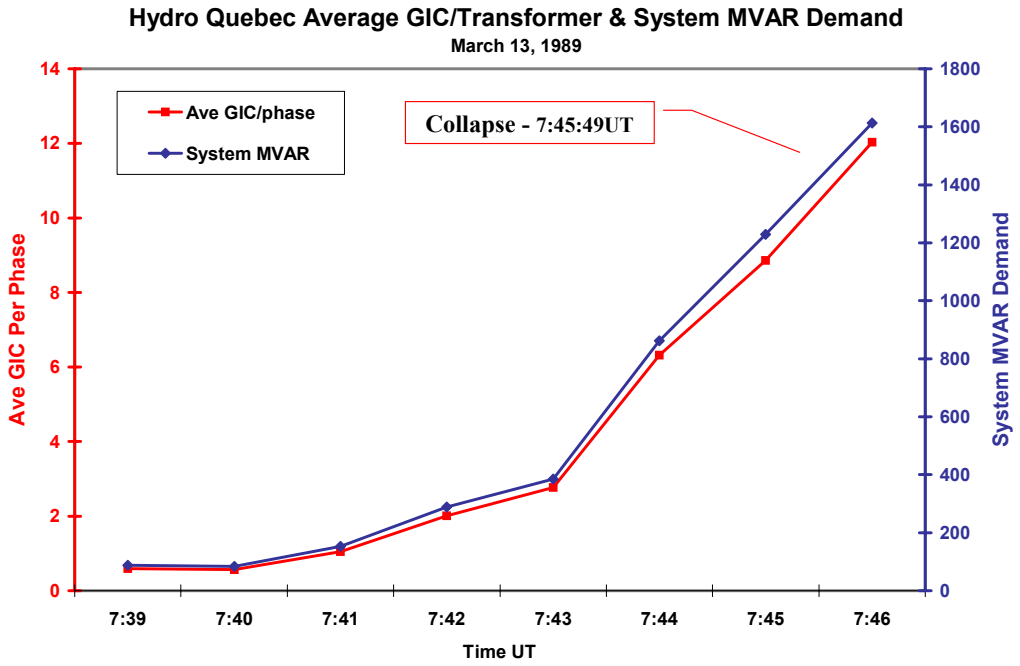

Figure 2-7. Average GIC per transformer and reactive demand, for Hydro-Quebec, for the time just before the system failure.

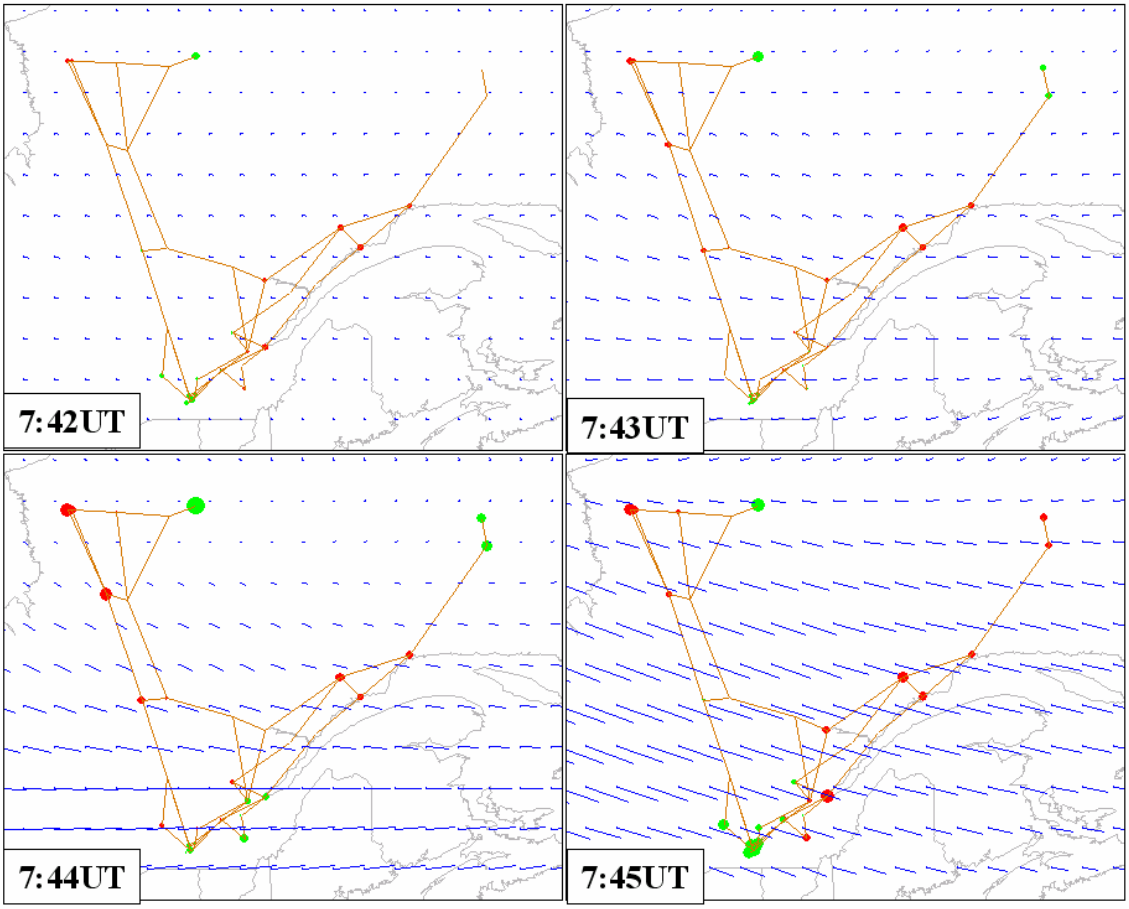

Figure 2-8. Four minutes of space weather/GIC conditions leading to Hydro Quebec collapse.

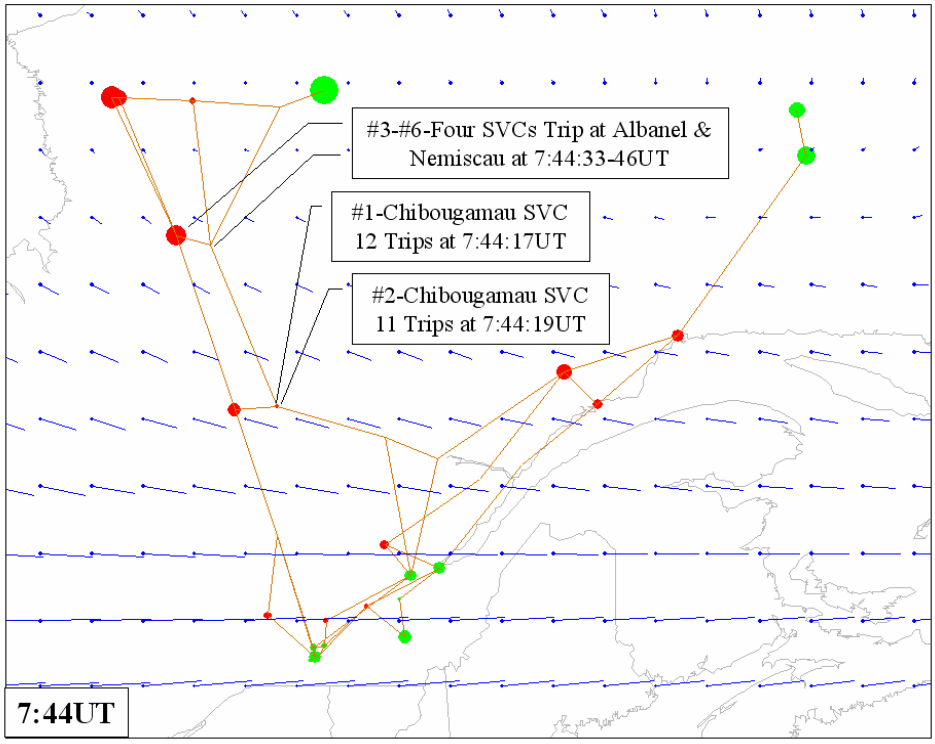

Figure 2-9. Details of 7:44 UT in the Hydro-Quebec collapse simulation.

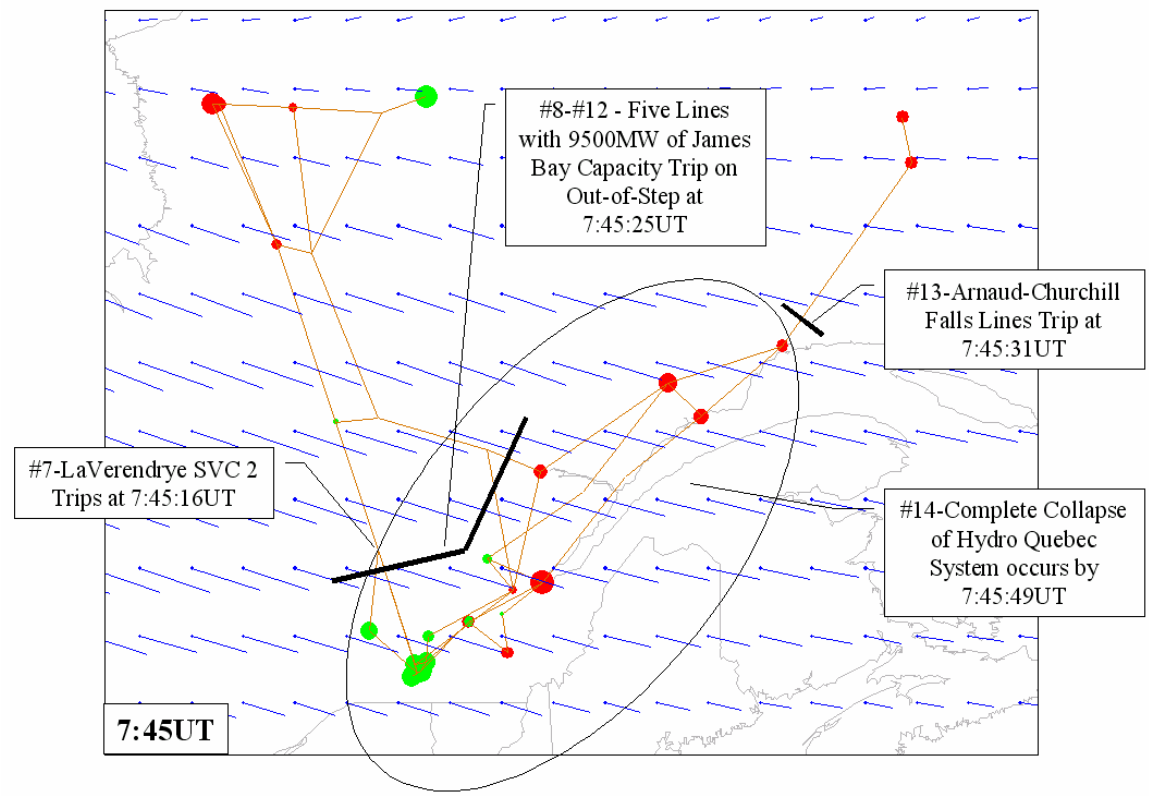

Figure 2-10. Details of 7:45 UT in the Hydro-Quebec collapse simulation.

Figure 2-11 provides a set of plots that summarize the geo-electric field intensities in the Montreal, James Bay and Churchill Falls region of Quebec. As summarized here, and as shown by vector icons in prior system maps, it is likely the initial intensification of the geo-electric field in the southern Montreal region of Quebec triggered most of the problems. The intensity of the geo-electric field is estimated to have only reached a level of ~1.5 V/km, a relatively low level compared to actual measurements that have approached 20 V/km during other more intense storms. Figure 2-12 shows the level of GIC at transformers at the sites where SVCs tripped. These results also indicate GIC levels sufficient to cause half-cycle saturation, but also levels that are not excessively large. The largest GICs were located in the transformers north and south of these SVC locations, and it is likely that harmonics from these locations contributed to the distortion overloads.

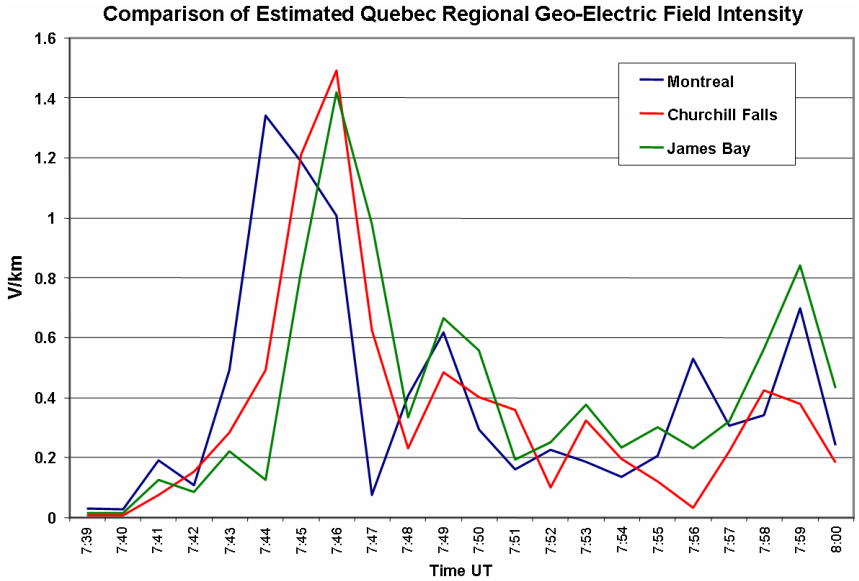

Figure 2-11. Simulated geo-electric fields at three Hydro-Quebec locations, just before the collapse.

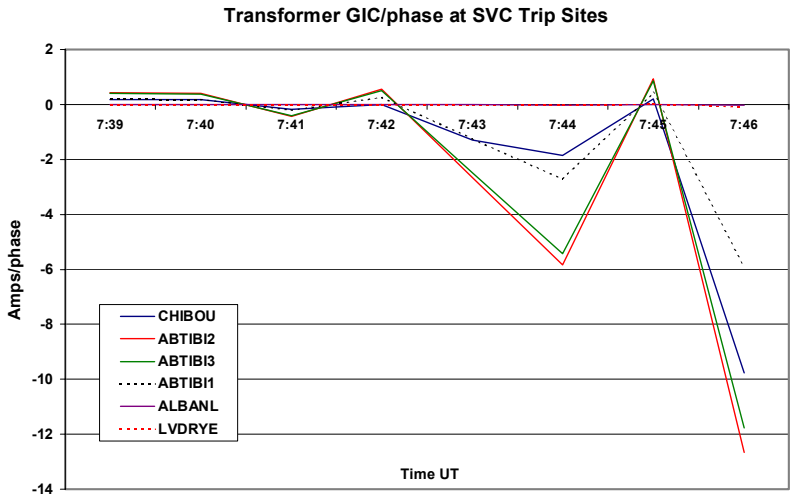

Figure 2-12. GIC, levels at the Hydro-Quebec SVC locations that tripped.

There are a number of lessons learned that should be mentioned, especially as it applies to broader implications and strategies for mitigation in the U.S. These lessons deal with the damage during the process of collapse that could occur from future GIC events, the difficulties posed by the restoration process itself, and GIC tripwires (such as new technology systems, i.e. SVC's) that are unknowingly present in today's system that will too easily initiate widespread grid collapse scenarios. During the process of collapse, permanent damage was inflicted on the Quebec power grid. The uncontrolled operation of circuit breakers in rapid succession across the grid added fuel to the fire, by causing temporary overvoltages (load-rejection overvoltages) on certain points in the network, which caused permanent damage to two 735kV transformers at the LG4 station in the James Bay complex, a 735kV shunt reactor at Nemiscau (located midway between James Bay and Montreal) and the failure of a 735kV lightning arrester. The restoration process is clearly hampered by damage of this type, as it may involve a critical circuit path for restoration of power. Fortunately, the Quebec system is almost exclusively hydro generation base, which means that restoration of generation is relatively simple and rapid. Even so, the restoration of a large complex network takes some time. The table below provides the restoration timeline that Quebec was able to achieve.

Table 2-1. Hydro-Quebec restoration

Time (EST)	Event	Status
0245	Collapse	Hydro-Quebec blackout
0700	Restoration	25% load restored (5,000 MW)
0900	Restoration	48% load restored (10,500 MW)
1100	Restoration	64% load restored (14,200 MW)
1300	Restoration	83% load restored (17,500 MW)

After 11 hours, 83% of the load was restored. However, with the predominant population of steam electric generation in the U.S., the restoration process is much more difficult, and similar restoration performance to that shown above is highly unlikely.

In retrospect, it is clear that the collapse occurred because of correlated multiple events causing a combination of the voltage regulation stress on the system from the storm, in combination with key relay malfunctions, separately caused by the storm. It is also evident that the first 7 relay actions, causing loss of all SVCs, was due to inappropriate and overly conservative relay settings, which were intended to protect a piece of equipment. This is too-often a preferred protection approach when the objective gets overly skewed towards limiting damage to the SVC device. However, these relay settings were a tripwire for collapse. When this protection philosophy is applied throughout the system and then that system is subjected to a common mode stress, the integrity of the system as a whole rapidly erodes. Because power system operators and planners have not had the luxury of storm analysis simulations, as employed in this study, they also have had very few insights into the risks posed by this environment.

One of the most important remedial actions that were undertaken was to revise the relay settings on the SVCs, and make other special protection modifications to allow more

generous levels of harmonic current loading before initiating a trip. It is also clear, from storm related events of this type in the U.S., that tripwires of this type might be waiting to surprise grid operators in future severe storms.

References

2-1 NERC Disturbance Analysis Working Group Report, The 1989 System Disturbances: March 13, 1989 Geomagnetic Disturbance, pages 8-9, 36-60, 1990.

2-2 Denis Larose, "The Hydro-Quebec System Blackout of March 13, 1989", IEEE Special Publication 90TH0291-5 PWR, Effects of Solar-Geomagnetic Disturbances on Power Systems, 1989, pg. 10-13.

2-3 Antonio Dutil, Impact of Geomagnetic Storms on Transenergie Transmission System-Situation at the Dawn of Year 2000, Report to NPCC, January 2000.

2-4 J.G. Kappenman, Chapter 13 - "An Introduction to Power Grid Impacts and Vulnerabilities from Space Weather", NATO-ASI Book on Space Storms and Space Weather Hazards, edited by I.A. Daglis, Kluwer Academic Publishers, II Mathematics, Physics and Chemistry, Vol. 38, pg 335-361.

2.2 Simulations and Review of Storm Impacts on the U.S. Power Grid

The effects of the March 13-14, 1989 Great Geomagnetic Storm were also widely felt on power grids throughout the U.S. The consequences of the storm in the U.S. were not as severe, compared to the complete blackout that occurred on the Hydro Quebec grid. However, the storm did pose serious and widespread threats to the operational integrity of the U.S. power pool at times. The storm also caused several cases of severe transformer damage. As previously discussed, four different substorm intervals were selected for detailed simulation and assessment using the U.S. Power Grid Model. The selected intervals also happened to coincide with the bulk of the power system problems reported to NERC and contained in the summary in Appendix 2 of this report. This forensic analysis allows for needed perspective on the levels of disturbance threat and resultant GIC flows that could trigger widespread power system problems. This simulation provides a means of further calibrating the assessments that are necessary to evaluate the potential consequences of future and potentially larger geomagnetic storm events on the U.S. power grid infrastructure.

2.2.1 Substorm Interval 7:40-8:00 UT

As previously described, the disturbance intensification primarily occurred in the vicinity of the U.S.-Canada border region. In the eastern part of North America the disturbance triggered the collapse of the Hydro Quebec grid, but also propagated disturbances effects into the neighboring U.S. regions as well. At the time of the Quebec collapse, the U.S. was importing 1949MW from Quebec. All of this capacity was lost due to the collapse. The most important loss involved the 765kV AC tie line that runs from upstate New York to the Montreal region, where a DC interconnection is made with the Quebec system.

As previously shown in Figure 2-4, the highest intensity observed from this storm in North America occurred in the southern Manitoba and northern Minnesota regions, reaching a peak of 892 nT/min at 7:45 UT. This intense disturbance caused an increase in reactive demands that was also observed – in one case the reactive power output of synchronous condensers increased by 420 MVARs, at one Manitoba 500kV substation. Figure 2-13 provides a map of the simulated geo-electric field conditions and resulting GIC flow conditions in the U.S. grid at the peak disturbance time of 7:45 UT. Also noted in this map are the locations of important reports of power system anomalies at this time, which clearly indicates they were caused by the storm environment. It is likely that less severe system impacts resulted due to the time of day of this substorm, in that this was 2:45 EST to 23:45 PST. These are all times of minimum system load across the U.S., and operating postures that would, in most cases, provide for highest reactive power reserves on the system.

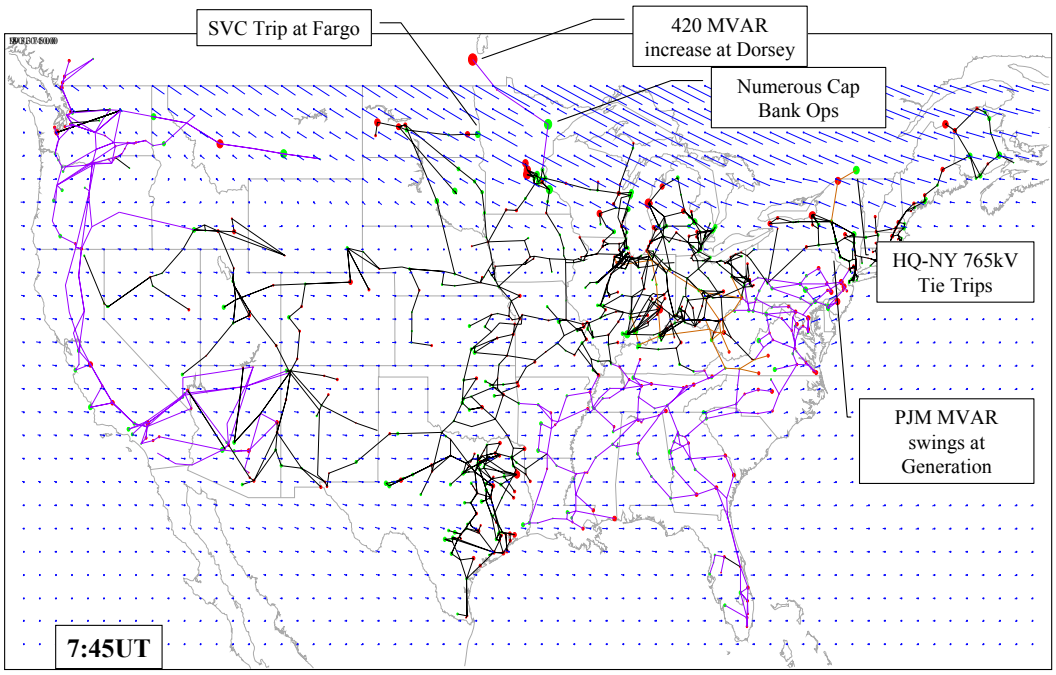

Figure 2-13. GIC and geo-electric field conditions – 7:45 UT, March 13, 1989.

2.2.2 Substorm Interval 10:50-12:00 UT

The substorm event of this time interval had location characteristics similar to those of the previously discussed interval. The source of the ground level geomagnetic field disturbance was an intensification of the westward electrojet, and the footprint of the disturbance primarily centered on the U.S.-Canada border. Figure 2-14 provides a depiction of the area at 11:26 UT. While the region is large, the intensity of this substorm was generally 20-50% less severe than the previous substorm. The most intense portion of interest was over portions of the eastern U.S. Figure 2-15 provides a summary map and table of a large number of reported power system events that were concentrated in this region over the time period from 6:60 to 6:30 EST (11:06-11:30 UT). These events largely involve capacitor switching to provide MVARs in response to the storm. Various alarms and associated event recorders were initiated, due to the highly unusual system events.

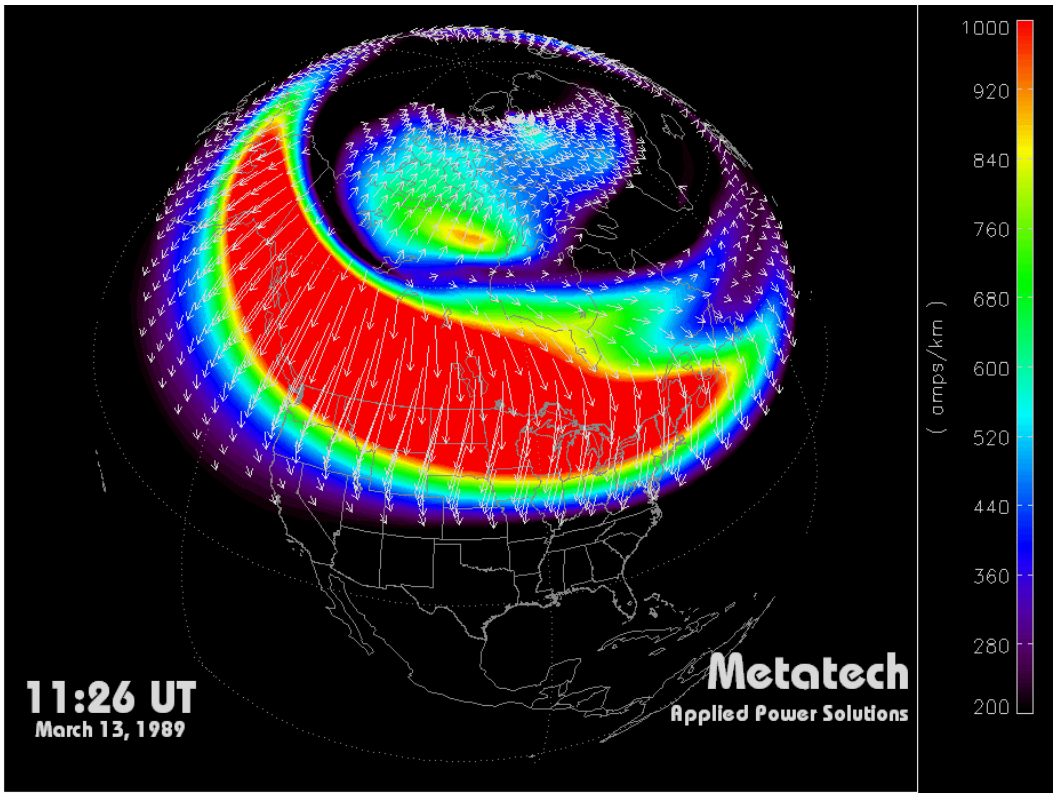

Figure 2-14. Simulation of geomagnetic conditions at 11:26 UT, on March 13, 1989.

Time (EST)	Area	Event
606	NIMO	Capacitor
608	Cent. Hud.	Capacitor
610	PJM	Voltage
613	NIMO	Capacitor
615	APS	Capacitor
615	Va. Pwr.	Capacitor
617	PJM	Oscillograph
618	NIMO	Capacitor
618	PJM	Recorder
618	PJM	MW
618	Va. Pwr.	Capacitor
618	Va. Pwr.	Capacitor
619	Va. Pwr.	Capacitor
619	PJM	Recorder
619	Cent. Hud.	Capacitor
620	Va. Pwr.	Capacitor
624	Va. Pwr.	Capacitor
624	Va. Pwr.	Capacitor
624	OH	Oscillograph
625	Va. Pwr.	Capacitor
630	Atl. Elec.	MVAR

Figure 2-15. Reported North American power system impacts, March 13, 1989, for time span of 6:06-6:30 EST (11:06-11:30 UT).

2.2.3 Substorm Interval 21:20-22:30 UT

The substorm activity during this time interval produced some of the largest and most widespread impacts observed across the U.S. power grid. Figure 2-16 provides a map

and table summary of reported events over the time period 16:00-17:23 EST (21:00-22:23 UT). As shown, a large number of events were reported across the entire continent, even as far south as Los Angeles. The power system problems were caused by a more complex pattern of storm intensification during this time interval than prior intervals. Also, the disturbance regions expanded to mid-latitude locations over the U.S., which exposed large portions of the U.S. grid to moderately intense disturbance conditions. The disturbance conditions at times 21:50 UT and 22:00 UT are shown in Figures 2-17 & 2-18. As shown, there was both a large westward electrojet extending from Europe to the center of the North American Continent and also a large eastward electrojet from the eastern U.S. through the Pacific Northwest. It is also evident from comparison that these disturbance regions were very dynamic, as they significantly expanded in area over the time interval shown. The environment was particularly harsh because of the lower latitude position of the eastward electrojet. The disturbance region exposed a large fraction of the U.S. grid, causing the large number of events reported. Since the reporting of these events was voluntary, it is likely that further events occurred that were unreported. This would be especially true for low latitude regions of the U.S. where most power system operators are much less familiar with GIC problems and may have dismissed anomalies to "cause-unknown". The other likely aspect explaining the higher relative impacts was the time of the disturbance intensification. The 16:00-18:00 EST time interval is during the peak electrical demand periods of the day for the entire U.S.; whereas the other two time intervals previously discussed were during early AM hours and minimum system load conditions.

Time (EST)	Area	Event
1600	Atl. Elec.	MVAR
1602	Va. Pwr.	Capacitor
1610	PJM	Noise
1615	PJM	Generator
1625	PJM	Oscillograph
1626	PJM	Oscillograph
1630	SC Edison	Current
1630	SC Edison	Current
1630	SC Edison	Noise
1640	PJM	Voltage
1644	PJM	Alarm
1644	PJM	Capacitor
1645	WPL	Voltage
1649	PJM	Recorder
1651	NIMO	Capacitor
1653	NIMO	Capacitor
1654	PJM	Alarm
1655	Minn. Power	Voltage
1655	Atl. Elec.	Voltage
1665	Atl. Elec.	MVAR
1658	BC Hydro	Voltage
1658	OH	Demand
1658	WAPA	Converter
1658	BPA	Noise
1658	WAPA	Line
1658	WKPL	Alarm
1658	BPA	Capacitor
1658	BPA	Transformer
1700	UPA	Voltage
1700	LILCO	Voltage
1700	IIGE	Voltage
1700	WEP	Noise
1701	PJM	Capacitor
1701	NIMO	Capacitor
1701	Va. Pwr.	Capacitor
1701	Va. Pwr.	Capacitor
1701	OH	Voltage
1701	OH	Oscilligraph
1703	Va. Pwr.	Capacitor
1708	UPA	Capacitor
1709	WAPA	Converter
1709	WAPA	Transformer
1709	WAPA-Fargo	Voltage
1709	WAPA	Line
1709	WAPA	Relay
1711	NIMO	Capacitor
1720	UPA	Voltage
1723	Va. Pwr.	Capacitor

Figure 2-16. Reported North American power system impacts, March 13, 1989, for time span of 16:00-17:23 EST (21:00-22:23 UT).

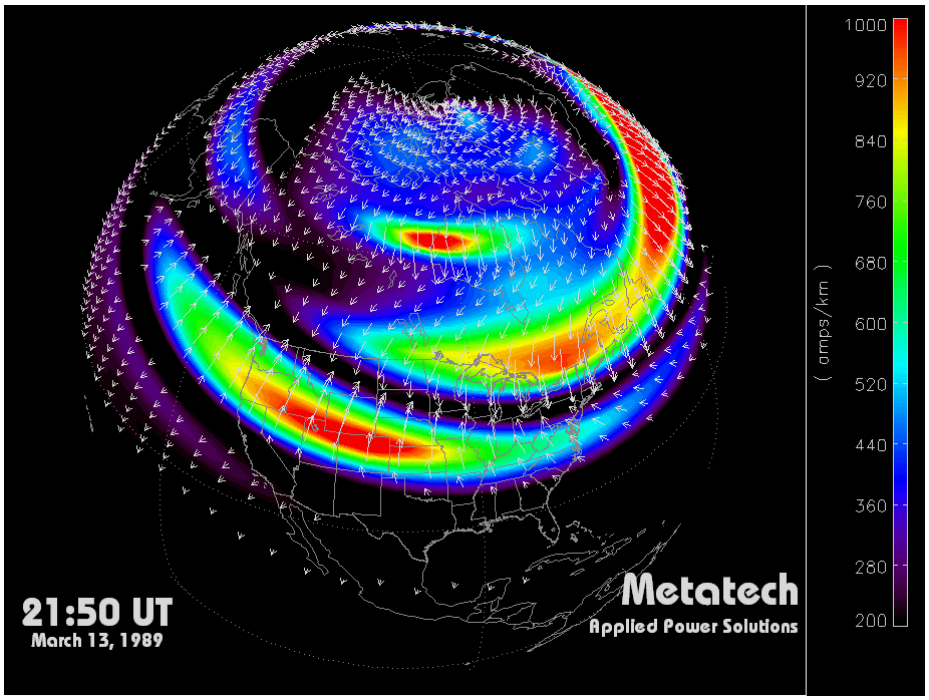

Figure 2-17. Simulated 21:50 UT, March 13, 1989, conditions.

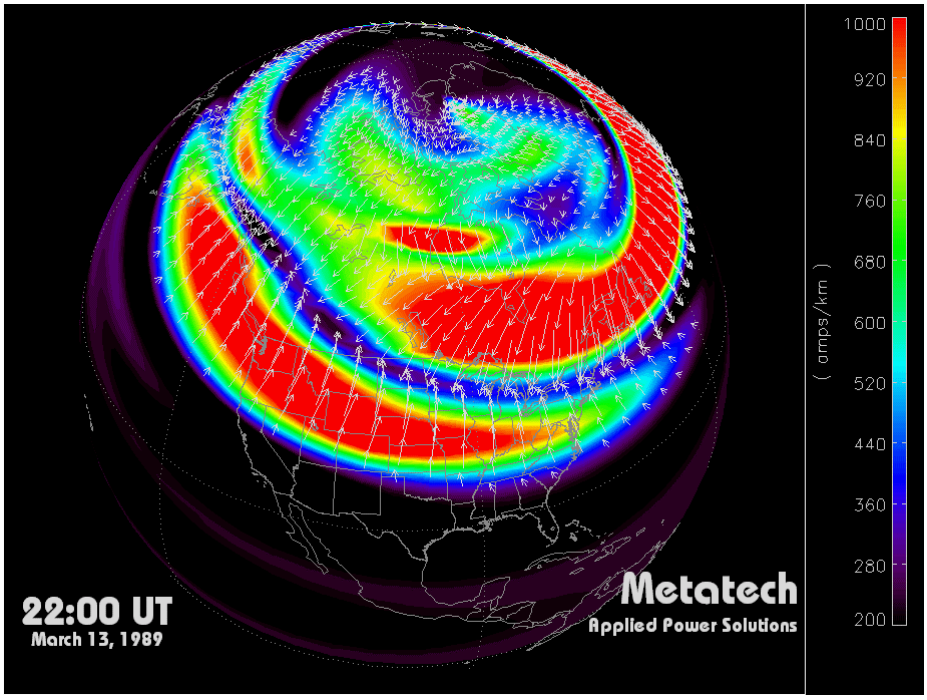

Figure 2-18. Simulated 22:00 UT, March 13, 1989, conditions. The intense geomagnetic field disturbance region at mid-latitudes of the U.S. is caused by an eastward electrojet intensification, while the higher latitude intensification extending back towards Europe is due to a westward electrojet current in the ionosphere.

The storm impacts can be assessed further by reviewing the geo-electric field conditions and the estimated GIC flows across the U.S. power grid at several key times. Figure 2-19 shows the conditions at time 21:44 UT. At this time, an intense geo-electric field extends from the mid-Atlantic region into the upper Midwest. Voltage regulation problems were reported in Wisconsin, along with a number of problem reports in the Pennsylvania and New Jersey regions. Figure 2-20 shows the conditions at 21:51 UT. Here, the storm is particularly intense over the Northeastern U.S. This also caused four capacitor banks to trip in New York. By 21:57 UT (Figure 2-21), the intense geo-electric field extends from the Mid-Atlantic/New England regions to the Pacific Northwest. This triggered a large number of problems all across the U.S., as noted in the figure. Figure 2-22 provides the conditions at 22:09 UT. The disturbances at this time caused trips of transmission facilities in the western North Dakota/Montana region and also trips of capacitor banks in upstate New York.

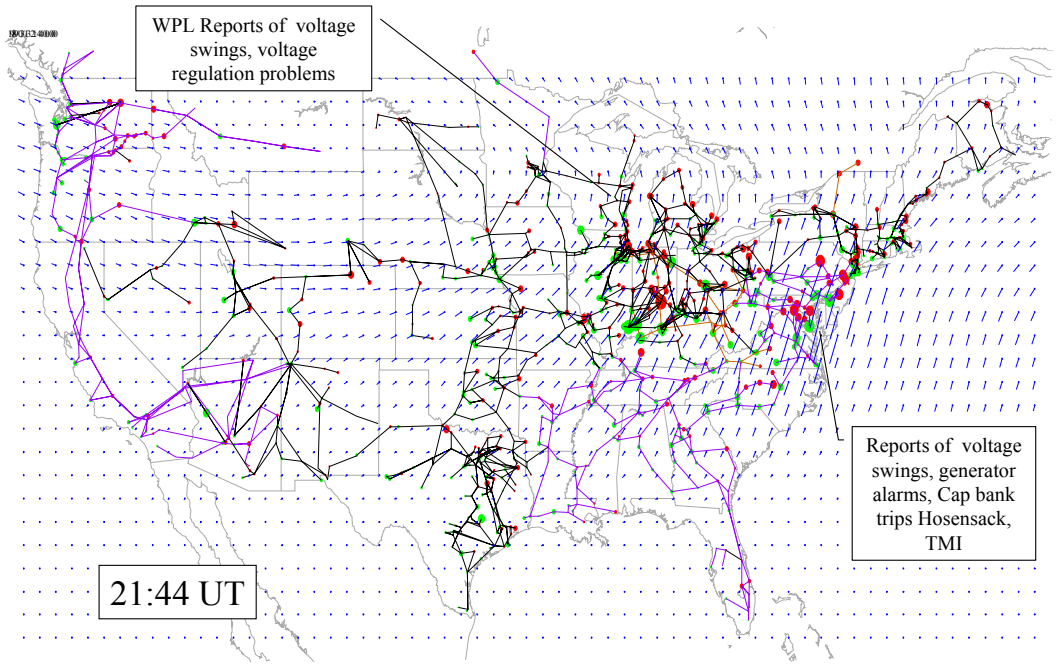

Figure 2-19. Simulation of U.S. power grid conditions at 21:44 UT on March 13, 1989.

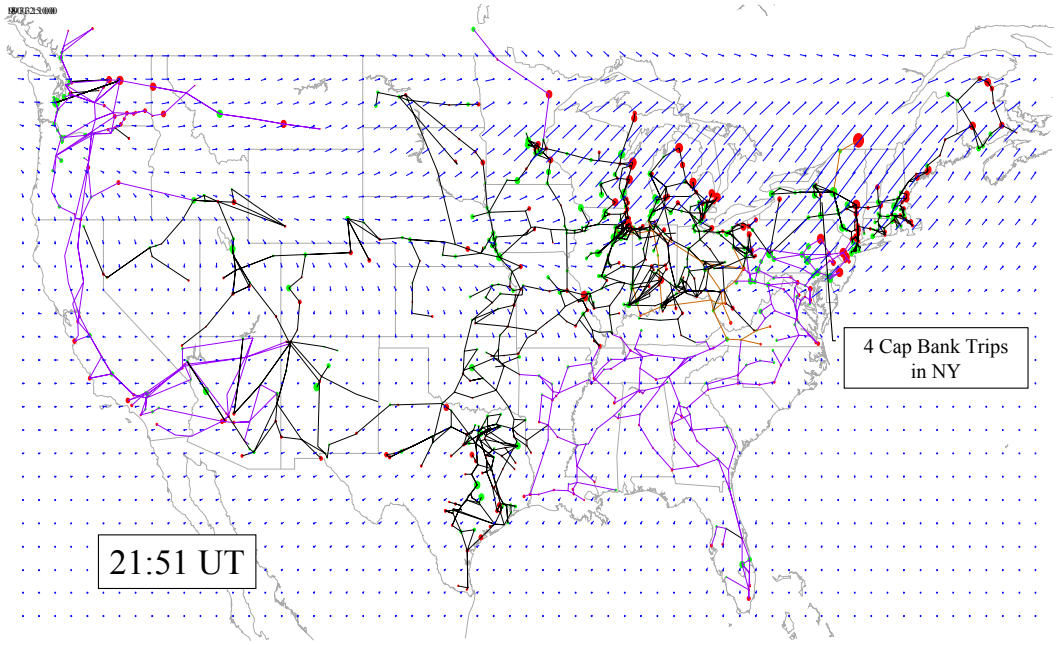

Figure 2-20. Simulation of U.S. power grid conditions at 21:51 UT on March 13, 1989.

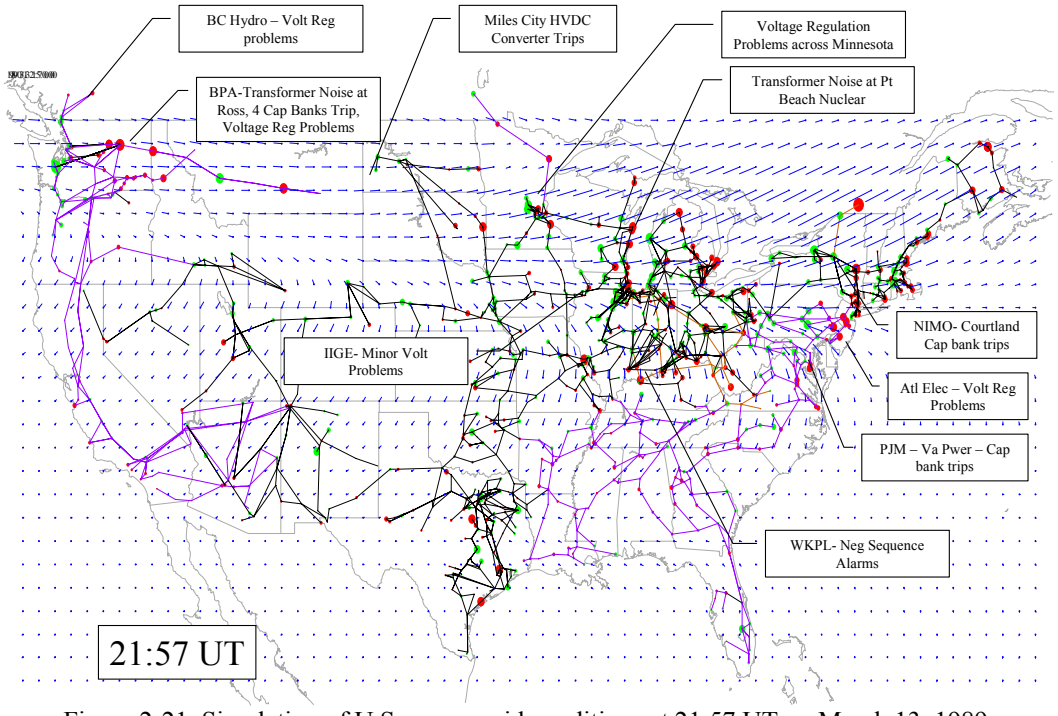

Figure 2-21. Simulation of U.S. power grid conditions at 21:57 UT on March 13, 1989.

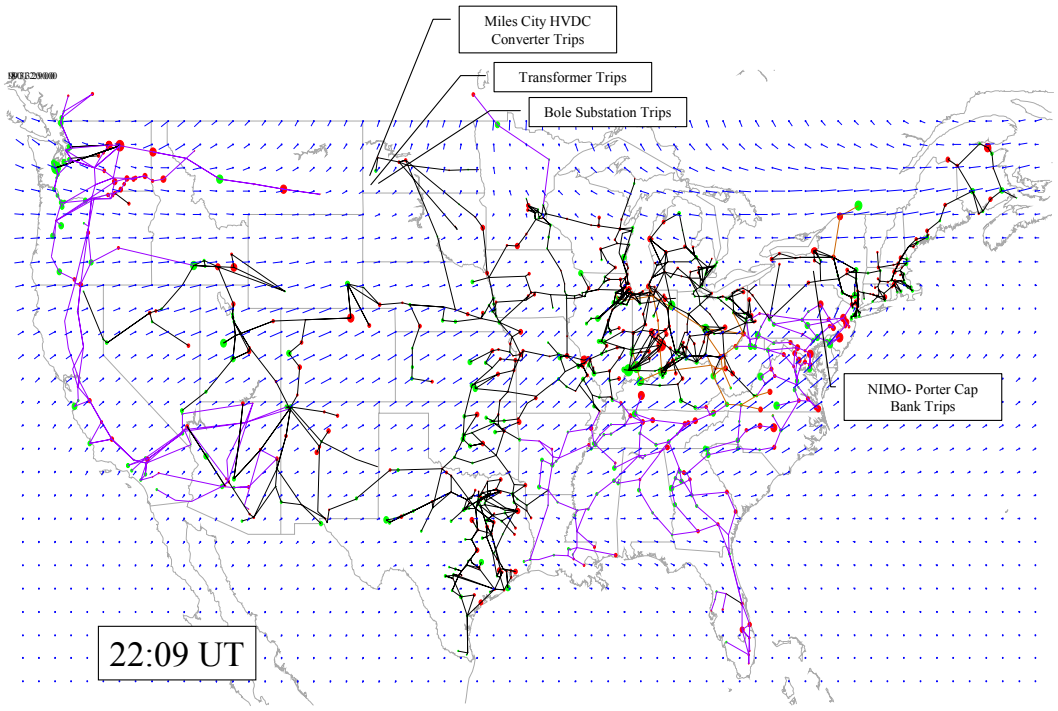

Figure 2-22. Simulation of U.S. power grid conditions at 22:09 UT on March 13, 1989.

2.2.4 Substorm Interval 0:30-2:00 UT March 14, 1989

The last interval of intense substorm activity occurred between 0:30-2:00 UT on March 14. As shown in Figure 2-23 for the time period from 20:00-20:32 EST, a large number of power system events were reported, with the impacts being particularly significant from the New England region through the upper Midwest. Figure 2-24 depicts one of the more intense disturbance periods during this interval. The large disturbance over the New England/Mid Atlantic to Midwest regions of the U.S. is due to a westward electrojet intensification. There are also less severe intensifications developing along the Florida panhandle and along the U.S./Mexico border region at this time as well. It is at this time that a dB/dt intensity of 461 nT/min was observed at Bay St. Louis, Mississippi, a level that was very close to the intensity that initiated the Quebec collapse. The EST time of this substorm also occurred during early evening peak load demand conditions on the U.S. grid. This may have acted to trigger additional power system problems.

Time (EST)	Area	Event
2000	NEPOOL	MVAR
2010	NEPOOL	MVAR
2010	NEPOOL	Voltage
2010	NEPOOL	Voltage
2010	NEPOOL	MVAR
2010	NEPOOL	Voltage
2010	LILCO	Voltage
2010	NEPOOL	MVAR
2010	INEPOOL	MVAR
2010	NEPOOL	Voltage
2010	NEPOOL	Voltage
2011	NIMO	Capacitor
2011	Va. Pwr.	Capacitor
2012	NEPOOL	Voltage
2012	NEPOOL	Voltage
2012	INEPOOL	Voltage
2012	INEPOOL	MVAR
2012	NEPOOL	Converter
2013	NEPOOL	MVAR
2014	PJM	Recorder
2014	NEPOOL	Voltage
2014	NYPP	Voltage
2015	NEPOOL	MW
2016	NEPOOL	MVAR
2015	INEPOOL	MVAR
2016	PJM	Alarm
2015	NEPOOL	MVAR
2015	NEPOOL	Voltage
2015	NEPOOL	Voltage
2016	NEPOOL	Voltage
2015	NEPOOL	MVAR
2016	OH	Generator
2016	OH	Capacitor
2017	NEPOOL	Converter
2017	NEPOOL	Voltage
2017	NEPOOL	Capacitor
2017	NEPOOL	Voltage
2017	NEPOOL	MVAR
2018	Va. Pwr.	Capacitor
2019	WEP	Alarm
2019	UPA	Alarms
2020	Atl. Elec.	MVAR
2020	APS	Transformer
2020	Atl. Elec.	Voltage
2020	OH	Generator
2020	UPA	Converter
2021	PJM	Capacitor
2022	UPA	Line
2022	PJM	Alarm
2024	CPA	Voltage
2024	CPA	Capacitor
2032	PJM	Capacitor

Figure 2-23. Reported North American power system impacts, March 13-14, 1989, for time span of 20:00-20:32 EST (1:00-1:32 UT).

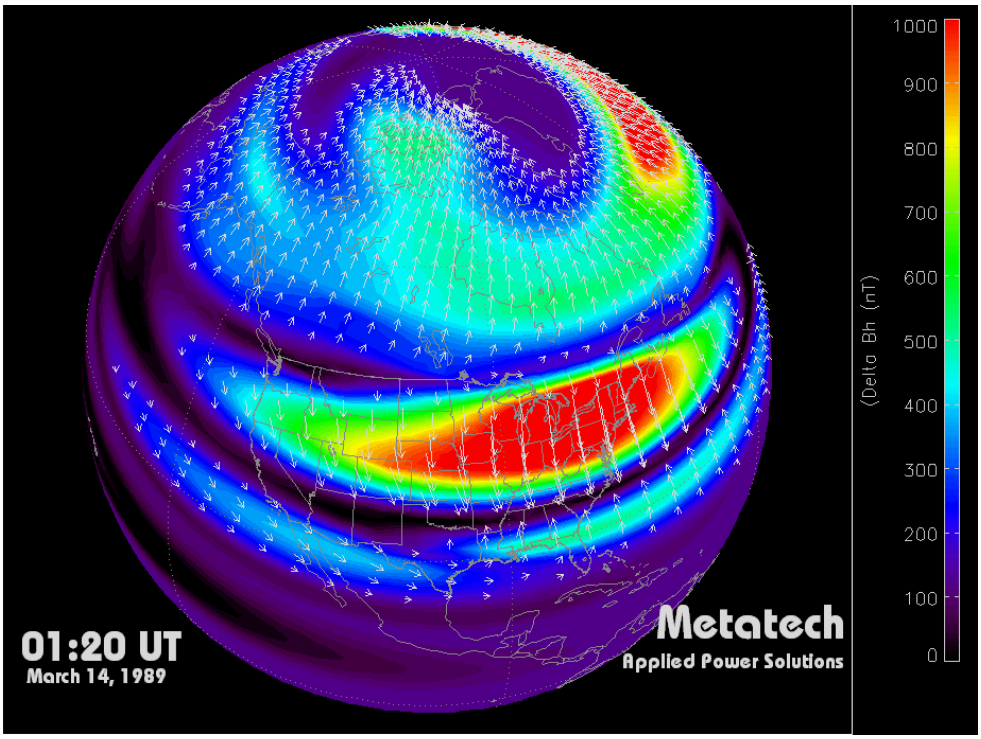

Figure 2-24. Simulated 01:20 UT, March 14, 1989, conditions.

2.2.5 Overview of U.S. power grid GIC flows and reactive power demands

While the previous summaries have provided important insights on the spatial and temporal features of disturbances across the U.S. power grid, from a power system operation and performance perspective, it is also useful to develop more aggregate measures of storm intensity and impacts as well. A sum of all GIC flows and all increased reactive demands provides one of the most meaningful metrics for assessment and comparison purposes. Figure 2-25 provides a comparison of the peak sum of GIC flows and associated sum of MVAR demands caused by the GIC for the U.S., along with the time-of-peak during each of the four major substorm intervals that were evaluated. It should be noted that MVAR levels could be higher due to reaction of the AC network as increased transformer reactive demands flow through the network. This would amplify the net impact even further. As was previously discussed, the substorm during interval 21:20-22:30 UT March 13, 1989 was the most severe, followed by the substorm during interval 0:30-2:00 UT March 14, 1989. Figure 2-26 provides a time plot of the variations in GIC and MVAR totals for the substorm during interval 21:20-22:30 UT, which further depicts the dynamic nature of the substorm.

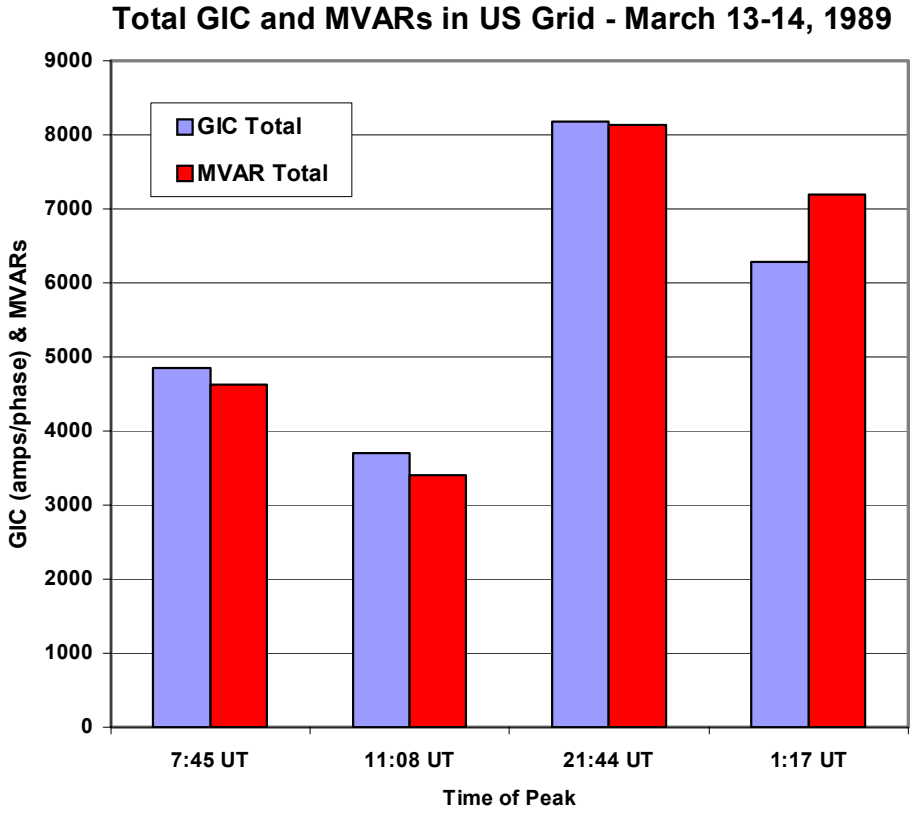

Figure 2-25. Peak sum GIC and MVAR demands for the U.S. power grid at four times during the March 13-14, 1989 geomagnetic storm.

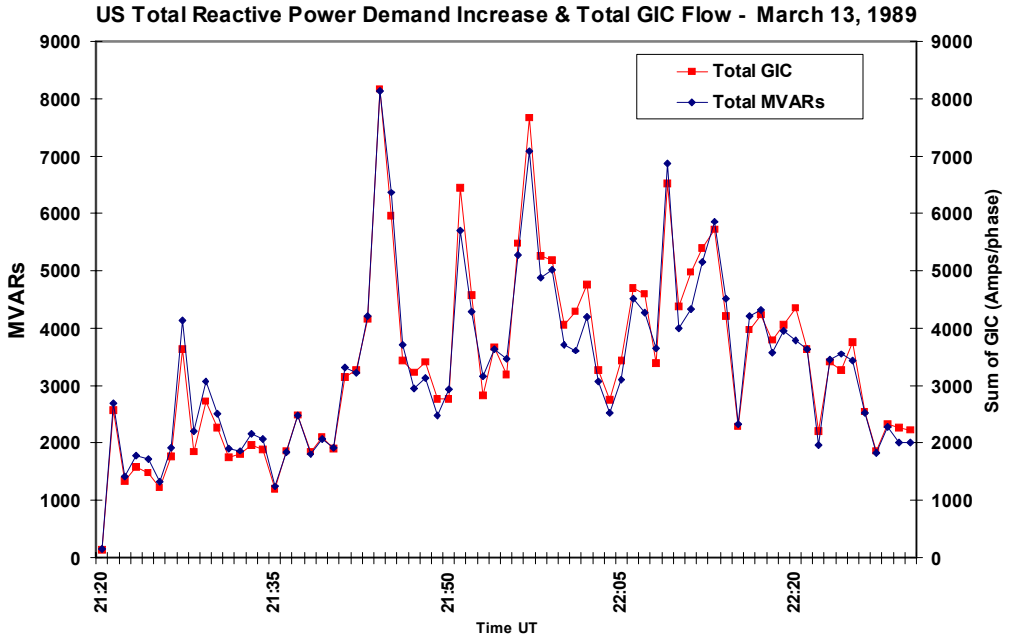

Figure 2-26. GIC and MVAR demand variations for the U.S. power grid during the March 13-14, 1989 geomagnetic storm from time 21:20 to 22:30 UT.

It is even more important to review the regional manifestations of the storm events. One of the more convenient ways of regionally classifying storm intensity and impacts is to summarize by power pool. Figure 2-27 provides a map of the major power pools in North America. Also noted on the map are two important subsets of the large NPCC pool, namely the NYISO and NEPOOL regions covering New York State and the New England regions respectively. Using these region boundaries, the intensity by geographic region can be reviewed to better quantify the impacts. Figure 2-28 provides a summary of the GIC and MVAR totals for the PJM pool. This region, like the U.S. totals, was most heavily impacted by the substorm during interval 21:20-22:30 UT. The peak GIC and MVAR demand for this region is ~940 amps and ~1550 MVARs; the time-of-peak was also 21:44 UT, as was the U.S. time-of-peak. The PJM region also experiences a secondary peak that is nearly as large, occurring at 22:13 UT. Immediately to the south of the PJM region is the SERC region, which also experienced a peak of GIC and MVAR demand during the 21:20-22:30 UT interval substorm. Figure 2-29 provides the time plot of total GIC and MVAR demand for the region. This region also experienced a time-of-peak at 21:44 UT, the total GIC reached ~1060 amps, and MVAR demand was ~1780 MVARs. To the immediate north of the PJM pool, the NYISO actually reached its peak GIC and MVAR demands during the latest substorm interval of 0:30-2:00 UT March 14, 1989. This region reached a peak GIC flow of ~890 amps and peak reactive demand of ~950 MVARs at 1:17 UT March 14. Progressing immediately west from the PJM pool is the ECAR pool, and the plot of GIC and MVAR demand is provided in Figure 2-31. This region also experienced a time-of-peak at 21:44 UT, as did the PJM and SERC regions. The total GIC was ~2420 amps and total reactive demand was ~2200 MVARs,

levels that are larger than either the PJM or SERC regions at this time-of-peak. Figure 2-32 provides the GIC flows and MVAR demands for the most westerly region in the model, the WECC. The WECC region experienced its largest impacts at 22:08 UT, rather than the 21:44 UT time of eastern U.S. pools. The aggregate totals for GIC flows and associated reactive demands for this region were ~1700 amps and ~2100 MVARs respectively. In general, these pools represent the bulk of the aggregate storm impacts that were observed, which is logical, given the enormous sizes and miles of transmission circuit exposure these regions presented to the storm conditions. Other mid to northern latitude pools such as NEPOOL, MAPP and MAIN did experience significant impacts, especially relative to their smaller sizes. Regions such as ERCOT and FRCC and the southern portions of SERC were not as consistently exposed as the more northerly located pools.

There is some Sub-Groupings between Reliability Regions and Power Pools

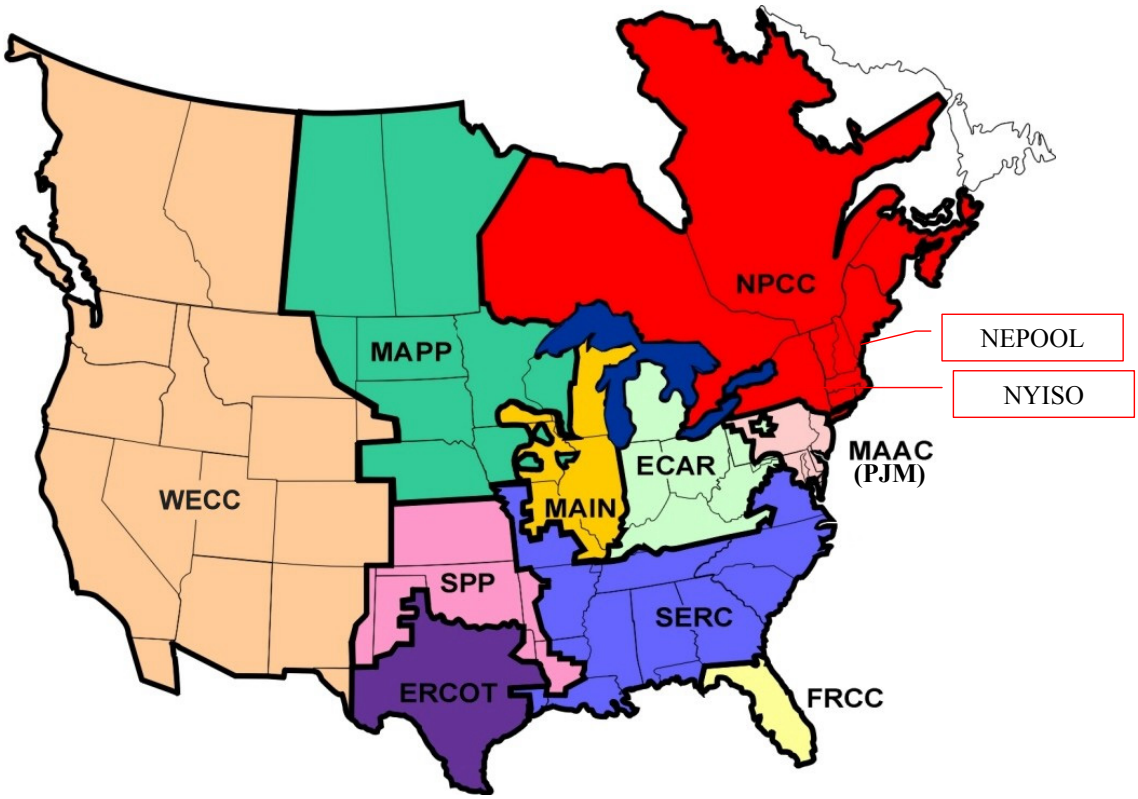

Figure 2-27. A road map of the U.S. power pools.

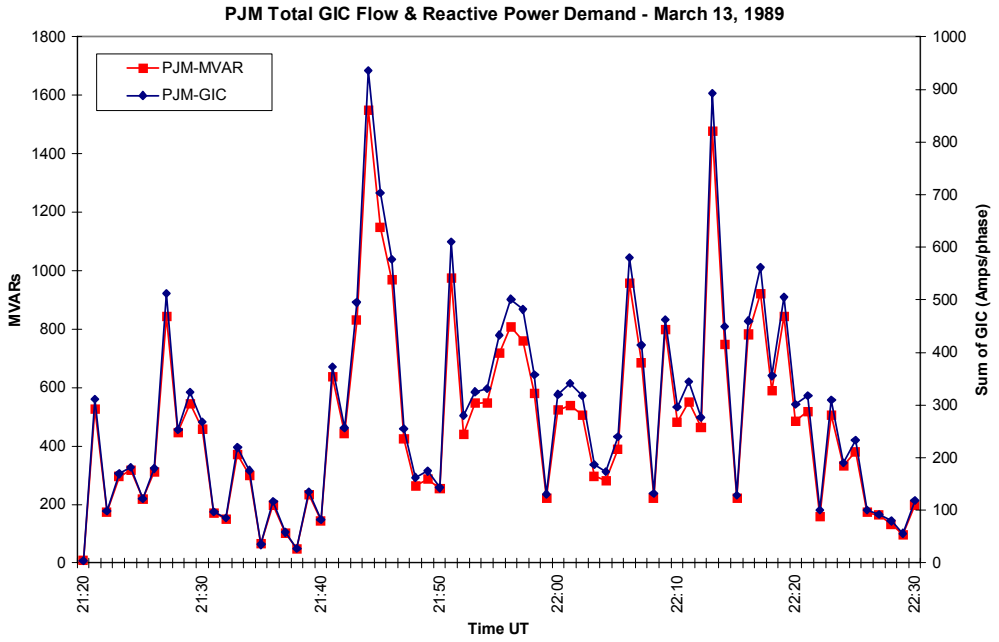

Figure 2-28. GIC and MVAR demand variations for the PJM pool during the March 13-14, 1989 geomagnetic storm.

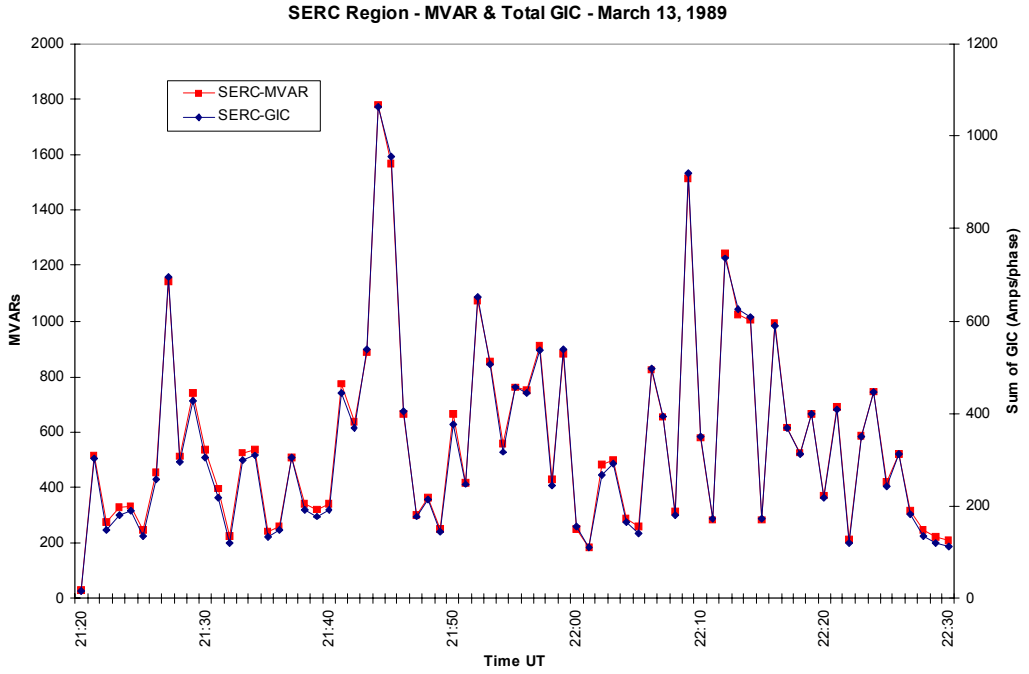

Figure 2-29. GIC and MVAR demand variations for the SERC pool during the March 13-14, 1989 geomagnetic storm.

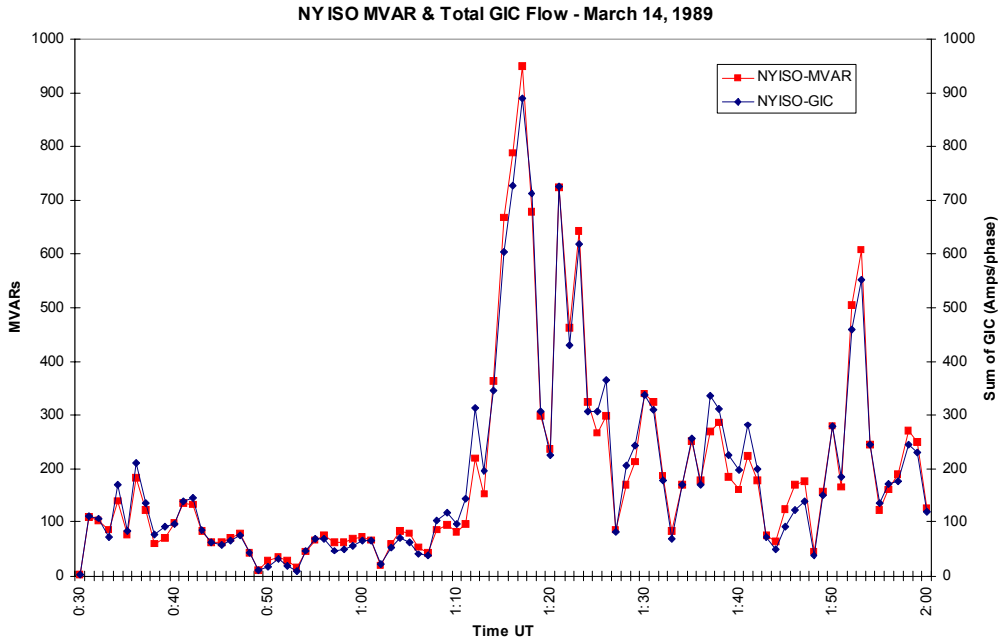

Figure 2-30. GIC and MVAR demand variations for the NYISO pool during the March 13-14, 1989 geomagnetic storm.

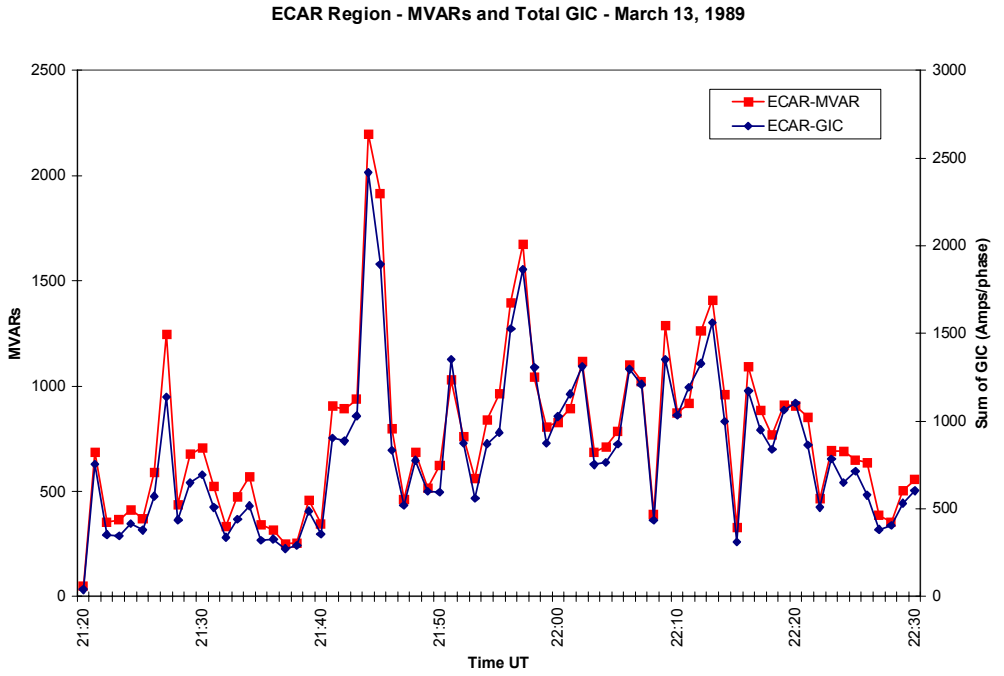

Figure 2-31. GIC and MVAR demand variations for the ECAR pool during the March 13-14, 1989 geomagnetic storm.

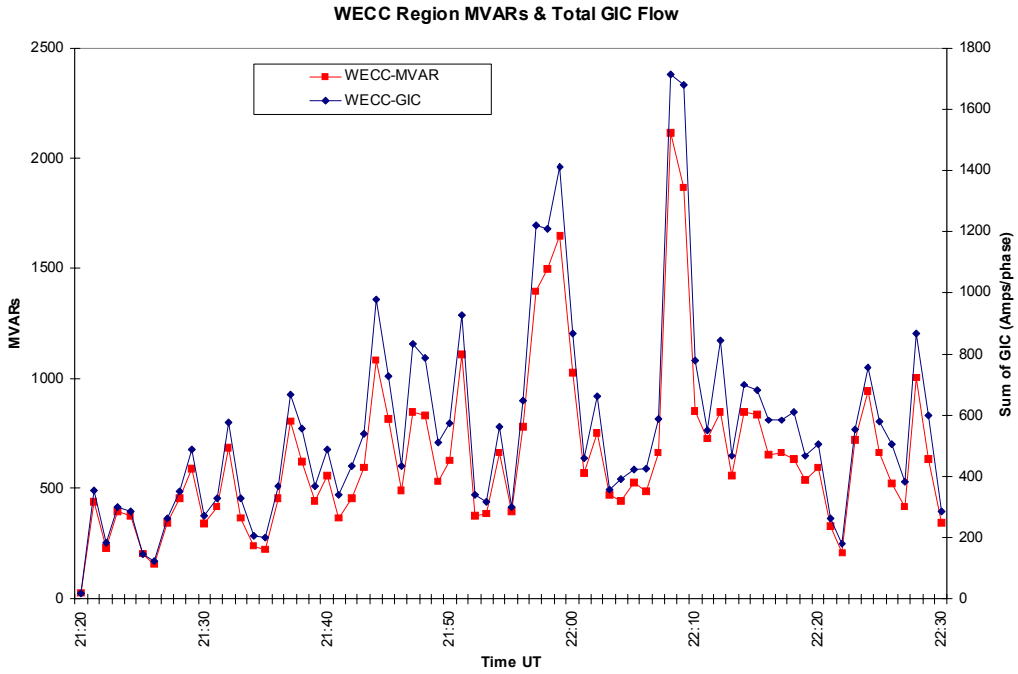

Figure 2-32. GIC and MVAR demand variations for the WECC pool during the March 13-14, 1989 geomagnetic storm.

2.3 Overview of Transformer Internal Heating – Examples from March 13-14, 1989 Storm and Other Incidents

The discussion to this point has been primarily regarding the threat to reliability of the system as a whole, due to the widespread and simultaneous nature of the stress across a large interconnected network caused by the March 1989 storm. Also of note from this particular storm is strong evidence that GIC-induced half-cycle saturation of transformers can indeed produce enough heat to severely damage or even destroy exposed large power transformers. The most noteworthy event of this storm was the complete loss of a large (~1000MVA) generator step-up (GSU) transformer connected to the 500kV transmission grid at the Salem Nuclear Plant in Lower Alloways Creek, N.J. Figure 2-33 provides a picture of one-phase of the transformer and several pictures of the extensive internal damage done to the 22kV low-voltage windings of the transformer. In spite of these core and windings being immersed in oil for insulation and cooling, the heating was so intense that it not only burned away all the paper tape winding insulation, but caused extensive melting of the windings, which are normally rated for ~3000 amps.

Figure 2-33. Damaged transformer at the Salem Nuclear Plant.

This damage was inflicted because of the high levels of stray magnetic flux and circulating currents that were occurring outside the transformer core due to half-cycle saturation. When these fluxes concentrate and impinge on regions of the transformer, such as windings and internal structural or tank members not expected to receive such exposure for normal operation, they can lead to almost immediate and severe hot-spot

heating insults to exposed internal windings and structures of the transformer. Thermal damage to paper tape winding insulation causes cellulose breakdown and is permanent. Also, damage may not be sufficient from one minor exposure to cause insulation failure, but can be accumulated over multiple insults to the point of failure. Because many transformers are of custom design in regard to winding configuration and tank/support structures, general guidelines on permissible levels of GIC exposure are not entirely useful. However, in general terms, the exposure risk for transformers is both a function of time and magnitude of the incident GIC. Figure 2-34 provides the estimated GIC flows in amps/phase in the Salem transformer for the four major substorm intervals that were simulated for the March 13-14, 1989 storm. As shown in this figure, the GIC per phase was estimated to reach a peak of ~90 amps/phase at 21:44 UT. Because this transformer is in a southern mid-latitude location, the highest sustained levels of GIC exposure to this transformer occurred during this substorm interval when the electrojet intensifications were situated over these regions.

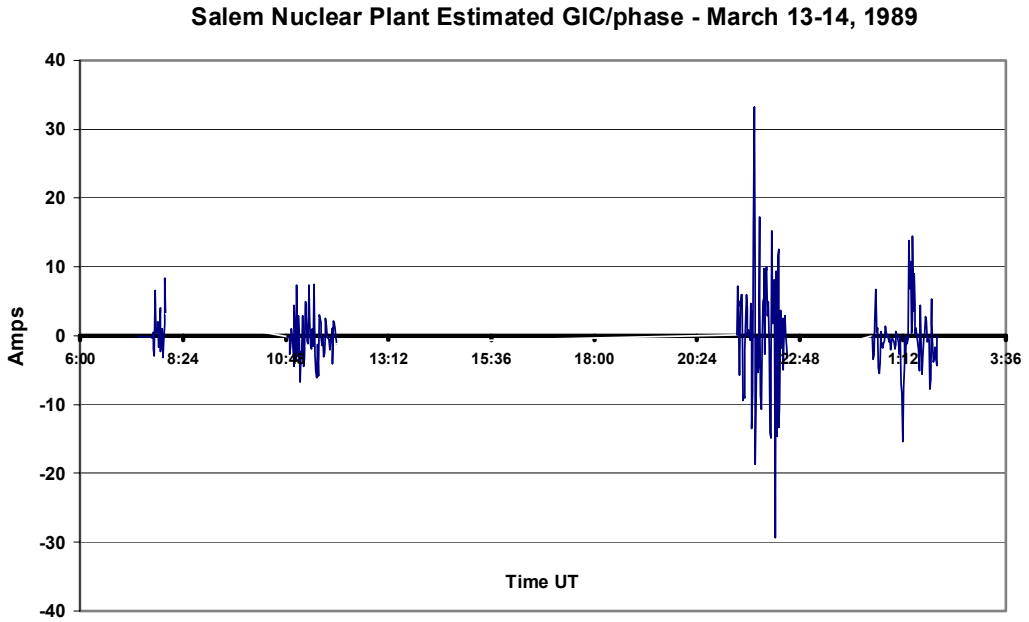

Figure 2-34. Estimated GIC at Salem Nuclear Plant.

The magnitude and duration of GIC events that transformers can withstand without damage are not well defined. Several controlled tests, looking at heating on select points internal to a transformer, have been conducted. However, the information from these staged-tests is limited because of the restricted accessibility for temperature measuring probe placement. It is difficult to even estimate where these critical hot-spots will develop, but even more so, it is difficult to monitor in the internal high voltage environments of a transformer, even if that hot-spot was fully known. In this regard, the March 89 storm provided another example of transformer stray-flux heating that helped to improve the understanding of the dynamics of transformer heating. This transformer was operated by Allegheny Power at the Meadowbrook substation in Virginia. This 500-

138kV, 350MVA transformer was removed from service on March 14, 1989 because of high gas levels in the transformer oil, which is a sign of unusual core and tank heating. External inspection of the transformer tank turned up four small areas of paint blistered by intense heat from stray flux. While no measurements were made for this storm, it is estimated that heat from the flux reached 400^{o}C in some spots. Since the transformer was not damaged sufficiently to permanently take out of service, the opportunity was available to monitor both neutral GIC and temperature variations at this known external hot-spot when the unit was returned to service.

During a storm on May 10, 1992 (a storm far less severe than March 13-14, 1989), observations were recorded of neutral GIC and tank wall temperature near the known hot-spot on the transformer. Figure 2-35 provides a summary of both the GIC and resulting transformer hot-spot measurements during this May 10, 1992 storm, and illustrates the relationship between GIC and transformer internal heating. As shown, the transformer neutral GIC increased to approximately 60 amps in a matter of about 10 minutes. Two transformer temperatures are shown. One is the top oil, which provides a measure of total bulk transformer temperature and did not experience any significant change over the brief monitoring window. The other is the temperature of the monitored hot-spot. This illustrates the rapid increase of hot-spot temperature on the transformer tank exterior, which increases to approximately 175^{o} C within a matter of minutes (interior hot-spot temperatures would be even higher) (Reference 2-5). Other staged tests provide insights to thermal response given step changes in various magnitude of GIC (Reference 2-6). Figure 2-36 shows the observed temperature changes due to the initial application of a 12.5 amp DC source, which was then followed by a 75 amp DC source. A number of different temperature locations and trends are shown in this plot, owing again to the limited flexibility of both knowing the location and then attempting to actually measure a hot spot from stray flux concentrations. Of these measurements, only the “top of tie plate” location provides an observation that could be used as a workable proxy to an actual hot-spot behavior. In particular, by analysis of the “top of tie plate” temperature, the impact of the higher DC excitation is primarily evident as both a higher internal temperature, but also an acceleration in temperature increase. These limited observations suggest that the magnitude of GIC is the more important exposure concern, as opposed to the duration of the GIC exposure. This also suggests that very large GIC exposures could further accelerate the onset of hot-spots.

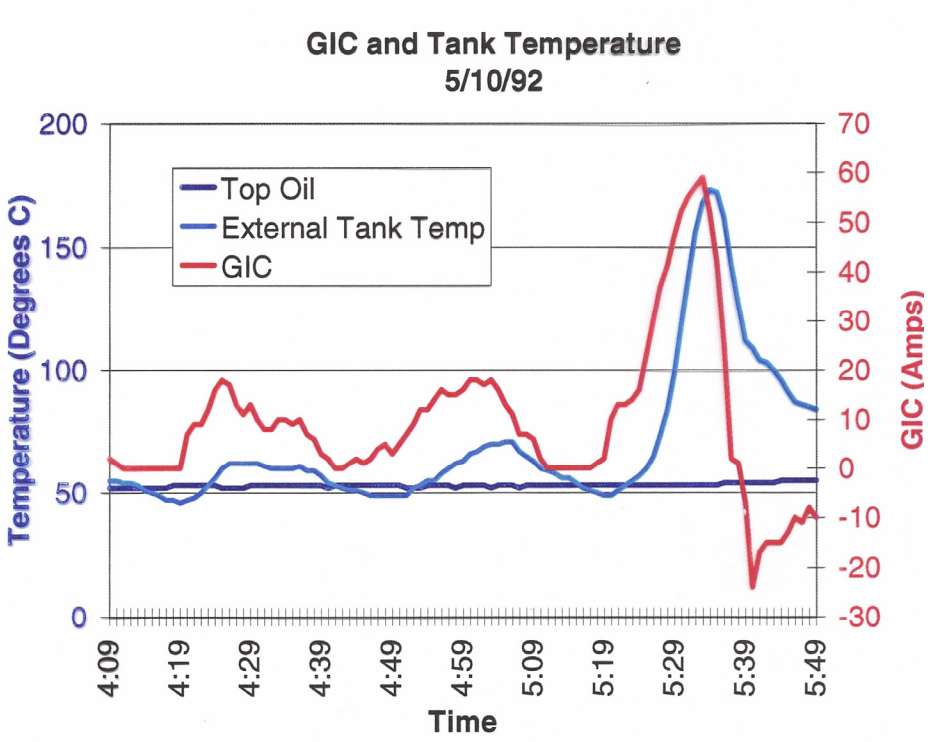

Figure 2-35. GIC and transformer tank temperature for May 10, 1992 geomagnetic storm.

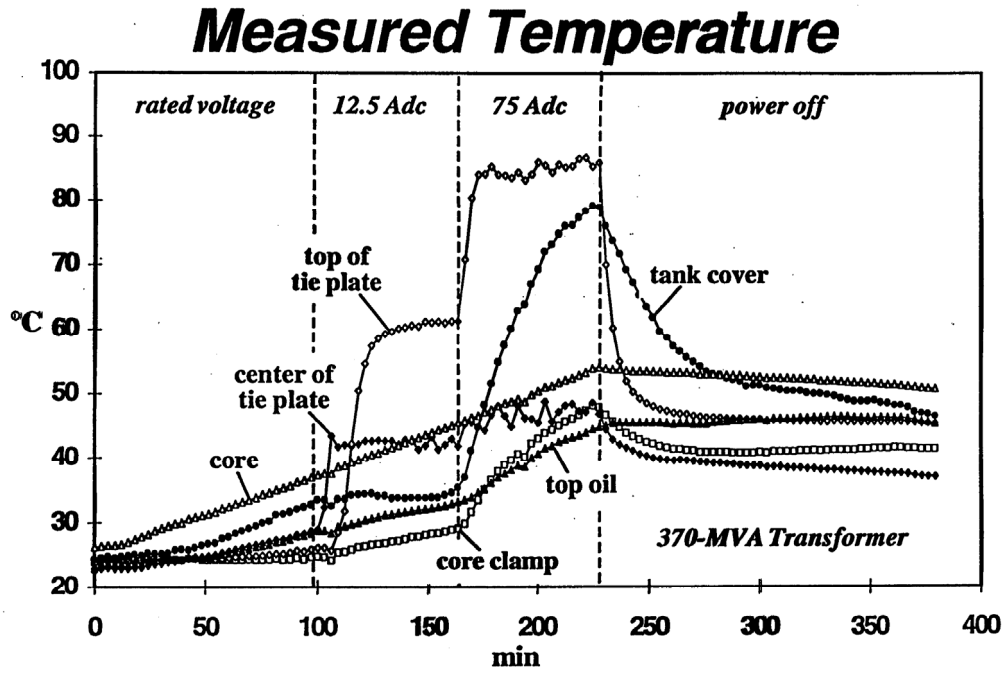

Figure 2-36. Various transformer temperatures, as DC current (12.5 amps, then 75 amps) is applied.

Other anecdotal evidence, post-March ’89, suggested that many other important transformers in the network sustained damage that eventually precipitated failures. Because the U.S. transformer population as a whole is very large and non-homogeneous, it is difficult to fully recognize trends, though studies have confirmed compelling associations between transformer failures over a 25-year period and geomagnetic storm activity (Reference 2-7). Rather, a rash of failures in the small and more homogeneous population of nuclear plant GSU transformers (~100 units) in the U.S. suggested a compelling linkage to the March ’89 storm and GIC exposure. Within 2 years after the March ’89 exposure, 11 nuclear plants noted failures of the large GSU transformers, in addition to the Salem failure (Reference 2-7). The previously mentioned failure incident at Salem was a case where damage was fortunately confined to the low voltage (22kV) windings of the transformer and not on the 500kV primary winding. In this case, the cooling oil in the transformer was able to provide sufficient insulation withstand to prevent a catastrophic failure of the transformer. In fact, the unit was not removed from service until the day after the storm.

This has not been the situation in other cases. On April 3, 1994 a moderate intensity storm occurred. During this storm a GSU transformer at Zion Nuclear plant (on the outskirts of Chicago) failed catastrophically. The failure was so severe that the transformer tank, containing thousands of gallons of oil, ruptured and started a major fire in the yard at the plant, which eventually involved control circuits and other sensitive systems. The fire also spread into the generator hydrogen cooled isobus inside the plant. In many postmortem analyses of transformer failures, it is very difficult to assess the failure cause, given unknowns about the unique design variations and unique operational exposure of each transformer. In particular, static electrification was a failure mode of transformers of this vintage, and would be unrelated to GIC exposure. Considering the unknowns and multiple plausible failure causes, very few definitive failure diagnoses can be expected. The operator of the plant facility has resisted the association of this failure with the geomagnetic storm event, however they had not been undertaking any effort to monitor for GIC in the transformer or at any other locations in their regional transmission network. Observations of GIC were made at utilities elsewhere north, south, east and west relative to their location. The space weather conditions that spawned the April 3, 1994 storm were associated with long-duration and recurrent solar activity sources. Therefore, storm conditions occurred from early April to mid-April. Over that same period of time, the local utility also experienced major GSU transformer failures at the Braidwood nuclear plant (April 5, 1994) and at the Powerton coal plant (April 15, 1994). Again, the operator has resisted the association of these failures with GIC, even though the timing of these events would appear to be extraordinarily coincidental.

Transformers of this size class (600MVA+) are large and expensive devices to replace. Operators of facilities such as these generally do not have spares readily available. In the best of cases, a large operator of a number of plants may have one or two un-energized spare transformers that could be re-located to one of many plants that they operate over a region. If no transformer is readily available, the delivery time on a newly manufactured unit typically runs to ~12 months or longer. Even with a readily available spare, the process of removing the old transformer, disassembling, shipping, assembling, and

installing the spare transformer (which includes filling with oil and pre-heating the oil in adverse temperature situations) is a process with a timeline of a few weeks or longer. If this failure is for a GSU transformer, in the intervening time, the important and usually baseloaded capacity source of the affected power plant is lost to the system. The GSU transformer is the only electrical path for plant output to the grid. Failure of other transformers embedded in the transmission network are somewhat less problematic, in that there is consciously more redundancy designed into the pool, because of multiple flow paths. However, multiple key failures in a network can also curtail or severely limit operating options in reconstituting a network. An especially large storm or GIC event could plausibly create the potential for widespread failure of many exposed transformers and hamper rapid restoration capabilities. In extreme cases, where replacements may take months, a situation may exist where the demand for electric service can only be partially supplied, raising the prospect of rationing and rotating blackouts to regions that are unable to be fully served.

Generators are another important apparatus that is potentially at-risk for permanent and debilitating damage due to unusually large GIC exposures. Prior investigative analysis has determined that there are two important aspects of vulnerability for generators that could lead to permanent damage (Reference 2-8). The high levels of harmonic currents flowing in the generator transformer due to half-cycle saturation are the immediate cause of both exposure concerns. The first concern is one of generator rotor electrical heating due to the coupling of various harmonic currents that act as negative sequence flows in the electrical windings of generators. There is considerable concern that standard relays designed to protect for rotor heating would not act properly in sensing this added current flow. The second and potentially more important concern arises from the interaction of the harmonic currents and the natural resonant frequencies of turbines on large MVA high-pressure turbine generators. Events that excite vibrations in the turbines at their natural frequencies can readily lead to mechanical damage to these high-speed, high-pressure blades. Permanent and widespread damage to large MVA generators in the U.S. would likely cause especially long-term debilitating damage to the power grid.

Additional References

2-5 Philip Gattens, Allegheny Power Corp., “Application of a Transformer Performance Analysis System”, Presentation at the Southeastern Electric Exchange, May 28, 1992.

2-6 P. Picher, et.al., Discussion to Paper “Study of the Acceptable DC Current Limit in Core-Form Power Transformers”, IEEE Winter Power Meeting, Baltimore MD.

2-7 J. G. Kappenman, “Geomagnetic storms and Their Impact on Power Systems: Lessons Learned from Solar Cycle 22 and the Outlook for Solar Cycle 23”, IEEE Power Engineering Review, May 1996, pg 5-8.

2-8 R.A. Walling, A.H. Kahn, “Solar-Magnetic Disturbance Impact on Power System Performance and Security”, EPRI Proceedings: Geomagnetically Induced Currents Conference, EPRI TR-100450, June 1992, pg 4-1.

Section 3
An Assessment of the Threat Potential to the U.S. Electric Power Grids from Extreme Geomagnetic Storms

This section provides an assessment of future geomagnetic storm threats to the U.S. power grids. Figure 3-1 illustrates an example of a massive coronal mass ejection that is the initiating event for extreme geomagnetic storms.

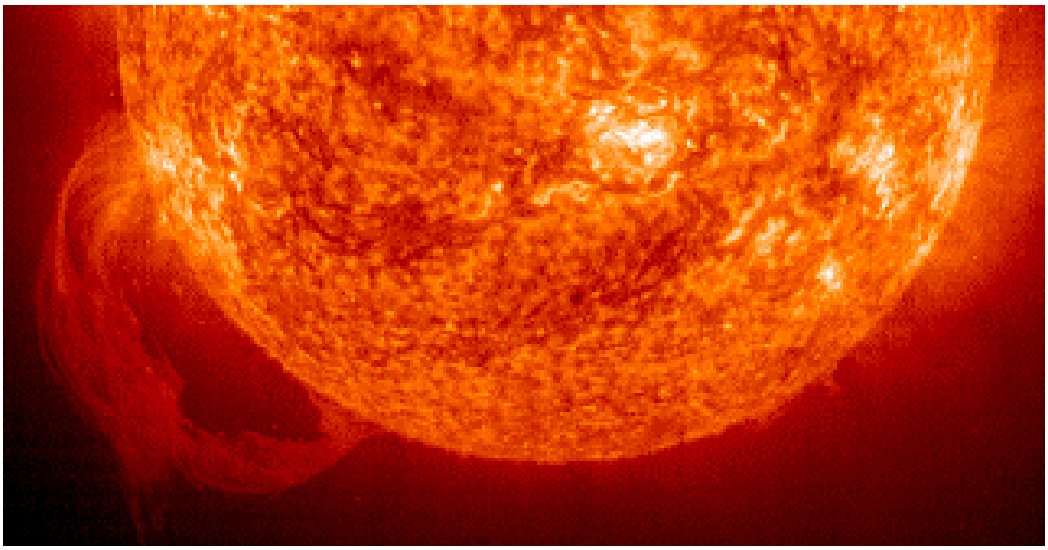

Figure 3-1. SOHO image, June 9, 2002.

3.1 Overview of Geomagnetic Disturbance Environments for Extreme Storm Scenarios

The footprints of a great geomagnetic storm can be extensive, and as power grids grow in vulnerability to disturbances from the space environment, the probability also increases for global consequences to these worldwide infrastructures. The previous section reviewed the impacts across North America during the March 13, 1989 storm. For perspective, the level of storm severity that best describes the disturbances that trigger large geo-electric fields and resultant GIC flows is the rate-of-change (dB/dt) of the geomagnetic field. At northern to mid latitude locations, the most severe impulsive geomagnetic disturbances are generally caused by rapid intensifications and movements of the over 1 million amp auroral electrojet currents at altitudes of ~100km. These intensifications are usually regional in nature but can have, at times, continental footprints of high intensity. At more equatorial and low-latitude locations, the ring current becomes the dominant influence on ground level geomagnetic disturbance patterns. Both current systems are closely coupled and will simultaneously enhance as the intensity of the storm increases. Other geomagnetic field disturbance processes have also been recently observed to cause high levels of GIC in power grids at all latitudes.

Long-term detailed climatology data on geomagnetic field disturbances are not available; the one-minute or faster cadence data from observatories needed for this type of analysis

only extends back to the early 1980's. Prior to that time, only index summaries of storm activity are available and cannot be reverse engineered to extract the more detailed and site-specific data necessary. Therefore, the extremes of dB/dt impulses and the resulting equatorward boundaries of such impulses are not well documented. Indices to classify the planetary severity of geomagnetic storms reach back somewhat further in time. Using the oldest measure of planetary average or index for storm classification, the Ap index, it is possible to look back at only ~80 years of magnetic storm history. Figure 3-2 provides a plot of all major geomagnetic storms (Ap>50) and the sunspot cycle from September 1933 through 2008. The March 13-14, 1989 storm as previously discussed has an Ap intensity of 285. Using the Ap Index as a guide to storm intensity only provides information back to 1932. However, considerable contemporary forensic evaluation has been undertaken to assess older storms dating back to famous storms from August/September 1859 and from May 1921. In fact, the 1859 storm heralded the advent of space weather and the impacts on human technology systems. Due to this storm, telegraph operations, a rather recent electrotechnology invention, were disrupted. It was reported that *Telegraph systems operating in the northeastern U.S. could at times be operated without the aid of batteries* (Reference 3-2). Using the Dst (an alternate storm index) as an estimate of the storm intensity, the 1859 storm is estimated to have reached a level of –1760, a level that is ~3 times larger than the March 13-14, 1989 Great Geomagnetic Storm (Reference 3-3). The important limitation of this measure is that equatorially located observatories are used as the input to this classification. Therefore, the Dst provides a more direct metric of the ring current intensification, leaving undefined the dynamics of electrojet intensifications at latitudes of concern for the U.S. power grid. However, it is not an unreasonable premise to expect that, in the closely coupled environments between the ring current and electrojet current systems, dB/dt intensities from electrojet intensifications at mid-latitude locations would also experience periods of dramatic enhancement as well, enhancements that could exceed those that had been observed in the storm of March 13-14, 1989.

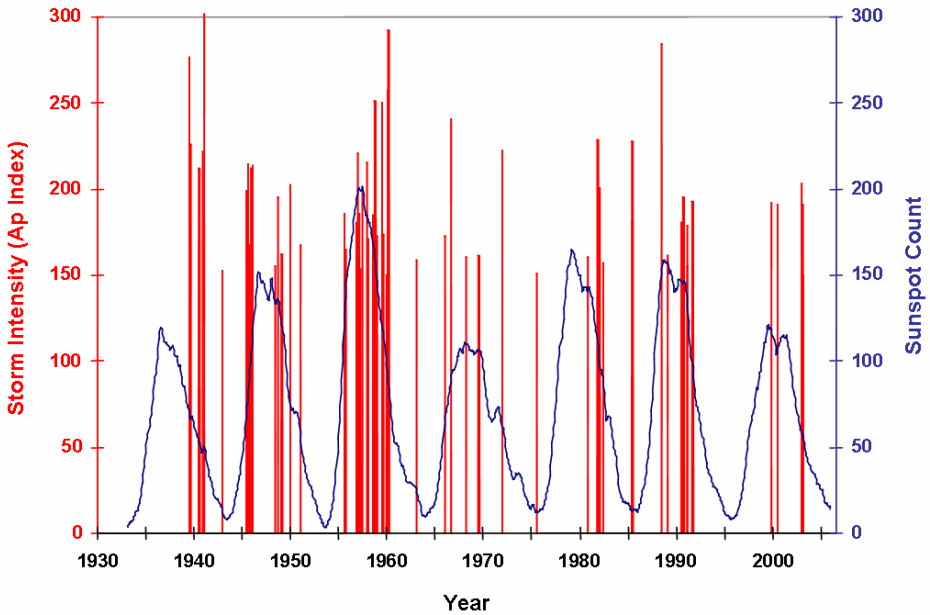

Figure 3-2. All major geomagnetic storms from September 1933 to 2006.

In assessing threat potentials for geomagnetic storms, it is useful to review peak dB/dt intensities from prior storms, and the equatorward expansion of these disturbances to characterize threat potentials. Large rate-of-change impulses in the geomagnetic field from the March 13-14, 1989 storm and other large contemporary storms can provide guidance for characterizing larger storm events that have not been well monitored. The Hydro Quebec collapse was triggered by a ~480 nT/min disturbance, which drove geo-electric fields of ~1.5 V/km in the region. The largest dB/dt observed in North America was ~900 nT/min, which occurred in southern Manitoba (an equivalent geomagnetic latitude to southern Quebec) and caused very large reactive power swings in that region as well. However, it should be noted that a large dB/dt (or associated electrojet intensification) in one location is due to coincidental aspects of the timing of substorm events, therefore these events can have equal probability of producing the same intensity disturbances at other locations around the world at equivalent geomagnetic latitudes (References 3-4a and 3-4b). By considering other world locations, a more complete perspective can be developed on the maximum bounds of the threat possible for the U.S. grid.

Again considering the March 89 superstorm, the largest dB/dt observed, a value of 2000nT/min (more than twice as large as any observed in North America), occurred at ~21:44 UT at a Danish magnetic observatory (Brorfelde or abbreviated BFE). Figure 3-3 provides an iso-telluric map showing the location of the BFE observatory and equivalent geomagnetic latitude locations across North America. As depicted, the disturbance, as observed at BFE, is at a geomagnetic latitude that extends well down into mid-latitude portions of the U.S. This alignment suggests that had this particular substorm occurred 5-7 hours later than 21:44-22:00 UT, then the location of this intense disturbance would have happened somewhere over mid-latitude portions of the U.S. The detailed data assimilation models provide an even better perspective on the intensity and geographic extent of this particular electrojet intensification. Figure 3-4 provides a synoptic of the ground-level geomagnetic field disturbance regions at 22:00 UT. The BFE disturbance, as shown, is embedded in an enormous westward electrojet complex during this period of time. The footprint of the westward electrojet disturbance region is so large that the depiction needs to be covered in two frames, the first frame showing a point of view over the Atlantic Ocean, the second frame from a perspective over North America. Also shown over North America, is the Harang Transition to the eastward electrojet, which simultaneously occupies a region across the mid-latitude portions of the U.S. However, the eastward electrojet is considerably weaker in intensity than the westward electrojet, yet this weaker structure was the source of the most serious U.S. power system threats from the storm. Focusing again on the more energetic westward electrojet, the disturbance region extends from Eastern Europe to central North America, a footprint greater than 120^{o} in longitude. The width of the most energetic portions of the disturbance region generally ranges between 5^{o} to 10^{o} in latitude. The size of this structure, had it developed 5 to 7 hours later, would have extended from east coast to west coast of the entire northern-latitude portions of the U.S. power grid, and is likely to have produced much more significant consequential impacts than those caused by the weaker eastward electrojet that occurred over the U.S. during this substorm.

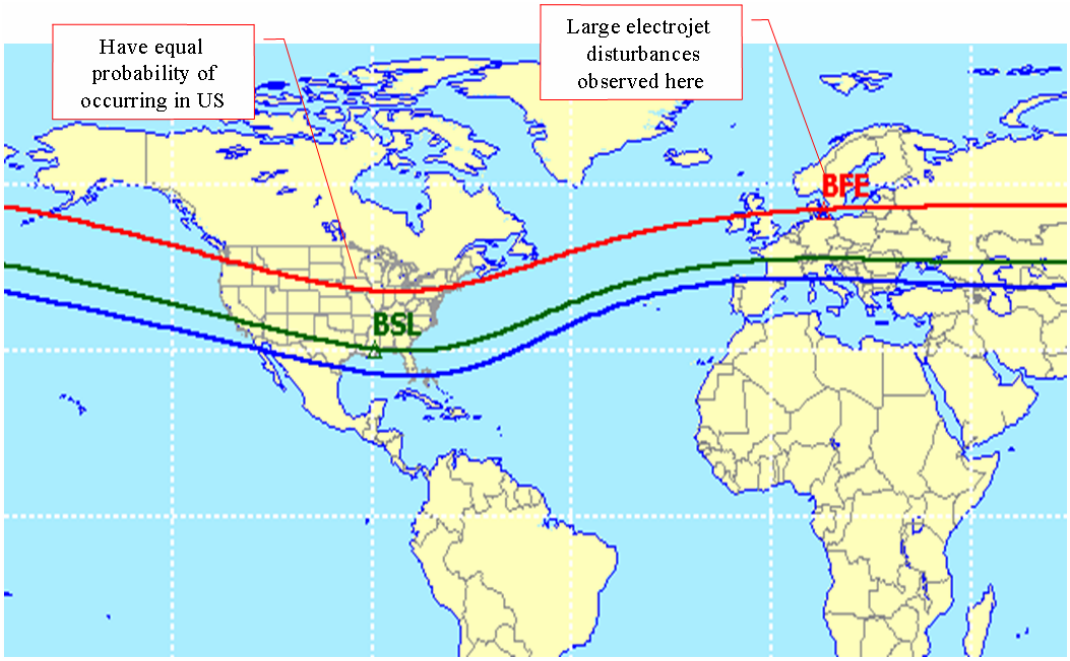

Figure 3-3. World climatology and developing great storm scenarios.

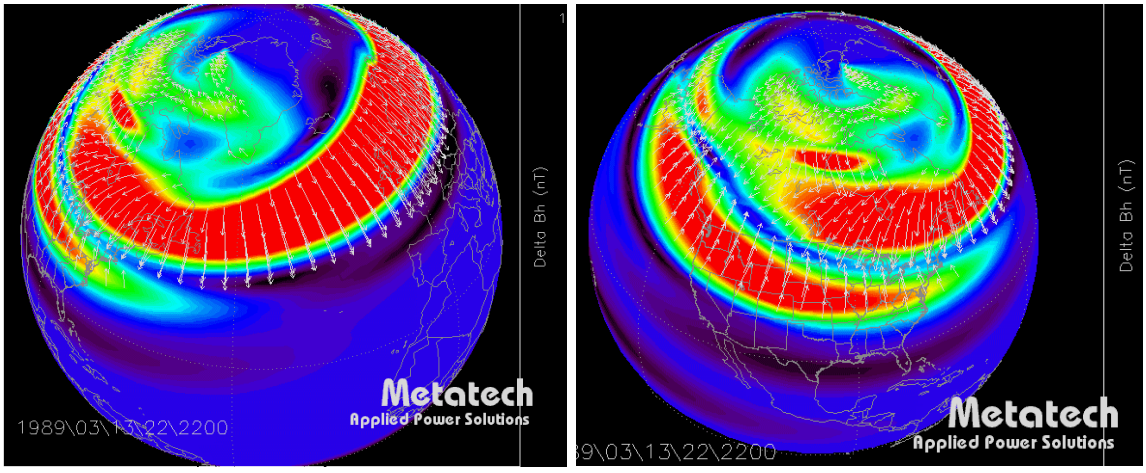

Westward electrojet extends from eastern Europe to central North America

Figure 3-4. Large westward electrojet intensification at 22:00 UT March 13, 1989
(left frame – view over Atlantic Ocean , right frame – view over North America).

In addition to magnetic observatory data, observations of geo-electric fields (or surrogate observations such as GICs, geo-potentials, etc. on technology systems) can provide valid scientific measurements that can extend the time horizons of forensic analysis of large and significant geomagnetic storm events beyond the limitations of current index classifications. For example, on August 4, 1972 a large dB/dt event was observed over North America, with the major impulsive disturbance occurring ~22:42 UT. This

disturbance was estimated to be at an intensity of ~2200 nT/min over extensive portions of North America (References 3-5 and 3-6). Electric power systems were impacted across the U.S. and Canada. Some of the more noteworthy observations were a neutral GIC that went off-scale at greater than 100 amperes peak in a 345/22kV transformer at J.M. Stuart Station near Dayton, Ohio, a level of unprecedented size in this region over the last 30 years. GICs of 100 amps were observed at Whitpain #1 transformer and 120 amps were seen at Whitpain #2 transformer near Philadelphia. Also near Philadelphia, a GIC of 63 amps was seen at Peach Bottom Nuclear Plant. GICs of over 100 amps (off-scale) were observed at several Manitoba locations. Large real and reactive power and voltage fluctuations were observed from Alabama, New Jersey, and Newfoundland and across to the BPA and Los Angeles regions on the western end of the continent; and nearly everywhere else in between. In the Grand Forks North Dakota area, the voltage collapsed to 64%. This area and surrounding regions of several states and provinces appeared to be near the epicenter of the disturbance (Reference 3-7). These large scale GIC observations and impacts also happened to occur at an embryonic stage in the development of the U.S. power grid, as less than half of the present transmission system (voltages 230kV and above) existed at the time of this storm (Reference 3-10). Higher GICs and associated system impacts would now be expected due to exposure to the same disturbance today, given the effectively larger GIC antenna of the present U.S. grid.

A large AT&T mid-continent telephony cable (L4) failed due to this storm near Plano, Illinois. Subsequent analysis indicated that the east-west geo-electric fields approached a level of at least 7 volts/km (Reference 3-5). This work also confirmed the large continental footprint of the disturbance around 22:42 UT, which agrees very closely with the comparable power system impact regions previously discussed.

Older storms provide even further guidance on the possible extremes of the environment. For example, the first reported power system problems associated with a geomagnetic storm occurred during a storm on March 24, 1940 (Reference 3-8). This was an era in which 115kV was typically the highest operating transmission voltage. Also, most power systems operated as islands instead of the tightly interconnection and geographically widespread pools common in the U.S. grid today. An analysis done at that time indicated geo-electric fields of ~5 volts/km as far south as Georgia (Reference 3-9). Correlations of geo-electric field measurements to simultaneous and high-resolution magnetic field observations provide opportunities for further contextual estimates of historically large events. A set of important observations was actually conducted by the operators of a rail system communication circuit in Sweden that extends back further than 80 years. Careful observations of telluric activity had been part of the normal operational practice of this facility. Figure 3-5 provides the route of a communication circuit between Stockholm and Torreboda, and a chart of the measured geo-potential observed on that circuit during a large storm on July 13-14, 1982. The communication circuit length is ~100km and the operators noted that the peak geo-potential observed during this event was 9.1 volts/km (Reference 3-11). The topology of the circuit is predominantly east-west, therefore the Bx (or north-south) component of magnetic field provided the driving force for this geo-electric field. This is also in the same region as the observation of the peak 2000 nT/min dB/dt during the March 13, 1989 superstorm. Coincident with the observed geo-potential

measurement on July 13-14 are two magnetometers just to the north and to the south of this circuit, the observatories Lovo (LOV) and Brorfelde (BFE). The approximate locations of BFE and Lovo are shown also in Figure 3-5. These observatories lie just north and to the south of the circuit and are separated north/south by ~5^{o} latitude. Figure 3-6 shows the delta Bx observed at BFE and Lovo during the hour of the peak disturbance on July 13, and for comparison purposes, the delta Bx observed at BFE on March 13, 1989 is also shown. This comparison illustrates that the comparative level of delta Bx is twice as large for the July 13, 1982 event as that observed on March 13, 1989. The Lovo observatory is the closest observatory to the circuit, being just north of Stockholm. The intensity of the dB/dt observed for this event at Lovo was ~2700 nT/min. This paired observation defines both a very large impulsive environment as well as the geo-electric field response, and also confirms that both impulsive disturbances are embedded in a large westward electrojet intensification. The large delta Bx peak of ~5000 nT, and rapid variations just before and after the peak on July 13-14, suggests that these large field deviations are very unstable and that even larger dB/dt's are possible, should a faster onset or collapse of the Bx field occur over the region. As was done for the large westward electrojet of March 13, 1989, it is also possible to define the footprint of this disturbance of July 13, 1982. The simultaneous observations of a similar magnitude delta Bx at BFE and Lovo reveals that the high intensity Bx disturbance was occurring north to south over the entire 5^{o} latitude separation between BFE and Lovo. Only a limited number of other world observatories are available for this storm, however, the simultaneous observatories in North America confirm that the westward electrojet extended over to the Manitoba, Canada. This defines the east to west dimensions of the westward electrojet extending at least 115^{o} in longitude, making this structure similar to the previously discussed westward electrojet of March 13, 1989.

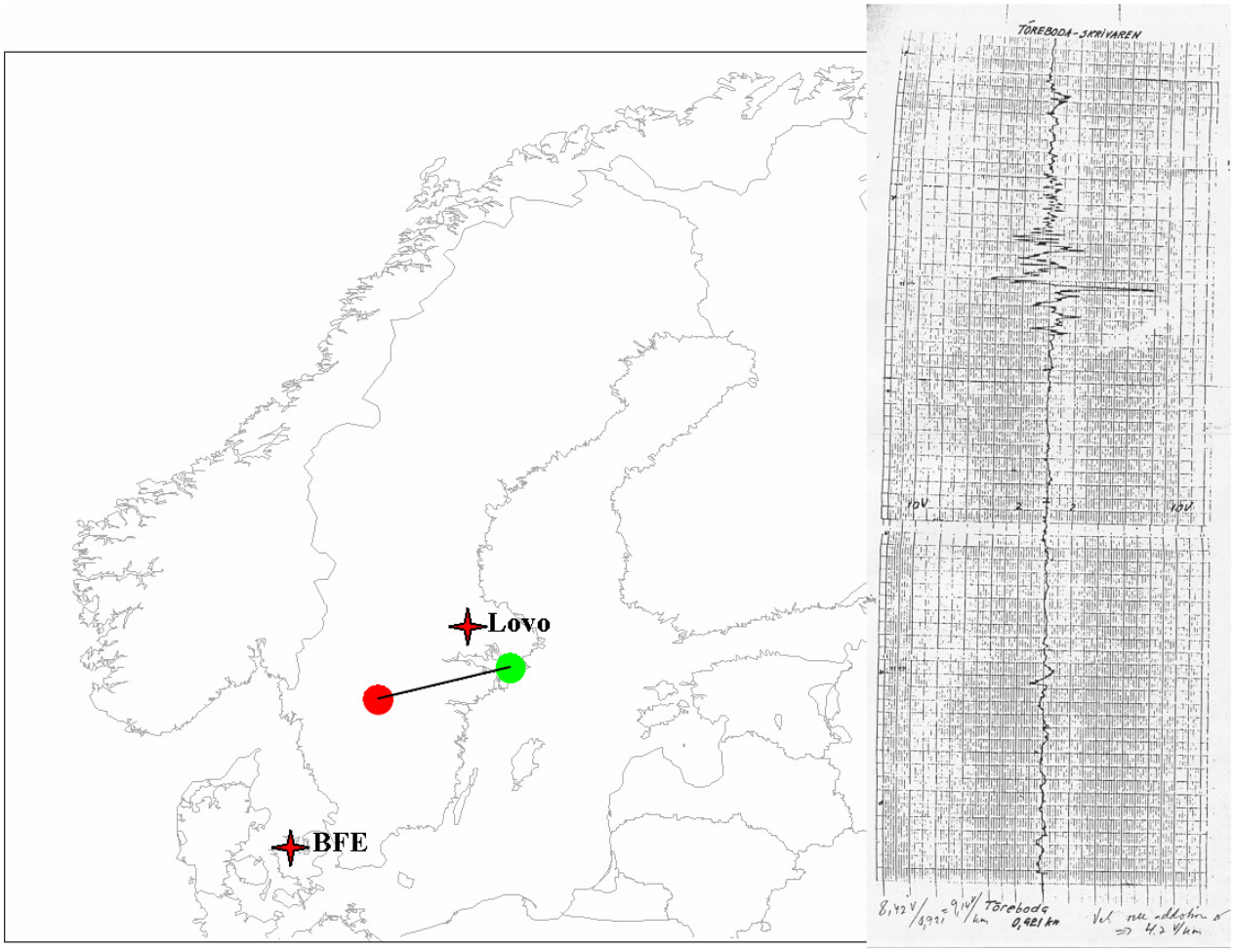

Figure 3-5. Observations of large geo-potential on the Stockholm-Toreboda rail communication circuit during July 13-14, 1982 storm event.

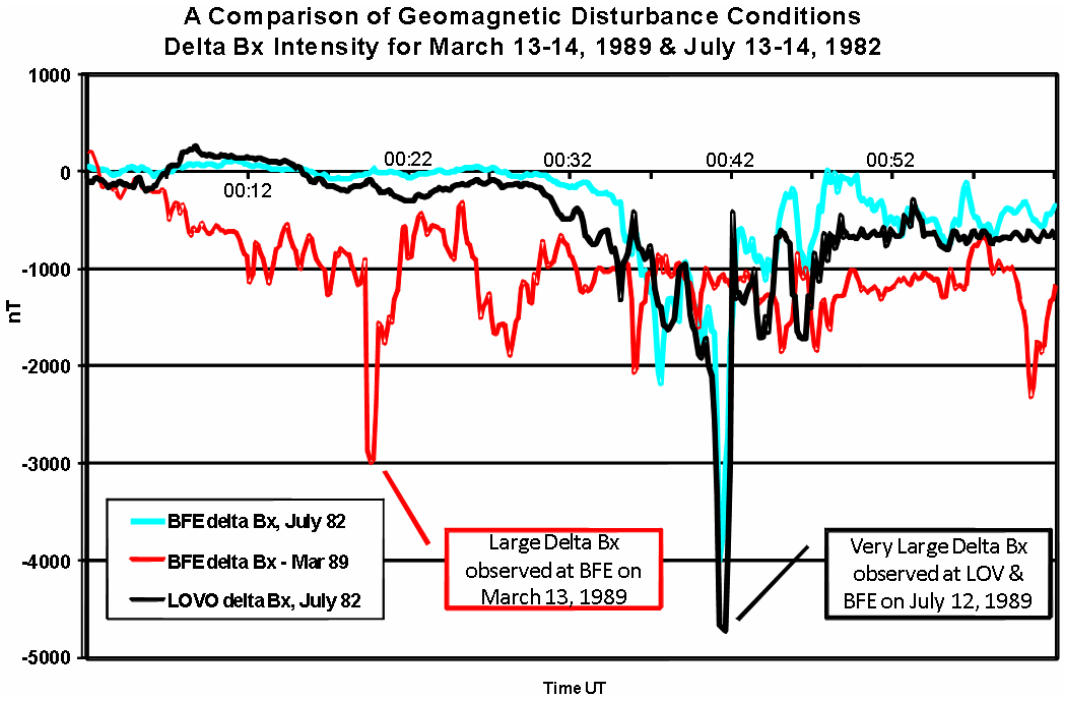

Figure 3-6. Delta Bx at BFE and LOV for the July 13-14, 1982 and March 13-14, 1989 storms.

Using this same communications circuit in Sweden, a storm that occurred in May 13-15, 1921 measured a geo-potential on the circuit of ~20 volt/km (References 3-4b, 3-12, and 3-13). This record provides the largest known geo-electric potential. Anecdotal reports of the storm indicate (from Karsberg, et al., 1959) that induced currents caused fires in telegraph equipment in Sweden. On the other side of the Atlantic, the New York Times reported in a May 15, 1921 article on a 14 May 1921 storm: "The voltage on some of the wires leading out of the city [New York] would be 150 degrees positive in one instant and in the next would have gone down to zero and on to 150 degrees negative. This fluctuation caused the wire to go up and down, in and out of service". There were also other reports about area impacts from Pittsburgh and Cleveland (Reference 3-14).

While these are colorful reports, they largely serve an anecdotal basis. However, Metatech has assembled other corroborating scientific information about this storm that adds support to the important 20 volt/km geo-potential observation. Because this observation is consistent with prior observations in the region, the data can be used to assess the source disturbance (Reference 3-4b). Therefore, this observation does make it possible to apply tendencies from prior disturbance events to further infer the parameters and context of this extreme event. No Baltic-region magnetometer data is available and this storm pre-dated any of the historic storm indices used for classification of geomagnetic storms. The forensic analysis of other available magnetometer data across North America and pacific equatorial regions indicates that this storm approached a DST index intensity of ~-1000, a level much larger than the March 1989 superstorm and nearly as intense as the level speculated for the 1859 storm. Also, based on the July 1982 paired observations and the linear behavior of geo-electric field response to the incident magnetic field environment, it is plausible to project that the disturbance intensity approached a level of ~5000 nT/min. While disturbances in either Bx or By can be the

source of moderate intensity impulsive disturbances, the most likely cause for disturbances of this size is that the disturbance is primarily driven from a disturbed Bx, similar to the March 89 and the July 82 events. No information is available on local-time of the manifestation (this would provide a better indication of an eastward or westward electrojet source), but observation tendencies of large impulsive events tend to be more associated with the westward electrojet. Assuming a westward electrojet, again tendencies further suggest that this local disturbance would be embedded within a geographically widespread westward electrojet structure of ~120^{o} longitudinal dimension and of at least 5^{o} latitudinal spread.

Others have also reviewed the 1859 storm as an example of important space weather extreme events. Previous to this work, Siscoe had done a more theoretical examination of self-consistent processes and had determined that the 1859 storm reached a Dst of -2000 (Reference 4-15). While the later Tsurutani effort includes improvements, both estimates provide the same approximate bounds. The work of Tsurutani et al., in classification of the 1859 storm, was based upon both terrestrial and solar observations of that era, and fitting these observations to contemporary understandings. This work also provides a comprehensive overview on the source constraints for large geomagnetic disturbances and offers added insight towards the classification of an extreme geomagnetic storm scenario. One of the important revelations of this work is that the solar activity (i.e. ejecta) that triggered the 1859 storm was not unique, and that there have been large flares that have been at least the equal, typically at intervals of at least one or more per decade over the intervening years. This non-unique perspective also applies to the downstream processes from the Sun, which also contributes to the storm manifestation process. What is of importance is the right convergence of factors from the sun, to the solar wind and its encounter with the Earth's magnetosphere that set the framework for the *Perfect Storm* scenario. A brief overview can provide further perspective on the role and variability of factors in defining the storm development process.

In looking at the solar source, the size of flares (as measured by X-ray emissions) provides one of the best and longest recorded classification methods. Figure 3-7 provides a plot of the observed large flares since 1972 (when reliable X-Ray observations of solar flares became available). The size scale of flares used by the NOAA Space Environment Center is a classification of M and X based on logarithmic decade change in the X-ray energy observed. There are several flares that have exceeded even the X category by another factor of 10, and are classified as X+. This is also a range in which instrument saturation begins to limit accuracy in determining total energy content of flares. However, the flare that was suspected of triggering the March 13, 1989 superstorm was only in the mid range of the X class, and not close to the most energetic events observed. What is more relevant is the location of the eruption on the solar disk and the resulting CMEs probable connection to the Earth. In particular, the large X22+ flare event of April 2, 2001, while ~30 times larger than the March 89 flare, was located at the far west limb of the Sun, and the resulting CME ejecta was not Earth-directed and only provided a small glancing blow upon arrival at the Earth.

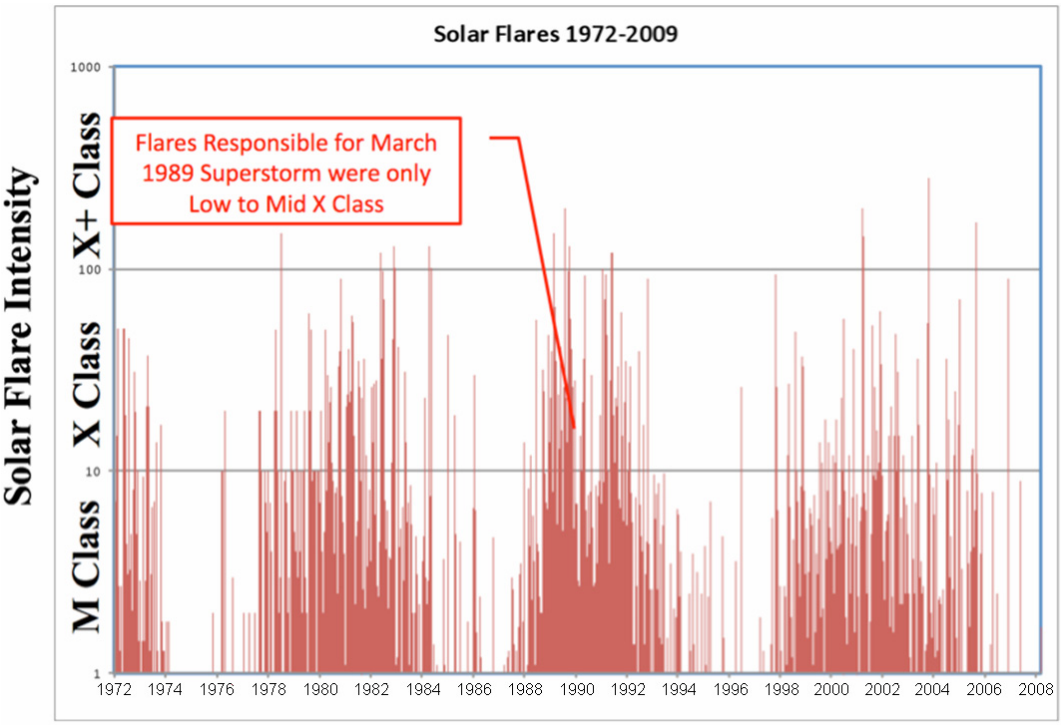

Figure 3-7. Observed solar flares since 1972.

As the ejecta leaves the Sun, a structure that is commonly called a coronal mass ejection (CME) begins to travel through interplanetary space, and generally in the direction of initial acceleration from the source. The CME, by the time it arrives at Earth, can be a massive structure, with a cross-sectional dimension measured along the Sun-Earth line that can be on the order of 0.5 AU or greater. These CMEs contain a magnetic structure which greatly enhances the Interplanetary Magnetic Field (IMF). The IMF intensity and orientation are important in defining the nature of the interaction with the Earth's magnetosphere. The most favorable orientation to produce a storm is when the IMF Bz component is negative, or southward oriented, and therefore opposite of the Earth's bipolar field. Under these conditions, a reconnection readily occurs between the IMF and the Earth's magnetosphere, allowing particles to enter and greatly enhance geomagnetic storm processes. IMF speed is also an important contributor, as well, to defining the level of energetics that the solar wind IMF delivers to the magnetosphere. The ability to continuously measure the solar wind has only been established over the past few years; therefore observations of this type are not available for the March 13-14, 1989 superstorm. However, one of the larger storms in the just completed solar cycle was observed on July 15-16, 2000. The nature of the coupling between the solar wind and the Earth's magnetosphere can be further illustrated. Figure 3-8 provides a plot of the rectified electric field (a measure of storm energetics) for a large CME cloud passage during July 15-16, 2000. Two plot areas are shown. In blue is a plot of the total solar wind energy, which is based on speed and B total of the IMF. As previously explained, it is only when Bz of the IMF is pointing southward that coupling with the magnetosphere

occurs. The red plot provides this fraction of the total solar wind cloud content that couples and produces storm activity. Because the solar wind IMF exhibited a bi-polar rotation of Bz during the passage of the cloud, only a fraction of total energy was able to couple. Figure 3-9 again shows the coupled solar wind energy, overlaid by a plot of the observed ground level geomagnetic field disturbances observed at Fredericksburg, MD (in nT/min) during the storm. This comparison indicates a fairly close coupling of the intensity variations over the storm interval. The July 15-16, 2000 event had many of the solar wind features that are considered to be approaching upper bounds. However, the storm, in total, was limited by the coupling efficiency. One way of measuring this coupling efficiency is to accumulate the energy content of the total solar wind and the coupled portion. In actuality, the coupling efficiency for this cloud passage was only at ~40% of total solar wind content. Figure 3-10 shows the solar wind energy content comparisons (total and coupled) for this storm as well as other noteworthy storms of 2000 and 2001. This summary indicates that the July 2000 storm had the highest solar wind content of the storms examined, and also the highest coupled content, with considerable size variations possible. It also indicates that the percentage coupling efficiency can be quite variable. For example, in the events considered here, the coupling efficiency ranges from a low of ~3% to a high of ~85%.

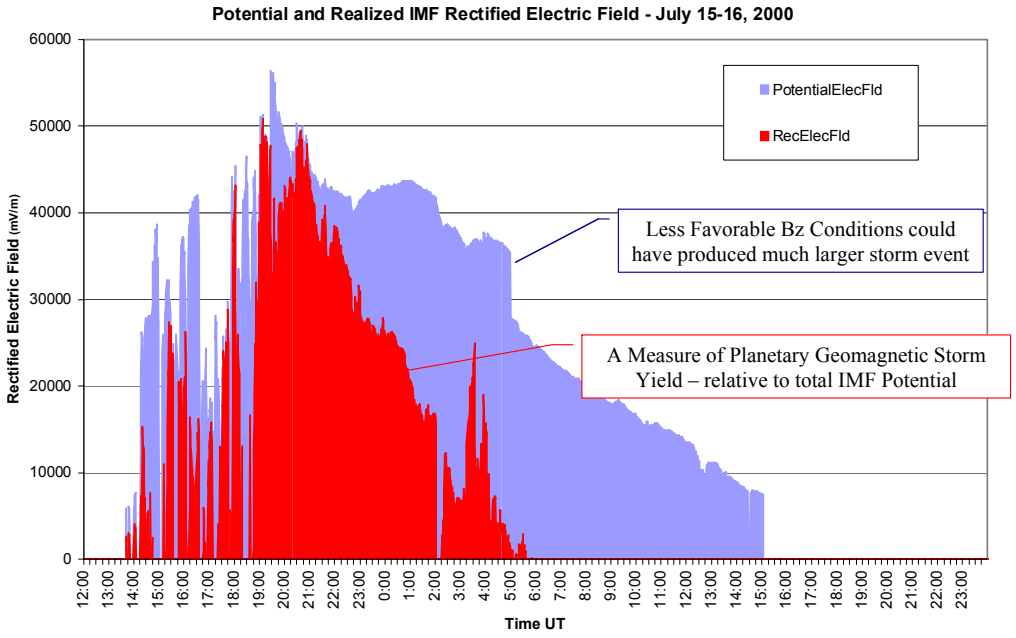

Figure 3-8. Rectified electric field from CME of July 15-16, 2002.

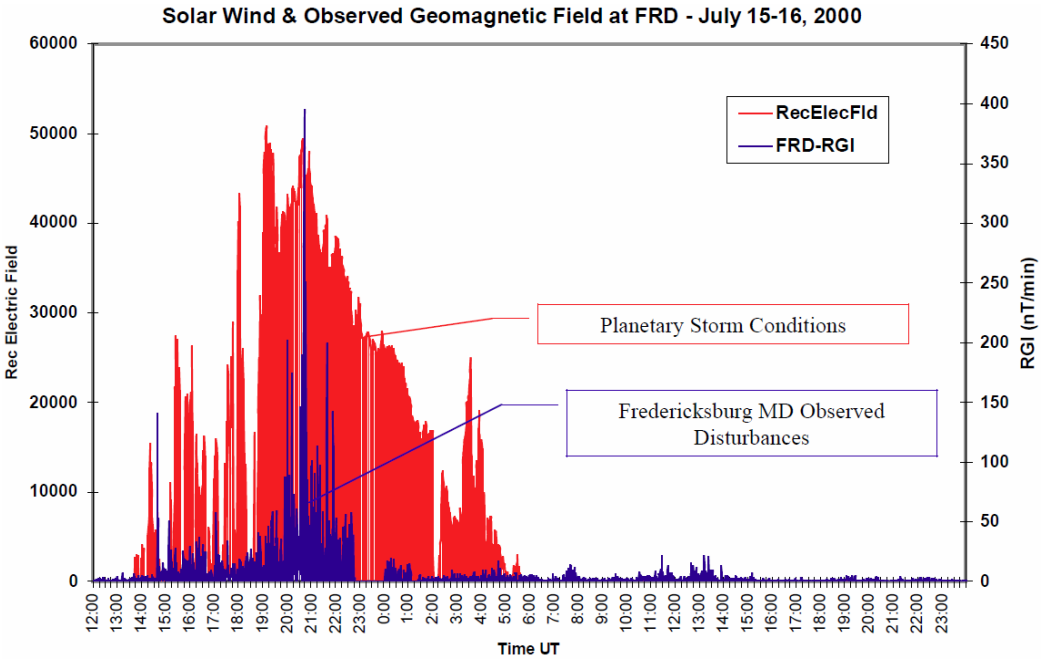

Figure 3-9. Coupled solar wind energy and observed geomagnetic disturbance for July 15-16, 2000 event.

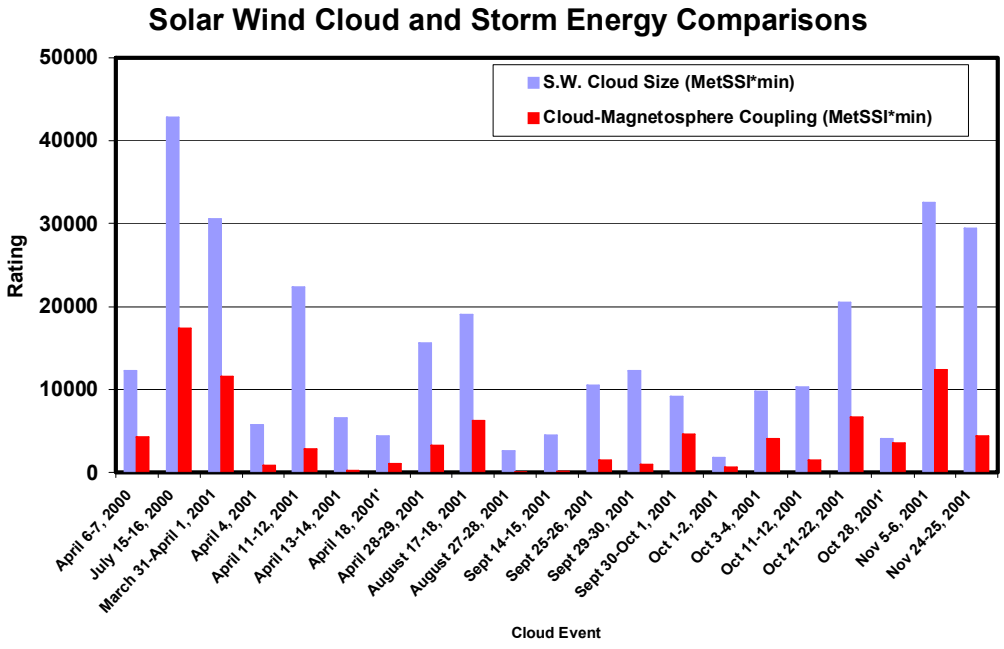

Figure 3-10. Solar wind energy for some 2000 and 2001 storms.

Again referring to Figure 3-8, the solar wind cloud passage for the July 15-16, 2000 storm represents a typical time-span for the passage of a large high-speed CME cloud.

The highest intensity portion of the cloud has a period of ~12-18 hours, as this cloud event was due to a single large CME ejecta from the Sun. There are important contrasts when looking at the duration of great storms, such as March 13-14, 1989, which lasted over 24 hours. The March 89 storm also had the most energetic substorms in late March 13 and into March 14 after about a 12 hour lull from substorms in the earlier AM hours of March 13. This suggests the possibility of passage of a second CME cloud that triggered the late energetic substorms. The magnetosphere has several modes of inertia and storage that play an important role in very long duration storms. Secondary solar wind cloud passages would encounter a magnetosphere with considerable momentum in convection patterns and initial storage of energy in the magnetospheric tail, which would readily set the stage for increasingly more energetic substorms, such as those on late March 13 and early March 14. From the historic data, other very large storms have also been multi-day events. The 1859 geomagnetic storm raged over a period from Aug 28 to Sept 2. The May 1921 storm lasted from the 13th to the 15th. Therefore, it appears that a necessary condition for large ground-level impulsive events would be a compounding effect of multiple solar wind cloud passages. Multiple CMEs are also not a unique feature of extremely active solar regions, as a number of regions appear each solar cycle that have produced multiple X-class flares over a several day period. These regions can also imprint a polarity characteristic on the CME. Therefore, a region that produces a CME with a favorable polarity for magnetospheric coupling can readily produce subsequent events as well. As the storm extends in time and becomes more energetic, the auroral oval exhibits equatorward expansion. This tendency infers that the later and very energetic impulsive events could occur at lower latitudes, which broadens the risk areas that need to be considered.

These summaries indicate that factors from solar activity, the IMF, and geomagnetic fields all have variations, and that all independent variations need to favorably converge to produce storm events. The extent of these convergences defines the character of the storm. In addition, the terrestrially-local manifestation of storm intensifications needs to be considered to determine the approximate threat to the North American continent. No organized effort has been expended by the space weather community to carefully document the dB/dt climatology of each storm and magnetic observations. Therefore, the large impulsive events of importance have more often been tipped-off by the observance of an important impact on a technology system that was upset by the storm's dB/dt event. Therefore, the probability estimate can only be roughly determined and may be understated. For example, the observation of a ~2000 nT/min dB/dt was observed in March 13, 1989 in Denmark, ~2700 nT/min in mid-Sweden in July 1982, ~2200 nT/min again in March 24, 1991 in southern Finland, and on Aug 4, 1972 in North America. This sampling indicates that a disturbance of this size class can be expected at a frequency of approximately once or twice per solar cycle, i.e. about a 1 in 10 year probability. Since the most intense portion of these disturbances tend to be part of a large electrojet structure of ~120^{o} longitudinal dimension, the odds for this structure erupting over North America would be expected to be 1 of every 3 occurrences. This provides a combined probability of ~1 in 30 years for a ~2400 nT/min disturbance for North America. As previously reviewed, the large ~5000 nT/min observed in May 1921 has occurred before and therefore is likely to occur again. More anecdotal data from other

large storms over the years, such as the March 24, 1940 storm documented by McNish and Davidson, also indicate geo-electric field effects in the May 1921 event. These two events, combined with the 1859 storm, a storm speculated to be somewhat larger than the 1921 storm, suggest that on a planetary basis, a cadence of 1 in 30 to 1 in 50 years is reasonable. Though it would arguably take over 150 years of continuous impulsive disturbance data to verify this cadence, this is not possible given the lack of measurement history. Locating the most severe impulsive event of the storm, such as a ~5000 nT/min disturbance, over North America produces a combined probability that places the overall risk closer to a ~1-in-100 year probability.

3.2 Simulations and Review of Storm Impacts on the U.S. Power Grid

Based upon the previously discussed observations and expected storm dynamics for extreme storm events, a number of simulation scenarios have been developed to review potential threat extremes to the U.S. Power Grid. To perform this analysis several simulation methods will be utilized. The first approach will focus on the July 13-14, 1982 storm that reached a large peak dB/dt value, which can be verified with modern digital data methods. Since a reasonably good collection of data observatories are available it is also forensically possible to recreate the dynamics of this storm in our environment model. The peak event occurred around 23:54-23:55 UT on July 13, 1982. Figure 3-11 provides a depiction of the geomagnetic field disturbances observed over North America at 23:54 UT (time of regional peak). This was coincident with the large GIC observations reported in North America earlier in this report. This disturbance region is demonstrably larger than the large disturbances centered around ~22:00 UT on March 13, 1989 (Figure 3-4). Further, the intense dB/dt disturbance of ~2700nT was observed over the Baltic Sea region at this same time (~120^{o} longitude from North America).

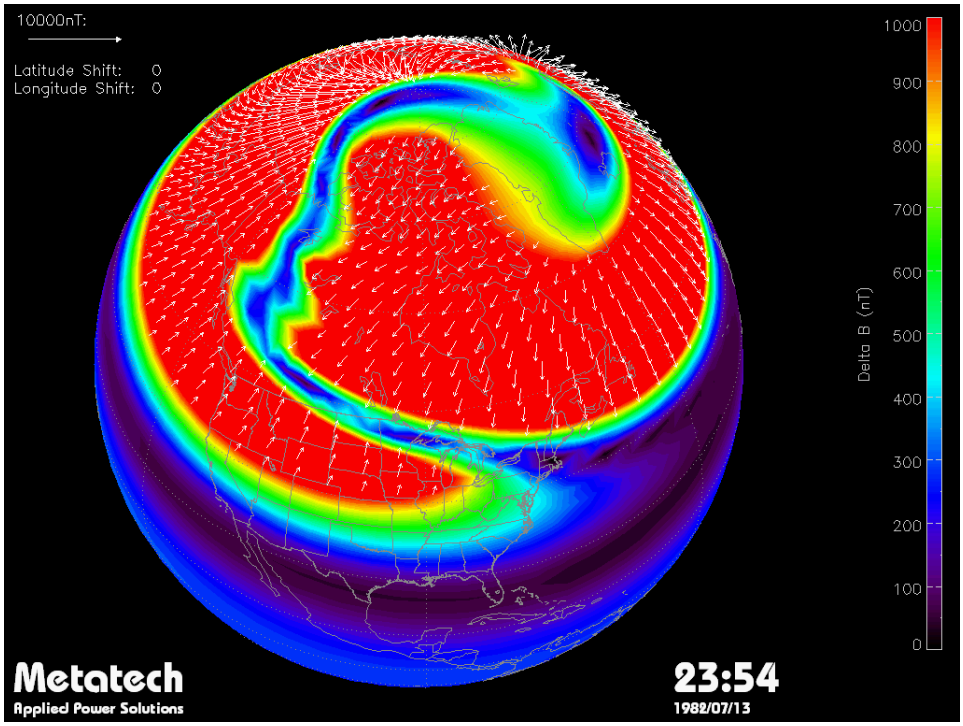

Figure 3-11. Geomagnetic field disturbances estimated over North America, July 14, 1982 at 23:54 UT.

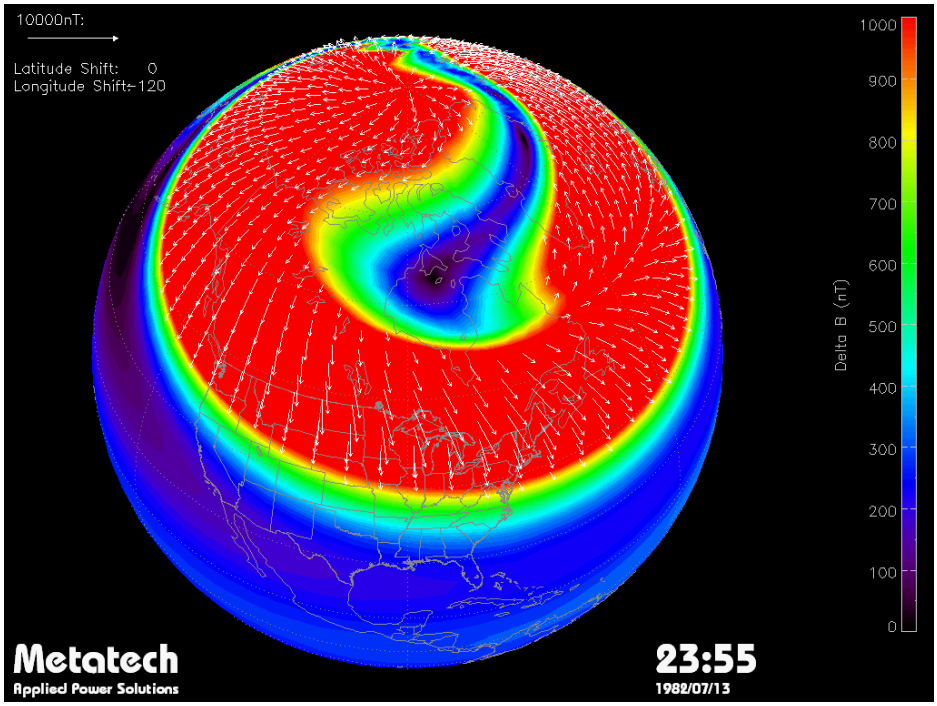

Figure 3-12. Geomagnetic field disturbances rotated by 120^{o} longitude over North America, July 14, 1982 at 23:55 UT.

The location of this region of intense dB/dt, as previously discussed, usually is located in the midnight to 6 AM. local time portions of the planet. The actual geographic laydown region is primarily a product of timing of the substorm event and could have equal probability of being centered over North America if this same substorm had been delayed by 6 to 7 hours in onset time. The environment model that has been created for this storm can also be utilized to rotate this storm over North America, while maintaining precise fidelity to all other aspects of the observed environments. This allows us to simulate for the today's U.S. Power Grid not only the actual 1982 storm that occurred, but also a more severe 1982 storm scenario where the intense dB/dt region is now centered over North America. Figure 3-12 provides a plot of this intense dB/dt region at 23:55 UT rotated by 120^{o} longitude over North America. As this illustrates, the environment over North America is now significantly more severe than any observed in the March 1989 storm. Further enhancements in the storm laydown region can be simulated by stretching the boundaries of the intense electrojet regions by 5^{o} and 10^{o} southward from the observed locations for the 1982 storm. This would represent a storm scenario that is only a slightly enhance version of the 1982 storm. Figure 3-13 provides a plot of the geographic regions over North America for this scenario with a 5^{o} latitude stretch.

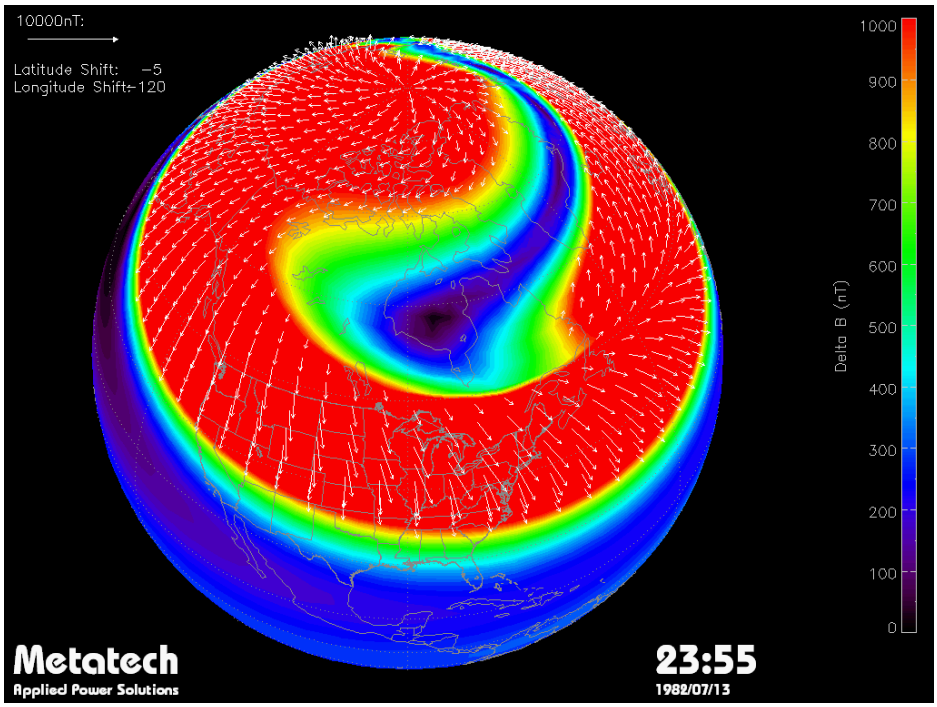

Figure 3-13. Geomagnetic field disturbances rotated by 120^{o} longitude and stretched southward by 5^{o} latitude over North America, July 14, 1982 at 23:55 UT.

It is also feasible to use these environments to estimate the potential problems that could occur for the current model of the U.S. Electric Power Grid. The peak time for the 1982 storm (non-shifted) was at 23:55 UT. Figure 3-14 provides a plot of the GIC flows and geo-electric field vectors across the U.S. at that time. In contrast to Figure 2-19, that

provided a similar plot for the peak of the March 13, 1989 storm at 21:44 UT, the levels of GIC flows are noticeably higher. Similarly, Figure 3-15 provides a summary of the reactive power demands (MVARs) and GIC flows for this July 13-14, 1982 storm on the present day U.S. Power Grid. This figure shows peak reactive demand reaching a level over 11,000MVARs, which contrasts to the results in Figure 2-26 for the March 13, 1989 storm where the peak was only 8000MVARs. These simulations confirm that the environment for the July 1982 storm was somewhat larger than the March 1989 storm.

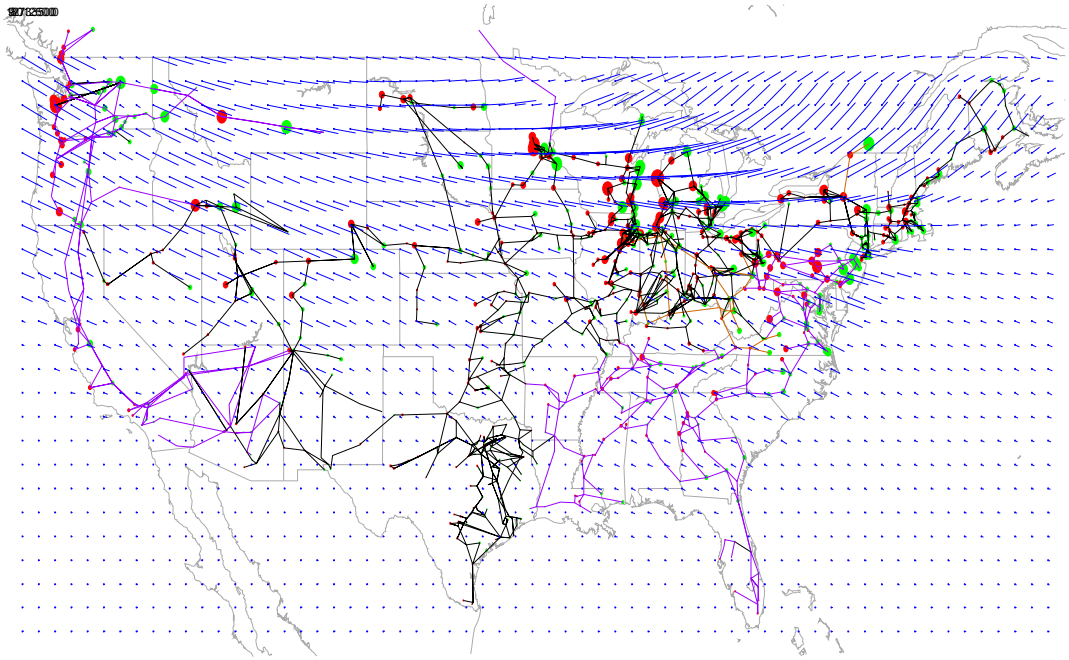

Figure 3-14. Simulation of U.S. power grid conditions at 23:55 UT on July 13, 1982.

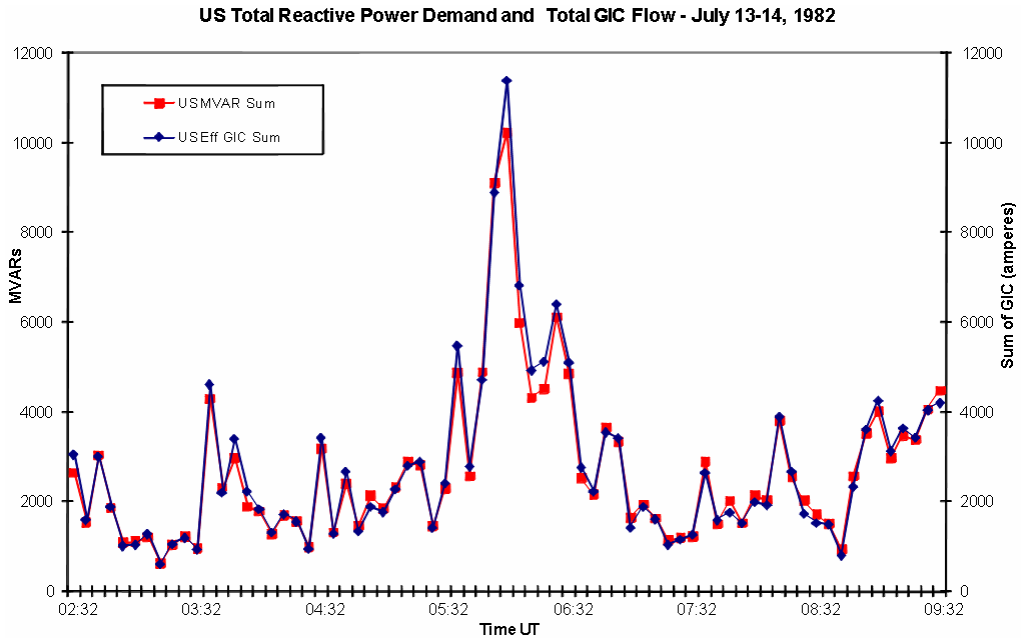

Figure 3-15. GIC and MVAR demand variations for the U.S. power grid during the July 13-14, 1982 geomagnetic storm.

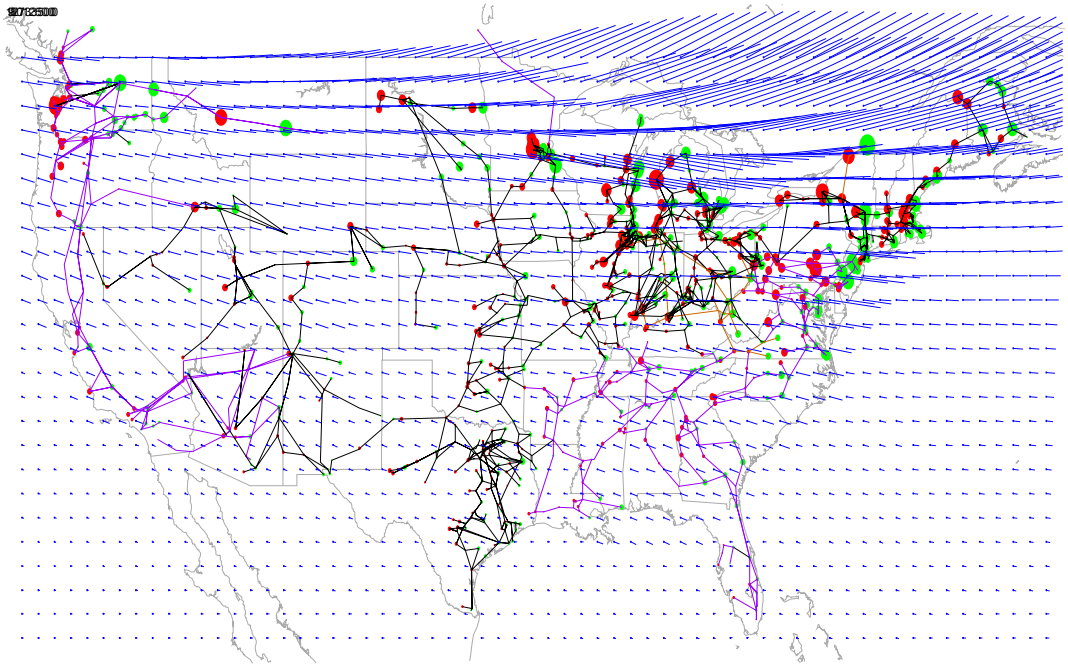

Figure 3-16. Simulation of U.S. power grid conditions.

The examination of simulations with the intense dB/dt region shifted by 120° longitude so that it falls over the North American continent reveals the degree of impact that such a scenario would pose for the U.S. Power Grid. Figure 3-16 provides a plot of the pattern of geo-electric fields and GIC flows in the U.S. Grid at 23:55 UT for this 120° location shift scenario. As illustrated, both higher electric fields and patterns of GIC flows are evident. Figure 3-17 provides a summary of total MVAR and GIC flows in the U.S. Power Grid for this time period with the 120° shift. As this calculation indicates, both GIC and MVAR levels continue to increase, reaching a peak reactive demand of ~16000 MVARs, a level that is nearly 3 times larger than peak levels reached during the March 1989 Superstorm.

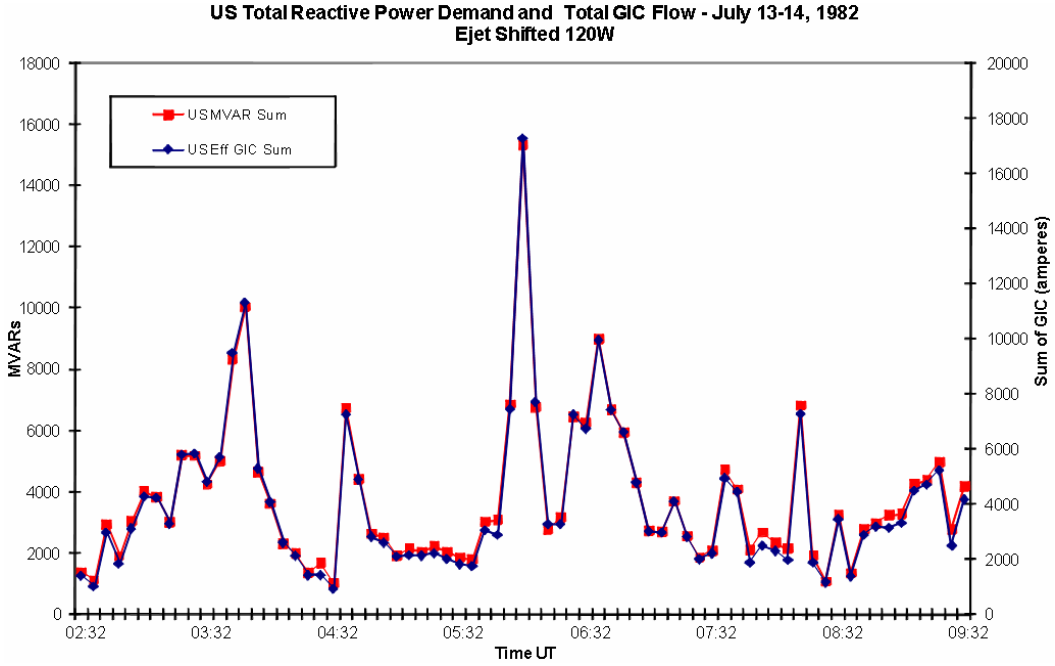

Figure 3-17. GIC and MVAR demand variations for the U.S. power grid during the July 13-14, 1982 geomagnetic storm with 120° longitude shift.

In addition to a longitude shift, both 5° and 10° latitude shifts were also simulated. This would have the effect of placing the intense dB/dt disturbance region at lower latitudes with respect to the U.S. Power Grid infrastructure. Figure 3-18 provides a map of the geo-electric field pattern and the pattern of GIC flows in the U.S. Power Grid for the 5° latitude shift case. Again, in comparison to the results provided in Figure 3-16, this scenario poses a noticeable increase in GIC flows across the network. This increase in impact is also confirmed by the analysis of total GIC flows and MVAR demand increases in the U.S. Grid as plotted in Figure 3-19. The MVAR demands as summarized now reach peaks of over 32,000 MVARs, which is about 4 times larger than similar increases estimated for the March 1989 superstorm.

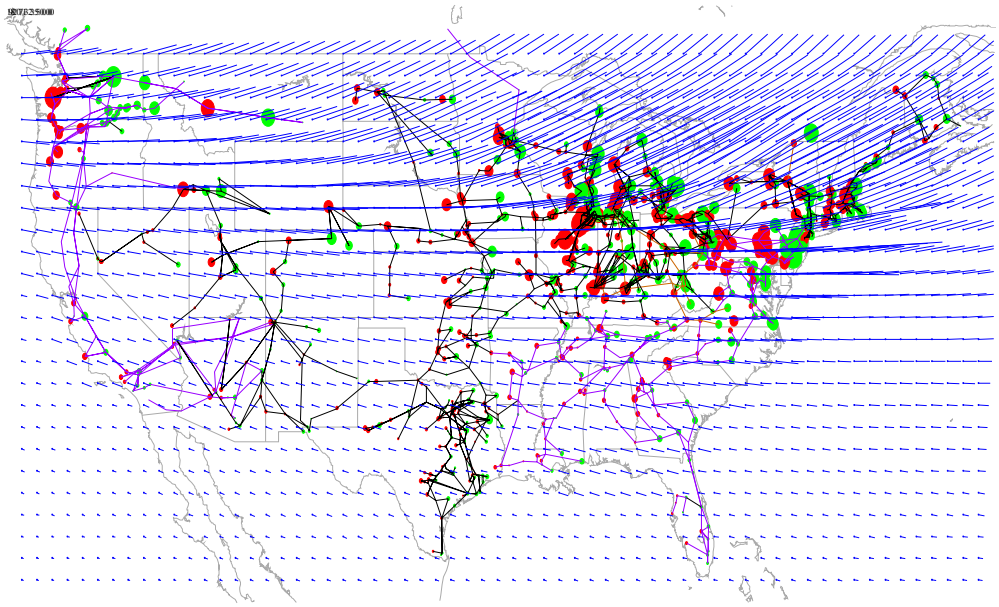

Figure 3-18. Simulation of U.S. power grid conditions at 23:55 UT with 120° longitude and 5° latitude shift on July 13, 1982.

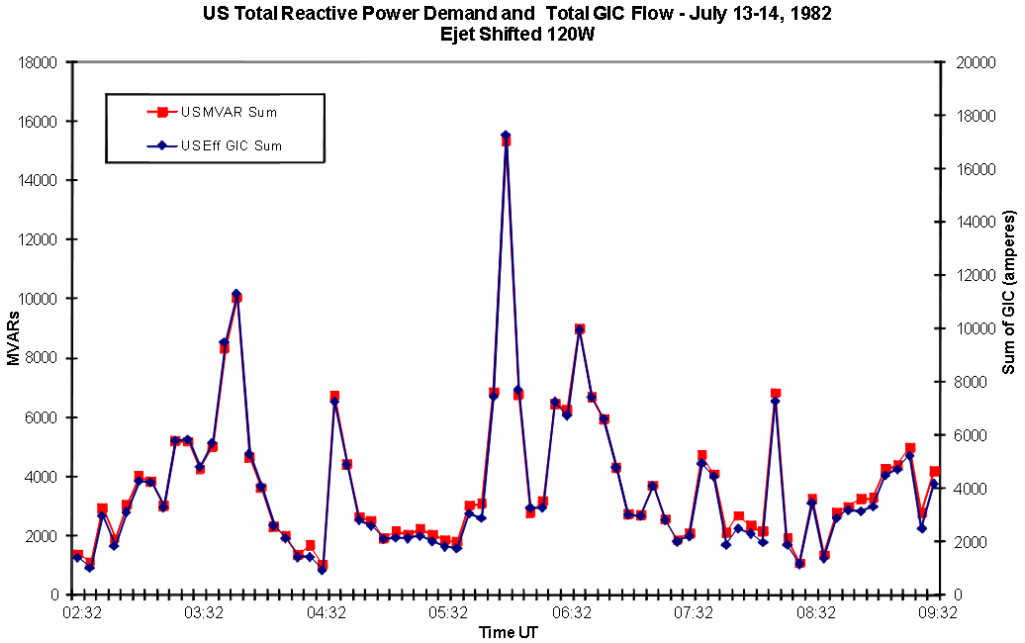

Figure 3-19. GIC and MVAR demand variations for the U.S. power grid during the July 13-14, 1982 geomagnetic storm with 120° longitude and 5° latitude shift.

Figure 3-20 provides an illustration of the geo-electric field and GIC flow patterns for the 10^{o} latitude shift storm scenario. This scenario illustrates an increase of GIC flows in mid-latitude locations across the U.S. Grid, while also showing some decrease in GIC flows for northern locations when compared to the 5^{o} shift scenario shown in Figure 3-18. In examining the total GIC and MVAR increase levels for the U.S. Grid (Figure 3-21), only a modest increase has now occurred in levels compared to Figure 3-19 (5^{o} shift). This suggests a possible plateau at this intensity level as location is shifted further southward across the U.S. Grid infrastructure.

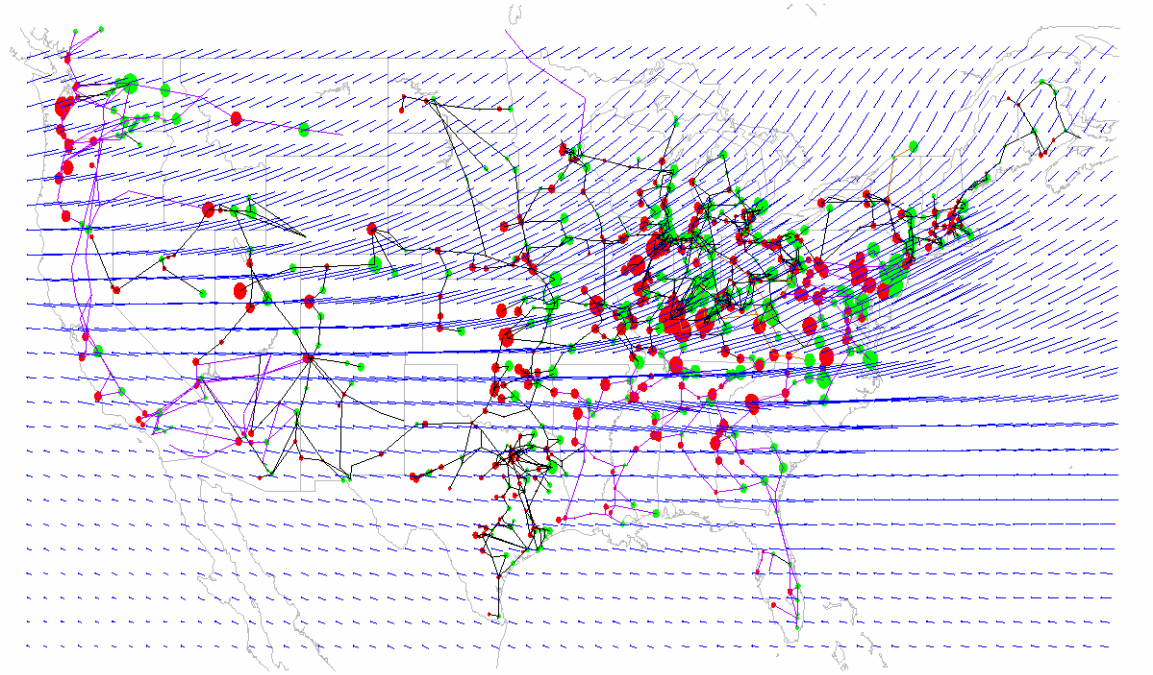

Figure 3-20. Simulation of U.S. power grid conditions at 23:55 UT with 120^{o} longitude and 10^{o} longitude shift on July 13, 1982.

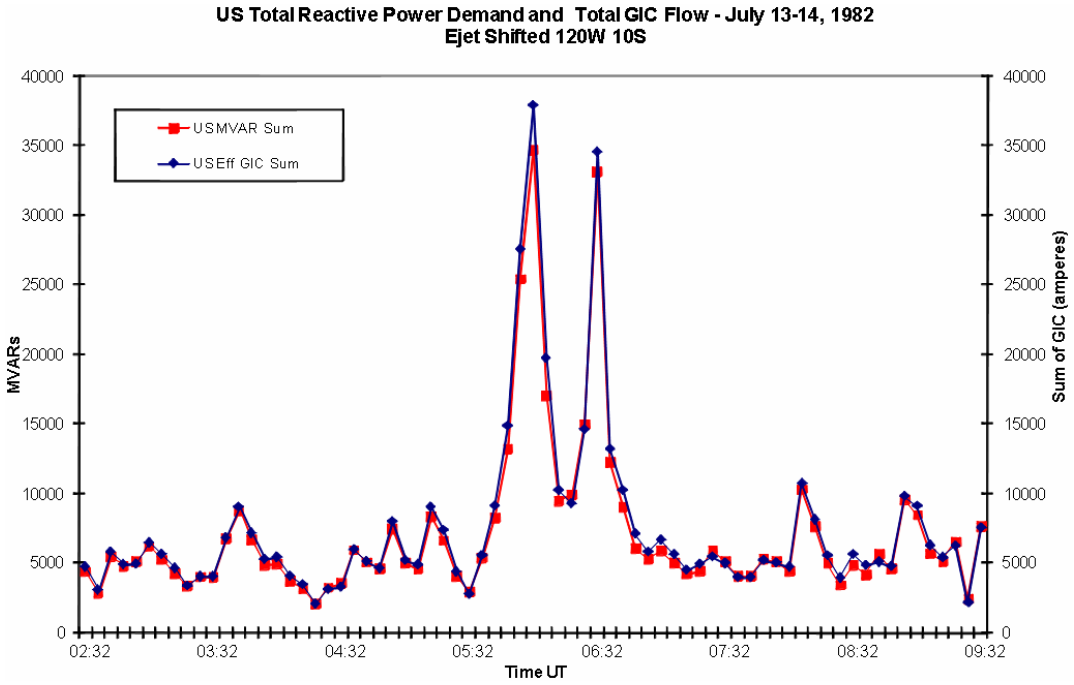

Figure 3-21. GIC and MVAR demand variations for the U.S. power grid during the July 13-14, 1982 geomagnetic storm with 120^{o} longitude and 10^{o} latitude shift.

As these simulations illustrate, the manipulation of the 1982 electrojet structure reveals that the potential impact to the U.S. Power Grid could increase many times over the levels actually experienced by the U.S. Grid during the March 1989 superstorm. As previously described, the intensity of the 1982 storm could also increase by about a factor of two as well. These results also show impact variation due to location (latitude), in that southward expansion of the electrojets over the U.S. Grid appears to increase impacts markedly, up to a point. To further explore both the impact of intensity variation and latitude locations that might be plausible in extreme storm events, further environment scenarios are simulated to allow a more rigorous examination of these features and potential impacts. These scenarios are based upon various levels of dB/dt and location of a complex westward electrojet structure with an approximate size of a ~120^{o} longitudinal by ~5^{o} latitudinal band placed over various U.S. locations. Three different levels of dB/dt have been selected at 2400 nT/min (~ intensity level similar to the 1982 storm), 3600 nT/min, and 4800 nT/min (~ intensity level for the 1921 storm). The 2400nT/min represents the intensity that is likely for a 1-in-30 year scenario, while the more severe disturbances would be more representative of the estimated 1-in-100 year scenario. The locations for each of these disturbance intensities will also be evaluated at various equatorward expansion locations over the U.S., with the disturbance intensity centered on 55^{o}, 50^{o}, 45^{o} and 40^{o} geo-magnetic latitudes across North America. Figure 3-22 illustrates the footprint of the disturbance for the simulations where it is centered on 45^{o} and 50^{o} latitude locations.

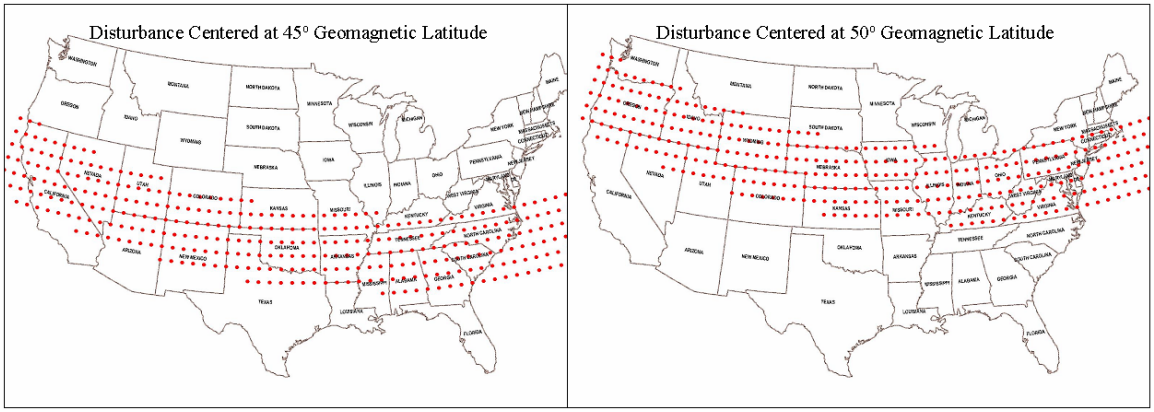

Figure 3-22. Disturbance regions for 45^0 and 50^0 geomagnetic latitude storms.

In this analysis of disturbance impacts, the level of cumulative increased reactive demands (MVARs) across the U.S. Power Grid provides one of the more useful measures of overall stress on the network. As previously noted, this cumulative MVAR stress was also determined for the March 13, 1989 storm for the U.S. Power Grid, and can also be used for comparison purposes in the evaluation of these threat assessments. Figure 3-23 provides a comparison summary of the peak cumulative MVAR demands that are estimated for the U.S. power grid for the March 89 storm, and for the 2400, 3600 and 4800 nT/min disturbances at the different geomagnetic latitudes. As shown, all of these disturbance scenarios are far larger in magnitude than the levels experienced on the U.S. Grid during the March 89 superstorm. The disturbance scenarios are sorted by geomagnetic location and, as shown, the highest MVAR demand at each disturbance intensity occurs for the disturbance at 50^o latitude and the lowest intensity occurs for the disturbance at 40^o latitude simulations. The difference in impact is primarily due to the location of the disturbance relative to the density and voltage level of the U.S. Grid circuit topology. The PJM, ECAR, and northern WECC regions in particular contain systems of dense 500kV and 765kV circuit topology.

All reactive demands for the 2400 to 4800 nT/min disturbance scenarios would produce unprecedented in size reactive demand increases for the U.S. Grid. The comparison with the MVAR demand from the March 89 superstorm further indicates that even the 2400 nT/min disturbance scenarios would produce reactive demand levels at all of the latitudes that would be from 3 to 6 times larger than those estimated for the March 1989 storm. At the 4800 nT/min disturbance levels, the reactive demand is estimated, in total, to exceed 100,000 MVARs. It should also be noted that peak reactive demands occur in all cases (2400, 3600 and 4800n nT/min) with a electrojet intensification located at 50 degree geomagnetic latitude, as this provides the broadest footprint across the highest density of the U.S. power grid. For the smallest disturbance scenario (2400 nT/min) a breakout of reactive demand by pool regions is provided for the 50^o latitude disturbance, as shown in Figure 3-24. The comparison with the March 1989 storm is also provided for each pool. As shown, each of the pools in or near to the disturbance zone generally experience reactive demand levels that are ~ 5 times larger than estimated for the March 1989 storm event.

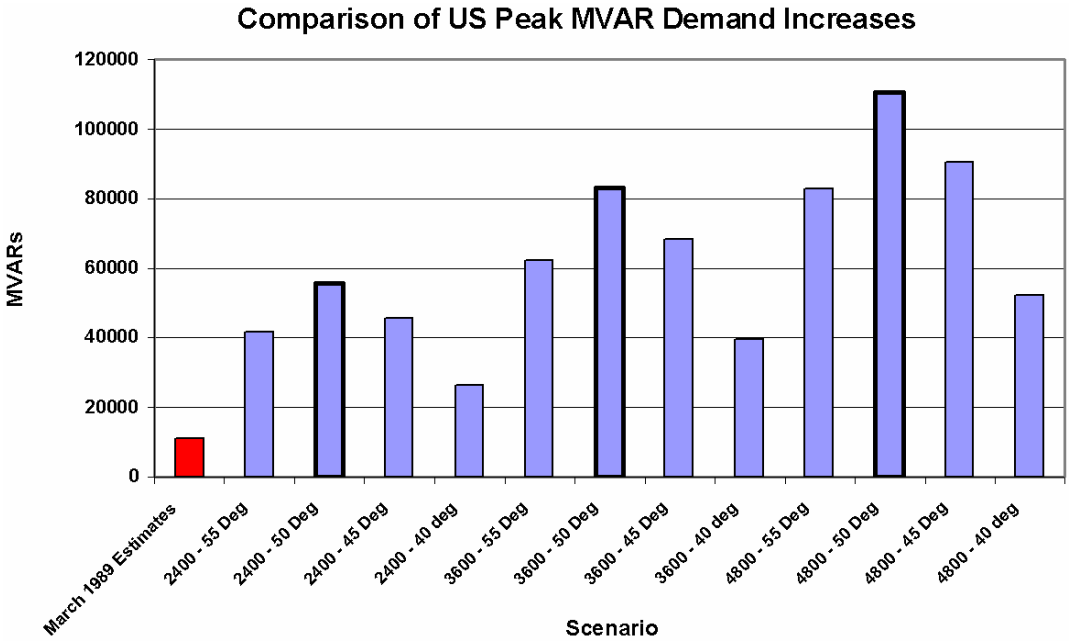

Figure 3-23. MVAR demands for the March 1989 storms, compared to various simulated storms.

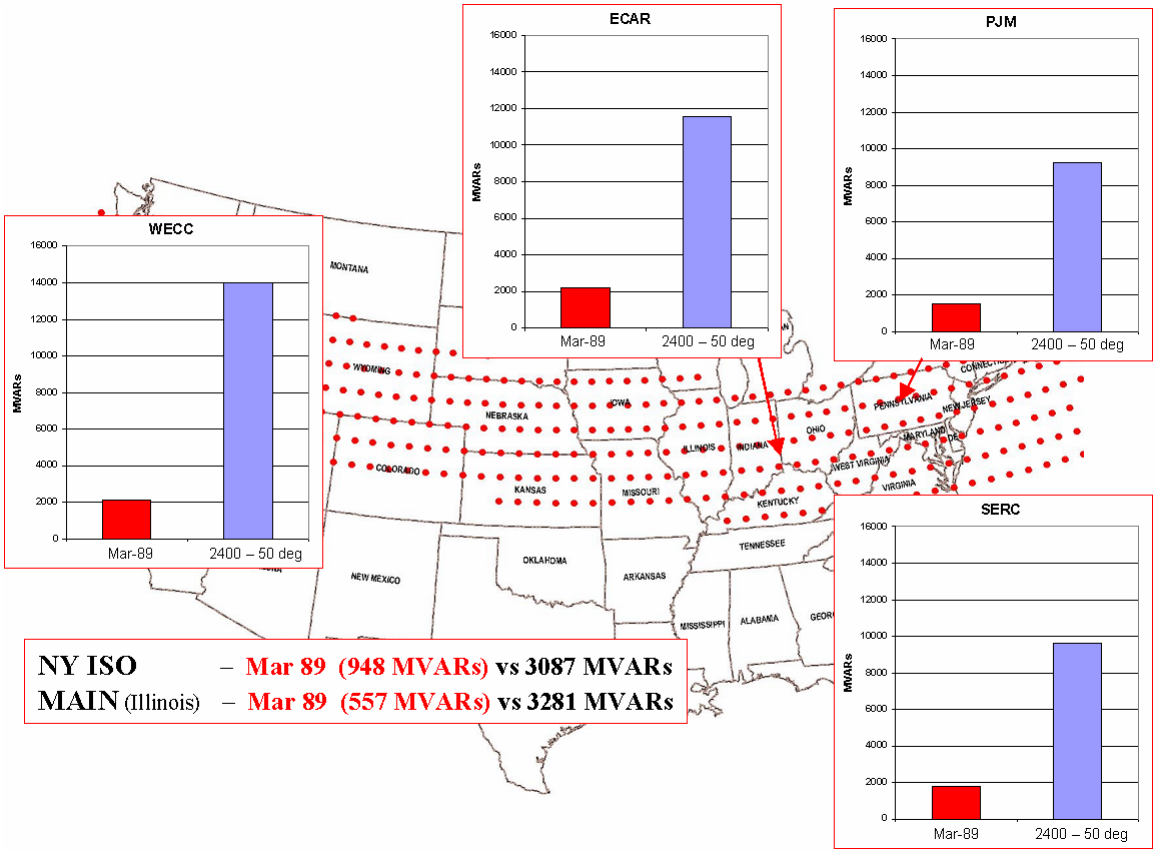

Figure 3-24. 1 in 30 year storm scenarios – 2400 nT/min.

The increased reactive demand constitutes only one aspect of the power grid threat that needs to be considered. The waveform distortion due to harmonics from transformer half-cycle saturation will also threaten network security, due to the high probability of relay and protective system malfunctions. The relay operational concerns can initiate in any number of relay systems, such as generators, transformers, capacitors and both AC and HVDC transmission lines. From a practical standpoint, this dual threat condition tends to make the estimates of reactive demands less relevant, in that collapse of the grid could occur at levels well below these estimated peak demands, as the loss of key system elements occurring simultaneously with a significant increase in storm MVAR stress can lead to rapid erosion of network security.

This disturbance environment was further adapted to produce a footprint and onset progression that would be more geo-spatially typical of an electrojet driven disturbance. For this scenario, the intensity of the disturbance is decreased as it progresses from the eastern to western U.S. The eastern U.S. is exposed to a 4800 nT/min disturbance intensity, while west of the Mississippi, the disturbance intensity decreases to 2400 nT/min. This simulation was also performed for the two highest impact and likeliest latitude locations at 45^{o} and 50^{o}. Using the impact criteria described in Appendix 1 and a 2-minute time window during the disturbance peak, the regions of expected power system collapse can be estimated. Figure 3-25 provides the outage regions that would be expected for a disturbance occurring at a 50^{o} latitude, while the regions for a 45^{o} disturbance latitude are shown in Figure 3-26. Even though the 45^{o} latitude disturbance scenario has a weaker overall disturbance energy, the region of resultant outage estimated is substantially larger than that resulting from the 50^{o} location scenario. While this would intuitively be unexpected by consideration of disturbance location alone and the prior peak MVAR summaries of Figure 3-23, the impacts continue to be sufficiently large to the regions just north of the disturbance to also cause failure. These regions, while less disturbed for the 45^{o} scenario, still have sufficient disturbance energy to cause failure, primarily due to these regions' inherently higher susceptibility because of the high kV ratings of the systems. In short, the 45^{o} location tends to have higher collateral impacts.

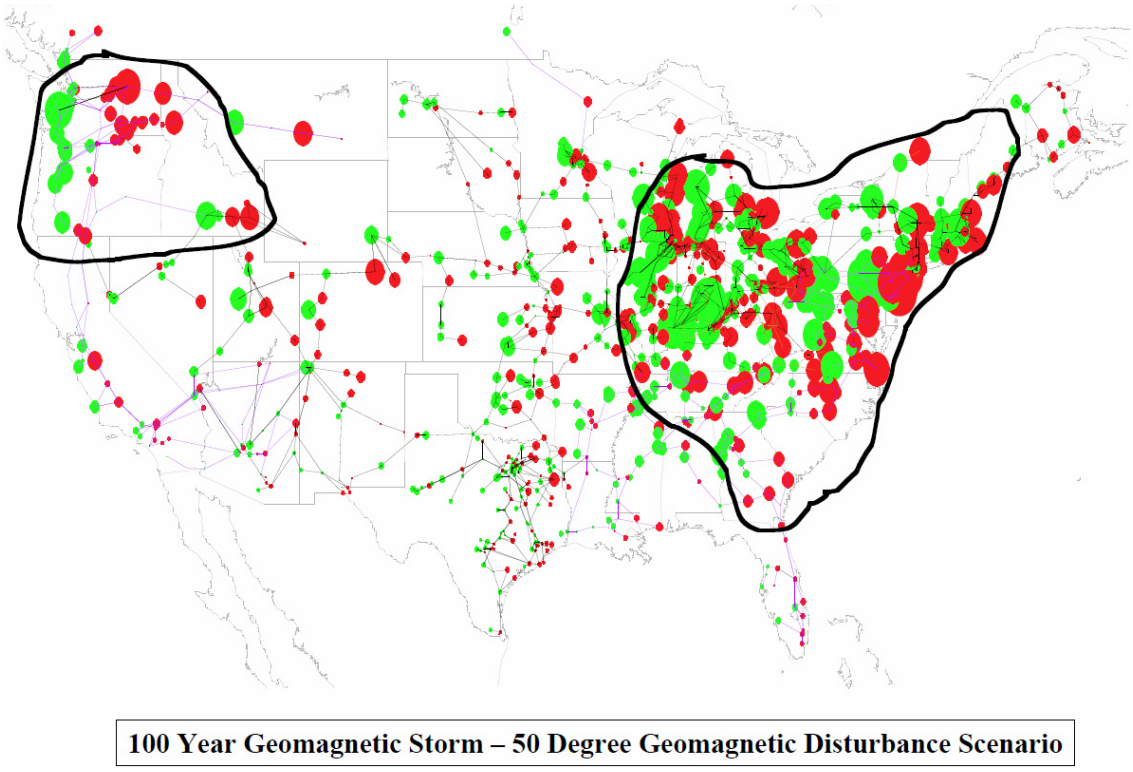

Figure 3-25. 100 Year geomagnetic storm – 50 degree geomagnetic disturbance scenario. The above regions outlined are susceptible to system collapse due to the effects of the GIC disturbance.

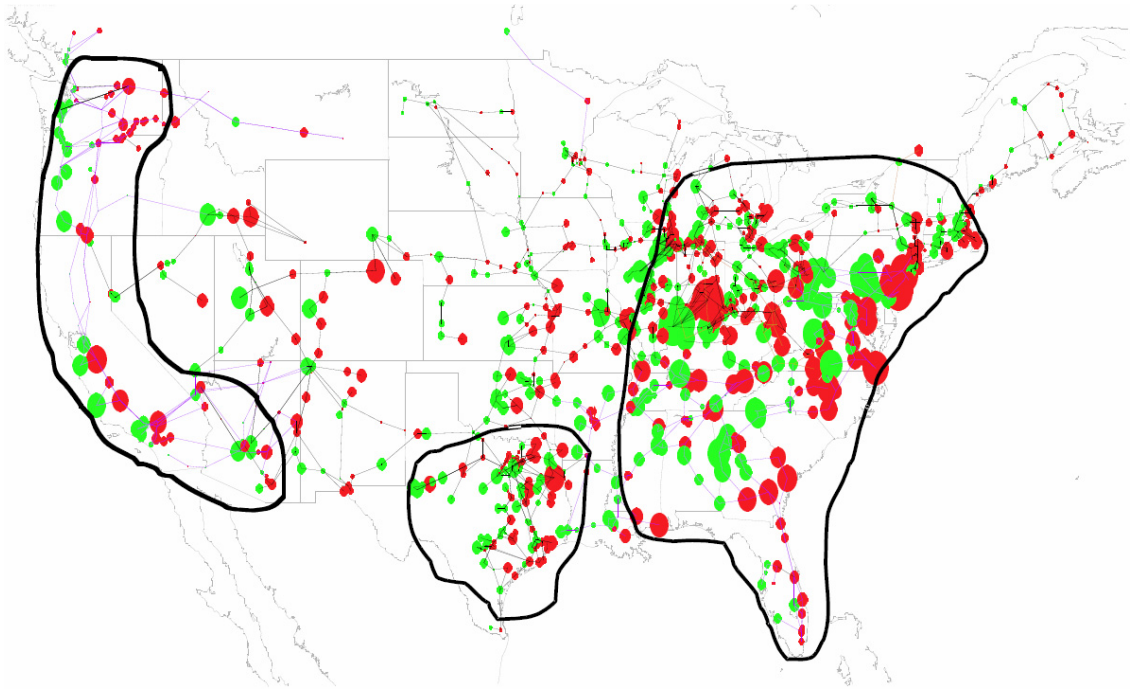

Figure 3-26. 100 Year geomagnetic storm – 45 degree geomagnetic disturbance scenario. The above regions outlined are susceptible to system collapse due to the effects of the GIC disturbance.

A 1-in-100 year storm lasting several days and achieving very high intensities would also have the potential for global power system impact implications. Most concerns of power system impacts have usually focused on power grids located at high latitudes that are directly exposed to electrojet intensifications. However, recent work has also established that power system impacts are being observed at low and equatorially located regions, due to simultaneous intensifications of the ring currents located over these terrestrial regions. While the disturbance intensity at these locations is greatly reduced, they can persist for very long periods of time. The power grid design factors that enhance GIC exposures for U.S. latitudes are also responsible for exposure enhancements at these lower latitudes. Figure 3-27 shows the onset of widespread GIC flows in the power grid of southern Japan (26^{o} geomagnetic latitude) during a storm on November 6, 2001. This disturbance, while only of moderate intensity, indicates that GICs of relatively large magnitude can occur. Modeling and benchmarking of this system can be used to extrapolate the threat conditions for more intense disturbance scenarios. This has been done for a number of storms including the Dst –600 storm of March 13-14, 1989. Figure 3-28 shows that a linear trend line provides a first-order prediction of expected GIC levels for this region. It would also be expected that a -1700 Dst 1-in-100 year storm may have the potential to produce ~3 times higher expected GIC levels at these equatorial and low-latitude locations than those anticipated for the March 1989 storm. These levels of GIC could also cause the possibility of widespread power system problems in these regions as well. For example, the Eskom grid (South Africa) sustained the loss of 14 large 400kV transformers over the October 29-31, 2003 geomagnetic storm. Therefore, these lower latitude regions in combination with high latitude regions of North America and Europe could all experience substantial disruptive events from an extreme storm, effects that could include permanent damage to key power system apparatus such as transformers and generators. In these scenarios, the world demand for replacement apparatus could dwarf the world capability to manufacture and supply replacement apparatus. While it would be difficult to accurately estimate world damage, the U.S. Grid simulations can provide a rough estimate of potential GIC-caused thermal damage to transformers. Using the 950 amp-min exposure determined for the Salem transformer from the March 89 storm, a review of transformers with this level of exposure and higher can be undertaken. Using the 2400 nT/min disturbance peak at each location latitude along with the three smaller substorms of March 1989 (to simulate a long-duration storm), a map of at-risk transformers is provided in Figure 3-29. This calculation estimates that ~216 large power transformers would be exposed to these at-risk levels.

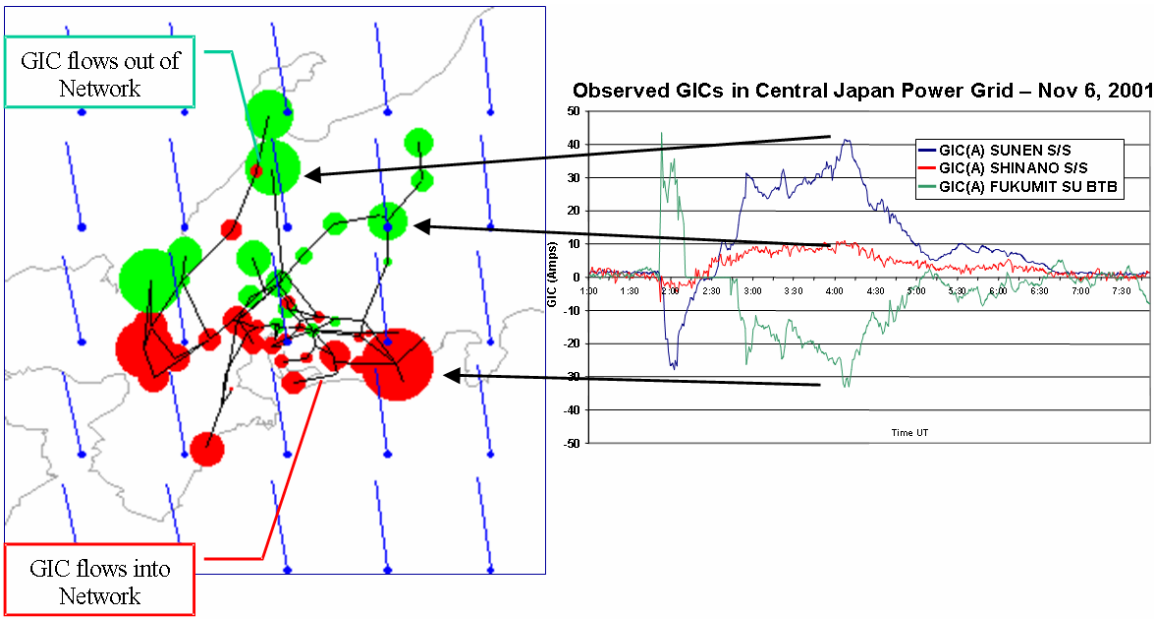

Figure 3-27. GIC flows in southern Japan for November 6, 2001 storm.

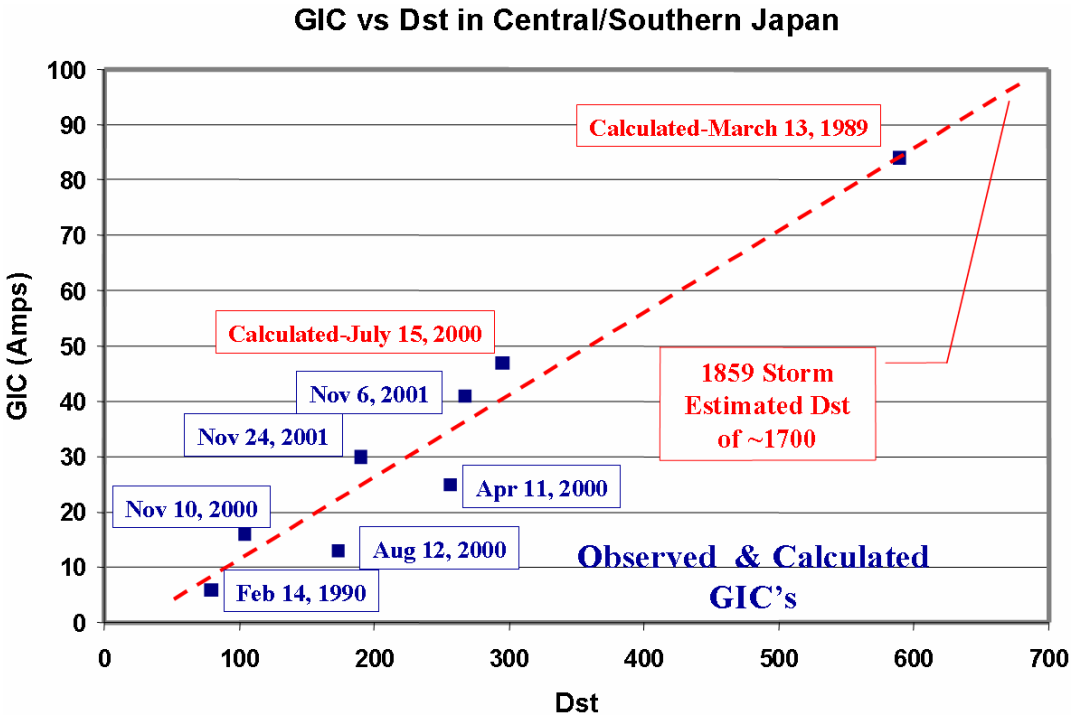

Figure 3-28. Ring current intensification and GIC risk at low latitudes.

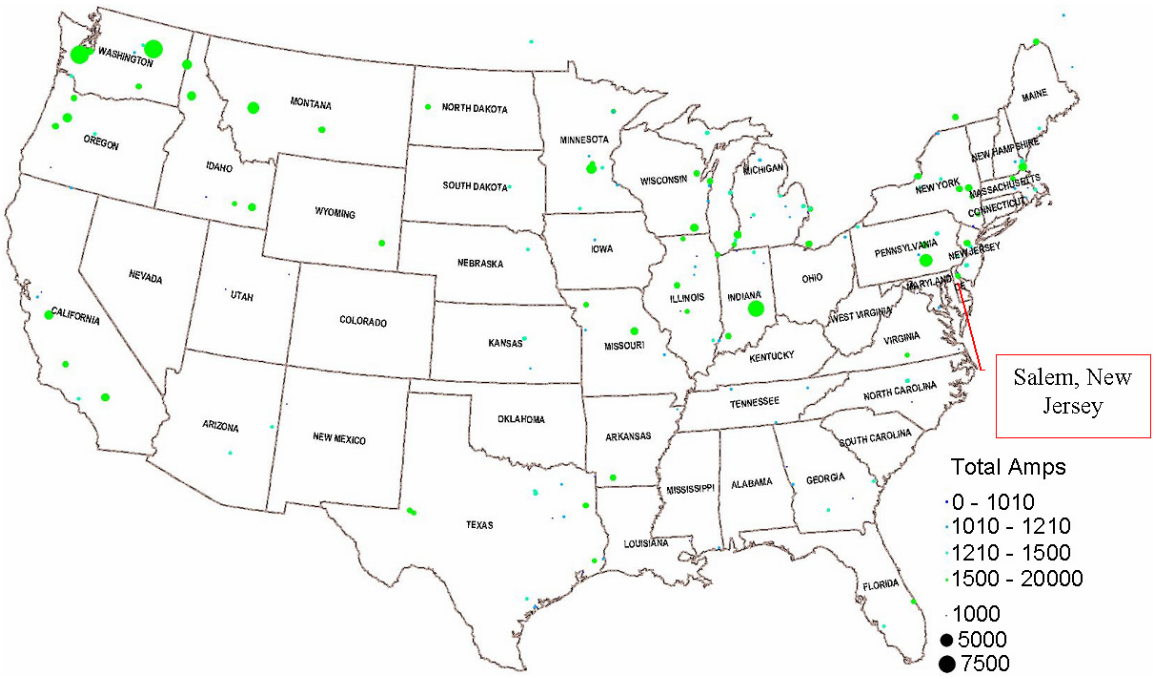

Figure 3-29. GIC exposure and transformer internal heating/failure for a 1 in 30 storm – 2400 nT/min scenario. Simulations indicate that ~216 transformers may receive GIC cumulative exposures that exceed the March 89 exposure of the Salem transformer.

References

3-1 Carovillano, R.L. and G.L. Siscoe, "Energy and Momentum Theorems in Magnetospheric Processes", Review of Geophys. and Space Phys., 11, 289, 1973.

3-2 L.J. Lanzerotti, G.P. Gregori, "Telluric Currents: The Natural Environment and Interactions with Man-made Systems, in the Earth's Electrical Environment", National Academy Press, Washington, 1986.

3-3 B.T. Tsurutani, W.D. Gonzalez, G.S. Lakhina and S. Alex, "The Extreme Magnetic Storm of September 1-2, 1859", Accepted for publication in Journal of Geophysical Research, 2002.

3-4a J.G. Kappenman, Chapter 13 - "An Introduction to Power Grid Impacts and Vulnerabilities from Space Weather", NATO-ASI Book on Space Storms and Space Weather Hazards, edited by I.A. Daglis, Kluwer Academic Publishers, pg 335-361, 2001.

3-4b John G. Kappenman, Great Geomagnetic Storms and Extreme Impulsive Geomagnetic Field Disturbance Events – An Analysis of Observational Evidence including the Great Storm of May 1921, Paper in Press for 35th COSPAR Assembly publication in Advances in Space Research, August 2005 Published by Elsevier Ltd on behalf of COSPAR.doi:10.1016/j.asr.2005.08.055

3-4c J. G. Kappenman, Chapter 16 – " Geomagnetic Disturbances and Impacts Upon Power System Operations", The Electric Power Engineering Handbook, 2nd Edition, edited by Leonard L. Grigsby, CRC Press/IEEE Press, pages 16-1 through16-22, published 2007.

3-5 Anderson, C.W., L.J. Lanzerrotti, C.G. Maclennan, "Outage of the L-4 System and the Geomagnetic Disturbances of August 4, 1972", Bell System Technology Journal, 53, 1817, 1974.

3-6 D.H. Boteler, J.G. Van Beek, "Mapping the March 13, 1989 Magnetic Disturbance its Consequences across North America", Solar Terrestrial Predictions IV, Proceedings of a Workshop at Ottawa, Canada May 18-22, 1992, Volume 3, pages 57-70.

3-7 V.D. Albertson, J.M. Thorson, "Power System Disturbances During a K-8 Geomagnetic Storm: August 4, 1972", IEEE PES Transactions Paper T 73 369-6, IEEE PES Summer Meeting, Vancouver, B.C., July 15-20, 1973.

3-8 W.F. Davidson, "The Magnetic Storm of March 24, 1940 – Effects in Power Systems", EEI Bulletin, May 7, 1940.

3-9 A.G. McNish, "Magnetic Storms", EEI Bulletin, May 7, 1940.

3-10 "Project UHV, Transmission Line Reference Book, 345kV and Above", EPRI, 1987.

3-11 Swedish Railway Authority measurements from July 13-14, 1982. Personal communication from Sture Lindahl, May 22. 2002.

3-12 J. Elovaara, et. al., "Geomagnetically Induced Currents in the Nordic Power System and their Effects on Equipment, Control, Protection and Operation", CIGRE Paper 36-301, 1992 Session.

3-13 J.G. Kappenman, V.D. Albertson, "Bracing for the Geomagnetic Storms", IEEE Spectrum Magazine, March 1990, pages 27-33.

3-14 Geological Survey of Canada, "Spaceweather – 150 Years of Geomagnetic Effects", Natural Resources Canada.

3-15 G.L. Siscoe, "A Quasi-Self-Consistent Axially Symmetric Model for the Growth of a Ring Current through Earthward Motion from a Pre-Storm Configuration", Planet. Space Sci., pp 285-295, Vol. 27, 1979

3-16 J. G. Kappenman, et al., "Application of Modeling Techniques to Assess Geomagnetically Induced Current Risks on the NGC Transmission System", CIGRE, Session 2002, paper 39-304.

Section 4
An Assessment of Geomagnetic Storm-Related At-Risk EHV Transformers and Potential Damage Estimates

The previous sections of this report focused upon the mechanisms for power system collapse due to geomagnetic storm disturbance environments, but also briefly discussed the possible permanent equipment damage that may result from these disturbances. In regards to this analysis, the ability to assess disturbance conditions that can trigger widespread power system collapse is at a higher level of certainty than the analysis of what permanent damage these environments may cause to the equipment itself. This discussion will attempt to provide perspectives, through experience of actual power system collapses, on both the nature of the initiating causes of the collapses and the potential level of damage that may be possible to the infrastructure. Section 3 indicated that in worst case situations, these types of disturbances could instantly create a loss of over 70 percent of the nation's electrical service. This could be a blackout several times larger than the previously largest, the North American blackout of 14 August 2003. The most troubling aspect of the analysis is the possibility of an extremely slow pace of restoration from such a large outage and the multiplying effects that could cripple other infrastructures such as water, transportation, and communications due to the prolonged loss of the electric power grid supply. This extended recovery would be due to permanent damage to key power grid components caused by the unique nature of the electromagnetic upset. The recovery could plausibly extend into months in many parts of the impacted regions. Also other space weather environment interactions can lead to loss of, or permanent damage to, satellites, communications, and other infrastructures, as has been widely reported in the space weather community. In both cases, the concerns become one of highly correlated multipoint failures that can adversely affect the entire infrastructure and the numerous and complex interdependencies that these systems may have with each other.

The onset of important power system problems can be assessed in part by experience from contemporary geomagnetic storms. At geomagnetic field disturbance levels as low as 60–100 nT/min (a measure of the rate of change in the magnetic field flux density over the Earth's surface), power system operators have noted system upset events such as relay malfunction, the offline tripping of key assets, and even high levels of transformer internal heating due to stray flux in the transformer from GIC-caused half-cycle saturation of the transformer magnetic core. Reports of equipment damage have also included large electric generators and capacitor banks. Power networks are operated using what is termed an "N–1" operation criterion. That is, the system must always be operated to withstand the next credible disturbance contingency without causing a cascading collapse of the system as a whole. This criterion normally works very well for the well-understood terrestrial environment challenges, which usually propagate more slowly and are more geographically confined. When a routine weather-related single-point failure occurs, the system needs to be rapidly adjusted (requirements typically allow a 10–30 minute response time after the first incident) and positioned to survive the next possible contingency. Both HEMP and space weather disturbances, however, can have a sudden onset and cover large geographic regions. They therefore cause near-

simultaneous, correlated, multipoint failures in power system infrastructures, allowing little or no time for meaningful human interventions that are intended within the framework of the N–1 criterion. This is the situation that triggered the collapse of the Hydro Quebec power grid on 13 March 1989, when their system went from normal conditions to a situation where they sustained seven contingencies (i.e., N–7) in an elapsed time of 57 seconds. The province-wide blackout rapidly followed, with a total elapsed time of 92 seconds from normal conditions to a complete collapse of the grid. For perspective, this occurred at a disturbance intensity of approximately ~480 nT/min over the region. As previously discussed, an examination by Metatech of historically large disturbance intensities indicated that disturbance levels greater than 2000 nT/min have been observed even in contemporary storms on at least three occasions over the past 30 years at geomagnetic latitudes of concern for the North American power grid infrastructure and most other similar world locations; on August 1972, July 1982, and March 1989. Anecdotal information from older storms suggests that disturbance levels may have reached nearly 5000 nT/min. Both observations and simulations indicate that as the intensity of the disturbance increases, the relative levels of GICs and related power system impacts will also proportionately increase. Under these scenarios, the scale and speed of problems that could occur on exposed power grids will hit system operators unlike anything they have ever experienced or even imagined in their careers. Therefore, as storm environments reach higher intensity levels, it becomes more likely that these events will precipitate widespread blackouts to exposed power grid infrastructures. The possible power system collapse from a 4800-nT/min geomagnetic storm is as shown in Figure 4-1.

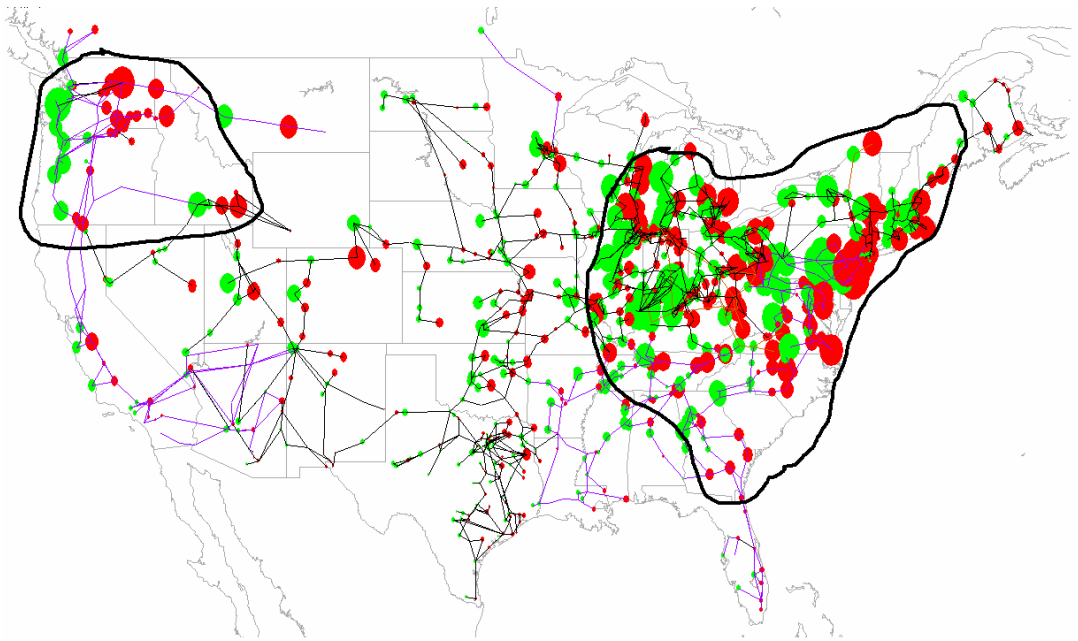

Figure 4-1. Severe geomagnetic storm with a 50 degree geomagnetic disturbance scenario. The above regions outlined are susceptible to system collapse due to the effects of the GIC disturbance.

The more difficult aspect of this threat is the determination of permanent damage to power grid assets and how that will impede the restoration process. As previously mentioned, transformer damage is the most likely outcome (although other key assets on the grid are also at risk). In particular, transformers experience excessive levels of internal heating brought on by stray flux when GICs cause the transformer's magnetic core to saturate and to spill flux outside the normal core steel magnetic circuit. Previous well-documented cases have noted heating failures that caused melting and burn-through of large-amperage copper windings and leads in these transformers. These multi-ton apparatus generally cannot be repaired in the field, and if damaged in this manner, they need to be replaced with new units, which have manufacture lead times of 12 months or more in the world market. In addition, each transformer design (even from the same manufacturer) can contain numerous subtle design variations. These variations complicate the calculation of how and at what density the stray flux can impinge on internal structures in the transformer. Therefore, the ability to assess existing transformer vulnerability or even to design new transformers to be tolerant of saturated operation is not readily achievable, except in extensive case-by-case investigations. Again, the experience from contemporary space weather events is revealing and potentially paints an ominous outcome for historically large storms that are yet to occur on today's infrastructure. As a case in point, Eskom, the power utility that operates the power grid in South Africa (geomagnetic latitudes –27° to –34°), reported damage and loss of 15 large, high-voltage transformers (400kV operating voltage) due to the geomagnetic storms of late October 2003 (Reference 4-1). This damage occurred at peak disturbance levels of less than 100 nT/min in the region.

While damage assessment is important in order to evaluate the restoration of the power grid, several factors also contribute to vulnerability of the power grid to EHV transformer damage. In addition to the concern about the ability of the GIC to damage these components, the condition of this infrastructure due to advancing age may be an important compounding factor. Analysis on EHV transformer population demographics provides some details on the trend in EHV transformer condition, growth trends, age, etc. Only limited data is publicly available on the age and condition of the transmission network apparatus and infrastructure, but the data that is available also suggests looming concerns. In 1999, the ECAR Region published a report titled "How Aging of Major Equipment Impacts Reliability". From this report, Metatech has been able to assess the age statistics on EHV transformers for approximately 20% of the U.S. Grid. Figure 4-2 shows the age distribution for installed EHV transformers (345kV and above) for the ECAR region. This also indicates that weighted average age for these facilities is greater than 30 years (out of a ~40 year economic life). The age of this infrastructure is rapidly approaching old-age. As previously mentioned, these key assets are at risk due to large GIC flows caused by both the E3 and severe geomagnetic storm threats that are possible. The failure of these devices will impair the transmission network and the ability to provide rapid restoration of electric power to regions.

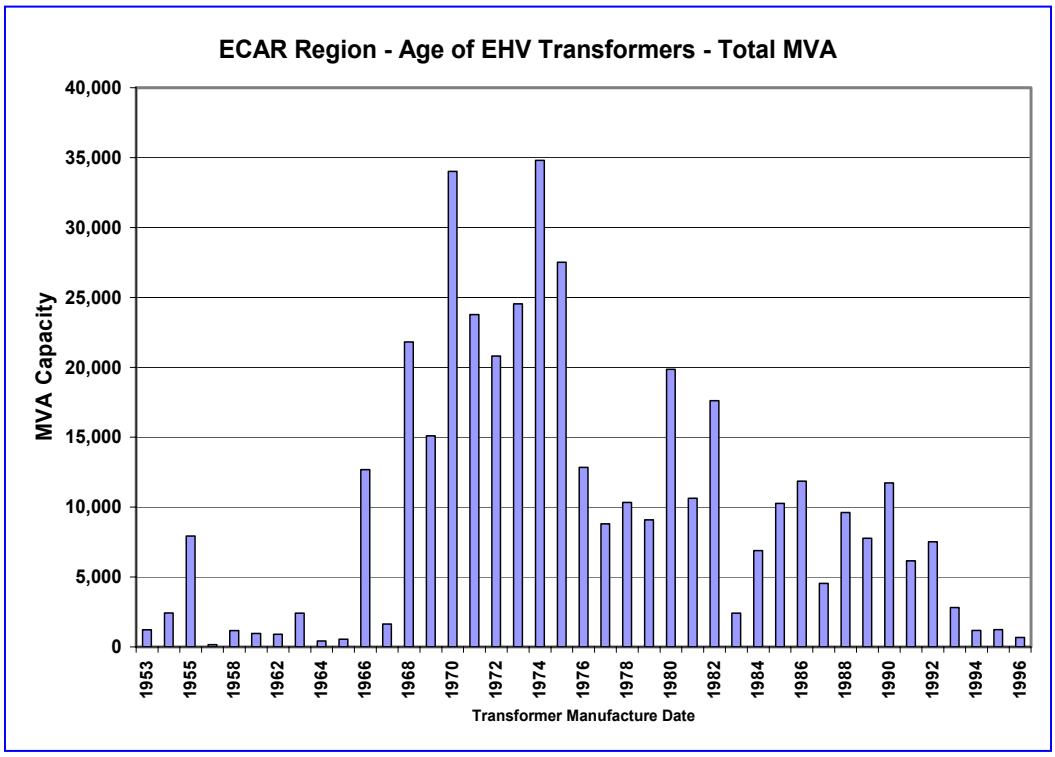

Figure 4-2. Age/manufacture dates of extra high voltage transformers in ECAR.

4.1 Transformer Internal Heating – Empirical and Analytical Data

While there is some uncertainty as to the threshold level of GIC that will cause transformer failure, there is both empirical evidence and engineering analysis that provide basic guidance as to overall trends and vulnerability issues. As previously noted, the Eskom network of South Africa experienced a large number of GIC-caused transformer failures due to storms in late October and early November of 2003 (Reference 4-1). These failures are suspected by them to have occurred at relatively low levels of GIC exposure. Their analysis also indicated that even 3-legged core form transformers were susceptible to half-cycle saturation at levels as low as 2 amps/phase. Price, in his analysis of transformer saturation, had determined that tank shunting is important in 3-legged core form transformers and that local heating is affected by the construction details (Reference 4-2). As both of these analysis efforts note, without adequate control of the flux under saturation conditions, local heating in parts of the transformer may not be cooled effectively. In turn, this leads to rapid temperature increase in some cases in small but sensitive areas. The intensity of overheating depends on the level of GIC but is also a function of various design parameters of the transformer itself. These include the saturation flux paths, cooling flow, and the thermal condition or loading of the transformer. When overheating occurs, it causes the breakdown of oil and paper insulation in the hot spot regions.

Observations from monitoring and field tests also empirically illustrate the concerns about internal heating and damage potential this could cause. In Section 2, Figure 2-35 showed the rise of monitored external tank hotspot on the Meadowbrook transformer during a minor storm on May 10, 1992. This same illustration is provided here as Figure 4-3. As measured, there is a very fast response (on the order of 2-4 minutes) between the onset of a large GIC spike and the sudden and sharp temperature rise at the known hotspot on this transformer tank wall. Since this transformer is located very close to the Fredericksburg Magnetic Observatory, the corresponding rate of change (dB/dt) of the regional geomagnetic field can also be described. Figure 4-4 provides a plot of the observed dB/dt in UT time (5 hour difference between local time used in Figure 4-3). The dB/dt responsible for the ~60 amp neutral GIC observed in the Pennsylvania transformer in Figure 4-3 reached a peak dB/dt of only ~55 nT/min. As previously noted, extreme storm scenarios can produce up to 5000 nT/min disturbance levels. This would be a level ~100 times larger. It is expected that this larger dB/dt could also produce ~100 times larger GIC levels in this same transformer.

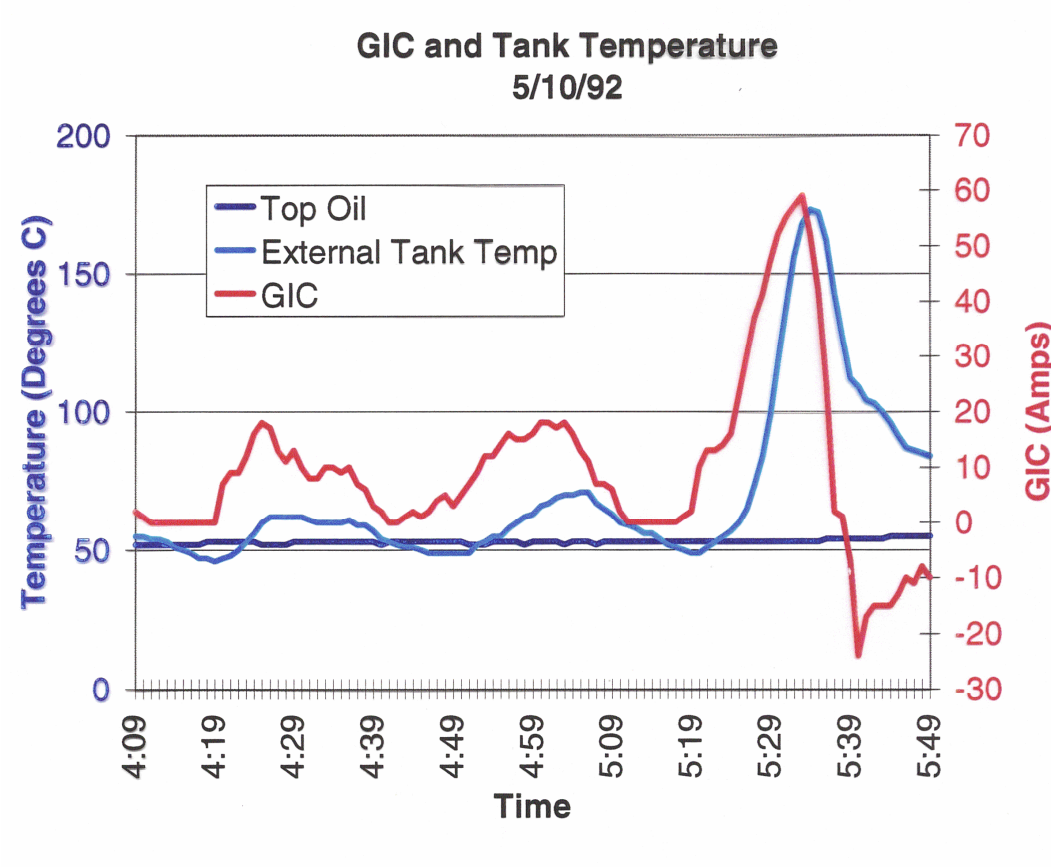

Figure 4-3. GIC and transformer tank temperature for May 10, 1992 geomagnetic storm

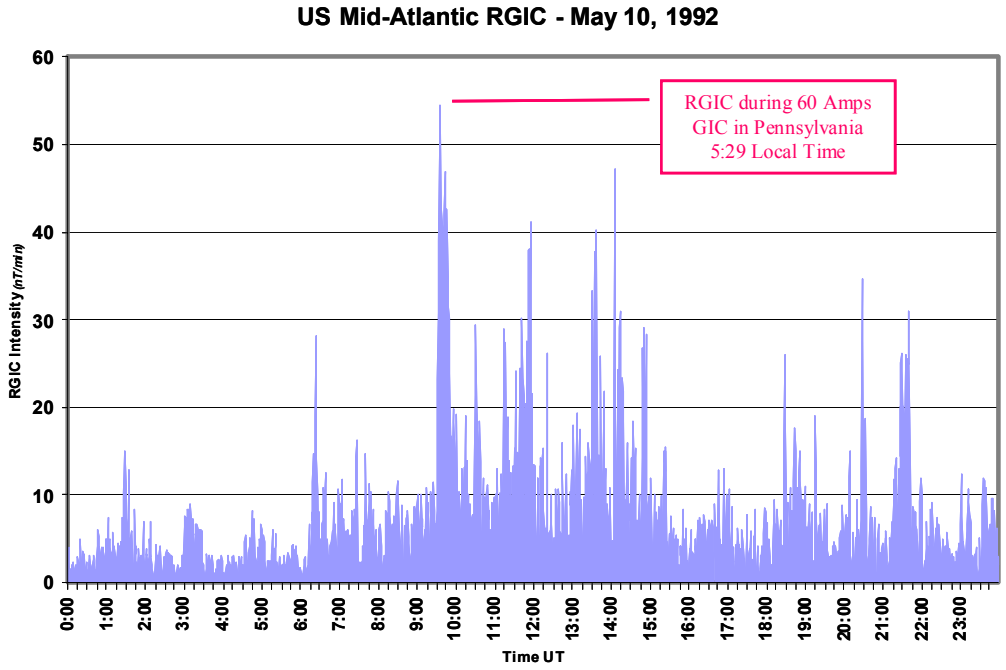

Figure 4-4. Observed dB/dt near Meadowbrook for May 10, 1992 geomagnetic storm.

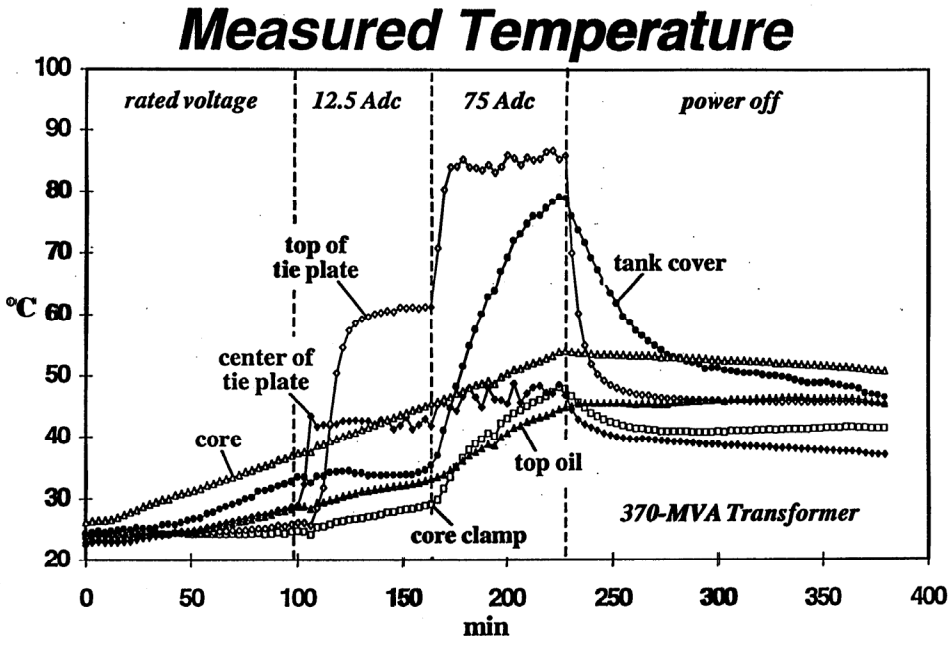

Figure 4-5. Observed temperature from Hydro Quebec tests showing response between two levels of neutral GIC (12.5 amps and 75 amps) and measured temperatures in the transformer in easy-to-access spots.

In Section 2, Figure 2-36 showed the results of measured temperature rises for DC testing of a transformer, which is also shown here as Figure 4-5. As clearly demonstrated by these tests (Reference 4-3), the intensity of the GIC plays an important role in both the level of internal heating and the rate of rise of this heating. Note that when the DC injection is suddenly increased from 12 amps to 75 amps, the temperature (top of tie plate) experiences a sudden increase over a time span of only three minutes.

Other reports also correlate sudden storm commencement (SSC) geomagnetic disturbances with incidents of transformer failures. Figure 4-6 provides a plot from a paper noting observations of the sudden onset of a geomagnetic storm with a transformer failure in New Zealand which occurred on Nov. 6, 2001 (Reference 4-4). The SSC has an onset and rise time very similar (though much smaller in GIC intensity) to that posed by an E3 HEMP threat scenario. This indicates that even brief duration GIC events can lead to transformer failures.

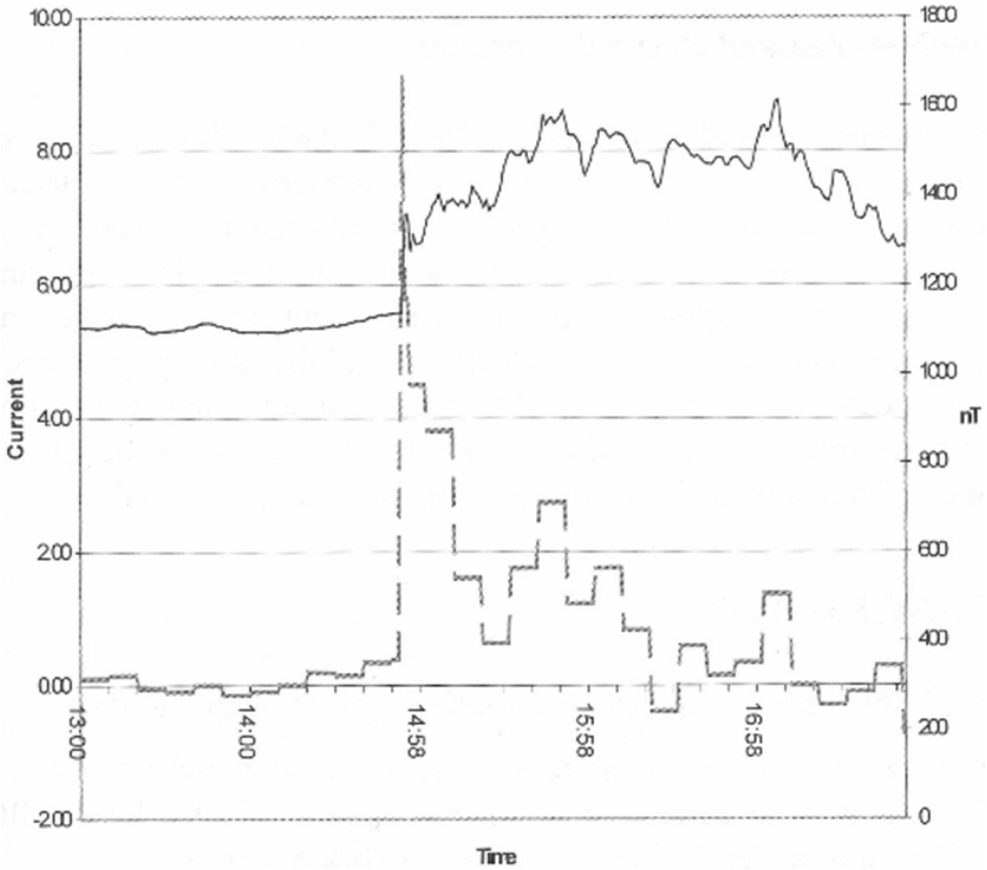

Figure 4-6. Observed SSC and sudden failure of New Zealand transformer, Nov 6, 2001.

Further analysis of the failure of the Salem Nuclear Plant GSU transformer also provides insights on possible large intensity but short duration GIC events and the potential for transformer failure. Figure 4-7 provides a plot of the dB/dt observed at Fredericksburg (FRD) which is nearby the Salem plant. As noted, several of the most energetic substorm intervals were simulated on the U.S. Power Grid Model to estimate GIC levels. It is also shown that the peak dB/dt of ~470nT/min was observed at 21:44 UT. As previously shown in Figure 2-34, the GIC in the Salem transformer was plotted over all four of the important substorm intervals, with the highest GIC occurring around 21:44 UT. The GIC reached a peak of ~90 amps/phase around the 21:44 UT peak dB/dt. Figure 4-8 provides a more expanded scale plot of the Salem GIC for the substorm time interval from 21:20 to 22:30 UT. As shown in this plot, the duration of the peak GIC levels are very brief (less than 2 minutes), yet were able to cause permanent and extensive damage to this large GSU transformer.

Subsequent analysis was undertaken by Girgis (Reference 4-5), providing analytical examinations of a transformer of this design, as well as another transformer that has design features that make it somewhat more tolerant of GIC exposure. Figure 4-9 provides a plot of the GIC level and load level that can be tolerated on a transformer of design like that at Salem. It should be noted that for a neutral GIC of as little as 90 amps (or equivalent to 30 amps/phase), the transformer can no longer have any load or there is risk of permanent damage. This situation would be particularly problematic for large baseload GSU transformers, as loading on these apparatus are nearly always operated at nameplate MVA rating.

Other analytical examinations of GIC thresholds came to similar conclusions. In their transformer design analysis (Reference 4-6), the authors Hurbert and Berthereau provide an equivalent of a short-time emergency overload guide to determine the amount of time that a transformer can withstand GIC. This overload guide is provided in Figure 4-10 and has DC current exposure limit results for the un-optimized transformer design similar to that noted by Girgis, et.al. The work by Hurlet also indicates that even optimized designs have limited time durations of GIC exposure, though with higher thresholds. Therefore if a storm occurs which produces 10 to 100 times higher GIC levels, then damage potential is plausible for these more robust transformer designs as well. It should further be noted that this work covers only a few of the multiple design variations that exist for these transformers and that this work also contained other limitations in the analysis on the scope of the problem. However, the summary of both empirical experience and various analytical determinations provides a basis for estimating potential at-risk transformers for large and severe storm events that are yet to occur on today's power grid infrastructure.

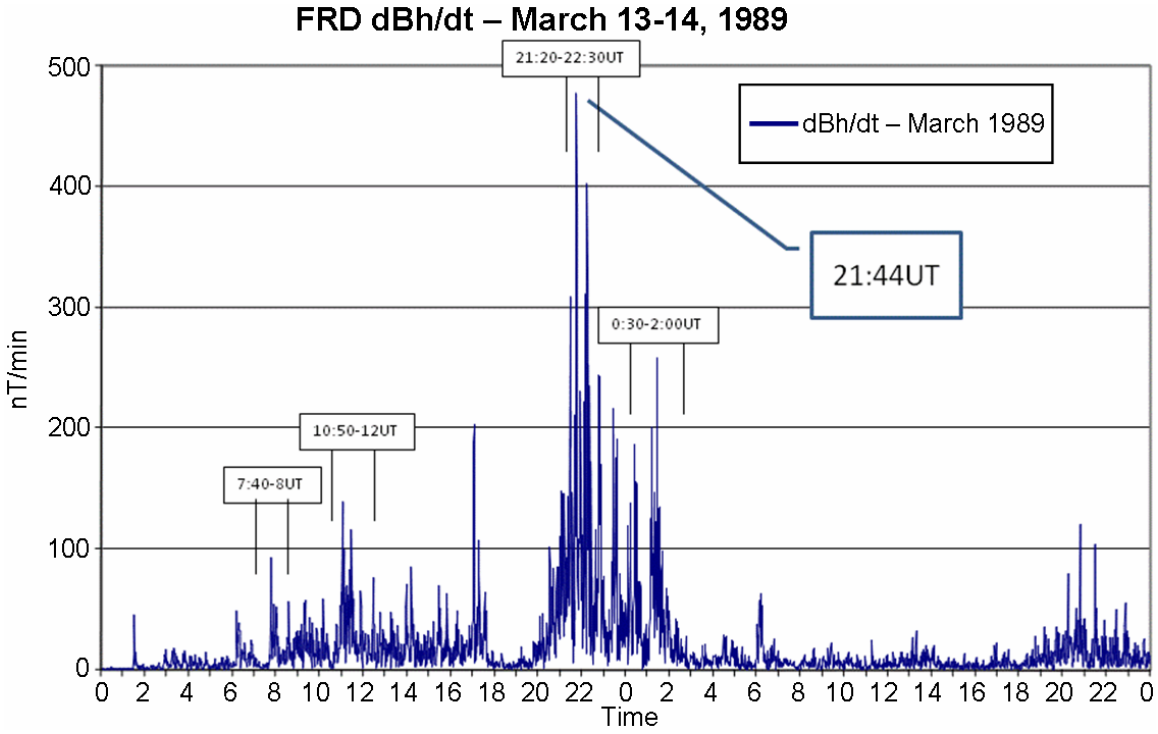

Figure 4-7. Specific storm intervals on March 13-14, 1989, selected for forensic analysis using FRD observatory.

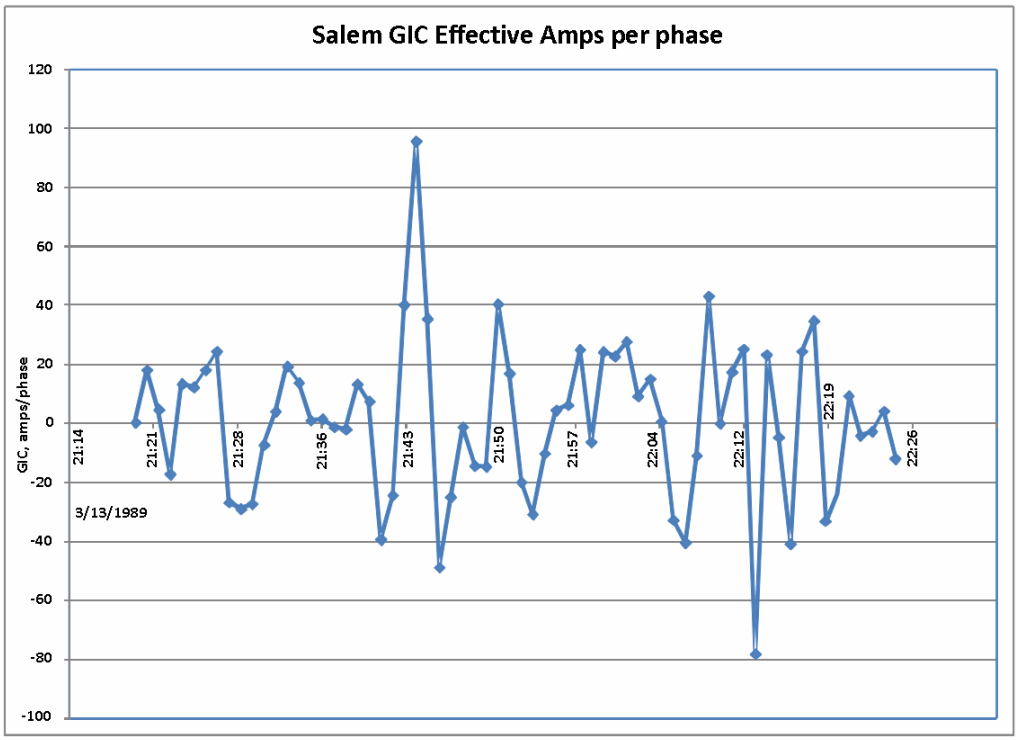

Figure 4-8. Estimated GIC in Salem GSU on March 13, 1989.

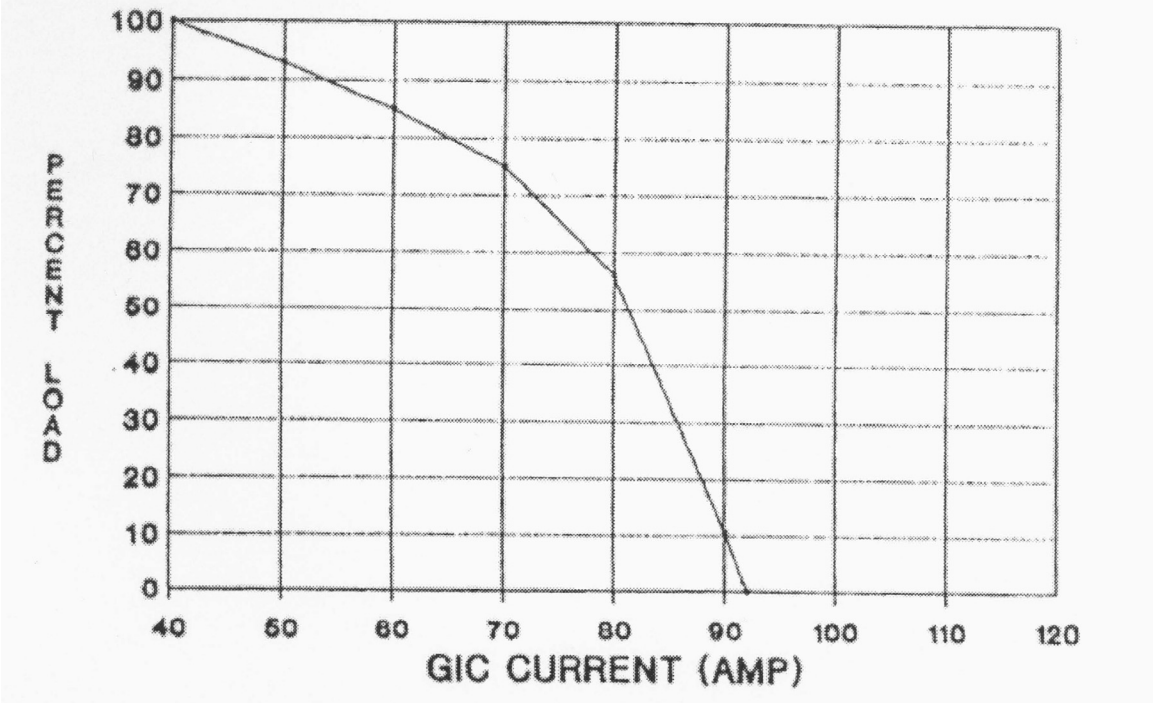

Figure 4-9. GIC vs loading for transformer (from Girgis, et al.). It is important to note that GIC plotted here is neutral current; therefore 90 amps would be 30 amps/phase.

Time withstand with GIC

	Time with optimisation and transposition	Time without optimisation and transposition
100 Amp Gic	23 mn	0 mn
50 Amp Gic	> 2h	3 mn
25 Amp Gic	> 2h	33 mn

Figure 4-10. Table of GIC time withstand, from Hurlet, et al.

4.2 Overview of Potential Impacts to EHV Transformers due to High GIC Levels

Very large GICs from extremely intense geomagnetic storms could pose the concern of large-scale and geographically widespread failures and permanent loss of the EHV transformers on the network. If enough of these key assets are lost, the restoration of the EHV power grid could also be considerably delayed. Because there is considerable uncertainty as to the threshold level of GIC that will cause transformer failure, two levels of minimum GIC (30 amps per phase and 90 amps per phase) were considered as the screening level for possible transformer failure for the severe geomagnetic storm 4800nT/min threat environment. For evaluations that were reported to the National Academy of Sciences and for the economic impact analysis performed for FEMA, a damage level threshold of 90 amps/phase was utilized, which makes overall estimates of damage levels more conservative. In contrast, a 30 amp/phase level is the approximate GIC withstand threshold for the Salem nuclear plant GSU transformer and possibly for others of similar less robust design in the legacy population of U.S. EHV transformers. Also, it is also important to note that other transformer failures have been observed at much lower thresholds and that other transformers have been exposed to levels higher than 30 amps/phase without indication of permanent damage. These variations largely stem from the diversity of design of the internal core and coil assemblies of large EHV transformers.

In this analysis, a determination is only being offered at this time for the 4800 nT/min storm scenario at 50 degree geomagnetic latitude for all 345, 500 and 765kV transformers in the U.S. Power Grid. Figure 4-20 provides a map of the location of all exposed EHV transformers with GIC of 30 amps per phase or greater in the eastern portion of the U.S., where generally the greatest levels of GIC occur and the at-risk transformer population is concentrated. The relative intensity of the GIC flow is also shown in this figure.

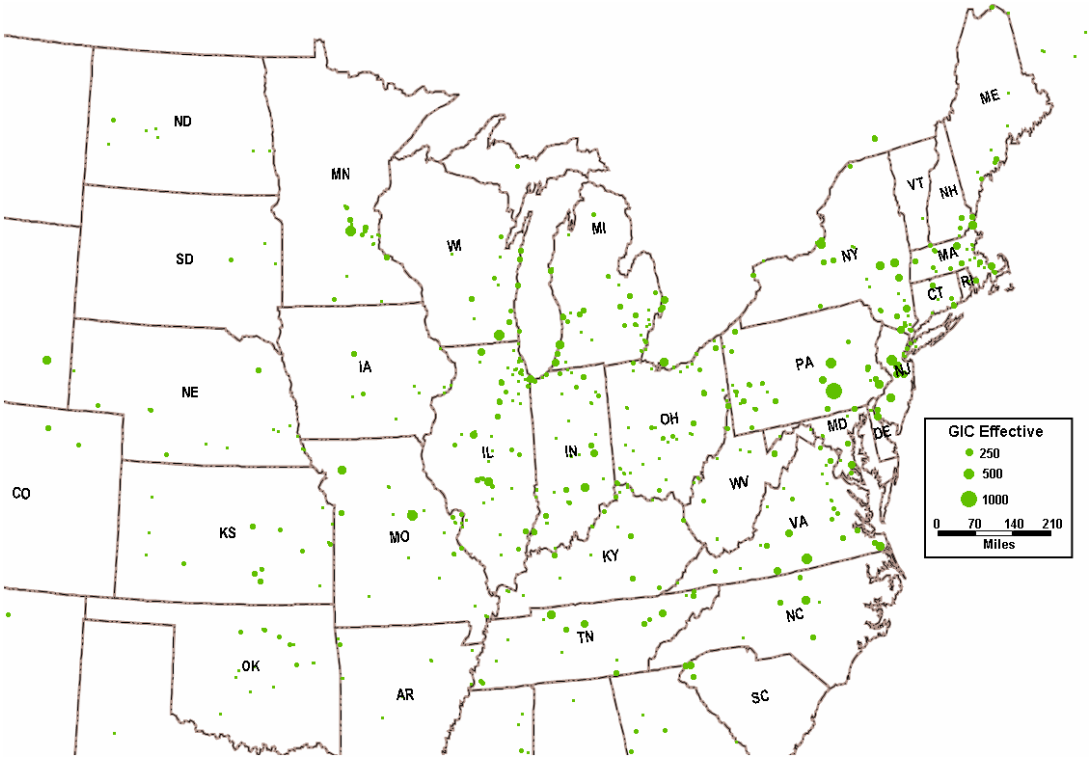

Figure 4-11. Transformers with GIC-effective of 30amps per phase or greater for the model that includes 765kV, 500kV and 345kV transformer detail. The threat environment is 4800nT/min at 50^{o} latitude.

To provide further perspectives on the intensity of the 4800 nT/min threat scenario, Figure 4-12 provides a comparison of GIC levels estimated for the peak conditions of the March 13, 1989 storm versus this more severe storm event. As displayed in this figure, the top 200 EHV transformer GIC flows are ranked for both of these storms. Because the 4800nT/min threat environment is ~10 times larger than the peak March 1989 storm environment, this comparison also indicates that resulting GIC peaks will also in general be nearly 10 times larger as well. For the March 1989 storm, peak GICs of less than 200 amps/phase were estimated, while the peak GIC levels are as much as 1800 amps/phase for the severe storm threat scenario.

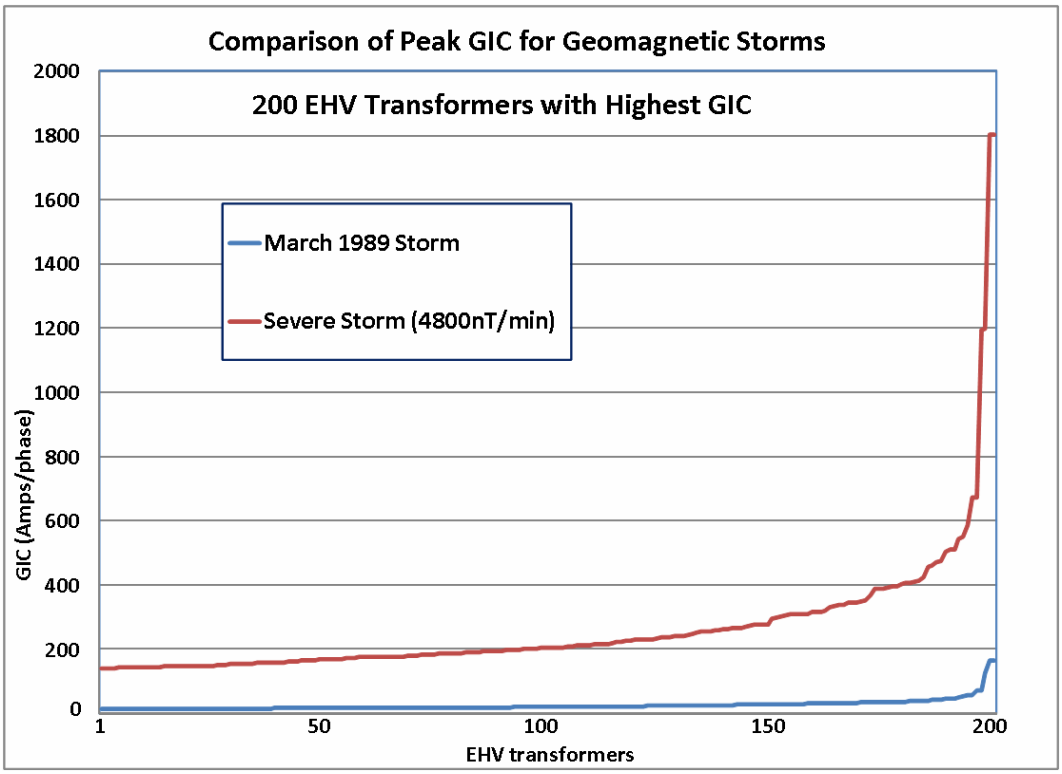

Figure 4-12. Comparison of peak transformer GIC levels for March 1989 storm and severe geomagnetic storm scenario.

Table 4-1 provides a summary for both a 90 amp (left hand side) and 30 amp at-risk thresholds. The left hand side of Table 4-1 provides a summary of the at-risk 345kV transformers for each state using a 90 amps/phase GIC threshold. The quantities provided are the at-risk MVA of 345kV transformer capacity for each state, the at-risk number 345kV transformers and the percent of the total 345kV transformer capacity at-risk for each state. The right hand side of Table 4-1 provides a similar summary for each state of the at-risk 345kV transformers only using a lower 30 amps/phase GIC damage threshold. In all cases, substantially greater percentages of the 345kV transformer infrastructure would be considered at-risk and permanently damaged due to this lower GIC threshold criteria. A summary is provided at the bottom of each threshold level that indicates that the lower GIC level could increase the damage by a factor of 2 or more.

Table 4-1. Comparison of 345kV at-risk transformers for 90 amp/phase and 30 amp/phase GIC levels

90 Amp GIC At-Risk Threshold

345kV At-Risk Transformers (90 Amp/phase GIC Level)

State	345kV MVA	# of At-Risk 345kV	% of MVA Capacity
AR	600	1	30.1%
CO	2,430	6	29.6%
CT	1,376	5	15.8%
IA	1,060	2	8.6%
ID	2,750	4	38.2%
IL	5,540	20	9.4%
IN	10,896	21	26.5%
KS	4,401	8	27.5%
KY	1,467	4	10.6%
MA	5,764	12	33.3%
ME	2,332	4	45.3%
MI	63,495	27	35.4%
MN	5,342	9	27.0%
MO	4,241	7	17.1%
ND	400	1	7.4%
NE	1,408	4	10.6%
NH	930	4	100.0%
NJ	1,385	2	38.1%
NM	235	1	1.7%
NV	680	2	11.3%
NY	12,274	20	29.0%
OH	8,555	15	15.0%
OK	1,049	3	6.3%
PA	2,234	4	14.7%
SD	400	1	11.5%
UT	3,638	6	23.4%
VT	448	1	29.6%
WA	3,944	6	86.8%
WI	6,459	13	35.6%
WY	690	1	24.6%
345kV Total	**156,423**	**214**	**20.0%**

30 Amp GIC At-Risk Threshold

345kV At-Risk Transformers (30 Amp/phase GIC Level)

State	345kV MVA	# of At-Risk 345kV	% of MVA Capacity
AR	1,400	3	70.2%
AZ	625	1	5.9%
CA	600	2	100.0%
CO	6,800	15	82.7%
CT	2,991	10	34.3%
IA	3,908	9	31.9%
ID	3,698	7	51.4%
IL	27,702	87	46.8%
IN	25,590	62	62.2%
KS	9,851	19	61.5%
KY	5,848	12	42.2%
MA	13,256	27	76.5%
ME	4,232	8	82.2%
MI	125,374	56	70.0%
MN	12,552	23	63.4%
MO	15,160	28	61.2%
ND	3,598	10	66.9%
NE	6,491	15	49.0%
NH	930	6	100.0%
NJ	1,385	2	38.1%
NM	3,547	9	25.3%
NV	3,300	12	54.8%
NY	25,530	55	60.4%
OH	32,500	69	56.9%
OK	10,800	21	64.7%
OR	554	1	100.0%
PA	9,049	18	59.5%
RI	479	1	24.6%
SD	1,000	3	28.7%
TX	7,620	13	6.4%
UT	10,721	25	69.1%
VA	732	1	32.9%
VT	1,512	3	100.0%
WA	4,544	7	100.0%
WI	10,620	27	58.5%
WV	3,277	6	39.9%
WY	2,700	4	96.4%
345kV Total	**400,476**	**677**	**51.2%**
Increase %	**156.0%**	**216.4%**	

Table 4-2. Comparison of 500kV at-risk transformers for 90 amp/phase and 30 amp/phase GIC levels

90 Amp GIC At-Risk Threshold

500kV At-Risk Transformers (90 Amp/phase GIC Level)

State	500kV MVA	# of At-Risk 500kV	% of MVA Capacity
AR	600	1	3.9%
CA	3,547	4	6.9%
GA	8,277	6	20.8%
ID	1,986	2	65.3%
KY	504	1	8.7%
MD	7,187	7	54.8%
MS	1,200	1	7.7%
MT	2,229	3	37.1%
NC	6,147	6	37.2%
NJ	12,637	13	100.0%
NY	995	1	100.0%
OR	16,908	16	71.0%
PA	17,518	25	77.7%
SC	1,459	3	60.4%
TN	10,899	9	37.8%
VA	16,919	18	47.2%
WA	18,784	16	33.7%
WV	3,557	5	45.7%
500kV Total	**131,353**	**137**	**28.4%**

30 Amp GIC At-Risk Threshold

500kV At-Risk Transformers (30 Amp/phase GIC Level)

State	500kV MVA	# of At-Risk 500kV	% of MVA Capacity
AL	2,544	2	13.3%
AR	6,522	12	42.1%
AZ	672	1	2.4%
CA	14,043	12	27.4%
DE	2,379	3	100.0%
GA	20,232	15	50.8%
ID	3,042	3	100.0%
KY	5,801	5	100.0%
MD	12,008	15	91.5%
MN	1,344	2	35.0%
MO	1,501	2	100.0%
MS	4,724	7	30.5%
MT	2,229	3	37.1%
NC	10,840	10	65.6%
NJ	12,637	13	100.0%
NM	1,680	2	39.2%
NV	866	2	13.5%
NY	995	1	100.0%
OR	18,610	22	78.1%
PA	21,603	33	95.8%
SC	1,459	3	60.4%
TN	24,007	21	83.3%
VA	31,882	42	88.9%
WA	37,296	36	66.9%
WV	6,401	18	82.3%
500kV Total	**245,317**	**285**	**53.0%**
Increase %	**86.8%**	**108.0%**	

Table 4-2 provides a similar state-by-state summary for the 500kV transformers that would be considered at-risk depending upon the current 90 amp GIC threshold or the lower 30 amp GIC threshold. This comparison also indicates that an approximate doubling of the at-risk 500kV transformers would occur using the lower 30 amp threshold. Table 4-3 provides the comparison summary for the 765kV transformers. This also shows a trend similar to that for the 345 and 500kV infrastructures which would place a much higher percentage of this infrastructure at-risk using the lower GIC thresholds.

Table 4-3. Comparison of 765kV at-risk transformers for 90 amp/phase and 30 amp/phase GIC levels.

90 Amp GIC At-Risk Threshold

765kV At-Risk Transformers (90 Amp/phase GIC Level)

State	765kV MVA	# of At-Risk 765kV	% of MVA Capacity
IL	6,240	6	65.0%
IN	1,680	1	13.4%
KY	1,587	1	100.0%
NY	1,872	2	38.6%
OH	1,660	1	14.9%
VA	4,755	4	59.4%
WV	3,087	2	21.1%
765kV Total	**20,881**	**17**	**31.8%**

30 Amp GIC At-Risk Threshold

765kV At-Risk Transformers (30 Amp/phase GIC Level)

State	765kV MVA	# of At-Risk 765kV	% of MVA Capacity
IL	9,600	9	100.0%
IN	6,218	6	49.6%
KY	1,587	1	100.0%
MI	3,208	2	100.0%
NY	4,848	4	100.0%
OH	6,640	3	59.6%
VA	6,465	5	80.7%
WV	11,310	11	77.2%
765kV Total	**49,876**	**41**	**76.0%**
Increase %	**138.9%**	**141.2%**	

These at-risk transformers also represent a diverse population of function and high and low side kV and MVA ratings. The at-risk populations are made up of auto and non-auto transformer types with a variety of primary and secondary voltage ratings and MVA capacity ratings that were designed specific to their grid location purposes. This diversity underscores the problems of providing spare equipment for such large scale infrastructure failures. Also from a world market manufacturing perspective, these numbers of failures exceeds the annual production in the world of transformers of this kV rating and MVA size class. Normally, only a handful of transformers of this size are purchased for U.S. locations on an annual basis. Therefore the immediate replacement of such a large scale failure of the infrastructure could pose serious challenges and add considerable delays to the restoration process for the power grid.

Of particular concern would be the permanent loss of large GSU (generator step-up) transformers at power plants in the northeastern region of the U.S. (i.e. NE Quad). The loss of these transformers causes a compounding of difficulties, in that the EHV transmission network is impaired along with the loss of output of vital and usually baseload nuclear, coal, and hydro-electric generation resources for the power grid. There are a considerable number of the large GSU transformers "at-risk" due to GICs of at least 30 amps per phase in these units. Approximately 128,000 MVA of GSU transformer capacity would be at-risk, which is ~63% of all large power plant GSU's in the NE Quad. In total there is ~430,000 MVA of generation capacity in the NE Quad, which means that nearly 50% of the generating capacity in the NE Quad are numerous smaller capacity units which connect into the power grid at 161kV and lower operating voltage levels. In general, it is likely that most of these smaller generating units would not be baseload, but would more likely be peaking units that would typically operate for a limited number of hours on an annual basis. It is also possible that these smaller generators may not be fully staffed or have sufficient fuel resources available to provide meaningful continuous operation during an emergency. From this larger base of generation, the large-size at-risk GSUs and associated generators constitute ~30% of all NE Quad generation resources. It would also be expected that these are predominantly baseload generators which are vital to operation of a stable interconnected grid. Figure 4-13 provides a graphic summary of the fuel types for the generators that are associated with the at-risk GSU transformers. As shown in this summary, ~82% of the generators at-risk are the large nuclear and coal fired power plants. The loss is particularly important for the nuclear capacity since ~92% of all nuclear generation in the NE Quad would be out of service long-term.

An analysis of at-risk GSU transformers was also carried out using the higher 90 amp per phase GIC threshold. As in the previous analysis of all at-risk transformers, the percentages decrease at this higher threshold, but still indicate potentially severe recovery problems for the NE Quad due to loss of these GSU transformers. A total of 94 GSU transformers are at-risk with a combined MVA capacity of ~64,000 MVA (~15% of total NE Quad generation capacity). Again this at-risk population would generally represent the largest and most important of the baseload generation in the NE Quad. Figure 4-14 provides a similar summary of the amount of at-risk generators by fuel type. Similar to the analysis performed at the 30 amp threshold, ~77% of the at-risk generators are coal and nuclear fuel types for the 90 amp threshold.

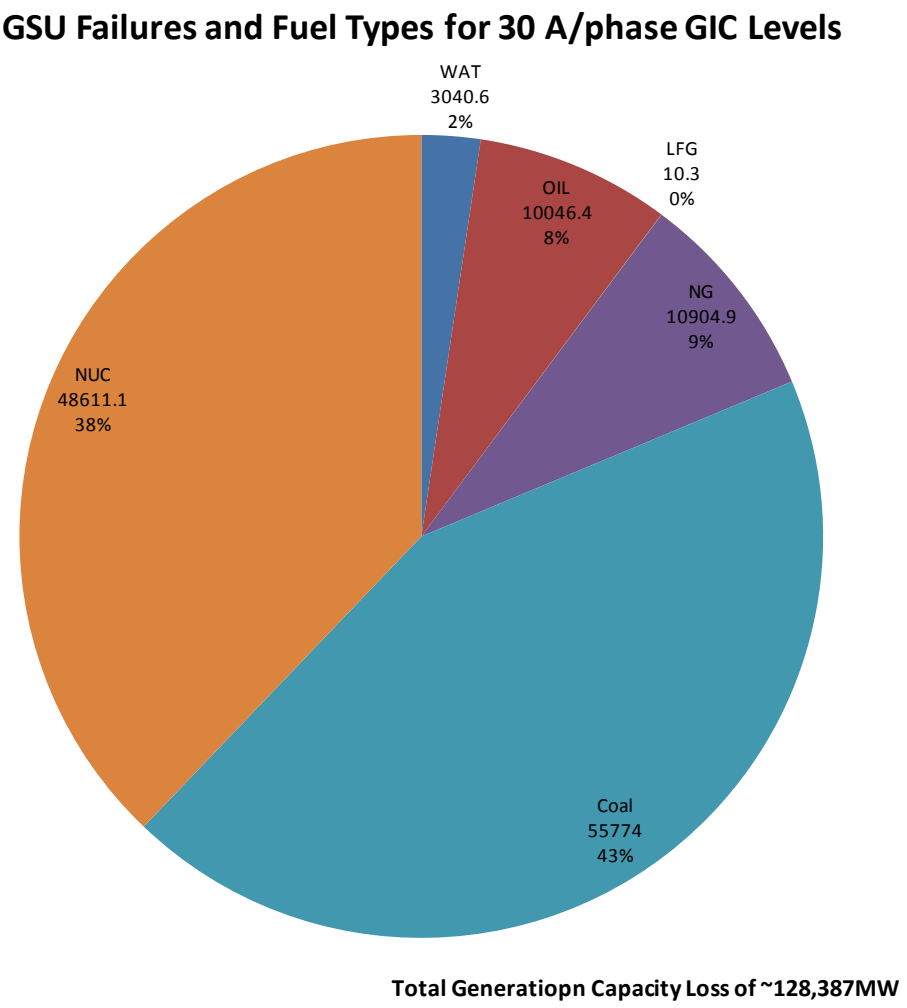

Figure 4-13. Fuel types for power plants associated with at-risk transformers with 30 amp/phase of GIC.

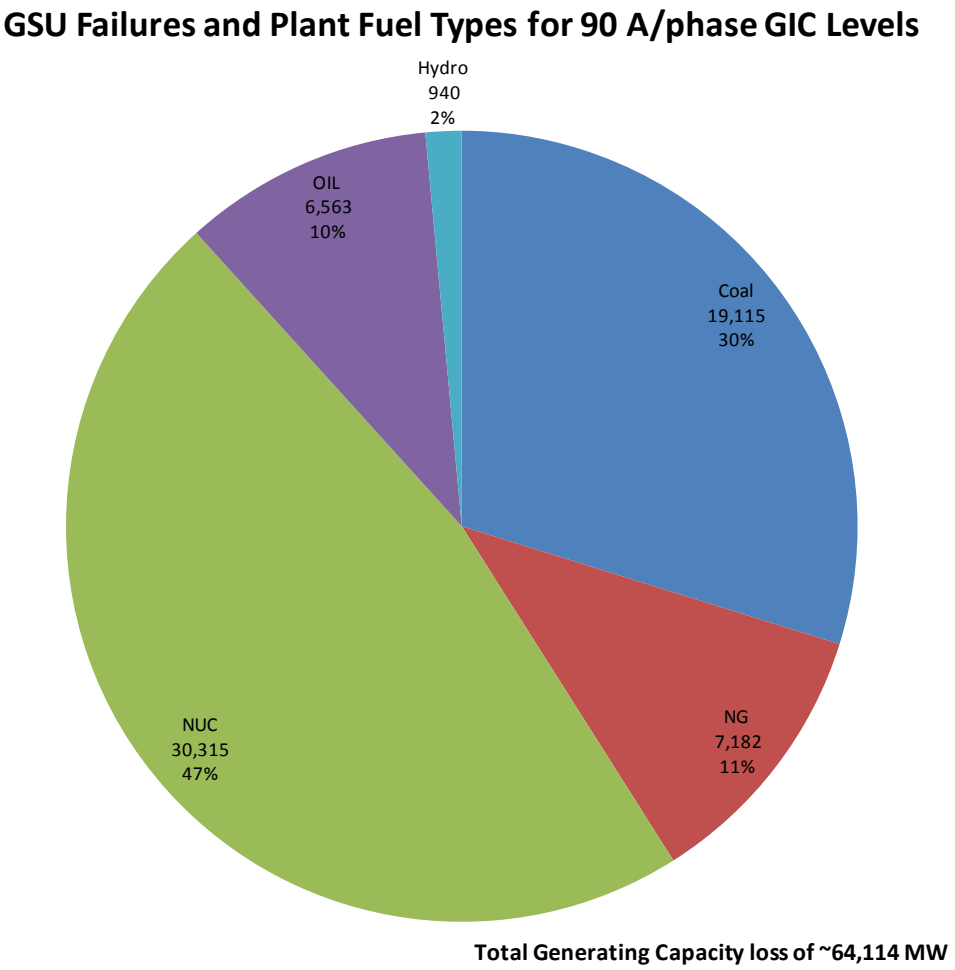

Figure 4-14. Fuel types for power plants associated with at-risk transformers with 90 amp/phase of GIC.

4.3 Overview of Emergency Replacement of EHV Transformers

The failure of many large EHV transformers and the need to suddenly replace a large number of them has not been previously contemplated by the U.S. electric power industry. Under normal conditions, the purchase placement of a single EHV transformer order in the 300-400MVA class has normally been quoted as taking up to 15 months for manufacture and test. For larger sizes of transformers and transformers with special reactance or tap-changer requirements, several months may need to be added to the above mentioned figure, and the suitability of qualified manufacturers may be more limited.

Of course, manufacturing and testing the equipment does not mean the story ends there. The equipment will then need to be transported to site and commissioned before being put into service. The size and weight of large EHV transformers precludes the concept of airlifting from an overseas destination for emergency replacements, even if a suitable spare is readily available. This means at least several weeks of ocean transport for apparatus of foreign source. When such heavy equipment arrives at the border or port, it

almost always requires permission from municipalities and highway/transport authorities, as they are slow moving and heavy. For example, it may take one week to move a 250MVA transformer a short distance in major metropolitan areas (larger ones up to 1000 MVA in size are even more problematic). Even the distance of a few miles may take an entire weekend, as a number of traffic lights have to be removed and reinstated as the load is moved at snail's pace in special trailers and the route taken has to be fully surveyed for load bearing capability by civil engineers and certified. In normal times, it is not unusual for some 6 months of notice being requested for the movement of such loads to coordinate all the certification details with each impacted local, state and federal unit of government involved in transportation and logistic details such as these. (Figure 4-15 provides a photo of several transformers being moved using specialty moving trailers). Once the transformer is at the site, then affixing oil radiators, installing bushings, filling with specialty transformer oil (heated if a cold-weather situation), drawing vacuum on the transformer before sealing to the atmosphere, installing oil circulating pumps, and various relay and control auxiliaries is required. An installation process can take several days with a large trained crew in the best of circumstances. If the replacement transformer is from an in-service unit, moved from an different location to a the existing location, then even more preparation steps are necessary to disassemble and prepare the unit for shipment; this includes the draining of oil, removal of bushings, radiators, and auxiliaries. The matter of compatible foundations and oil-containment substructures is also a site-specific challenge, along with various EHV bus re-configurations due to differing heights and layouts of connections at primary and secondary voltage levels.

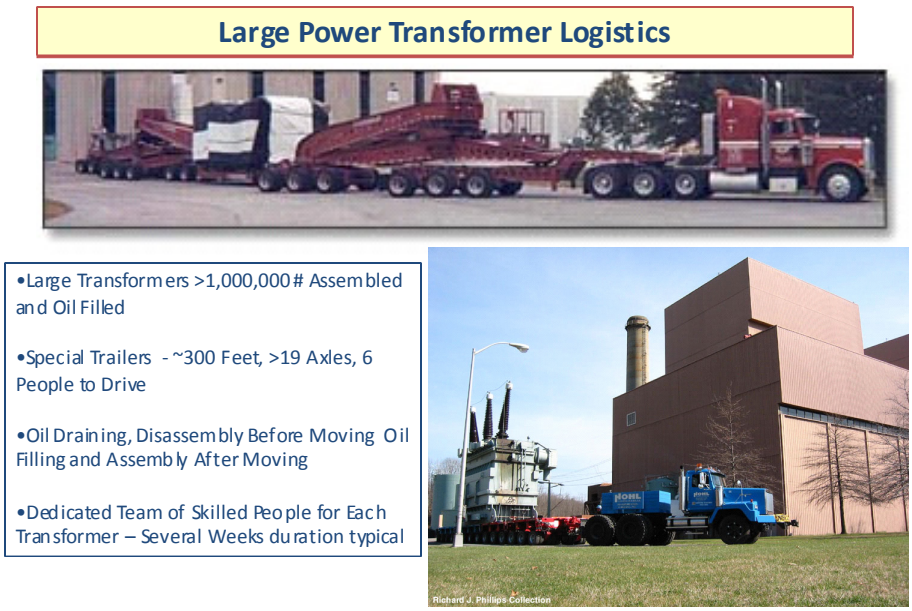

Figure 4-15. Top photo is transformer with EHV bushings and external oil cooling radiators removed for transport. Bottom photo is 230kV class transformer being relocated at a power plant site. The smaller size of this transformer and the short distance of move (within the power plant property) did not require removing HV Bushings from transformer.

Shipment of large MVA transformers may also require specialty railcars (Schnabel cars for instance), to meet height/weight limitations on most corridors in North America. Also specialty high axle trailers and heavy lift cranes to transport units may be needed from the nearest available rail siding to actual substation location.

Of course, in modern utilities there is always some heavy electrical equipment surplus due to requirements or retired equipment that is out of service. For example, a typical utility may have a few 40-year old transformers in the 115 to 230kV class and circuit breakers and capacitors that are not connected but have been left at the site at which they were originally installed. Moving these items in an emergency will inevitably cause further disruption and of course there is no full guarantee that the equipment which has not been energized for a long time will instantaneously work. Such equipment will still need to be rigorously checked and tested before being put into service. At EHV levels, the standard approach to spares has been to purchase an extra single phase transformer for a three phase bank. The transmission network at these voltage levels is generally designed to be somewhat redundant. However, with high utilization of the transmission network brought on by increased wholesale market activities, generally high rates of transmission network congestion and utilization are becoming the norm in the U.S. For large GSU (generator step-up unit) transformers, a pooling arrangement is generally done for spares, where one unit can be used to serve as a spare at as many as 6 different plant locations. This works conceptually if there is no wide spread rate of failures. Com Ed (Chicago area) experienced 4 large GSU transformer failures in a month in 1994,

possibly due to recurrent low level geomagnetic storm activity, and as a result had to arrange to borrow spares outside their system when they could no longer recover from the outages with their own inventory of spare GSU transformers.

With such long lead times for most transmission assets, and in order to be able to adequately respond to incident recovery, it has been essential that utilities develop strategies for asset procurement, the holding of strategic spares, and the way the system can be used to provide redundancy. However, not all systems can boast having the luxury of adequate redundancy for such eventualities. NERC has facilitated some coordination of spare parts and equipment inventories under their STEP program. While the details are not publicly available, this program does not include EHV GSU transformers, rather only bulk auto and non-auto transformers on the 500, 345, and 230kV portions of the network. Since only a few electric utilities own 765kV equipment, this kV rating is not included in the STEP program. About 170 spare or working transformers are committed to this program, but details as to size and winding configuration specifics are not publicly available.

Spare transformers on a loan basis is also problematic and the concept has limited utility due to the large diversity of kV and MVA ratings that are common in many custom built transformers. For example, as shown in Figure 4-16, transformers across the New York, New England, and Pennsylvania region have differing designs and cannot be readily substitutable in any specific location. Further, a large catastrophic event would cause simultaneous needs to develop in many locations for the limited spares that would be available for EHV apparatus.

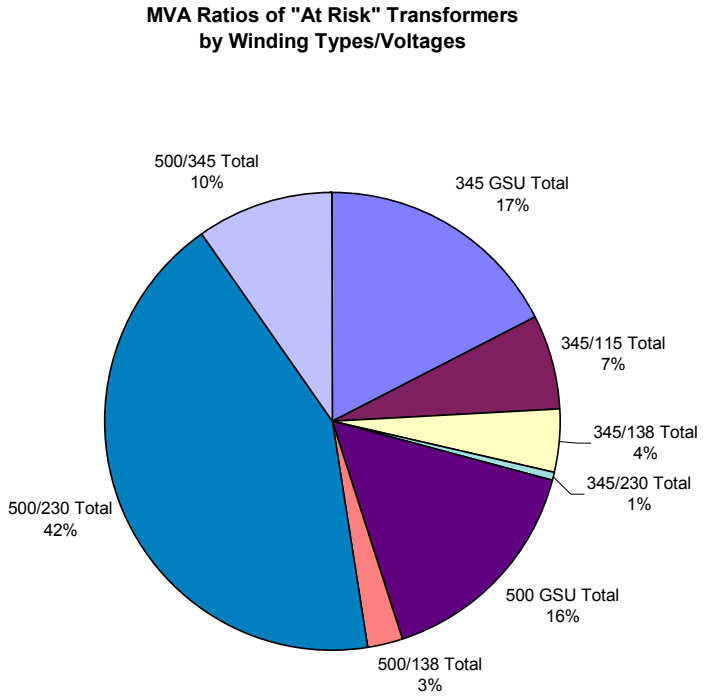

Figure 4-16. Diversity of transformer operating voltages design type is quite high in the New England through Pennsylvania region of the U.S., making substitution of shared spares a largely unworkable concept.

Along these lines but not related to severe geomagnetic storm scenarios, a rapid recovery option had been explored to deal with potential damage to large transformers and other transmission line equipment. This is the approach of buying and pre-positioning equipment (primarily small but transportable extra high voltage transformers) over a period of many years. This approach was investigated by EPRI for the Department of Homeland Security as a response to coordinated physical terror attacks on major substations on the high voltage grid. Because these transformers can take a year or more to replace, the impact of coordinated physical attacks could cause long-term disruption of power supply in one or more of the targeted major metropolitan areas (Reference 4-7). The benefit of this approach is that there may also be a partial option for rapid recovery due to a severe geomagnetic storm that would cause an even wider degree of transformer damage. This program was conceived to cover terrorist damage to unmanned high voltage substation transformers (about one-half the population of key transformers). This program could also offer mitigation assistance for GIC damage scenarios/concerns, but there are important limitations and gaps:

- The spares are only intended to cover terrorist damage to unmanned high voltage substation transformers (about one-half the population of key transformers).
- Important generator step-up (GSU) transformers, which are at manned stations (and therefore unlikely targets for a terrorist attack), are not being considered for a physical attack threat.
- MVA size of the specially designed replacement transformers will be very limited, ~300 MVA without supplemental oil cooling equipment and may need to fit into +1000 MVA slots (requiring reduced/limited transfer levels).
- Will be auto-transformer only design: non-auto, tap changers, and phase shifters which are important in some metropolitan regions are not being considered.
- Because of a large number of diverse voltage configurations, even for auto-transformers, a large number of devices need to be procured.

Important EHV generator step-up transformers, which are at manned stations, are not being considered for a physical attack threat but would be heavily exposed to GIC from severe geomagnetic storm scenarios. Rapid recovery of the power grid without taking into consideration these key transformers would not be possible, furthermore, a small transportable transformer design may not be applicable to replace the very large capacity generator transformers. However, there are potential benefits to incorporating this possible future set of resources into the analysis that will be needed to determine the optimal mix of GIC hardening and mitigation strategies.

References

4-1 C. T Gaunt, G. Coetzee, “Transformer failures in regions incorrectly considered to have low GIC-risk”, IEEE Power Tech 2007, 1-5 July 2007, Lausanne, Switzerland, Paper 445.

4-2 P. R. Price “Geomagnetically induced current effects on transformers”, IEEE Trans on Power Delivery, vol 17, no 4, October 2002, p1002-1008.

4-3 P. Picher, et.al., Discussion to Paper "Study of the Acceptable DC Current Limit in Core-Form Power Transformers", IEEE Winter Power Meeting, Baltimore MD.

4-4 J. Beland, K. Small, "Chapter 15: Space Weather Effects on Power Transmission", Effects of Space Weather on Technology Infrastructure, edited by I. A. Daglis, Kluwer Acad., Norwell, Mass., pages 287-300, vol. 176, 2004.

4-5 R.S. Girgis, C.D Ko, "Calculation Techniques and Results of Effects of GIC Currents as Applied to Two Large Power Transformers", IEEE Transactions on Power Delivery, Vol. 7, No. 2, April 1992.

4-6 P. Hurlet, F. Berthereau, "Impact of geomagnetic induced currents on power transformer design", IEEE Conference MATPOST'07 - LYON (France), JST Transformateurs, France.

4-7 Craig L. Stiegemeier, Ramsis Girgis, "Rapidly Deployable recovery Transformers", IEEE Power and Energy, Vol 4, Number 2, March /April 2006, pp. 38-45.

Appendix 1
Disturbance Impact Criteria for the U.S. Power Grid

Low voltage electric distribution systems are designed to operate radially and over geographically small subsystems. Unlike the distribution system, which is compartmentalized to protect from widespread risks, the transmission network is tightly interconnected and every station has redundant feeds from a geographically widespread grid. However, this design feature introduces new failure concerns in that a distinguishing characteristic of bulk transmission systems is that severe disturbances that occur in them can have a system-wide impact. Because the transmission networks in the U.S. are tightly interconnected, the concern also becomes failure modes that can cascade a failure or collapse from one region into neighboring interconnected and unaffected regions as well.

A1.1 Overview of U.S. Transmission Grid Design Criteria

Because these bulk transmission systems are geographically widespread and critical infrastructures, it is not possible to physically test the reliability of the power grid to the multitude of probable and severe disturbances that can occur. Rather, these networks have been designed by use of deterministic design criteria and, for the most part, tested through the application of large-scale network simulation models. The design and operating criteria are aimed at limiting the risk of widespread shutdowns and blackouts, and require grids to be operated in a manner in which they are prepared to survive the most severe contingency. The criteria are commonly called the N-1 design criteria and their application has generally required substantial redundancy in network design, to accommodate the loss of any single element under any probable operating condition. The N-1 design criteria applies to real and reactive power capacity sources, as well as the delivering transmission lines and transformers. The deterministic criteria for bulk power systems will typically include the following requirements:

- Severe Disturbances which include 3 Phase Normal Clearing Faults (~4-5 cycles) and Single Phase Delayed Clearing Fault (~10-12 cycles).
- System operated to withstand Generation Capacity Outage Contingency due to unanticipated loss of single largest generation plant in the pool or region, typically around 1000-1200 MW (Spinning Reserves).
- Withstand extreme contingencies such as simultaneous outage of two parallel lines or entire substation.

These contingencies are tested in simulation through the application of large network models.

This design approach has generally served the power industry very well and has in particular made the U.S. power grid highly reliable. The conventional stresses contemplated above are very localized in nature. This means there are limitations inherent in this design approach when stressed by simultaneous and geographically widespread disturbances, such as those associated with severe geomagnetic storms and HEMP E3 threats. These threats pose a common-mode stress to the network, as these threats can cause simultaneous stresses to occur at multiple locations, and multiple outage

events can arise from independent incident stresses. There are three important failure progressions that are commonly considered in design of the power system: 1) Thermal overload of elements, causing protective systems to interrupt the line or apparatus; 2) Transient instability due to angular accelerations from an initiating disturbance; 3) Voltage instability, where widespread progressive drops in system voltage occur, initiating a complete system collapse. Voltage instability is the most recent and most emergent of the three mechanisms for widespread system failures (Reference AP1-1). Several factors have contributed to this situation. The building of new transmission capacity is more difficult and often delayed, while network loads continue to increase unabated. NERC indicates that between 1990 and 2000 electric power demand in the U.S. increased by 29.4%, while the addition of transmission capacity (345kV and higher) has grown by only 4%.

The increasingly heavy use of the transmission network to accommodate higher power transfers causes burdens on voltage regulation capability, as these power transfers in and of themselves consume considerable reactive power through I^2X losses over the network lines and transformers. To counter some of the concerns of voltage instability, additional design criteria have been adopted, which essentially require that systems provide adequate voltage regulation resources locally. In response, the power industry has employed frequent use of shunt compensation to support voltage profiles on the network. This application of shunt compensation has had the effect of bringing the system instability point closer to normal voltage operating conditions. In many cases, the failure thresholds are so close to normal operating conditions that relatively minor disturbances can and have propagated widespread failures across portions of the U.S. power pools. Figure A1-1 best illustrates these operating concerns. In this figure is a plot of voltage versus power flow across an important transmission network interface between upstate and downstate New York on the New York power pool (Reference AP1-2). This shows the relative sensitivity in this region to increased power flows. Notice at certain transfer levels the voltage starts a steep decline. In essence, the system has been operated over the edge of the cliff and complete voltage collapse is now occurring. What is even more alarming is that this point of collapse is occurring at a network voltage of ~97% of normal, rather than the 70-80% levels that occurred in the past. This sudden transition can, at times, limit the operator's ability to fully recognize when the network has entered a precarious operating posture. Further, the two curves in this case are the system transfer capability, either with or without a 200 MVAR capacitor bank, at the EDIC station being in-service. This is a relatively small change in reactive supply and, as will be shown in the course of this study, sudden increases in system-wide reactive power demands across the state of New York can easily exceed 3000 MVARs due to GIC events, which essentially dwarfs the beneficial attributes of this single capacitor bank being analyzed.

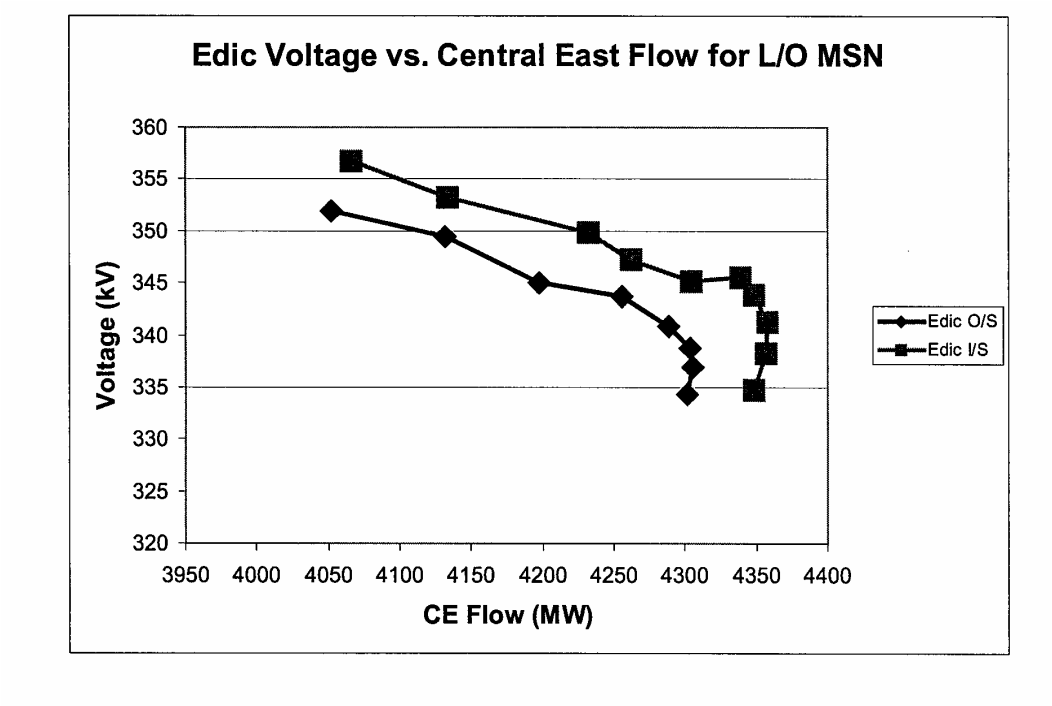

Figure A1-1. NY ISO voltage collapse threshold for system transfers.

Restructuring is also raising concerns over the reliability of the nation's electricity grid, as evolution to a competitive market structure has created substantial new operating and planning challenges for reliability. In this environment, operators are faced with large volumes of transactions, larger areas to control, new players, changing operational responsibilities, movement of power over long distances in response to market signals, shrinking and changing definitions for reserve margins, unpredictable system behavior, and finally, an environment of having to manage systems with operational tools that were designed for a centrally planned and controlled electric grid (Reference AP1-3). Reactive power management is one of the more pressing and yet unmet needs for the power industry. While existing and developing threats require precise knowledge of the available reactive power and voltage regulation reserves on the network, very limited knowledge, in practice, exists in most networks.

These limited disturbance/voltage stability margins and ability to control the system heighten the concern about the capability of the today's network to withstand future probable and severe geomagnetic storm threats, and also increases the likelihood of wider failure footprints for E3 threats to the grid. Until recent developments, power grid operators have generally not had a comprehensive understanding of the threat potentials that could be caused by probable and severe geomagnetic disturbances. Much work has been done on power grids in other world locations (Reference AP1-3), but has not, until this study, been undertaken in large scale for the U.S. (Reference AP1-4). For cases in which power grid operators have performed such analysis, the assessment of impact results indicate that a severe geomagnetic storm event may pose greater stress on the

network than the conventional threats of the design criteria now in use (Reference AP1-5).

This expedited study of U.S. Power Grid infrastructure did not allow sufficient time and resources to perform the wide range of power flow and transient stability simulations of AC power system response due to impacts of storms threats. From a practical standpoint, comprehensive studies of power system behavior under GIC threat conditions are not able to replicate all risk factors. Load flow studies alone provide insights on the voltage regulation risks posed to the system by increased transformer reactive demands (Reference AP1-6). However geomagnetic storms have dual threat concerns: voltage collapse caused by increased MVARs combined with disruptive affects of harmonics/waveform distortions on relay and protective systems, and resulting possibility of wide-spread common-mode failures of critical system elements (i.e. tripping of capacitor banks, when that device is needed for voltage support, can rapidly escalate decay of system integrity). A comprehensive assessment of harmonic interactions would require, as a starting point, large-scale harmonic load flow calculations, which have not previously been performed on bulk transmission system models. Still, such studies would not take into account relay malfunction impacts, and a review of all possible relay malfunctions is also beyond the scope of this effort. As an appropriate screening guide for assessment of potential collapse, a disturbance energy function is derived from the deterministic design criteria and assessments of operational experience from prior storm threats. This provides a means to assess the accumulated impacts of prospective widely spread increases in reactive power demands, and evaluate against a set of thresholds based upon more conventional threats that are likely to precipitate widespread failures of the system. While this provides an estimated threshold for collapse in this study, it is conceivable that a collapse may actually initiate at lower levels because of the unusual nature of this common mode threat to the grid.

A1.2 Disturbance Intensity and Energy Thresholds for System Failure

An important aspect of assessing failure thresholds is having to take into consideration the ability of the system to meet an instantaneous large change in reactive demand. This level of failure threshold can readily take into consideration relevant operating experience examples. For instance, the Hydro Quebec collapse from the March 1989 geomagnetic storm has been estimated to have caused about a 1600 MVAR increase in reactive demand and related harmonic distortion impacts on the system. This demand increase is at a level that is ~7% of the Hydro Quebec system load. In a subsequent study and report to the NPCC, TransÉnergie (the new name for Hydro Quebec), estimates that they have typical reactive reserves of ~ 3000 MVARs (Reference AP1-7). While this network has gone to extraordinary efforts to develop fast response VAR resources, this capability is still only a level that is ~9% of 2002 peak load for the system. National Grid (England/Wales) estimates that geomagnetic storm collapse could occur for 2000-3000 MVARs for their system, a level that is 4 - 6% of peak system demand (Reference AP1-4). The DOE Power Outage Study Team Report and several other reports indicated a number of system events where extreme load demands and/or capacity shortages pushed systems very close to, or actually into, voltage collapse in regions such as the NEPOOL,

PJM, SERC, and WECC power pools (References AP1-8, AP1-9, and AP1-10). Regional pools are also required to provide for a spinning reserve margin for contingency loss of real power capacity. This reserve requirement generally falls in the range of 1000 to 1500 MW, and provides useful guidance as a surrogate bound for reactive power reserve margins as well, lacking any better information.

In combination with the instantaneous demand of reactive power increases, the duration of the impulsive event needs to be considered. A useful measure is a Disturbance Energy Estimate and Threshold, as adapted from Standard System Design Criteria. This design criterion requires all systems to withstand creditable fault events. Using this event criterion as a measurable threshold, a calculation of MVA-Seconds Disturbance Energy can be applied to the power grid in each state. For example, on a 500kV system with a 3-Phase /60kA fault (a very high magnitude fault current) lasting 4 cycles (66.6msec), the total disturbance energy applied to a power grid would be 3464 MVA-sec. Since all power grids of 500kV design would be expected to successfully survive this level of threat, a much larger disturbance needs to be set as the threshold for failure. Most power grids would be expected to fail for such a fault extended to 30 cycles accompanied by simultaneous loss of key elements, which is analogous to the dual threat of GIC disturbances. GIC from geomagnetic storms and E3 threats are not single-point disturbances, but widely scattered, causing smaller MVA increases at each affected transformer. However, when accumulatively considered these events can be cumulatively very large disturbances to the network. To allow for reasonable margins of uncertainty, a cumulative disturbance energy based upon a 3-Phase 30 cycle fault was used as a threshold applied to each state region as the basis to determine geographic boundaries and thresholds for likely power grid collapse. For states with a predominant 765kV infrastructure, the threshold disturbance energy would be 39749 MVA-sec. For regions with predominant 500kV or 345kV systems, the respective disturbance energy thresholds would be 25980 MVA-sec and 17926 MVA-sec. Because there are several states that have sparse infrastructure, it is likely these regions will not have cumulative energy to meet these levels. The criteria would then need to include evaluation of GIC levels at available locations and assessment of neighboring regions that would collapse. Under these conditions, it would be reasonable to expect a cascading collapse to these sparse regions. Further, in application, both the instantaneous demand and disturbance energy thresholds must be exceeded.

A1.3 System Operating State Considerations

Stress calculations can be made for GIC threats, but there is considerable uncertainty, as the measurement of stress caused by a disturbance has to be weighed against the ability of the network to survive the stress. System uncertainty primarily arises from the large variability that can occur in system loads or operating posture of the system as a whole. Figure A1-2 provides a comparison of the power demand on the NY-ISO pool on July 15, 2000, the day of one of the largest geomagnetic storms during Cycle 23, and the load demand on August 7, 2001, during an extreme heat wave. As shown, the power demand for the region was effectively twice as high on August 7. Adverse demand conditions on this day strained the capability of the system and every available resource and, public

appeal to limit demand was employed. While a moderately severe geomagnetic storm occurred on July 15, 2000, the NY-ISO had considerable available capacity, due to the much reduced network demand, and no important system upset events occurred. The same storm scenario coincident with the system conditions of August 7, 2000 could have had much more serious consequences.

Figure A1-3 provides a graphic illustration of these combined probability considerations. The red curve represents a distribution of GIC disturbance impacts from geomagnetic storm conditions. This curve shows a normal distribution of storm related stress to the power grid, such that a large number or probability of small storm events will produce limited amounts of stress to the exposed power grid. As storm related intensity increases dramatically, these extreme storm events are far less probable. The blue curve represents a distribution of power grid operating posture or reserves available to counter disturbance events. The further to the right the system operating posture is, the greater the ability to withstand a stress environment such as that posed by a geomagnetic storm. Both the previously illustrated conditions of adverse load demands, as well as the desire to maintain economic operations, prevent the system from being maintained continuously in a highly resistant operating posture, hence a gaussian type distribution is assumed for this example. Where the stress and capability curves overlap, then network stress exceeds the ability of the network operating posture to successfully absorb that imposed stress, which indicates that failure would be expected.

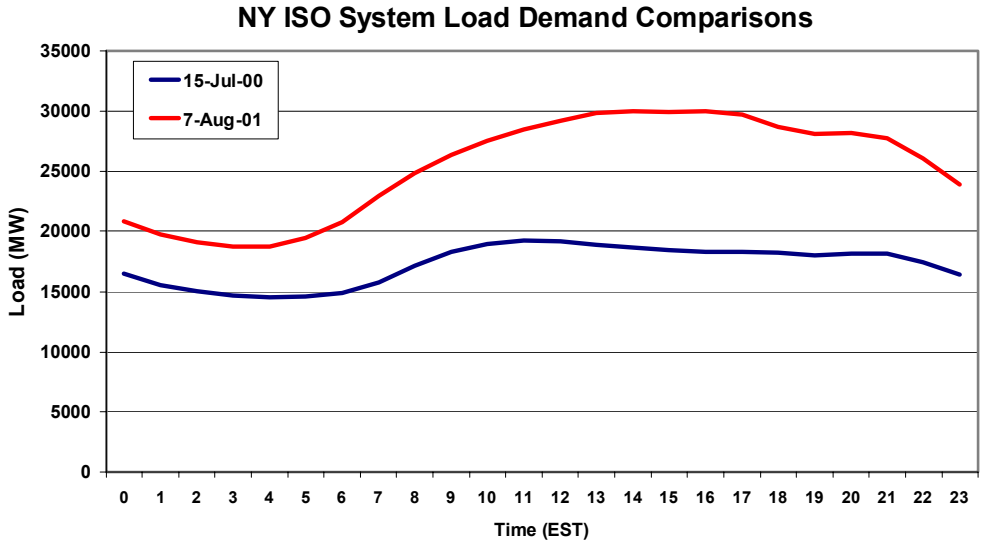

Figure A1-2. Comparison of NY ISO load for July 15, 2000 storm date and peak load conditions on August 7, 2001.

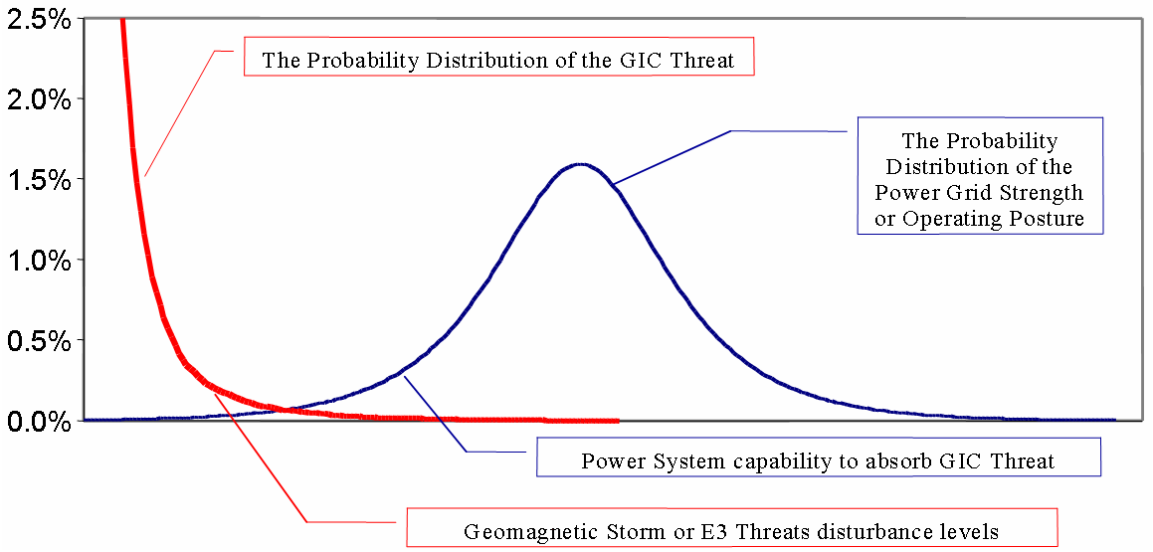

Figure A1-3. Power grid failure probability analysis from GIC threat scenario.

In this state-space depiction, Figure A1-4 illustrates how the system operating reserves can rapidly erode for sudden real or reactive demand changes on the grid, a scenario that is plausible under GIC threat events. Also as previously discussed, the consensus viewpoint has been that the electric industry restructuring that is occurring has produced a secular change in the overall reliability and operating capability of the U.S. Power Grid. This decline in capability can be represented by the shifted system capability distribution that is shown in Figure A1-5. While the operating state of the network is an important consideration in the assessment of network failure, there is also no practical means to assess the range of operating postures that could be present during severe GIC events, either from natural geomagnetic storm processes or from HEMP E3 threat scenarios. In the prior discussed disturbance energy assessments, the underlying assumption in the threshold levels that were developed is that the network condition is robust and not overly weakened at the time of the GIC event.

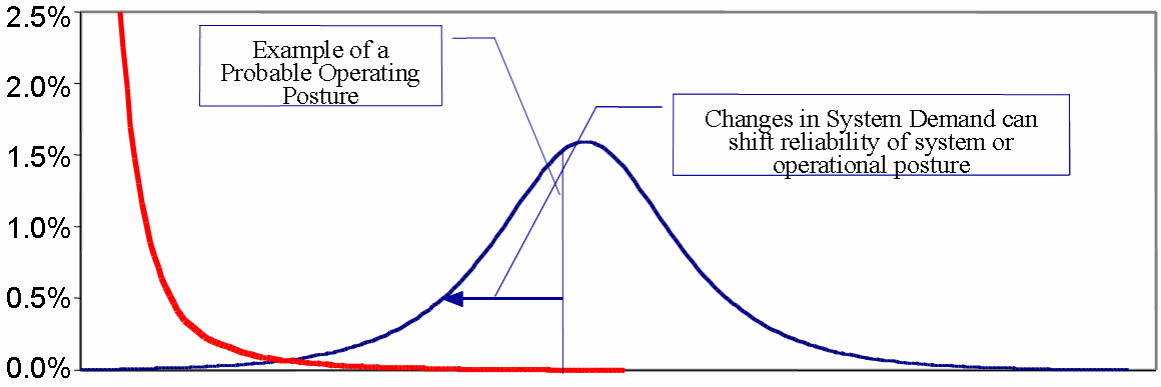

Figure A1-4. Power grid failure probability analysis from GIC threat scenario and cross section at a particular grid operating posture.

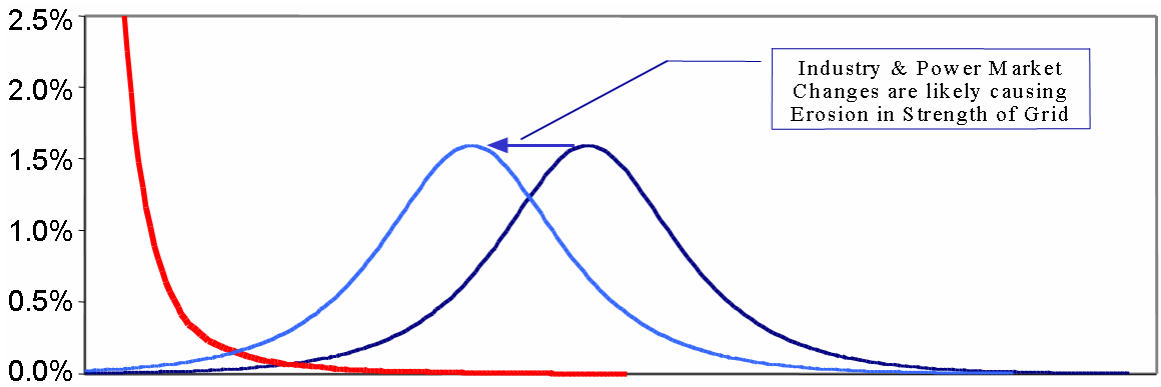

Figure A1-5. Power grid failure probability analysis from GIC threat scenario and impact of secular changes to power grid operating reliability.

In the estimate of power system impacts due to severe geomagnetic storms, the primary concern is increased reactive power, as measured by cumulative estimates of increases of reactive power losses at individual exposed transformers, which will be widely distributed around the network. There is the possibility of further AC power system responses that could act to compound the already large increase in reactive power demand. As reactive power demand increases in saturated transformers, the supply of the reactive power will result in an incremental increase in AC current flow in exposed portions of the power grid. This incremental current flow will also produce an incremental I^2X reactive power loss in the network, which adds to the increased reactive power loss due to this GIC event. In effect, this network response compounds the severity of the initial GIC event impacts even further. In order to estimate these impacts, it would be necessary to identify all base AC current flows on the exposed network and to perform a set of comprehensive load flow studies. Again, because of the limitations of this investigation, only a screening analysis can be considered, to establish creditable upper bounds on this impact adder.

An example of the WECC system (Western U.S.) will be used to illustrate the potential magnitude of this I^2X reactive demand adder. As will be shown in the course of this study, there are creditable geomagnetic storm and E3 threats that are likely to cause an increase of reactive demand in the WECC system by 11,000 MVARs or greater. Based upon the load and line flow conditions for the WECC Heavy Spring Load model, a calculation of I^2X increases can be made. The WECC load in this heavy spring model is 109,123 MW. Therefore, an 11,000 MVAR GIC-caused reactive demand increase represents an approximate 10% increase in net system demand. While reactive load, in theory, needs to be supplied locally, in real systems substantial flows across the network will need to occur, as not all fast-response reactive sources are homogeneously distributed. Given the uncertainty and lack of detailed information to compute all possible exact increases, a reasonable approximation can be made by assuming that all transmission line AC currents will increase by an average 10% from base conditions in response to the GIC event. Using this assumption, it can be calculated for the WECC region that the GIC-caused 11,000 MVAR increase will also result in an added I^2X loss on transmission lines of an additional ~5800 MVARs, a 52% adder to increased MVARs. If AC current flows also increase in network transformers, this would add even further to

incremental I^2X losses. For GIC threats of even larger magnitude as a percentage of system load, the percentage adder due to I^2X response of the network could be even larger.

While the I^2X response adder is not specifically calculated in the GIC threat scenarios, due to lack of sufficient AC line flow data, it is reasonable to assume that a significant percentage increase will occur and that estimates of disturbance energy functions described previously are conservative estimates of grid failure, and that wider spread disturbances than estimated could actually result for any of the studied scenarios.

A1.4 An Overview of GIC Threats and Relay Misoperation Concerns

Relay malfunctions during GIC events are a primary source of system reliability threats as well. This threat is usually caused by harmonic interactions with protective systems, but can also occur due to other causes, such as transformer current saturation or other secondary interactions (Reference AP1-11). While a comprehensive review of this threat is beyond the scope of this investigation, a brief overview of some potential areas of concern can be provided. In the U.S. it is estimated that there are ~40,000 transmission and distribution substations. Of the very largest and most important substations, which operate at voltage levels of 345kV and above, there are over 2000 stations. Figure A1-6 provides a schematic of a typical 500/230/138kV substation. At this substation there are 3 - 500kV lines entering, and 2 - 230kV lines and 2 - 138kV lines exiting. There are also 4 large power transformers, 4 busses, and 11 large circuit breakers. In addition, there is considerable other associated equipment, such as current transformers and potential transformers (CTs and PTs). In general, each piece of apparatus, line exit and bus zone in this substation has redundant levels of protection to sense fault events and remove the faulted device from the network as soon as possible. For a substation of this caliber, relay times are as fast as 70 msec for Primary Schemes (1-2 cycles to sense fault, 2-3 cycles for breaker to operate). The Secondary Protection is in case of relay failure, breaker failure, CT failure, etc. and is generally set to operate and sense at lower thresholds than primary, with a delay in time in the range of 100-150 msec. In cases of additional relay system malfunction, a more rudimentary backup protection is set to be very sensitive, but delayed a very long time, typically 0.5 seconds (30 cycles). When called upon to operate, these backup schemes usually result in tripping of an entire station or portion of a network. Relative to other conventional threats that relay systems are designed to address, GIC events last a very long time, many times longer than the slowest backup time delay for protection schemes. Because of this, and harmonic interactions, GIC events have been shown to adversely effect nearly every type of relay system. In this example substation, there could be over 45 different relays, up to 3 relays to protect each line, bus, and transformer at this one station alone, and with overlapping protection as well. Any of these relays could malfunction due to GIC, and precipitate wider-spread system reliability problems in the process.

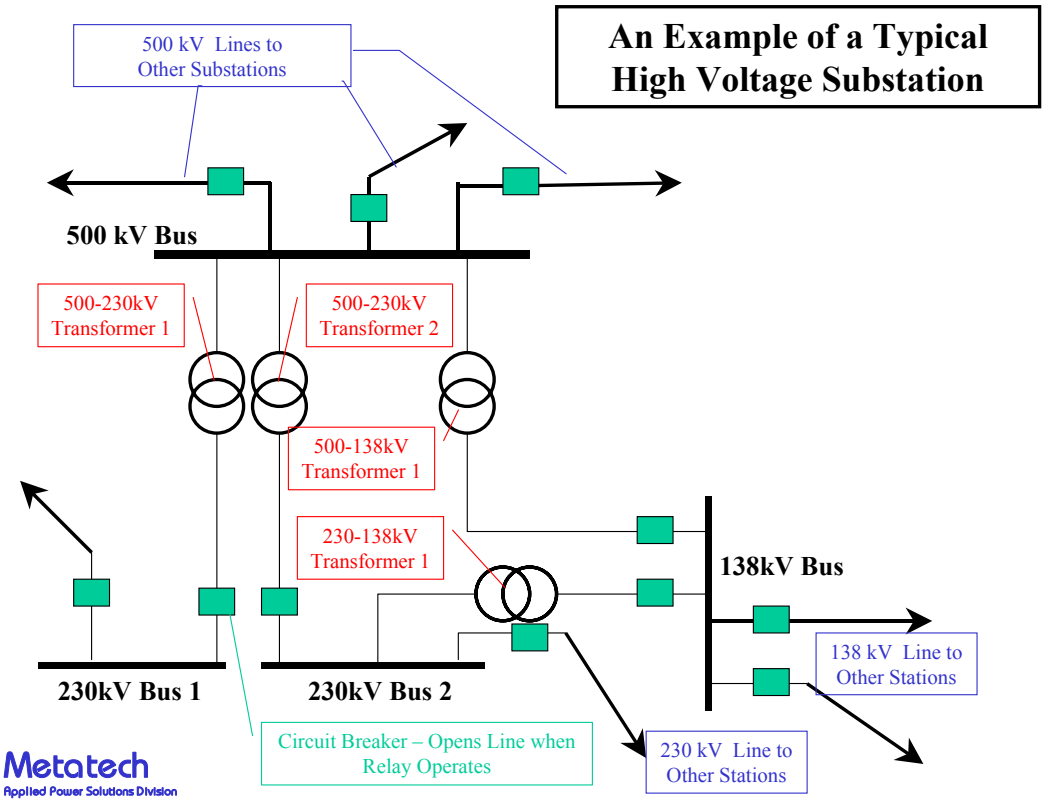

Figure A1-6. One line diagram of example 500kV, 230kV, 138kV substation.

A1.5 Capacitor Banks, General Relay and Overload Protection Concerns due to GIC

For a Shunt Capacitor or SVC (simple schematic as shown in Figure A1-7), the primary protection of the capacitor is based on over-current sensing. Since a capacitor is a high-pass filter, harmonics from nearby GIC saturated transformers will inrush to the device and cause large increases in total current flow. Some relays do not distinguish between fundamental and harmonic frequencies and can false-trip due to even a modest increase in harmonics current. These systems in particular were the primary culprits of failure in storms during Solar Cycle 22. Failure of these key fast response reactive sources is a significant loss to the system as a whole, as these capacitive devices are the key response to compensate for the increased reactive power demand from the GIC event itself. Rapid erosion of power network integrity or voltage collapse can occur when compounded by these device failures. More modern relays have the ability to differentiate between fundamental frequency and harmonics and, as a result, are less likely to malfunction. However, under extreme GIC events, the current rating of the capacitor can be exceeded. Figure A1-8 shows several cycles of AC current in a 500kV capacitor bank at the Three Mile Island station in Pennsylvania for a 1-in-30 geomagnetic storm threat scenario. Shown is both a normal capacitor bank current (blue curve), while the red curve shows the harmonic distorted capacitor bank current due to saturation of a nearby transformer from a GIC of 400 amps/phase. This simulation result indicates that the substantial

harmonic flow will cause a nearly 400% overload condition in total current flow in the capacitor bank, sufficient to initiate bank trip for any properly designed relay system.

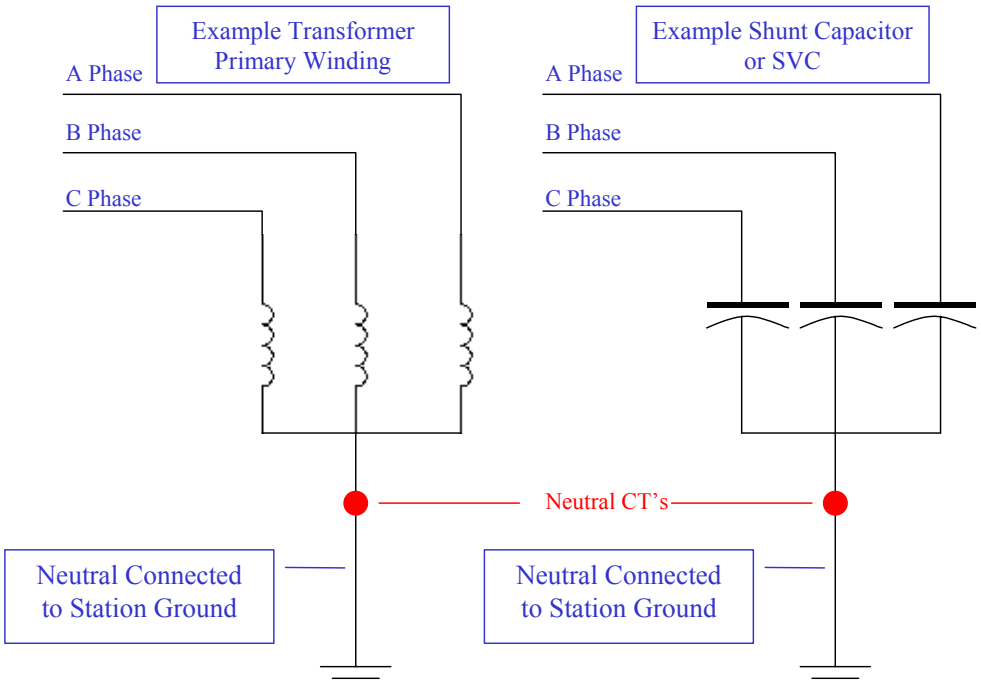

Figure A1-7. Schematic of shunt reactor and shunt capacitor.

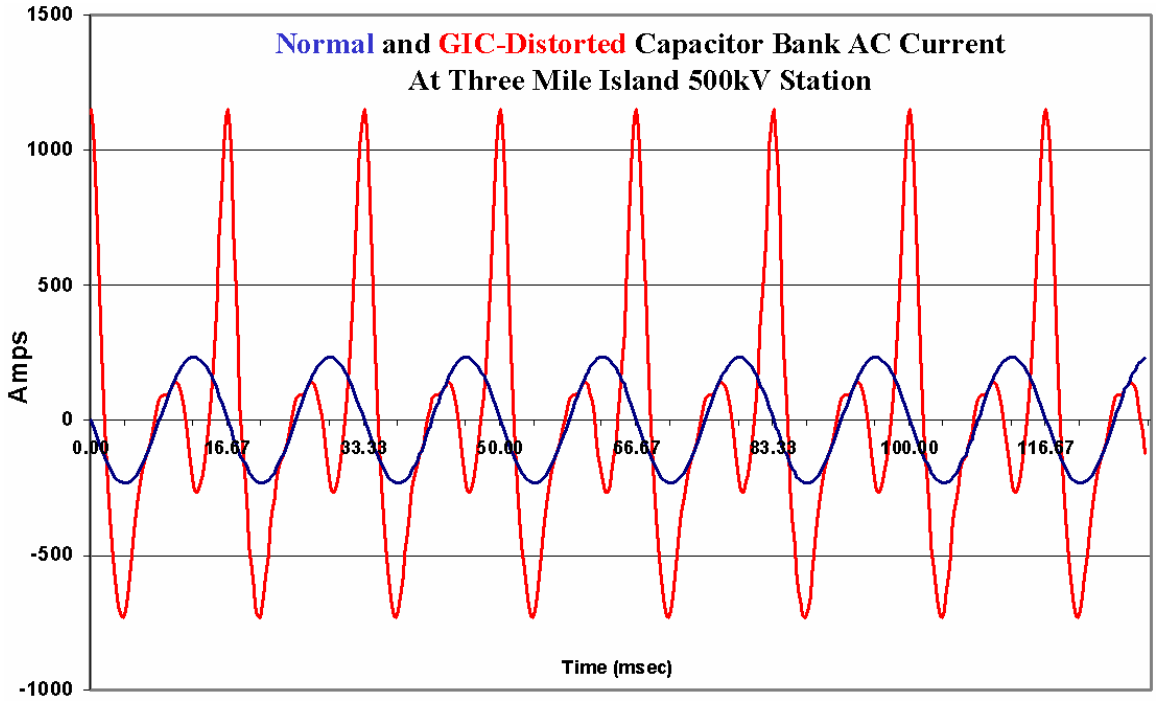

Figure A1-8. Normal and GIC-distorted 500kV capacitor bank current at Three Mile Island for severe geomagnetic storm threat.

Another example of relay operation due to GIC is presented in Figure A1-9. The two curves represent the GIC threat over a 40 second duration in the top graph. The bottom graph is the envelope of the AC waveform of the exposed transformer as it is experiencing harmonic distortion from half-cycle saturation. The transformer's normal ~600 amp peak AC waveform rapidly increases to a peak AC of ~2400 amps (a ~300% increase in current level). This current will also flow from each transformer into the system and through each line, breaker, and the CTs that sense these large currents. Since these over-currents last for many 10s of seconds, it is highly likely that either primary, secondary, or back-up protection systems on transmission lines, busses, transformers, and cap banks, will sense the disturbance and likely initiate a trip of some kind during this event. Instantaneous relay trips will occur if current levels exceed trip settings. But because of long duration, secondary and back-up systems are more likely to trip even if primary systems do not operate, as these back-up protection systems, while delayed by 100 milliseconds to 0.5 seconds, are set to trip at much lower over-current levels. Extreme levels of harmonic distortion are likely to cause relay malfunctions, as well as lead to scenarios of large-scale simultaneous tripping of devices outside of the high current overload zones. If numerous transformers are exposed and begin operation simultaneously in this manner, widespread tripping of key assets across the transmission network will occur. If these trips of key apparatus are sufficient in number or location, this can readily result in cascading collapse of the network as a whole.

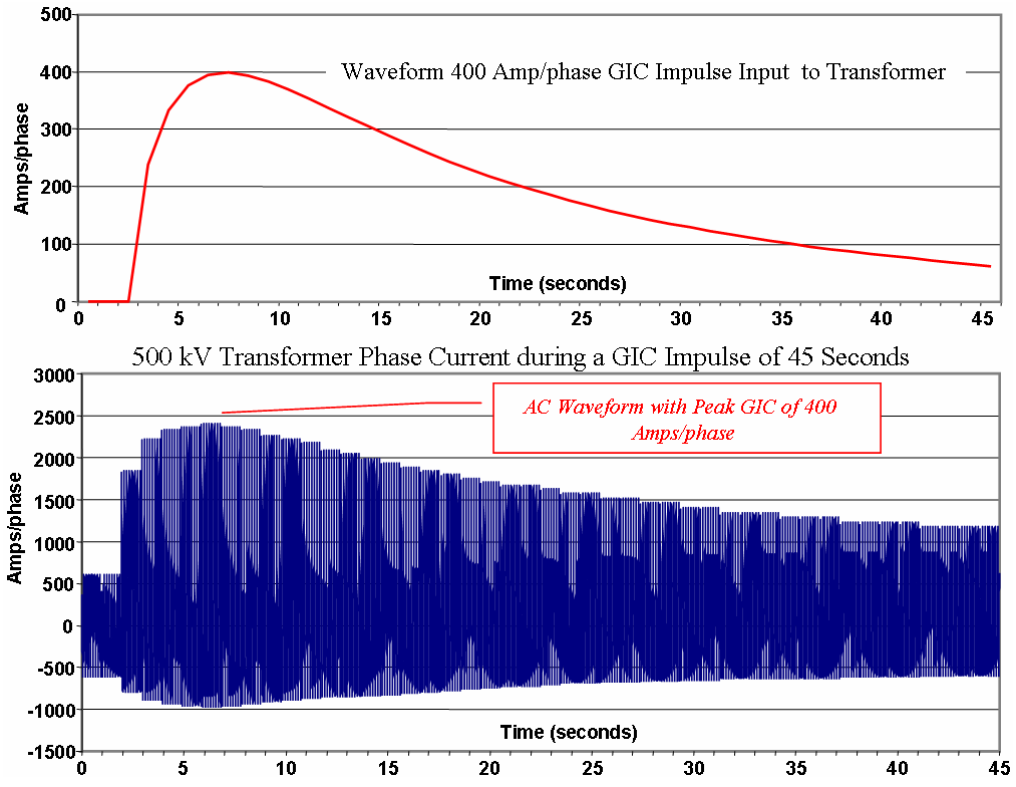

Figure A1-9. Top plot – GIC current versus time in 500kV transformer, bottom plot – AC current versus time of saturated 500kV transformer.

Appendix 1 References

AP1-1 Thierry Van Cutsem, Voltage Instability: Phenomena, "Countermeasures, and Analysis Methods", Proceedings of IEEE, Vol 88., No. 2, Feb 2000, pg 208-227.

AP1-2 "Central East Voltage Analysis – For Addition of 200MVAr Capacitor Bank at the Eidc 345kV Substation", NYISO Operations Engineering, March 2002.

AP1-3 J. Eto, C. Martinez. et. al., "Grid Management Tools", IEEE Winter Power Meeting, January 28-31, 2001.

AP1-4 J. G. Kappenman, et. al., "Application of Modeling Techniques to Assess Geomagnetically Induced Current Risks on the NGC Transmission System", CIGRE, Session 2002, paper 39-304.

AP1-5 J.G. Kappenman, Chapter 13 - "An Introduction to Power Grid Impacts and Vulnerabilities from Space Weather", NATO-ASI Book on Space Storms and Space Weather Hazards, edited by I.A. Daglis, Kluwer Academic Publishers, II Mathematics, Physics and Chemistry, Vol. 38, pg 335-361.

AP1-6 V. D. Albertson, J. G. Kappenman, N. Mohan, G. A. Skarbakka, "Load-Flow Studies in the Presence of Geomagnetically-Induced Currents", IEEE PAS Transactions, Vol. PAS-100, February 1981, pp. 594-607.

AP1-7 Antonio Dutil, "Impact of Geomagnetic Storms on TransÉnergie Transmission System- Situation at the Dawn of Year 2000", Report to NPCC, January 2000.

AP1-8 DOE, "Consortium for Electric Reliability Technology Solutions – Grid of the Future, White Paper on Review of Recent Reliability Issues and System Events.

AP1-9 "The Electric Power Outages in the Western United States, July 2-3, 1996", Report to the President, U.S. Department of Energy, August 1996.

AP1-10 Interim Report of the U.S. Department of Energy's Power Outage Study Team, Findings from the Summer of 1999, January 2000.

AP1-11 J. G. Kappenman, V. D. Albertson, N. Mohan, "Current Transformer and Relay Performance in the Presence of Geomagnetically-Induced Currents", IEEE PAS Transactions, Vol. PAS-100, March 1981, pp. 1078-1088.

Appendix 2
Detailed Summary of Power System Impacts from March 13-14, 1989 Geomagnetic Superstorm

In this appendix, a summary of power system impacts observed across North America due to the March 13-14, 1989 superstorm is provided. The bulk of the information contained here is primarily a chronological list of significant events and anomalies that were voluntarily reported shortly after this storm. The North American Electric Reliability Council, at that time, would annually review significant system disturbances and provided a report on the most important of these system disturbances, in order to share information and insights on the disturbances and what lessons may be gained from these experiences. The 1989 System Disturbances report included discussions on the San Francisco Bay Area Earthquake, the impacts of Hurricane Hugo, and several other disturbances, most of which were tied to extreme environment disturbances. This report also provided a detailed discussion of the March 89 Geomagnetic Superstorm, which entailed ~50% of the entire 67 page report. This provides an indication of the widespread impacts that were observed across the continent. The events chronology list, provided here, is largely a verbatim recreation of the *Chronology of Reported Events* table from this report, which covered pages 57-60. The only modification that has been made is the addition of new information in the first column, which provides an added assessment on the nature of the event reported.

At the time that the 1989 NERC System Disturbances report was prepared, a less detailed understanding was available of some of the event causes and interactions on the power grid between primary and secondary effects of the storm. This added commentary provides some guidance as to the likely nature of the event interaction that was reported. Power system impacts can result from both primary and secondary interactions of the space and geomagnetic field environments with the power grid infrastructure.

- Primary interactions with the power grid are a direct result of the flow of GIC in power system transformers, causing half-cycle saturation and a resulting large increase in reactive power demand in the transformer. Because many storms have a very geographically widespread footprint, GIC can be flowing at high levels in many transformers simultaneously. This can lead to multiple correlated failures and/or voltage regulation problems that can be severe enough to threaten network collapse.
- Secondary interactions arise from AC harmonics, from transformer saturation, that flow into other network devices or equipment and cause malfunctions of associated relay and protective systems, etc. For example, shunt capacitor banks or SVCs that are needed for voltage regulation at many locations on the network become a high-pass filter for harmonics. When the harmonics are present at very high levels, from severe transformer saturation, the large flow of harmonics in a capacitor bank can be sensed as an overload condition, causing protective relays to trip the device off. The loss of key apparatus such as this, at the time of system voltage regulation stress caused by the storm, becomes a double impact and can rapidly degrade the reliability of the network. Secondary interactions from

geomagnetic storms have been observed with nearly every piece of apparatus on the power grid, involving capacitors, HVDC terminals, generators and all manner of relay and protective system. Secondary interactions also include internal heating in transformers and generators, and possible long-duration outages that could result.

The large volume of significant events reported provides appropriate perspective on the geographically widespread nature of the threat, and that large numbers of simultaneous impacts posed by geomagnetic disturbances are a significant power system reliability concern.

March 13, 1989 Geomagnetic Disturbance
Chronology of Reported North American Power Grid Events

System Impact Type	Event#	Date	Time (EST) At(From) (To)	Area or System	Event	Base kV	Base MVAR	Voltage Range Low	Voltage Range High	Comments
Primary System Impact	1	3/11/1989	727	PJM	Oscillograph					Brandon Shores voltage below 224 kV
Primary System Impact	2	3/11/1989	744	PJM	Oscillograph					Brandon Shores voltage at 232
Primary System Impact	3	3/11/1989	1404	PJM	Oscillograph					Granite Substation
Primary System Impact	4	3/11/1989	1422	PJM	Oscillograph					Brandon Shores
Primary System Impact	5	3/12/1989	NA	SC Edison	Noise					115/55 kV transformer near Bishop CA Permissive trip & pilot relay alarms
Primary System Impact	6	3/12/1989	3	PJM	Alarm					Permissive trip monitor Alarms reset
Storm K Index	7	3/12/1989	100		K2					
Primary System Impact	8	3/12/1989	119	PJM	Alarm					Backup permissive trip monitor alarms Alarms reset
Primary System Impact	9	3/12/1989	138	PJM	Alarm					Alarms reset
Storm K Index	10	3/12/1989	400		K2					
Storm K Index	11	3/12/1989	700		K3					
Storm K Index	12	3/12/1989	1000		K3					
Storm K Index	13	3/12/1989	1300		K4					
Storm K Index	14	3/12/1989	1600		K3					
Storm K Index	15	3/12/1989	1900		K3					
Primary System Impact	16	3/12/1989	2029	Man. Hydro	Alarm					Neg. seq. alarm at Dorsey station
Storm K Index	17	3/12/1989	2200		K6					
Primary System Impact	18	3/12/1989	2215	OH	0scillograph					Essa station
Primary System Impact	19	3/13/1989	0-100	PJM	Noise					Calvert Cliffs GSU transformer
Storm K Index	20	3/13/1989	100		K7					
Primary System Impact	21	3/13/1989	119	Minn. Power	Capacitor	230	70			Forbes substation. Tripped by neutral overcurrent relay
Primary System Impact	22	3/13/1989	119	Man. Hydro	Alarm					Negative sequence alarms at Dorsey
Primary System Impact	23	3/13/1989	119	NIMO	Capacitor					Reynolds Rd. capacitor trip
Primary System Impact	24	3/13/1989	200	Man. Hydro	Alarm					Grand Rapids unit #1 phase unbalance alarm
Primary System	25	3/13/1989	239	Man. Hydro	MVAR			-140	280	Dorsey synchronous

Impact									condenser output varying
Primary System Impact	26	3/13/1989	239 -247	Man. Hydro	Voltage		-2.5		Winnipeg voltage. Freq. -0.04 Hz
Secondary System Impact	27	3/13/1989	243	Minn. Power	Capacitor				Numerous banks switched on line
Primary System Impact	28	3/13/1989	243	Minn. Power	Voltage	235	226		
Secondary System Impact	29	3/13/1989	245	Minn. Power	Capacitor	115 37			Lost capacitor bank at Nashwauk. Neut overcurrent relay
Secondary System Impact	30	3/13/1989	245	HQ	SVC				Hydro-Quebec blackout
Primary System Impact	31	3/13/1989	245	PJM	MVAR				MVAR generation swing
Secondary System Impact	32	3/13/1989	245	Man. Hydro	Generator				Brandon station. Ghost marks on #5 slip rings.
Secondary System Impact	33	3/13/1989	245	OH	Generator				Harmon Hydro trips on phase unbalance
Secondary System Impact	34	3/13/1989	245	WAPA-Fargo	SVC				SVC trip
Secondary System Impact	35	3/13/1989	246 -255	WAPA	SVC				Tripped on harmonic unbalance
Secondary System Impact	36	3/13/1989	246	OH	Generator				Harmon phase unbalance
Primary System Impact	37	3/13/1989	255	WAPA-Fargo	Voltage	230	-8	14	Fargo bus
Primary System Impact	38	3/13/1989	258 -303	Man. Hydro	MVAR		-130		Dorsey synchronous condenser varying Dorsey synchronous condenser varying
Primary System Impact	39	3/13/1989	335 -340	Man. Hydro	MVAR		-125	25	Dorsey synchronous condenser varying Dorsey synchronous condenser varying
Storm K Index	40	3/13/1989	400		K9				
Secondary System Impact	41	3/13/1989	458	NYPP	Generator				Poletti unit tripped (700 MVV)
Secondary System Impact	42	3/13/1989	458	NYPP	Generator				Poletti trips on lost exciter control
Secondary System Impact	43	3/13/1989	606	NIMO	Capacitor				Rotterdam capacitor trip
Secondary System Impact	44	3/13/1989	608	Cent. Hud.	Capacitor	69			Pulvers Corners capacitor trip
Primary System Impact	45	3/13/1989	610 -630	PJM	Voltage	500	-6	14	Voltage swings at Whitpain
Secondary System Impact	46	3/13/1989	613	NIMO	Capacitor				Reynolds Rd. capacitor trip
Secondary System Impact	47	3/13/1989	615	APS	Capacitor	138 44			7 Capacitors tripped
Secondary System Impact	48	3/13/1989	615	Va. Pwr.	Capacitor	230 -162			Loudoun
Primary System Impact	49	3/13/1989	617	PJM	Oscillograph				Peach Bottom and Whitpain
Secondary System Impact	50	3/13/1989	618	NIMO	Capacitor				Cortland and Teall Ave. capacitor trip
Primary System Impact	51	3/13/1989	618	PJM	Recorder				Alburtis fault recorder
Primary System Impact	52	3/13/1989	618	PJM	MW				Safe Harbor and Brunner generation swings
Secondary System Impact	53	3/13/1989	618	Va. Pwr.	Capacitor	230 162			Carson
Secondary System Impact	54	3/13/1989	618	Va. Pwr.	Capacitor	115 64			Virginia Beach
Secondary System Impact	55	3/13/1989	619	Va. Pwr.	Capacitor	230 117			Chuckatuck

Primary System Impact	56	3/13/1989	619	PJM	Recorder			Wescosville fault recorder for no reason
Secondary System Impact	57	3/13/1989	619	Cent. Hud.	Capacitor	115		Hurley Ave. capacitor trip
Secondary System Impact	58	3/13/1989	620	Va. Pwr.	Capacitor	230	117	Yadkin
Secondary System Impact	69	3/13/1989	624	Va. Pwr.	Capacitor	230	164	Elmont
Secondary System Impact	60	3/13/1989	624	Va. Pwr.	Capacitor	230	162	Dooms
Primary System Impact	61	3/13/1989	624	OH	Oscillograph			Essa and Bruce A
Secondary System Impact	62	3/13/1989	625	Va. Pwr.	Capacitor			Valley
Primary System Impact	63	3/13/1989	630	Atl. Elec.	MVAR			Increase In MVAR generation
	64	3/13/1989	700	HQ	Restoration			25% load restored (5,000 MVV)
Storm K Index	65	3/13/1989	700		K8			
Primary System Impact	66	3/13/1989	800 -1015	PJM	Noise			Calvert Cliffs GSU transformer
Primary System Impact	67	3/13/1989	825	VMPC	Radio			Radio problems
	68	3/13/1989	900	HQ	Restoration			48% load restored (10,500 MW)
Secondary System Impact	69	3/13/1989	926	Man. Hydro	Line	230		Radisson-Churchill line trip by 5ON relay
Storm K Index	70	3/13/1989	1000		K7			
	71	3/13/1989	1100	HQ	Restoration			64% load restored (14,200 MW)
Secondary System Impact	72	3/13/1989	1102	Man. Hydro	Line	230		Radisson-Churchill line trip by 5ON relay
Secondary System Impact	73	3/13/1989	1151	Man. Hydro	Line	230		Radisson-Churchill line trip by 5ON relay
Secondary System Impact	74	3/13/1989	1159	Man. Hydro	Line	230		Radisson-Churchill line trip by 5ON relay
Storm K Index	75	3/13/1989	1300		K7			
	76	3/13/1989	1300	HQ	Restoration			83% load restored (17,500 MW)
Primary System Impact	77	3/13/1989	1405	Portland GE	Noise			360 Hz noise at Boardman
Secondary System Impact	78	3/13/1989	1528	Man. Hydro	Line	230		Radisson-Churchill line trip by 5ON relay
Secondary System Impact	79	3/13/1989	1545	Cent. Hud.	Capacitor			Hurley Ave. capacitor trip
Primary System Impact	80	3/13/1989	1600 -2200	Atl. Elec.	Voltage			
Storm K Index	81	3/13/1989	1600		K8			
Primary System Impact	82	3/13/1989	1600 -2200	Atl. Elec.	MVAR			
Secondary System Impact	83	3/13/1989	1602	Va. Pwr.	Capacitor	230	162	Valley
Primary System Impact	84	3/13/1989	1610	PJM	Noise			Calvert Cliffs GSU transformer
Secondary System Impact	85	3/13/1989	1615	PJM	Generator			Mickleton CT trip (related to SMD?)
Primary System Impact	86	3/13/1989	1625	PJM	Oscillograph			TMI oscillograph on 230 kV
Primary System Impact	87	3/13/1989	1626	PJM	Oscillograph			Whitpain
Primary System Impact	88	3/13/1989	1630	SC Edison	Current			Elevated neutral current at 220166 kV transformer
Primary System Impact	89	3/13/1989	1630	SC Edison	Current			Neutral current of 15-30 A at 500/220 transformer
Primary System	90	3/13/1989	1630	SC Edison	Noise			500/220 kV transformer

Impact									at Mira Loma
Primary System Impact	91	3/13/1989	1640	-1700	PJM	Voltage	500	-18	18 VVhitpain
Primary System Impact	92	3/13/1989	1644		PJM	Alarm			Conastone substation general alarm
Primary System Impact	93	3/13/1989	1644		PJM	Capacitor			All capacitors tripped at Hosensack and TMI
Primary System Impact	94	3/13/1989	1645	-2000	WPL	Voltage	138	-2	2 Various voltage problems. Regulators hunting
Primary System Impact	95	3/13/1989	1649		PJM	Recorder			Alburtis-Wescosville fault recorder
Secondary System Impact	96	3/13/1989	1651		NIMO	Capacitor			Cortland, Teall Ave, Porter caps. trip
Secondary System Impact	97	3/13/1989	1653		NIMO	Capacitor			Reynolds Rd. capacitor trip
Primary System Impact	98	3/13/1989	1654		PJM	Alarm			Conastone substation general alarm
Primary System Impact	99	3/13/1989	1655	-1715	Minn. Power	Voltage	230	237	240 System voltage
Primary System Impact	100	3/13/1989	1655		Atl. Elec.	Voltage	69	-2	
Primary System Impact	101	3/13/1989	1665		Atl. Elec.	MVAR			
Primary System Impact	102	3/13/1989	1658		BC Hydro	Voltage	600	-20	20 4% voltage fluctuation
Primary System Impact	103	3/13/1989	1658		OH	Demand			Demand fluctuating by 200 MW
Secondary System Impact	104	3/13/1989	1658	-1700	WAPA	Converter			Miles City converter tripped
Primary System Impact	105	3/13/1989	1658		BPA	Noise			Ross Substation (near Vancouver, WA)
Secondary System Impact	106	3/13/1989	1658		WAPA	Line			Miles City-Custer. By neg. seq. relay
Primary System Impact	107	3/13/1989	1658		WKPL	Alarm			Negative sequence alarms
Secondary System Impact	108	3/13/1989	1658		BPA	Capacitor	115		Tripped by neutral time ground at 4 substations
Primary System Impact	109	3/13/1989	1658		BPA	Transformer			Hunting between taps 14 and 6
Primary System Impact	111	3/13/1989	1700		UPA	Voltage	230		Fluctuations at Willmar substation
Primary System Impact	112	3/13/1989	1700		LILCO	Voltage			Voltage fluctuations
Primary System Impact	113	3/13/1989	1700		IIGE	Voltage			Minor System Fluctuations
Primary System Impact	114	3/13/1989	1700	-2100	WEP	Noise			Low frequency noise at Point Beach Plant
Secondary System Impact	115	3/13/1989	1701		PJM	Capacitor	500		Hosensack capacitors tripped
Secondary System Impact	118	3/13/1989	1701		NIMO	Capacitor			Cortland capacitor trip
Secondary System Impact	117	3/13/1989	1701		Va. Pwr.	Capacitor	230	117	Chuckatuck
Secondary System Impact	118	3/13/1989	1701		Va. Pwr.	Capacitor	230	162	Carson
Primary System Impact	119	3/13/1989	1701		OH	Voltage			Overvoltage alarms on Waubaushene
Primary System Impact	120	3/13/1989	1701		OH	Oscilligraph			Esssa station
Secondary System Impact	121	3/13/1989	1703		Va. Pwr.	Capacitor	230	108	Idylwood
Secondary System Impact	122	3/13/1989	1708		UPA	Capacitor			Cap at Milaca sub switched in automatically
Secondary System Impact	123	3/13/1989	1709	-1725	WAPA	Converter			Miles City converter tripped
Secondary	124	3/13/1989	1709		WAPA	Transformer			Trip

System Impact									
Primary System Impact	125	3/13/1989	1709	WAPA-Fargo	Voltage	230	-8	14	Fargo bus
Secondary System Impact	126	3/13/1989	1709	WAPA	Line				Miles City-Custer. By neg. seq. relay
Secondary System Impact	127	3/13/1989	1709 -1827	WAPA	Relay				Bole Substation isolated by diff relay
Secondary System Impact	128	3/13/1989	1711	NIMO	Capacitor				Porter capacitor trip
Primary System Impact	129	3/13/1989	1720	UPA	Voltage	230			Swings on Wilmer 230 kV system
Secondary System Impact	130	3/13/1989	1723	Va. Pwr.	capacitor	230	164		Elmont
Primary System Impact	131	3/13/1989	1742	PJM	Alarm				500 kV line carrier low signal alarm
Secondary System Impact	132	3/13/1989	1827	Va. Pwr.	Capacitor	230	162		Carson
Secondary System Impact	133	3/13/1989	1829	Va. Flwr.	Capacitor	230	162		Yadkin
Primary System Impact	134	3/13/1989	1830	PE	Voltage	500		-10	Peach Bottom
Secondary System Impact	135	3/13/1989	1832	NEPOOL	Capacitor				Blown fuse at Orrington
Primary System Impact	136	3/13/1989	1840	Alt. Elec.	MVAR				
Primary System Impact	137	3/13/1989	1858	NEPOOL	Oscillograph				Maxcys substation
Storm K Index	138	3/13/1989	1900		K9				
Secondary System Impact	139	3/13/1989	1910	Va. Pwr.	Capacitor	230	164		Elmont
Primary System Impact	140	3/13/1989	2000	NEPOOL	MVAR				Connecticut Yankee 50 MVAR increase
Primary System Impact	141	3/13/1989	2010 -2024	NEPOOL	MVAR				Merrimack units MVAR swings
Primary System Impact	142	3/13/1989	2010 -2020	NEPOOL	Voltage	230	228	234	Comerford 230 kV station voltage swing
Primary System Impact	143	3/13/1989	2010 -2020	NEPOOL	Voltage	230	232	236	Moore 230 kV station voltage swing
Primary System Impact	144	3/13/1989	2010 -2024	NEPOOL	MVAR		100	200	Newington MVAR and voltage swing
Primary System Impact	145	3/13/1989	2010 -2020	NEPOOL	Voltage	345	351	3.54	Vermont Yankee 345 kV voltage swing
Primary System Impact	146	3/13/1989	2010 -2100	LILCO	Voltage				Severe voltage fluctuations
Primary System Impact	147	3/13/1989	2010 -2030	NEPOOL	MVAR				Salem Harbor & New Boston minor swings
Primary System Impact	148	3/13/1989	2010 -2020	INEPOOL	MVAR		4	8	Schiller station
Primary System Impact	149	3/13/1989	2010 -2024	NEPOOL	Voltage	345	350	336	Maine Yankee voltage drop
Primary System Impact	160	3/13/1989	2010 -2030	NEPOOL	Voltage	345	357	360	Mystic 345 kV stations voltage swing
Secondary System Impact	151	3/13/1989	2011	NIMO	Capacitor				Reynolds Rd. capacitor trip
Secondary System Impact	152	3/13/1989	2011	Va. Pwr.	Capacitor	230	162		Dooms
Primary System Impact	153	3/13/1989	2012 -2020	NEPOOL	Voltage		111.6	109.8	Bennington voltage fluctuations
Primary System Impact	154	3/13/1989	2012 -2016	NEPOOL	Voltage		355	352	Long Mountain voltage drop
Primary System Impact	155	3/13/1989	2012 -2020	INEPOOL	Voltage		232	227	Bear Swamp voltage fluctuations
Primary System Impact	166	3/13/1989	2012 -2024	INEPOOL	MVAR		100	300	Maine Yankee MVAR output swing
Secondary System Impact	157	3/13/1989	2012 -2016	NEPOOL	Converter				Comerfored filter bank tripped

Primary System Impact	158	3/13/1989	2013	NEPOOL	MVAR				Mystic 100 MVAR swing
Primary System Impact	159	3/13/1989	2014	PJM	Recorder				Alburtis-Wescosville fault recorder
Primary System Impact	160	3/13/1989	2014 -2028	NEPOOL	Voltage			355	352 Berkshire voltage drop
Primary System Impact	161	3/13/1989	2014	NYPP	Voltage				Voltage decline at Goethals, Flainey, Gilboa, Edic
Primary System Impact	162	3/13/1989	2015 -2030	NEPOOL	MW				Deerfield generation swings
Primary System Impact	163	3/13/1989	2016 -2030	NEPOOL	MVAR				Brayton Pt reactiv; output
Primary System Impact	164	3/13/1989	2015 -2030	INEPOOL	MVAR				Canal Station 20 MVAR swing
Primary System Impact	165	3/13/1989	2016	PJM	Alarm				Juniata
Primary System Impact	166	3/13/1989	2015 -2030	NEPOOL	MVAR			190	325 Millstone Unit 3 MVAR swings
Primary System Impact	167	3/13/1989	2015 -2030	NEPOOL	Voltage	345		358	359.5 Millstone Station voltage swings
Primary System Impact	168	3/13/1989	2015 -2030	NEPOOL	Voltage	345		350	353 Brayton Pt voltage dip
Primary System Impact	169	3/13/1989	2016 -2030	NEPOOL	Voltage				Webster St. voltage dip and swings
Primary System Impact	170	3/13/1989	2015 -2030	NEPOOL	MVAR				Middletown #4 20 MVAR
Secondary System Impact	171	3/13/1989	2016	OH	Generator				Phase unbalance at Bruce Nuclear Generator
Secondary System Impact	172	3/13/1989	2016	OH	Capacitor		32		Belleville capacitors trip
Secondary System Impact	173	3/13/1989	2017	NEPOOL	Converter				Madawaska dc tie run-back
Primary System Impact	174	3/13/1989	2017	NEPOOL	Voltage	345		-24	Voltage on Orrington 346 kV bus
Secondary System Impact	175	3/13/1989	2017	NEPOOL	Capacitor	115	67		Orringion capacitors (1.2,&3) opened and would not close
Primary System Impact	176	3/13/1989	2017	NEPOOL	Voltage				General voltage instability
Primary System Impact	177	3/13/1989	2017	NEPOOL	MVAR				Yarmouth reactive output exceeded 300 MVAR
Secondary System Impact	178	3/13/1989	2018	Va. Pwr.	Capacitor	230	162		Ox
Primary System Impact	179	3/13/1989	2019	WEP	Alarm				Point Beach plant
Primary System Impact	180	3/13/1989	2019	UPA	Alarms				Rush City MW and MVA@ alarms
Primary System Impact	181	3/13/1989	2020 -2030	Atl. Elec.	MVAR		85		
Secondary System Impact	182	3/13/1989	2020	APS	Transformer				Autotransformer at Meadowbrook damaged. 9.2 THD
Primary System Impact	183	3/13/1989	2020 -2030	Atl. Elec.	Voltage	138	-2.5		
Secondary System Impact	184	3/13/1989	2020	OH	Generator				Chats Falls MW and MVAR fluctuations
Secondary System Impact	185	3/13/1989	2020	UPA	Converter				Coal Creek pole #2 at 375 kV
Secondary System Impact	186	3/13/1989	2021	PJM	Capacitor				TMI capacitors tripped. Returned at 2139
Secondary System Impact	187	3/13/1989	2022 -2024	UPA	Line	230			Benton Co.-Milaca line opened
Primary System Impact	188	3/13/1989	2022	PJM	Alarm				Conastone
Primary System	189	3/13/1989	2024 -2064	CPA	Voltage				Voltage fluctuations

Impact									
Secondary System Impact	190	3/13/1989	2024	-2054	CPA	Capacitor			Capacitor banks switched on
Secondary System Impact	192	3/13/1989	2032		PJM	Capacitor	69		Nazareth Capacitors tripped
Storm K Index	193	3/13/1989	2200			K9			
Primary System Impact	194	3/13/1989	2300		PE	Voltage	500	-10	
Storm K Index	195	3/14/1989	100			K6			
Primary System Impact	196	3/14/1989	153		Nebraska	Alarm			Unexplalned frequency alarms
Primary System Impact	197	3/14/1989	233		Nebraska	Alarm			Unexplained frequency alarms
Primary System Impact	198	3/14/1989	240		Nebraska	Alarm			Unexplained frequency alarms
Primary System Impact	199	3/14/1989	240	-250	East ND	Voltage	230	-3	15
Storm K Index	200	3/14/1989	400			K8			
Primary System Impact	201	3/14/1989	628		PJM	Recorder			Wescosville fault recorder
Storm K Index	202	3/14/1989	700			K4			
Primary System Impact	203	3/14/1989	819		PJM	Alarm			Juniata miscellaneous alarms
Storm K Index	204	3/14/1989	1000			K4			
Storm K Index	205	3/14/1989	1300			K4			
Storm K Index	206	3/14/1989	1600			K6			
Primary System Impact	207	3/14/1989	1720	-1730	East ND	Voltage	230	-3	15
Storm K Index	208	3/14/1989	1900			K7			
Primary System Impact	209	3/14/1989	2020	-2040	East ND	Voltage		-3	15
Primary System Impact	210	3/14/1989	2104		Man. Hydro	Alarm	500		SMD alarm at Dorsey station
Storm K Index	211	3/14/1989	2200			K5			

Appendix 3
Geomagnetic Storm Validation Simulations of U.S. Grid Model

Geomagnetic storms have provided an ideal opportunity to validate the model components that will be used to assess the E3 threats to the U.S. Power Grid. Storms are relatively frequent events, and observations of magnetic fields, electric fields, and GICs in power grids provide observation data that can be used to validate simulation models. Power system GIC flows and overall current flows are the most difficult data to obtain, as it requires the installation of special monitoring equipment by the concerned utility company to measure GIC flows, and because of the effort and expense, these measurements are very sparse relative to the size of the power grid. In spite of these limitations, a relatively large number of observations and storms have been selected to perform validations. In some cases, the validation confirms individual model components, such as the response of the ground conductivity model in terms of geo-electric field. In many cases, validations are done of combined models, such as the ground model and the power circuit model, to validate the GIC flow in a particular set of transformers due to a geomagnetic field disturbance. This introduces a small amount of uncertainty in that some benchmark storm events are approximately 10 to 20 years old and some minor changes have occurred to the transmission network in intervening years. In aggregate, the changes to the power grid have been small. For example, NERC reports that between 1989 and 2000, only 192 miles of 345kV transmission have been added (0.4% increase in total miles) (Reference AP3-1). Therefore, as a whole, the model of the present U.S. grid is reasonably close to the size of the grid at the time of most storms. There is also the possibility of more significant changes of a local nature, which will mean some disagreement may be possible at specific sites, while valid at most other locations. This could occur, for example, due to the addition of a second transformer at an old monitoring site that would now cause the GIC flow modeled in today's network to be shared between the two transformers.

For many storm events, the ground model and Power Grid Model are confirmed simultaneously at many observation points across the U.S. power grid. These confirmations indicate that all aspects of the complex and geographically widespread storm events and models are providing creditable results, and therefore can reliably predict disturbance events of a more severe nature that are to be investigated in this study. Because there is uncertainty in both the ground model and in the Power Grid Model, agreement within a factor of two is a goal, though agreement in most cases is far better than this goal. In Section 2 of the this report, several model validations were discussed for three storm events: a validation of the ground models in northern Minnesota (storm on Nov 4, 1993) and central Alaska (storm on Oct 3, 1981), along with the validation of both the ground model and Power Grid Model for the power system in Maine during a storm on May 4, 1998. In addition to these cases, validations were also undertaken during storms on March 24, 1991, Oct 28, 1991, May 10, 1992, and Feb 21, 1994. The results of each will be described in the following sections.

A3.1 Benchmarking the U.S. Grid Model – Feb 21, 1994 Storm

The storm on Feb 21, 1994, while relatively small in intensity and duration, was simultaneously observed at several locations. Therefore, this storm presents a good opportunity for validation of the model components. Figure A3-1 indicates the locations in the U.S. of storm observations that can be used to benchmark various models and regions of the U.S. model. As shown in Figure A3-1, observations of GIC were made at the Rockport and Marysville substations on the AEP transmission system in Indiana and Ohio.

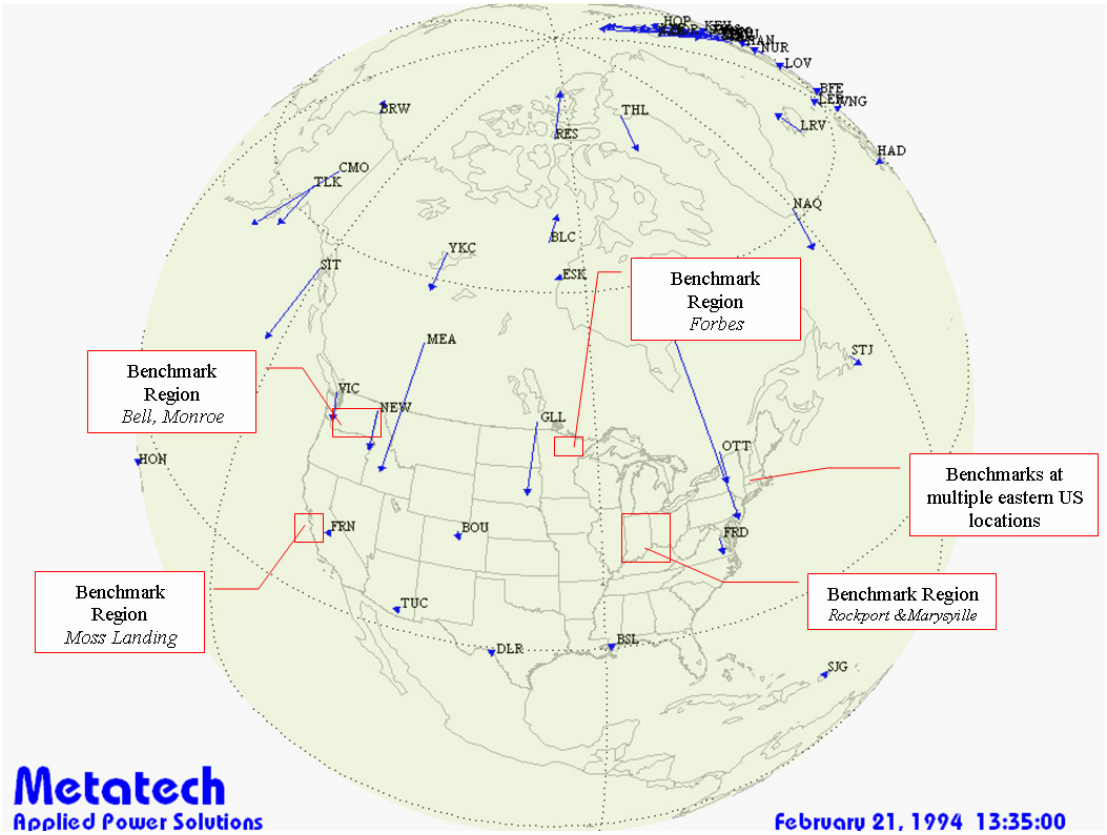

Figure A3-1. Benchmark areas and magnetic observatory locations for Feb 21, 1994 geomagnetic storm.

Figure A3-2 shows a more detailed view of the power grid region of interest, which involves a region of extensive 765kV transmission development. This region is also relatively remote and in a mid-point between 4 surrounding observatories, therefore this provides an opportunity to evaluate the performance of the geomagnetic storm specification model, the ground model, and the Power Grid Model components. The modeled geomagnetic field environments at times 13:35 and 14:04 are shown respectively in Figures A3-3 and A3-4. As shown, the intense electrojet regions are at very high latitudes, therefore storm conditions at the lower latitude regions of

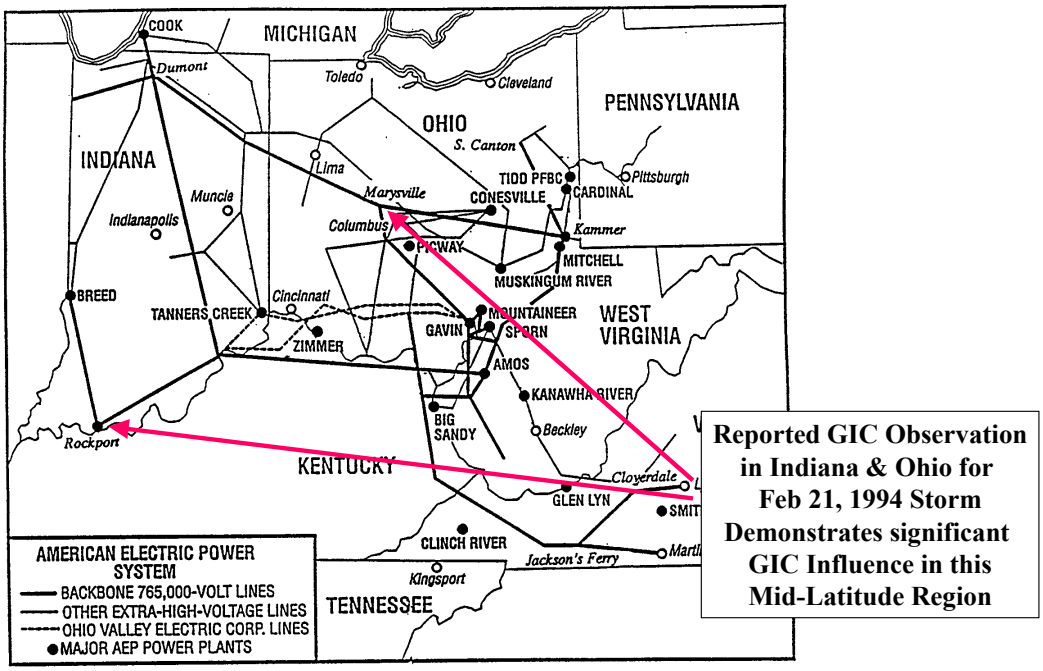

Figure A3-2. AEP-reported GIC observations at Marysville and Rockport on Feb 21, 1994.

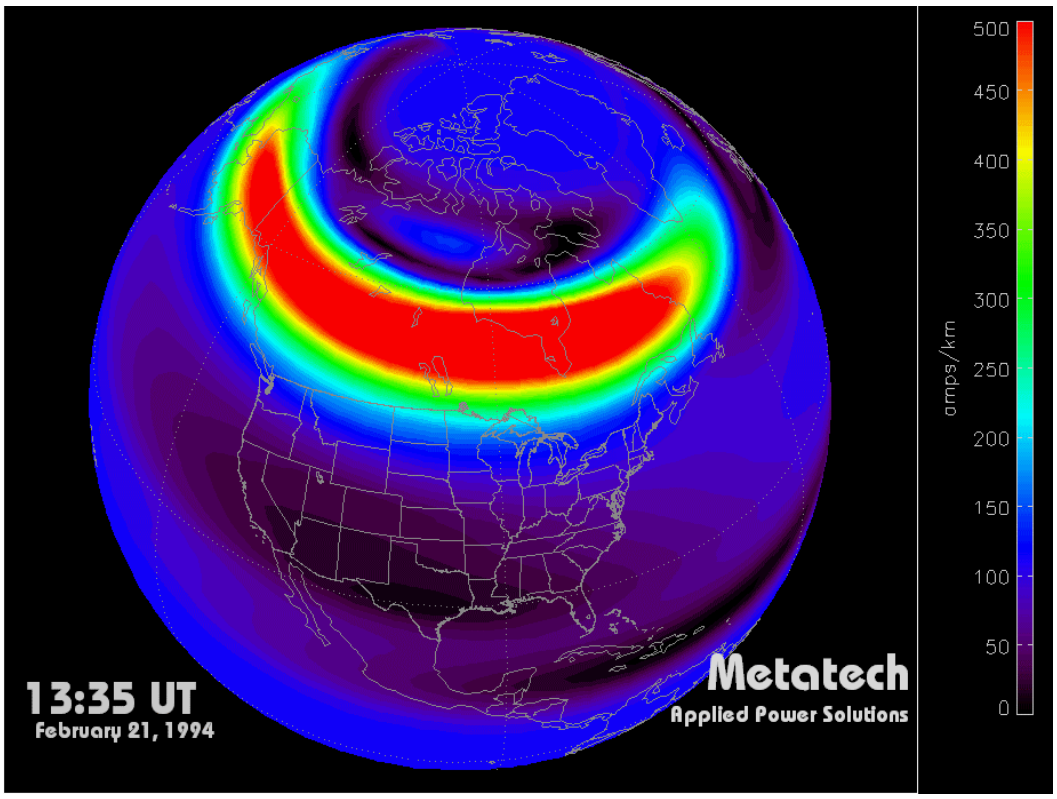

Figure A3-3. Geomagnetic storm conditions at 13:35 UT Feb 21, 1994.

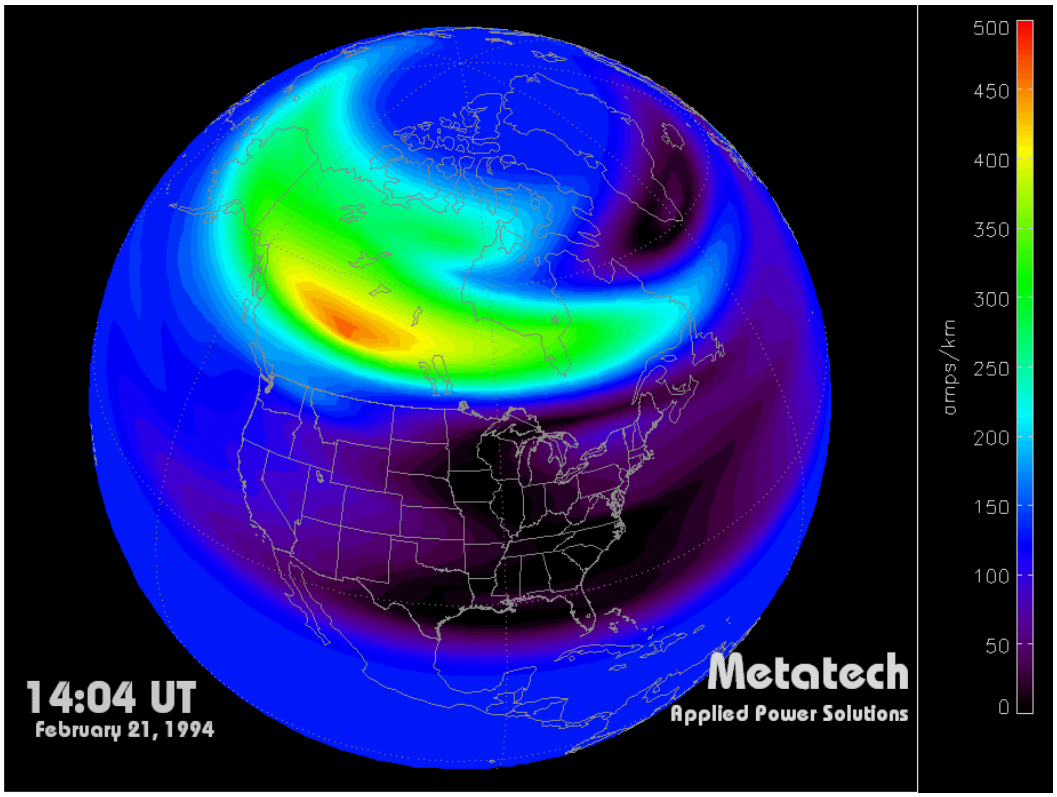

Figure A3-4. Geomagnetic storm conditions at 14:04 UT Feb 21, 1994.

Ohio/Indiana will be significantly weaker, as expected. The intensity (in nT/min) of the observed geomagnetic fields at two observatories east of the region (Fredericksburg, VA and Ottawa, Ontario) are shown in Figure A3-5. These observations also confirm the relatively weak storm conditions over the time interval of interest. In Figures A3-6 and A3-7 provide a comparison of the observed and simulated GIC at the Rockport and Marysville locations (Reference AP3-2). In general, the agreement is very good in respect to both magnitude and overall wave shape. In addition, it is evident that a timing error occurred in the observation of GIC at the Marysville location (a common occurrence given the experimental nature of these measurements).

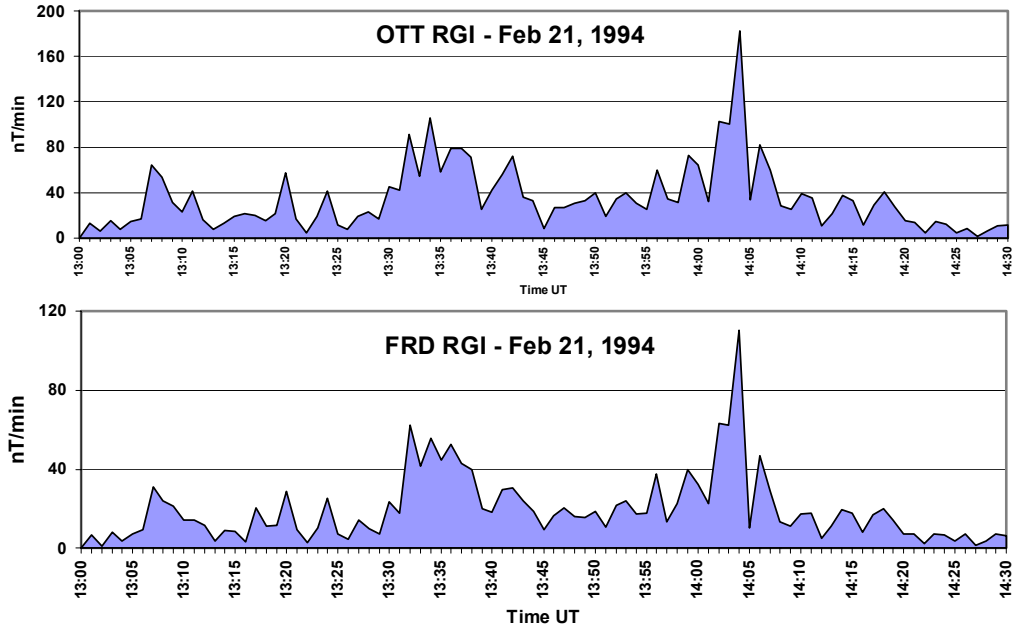

Figure A3-5. Intensity of geomagnetic storm in nT/min on Feb 21,1994 as measured at Ottawa (top) and Fredericksburg (bottom).

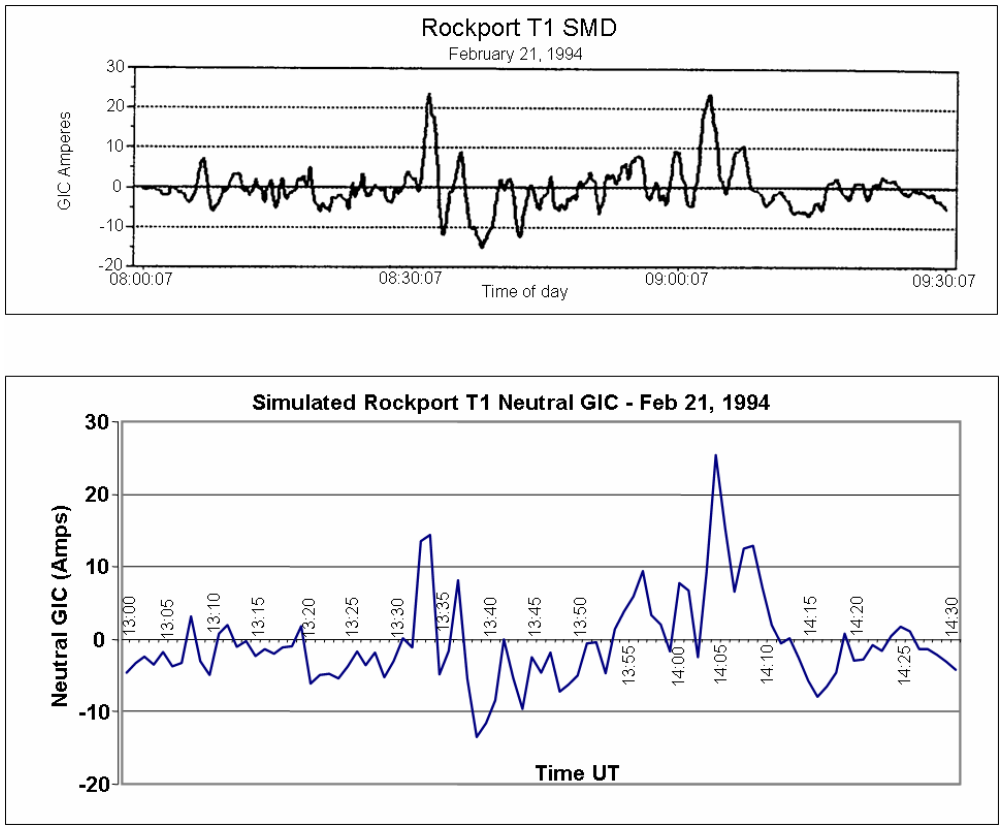

Figure A3-6. Observed GIC (top) and calculated GIC (bottom) for Rockport on Feb 21, 1994.

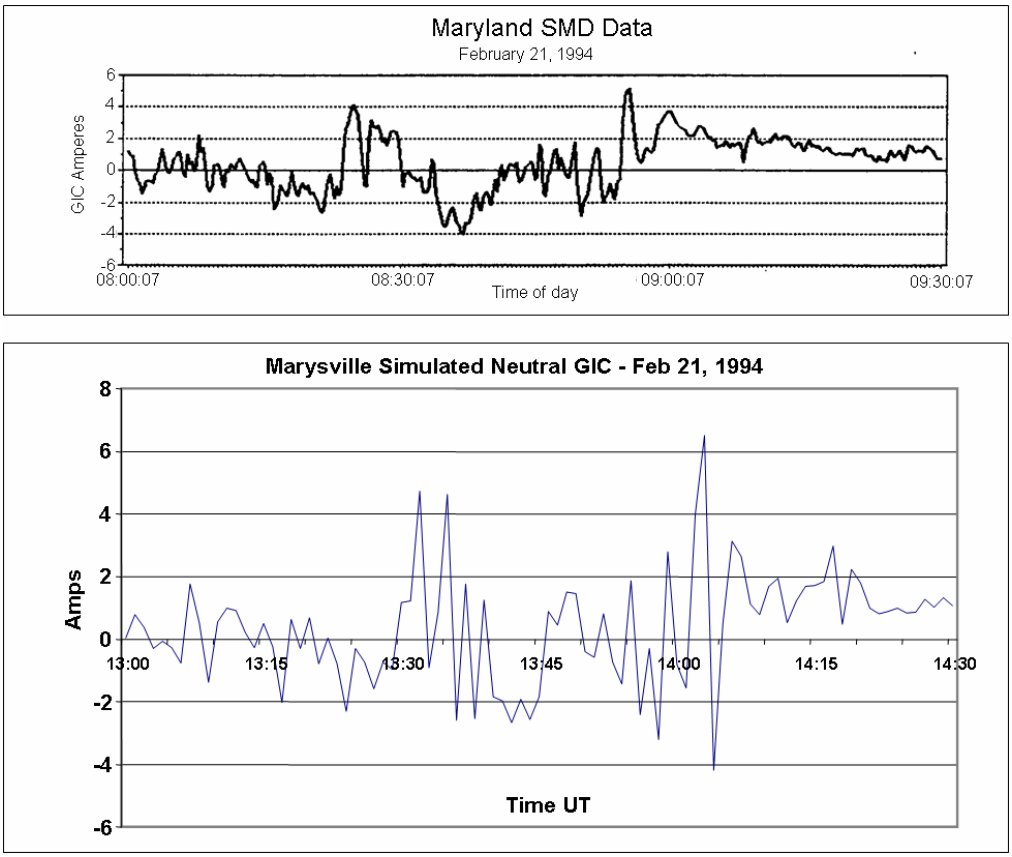

Figure A3-7. Observed GIC (top) and calculated GIC (bottom) for Marysville on Feb 21, 1994.

Other observations can be validated during this same storm. Figure A3-8 shows very good agreement between measured and calculated GIC observed at the Forbes substation in northern Minnesota (Reference AP3-3). Figure A3-9 shows the comparison of peak measured and peak calculated GIC at 10 locations around the U.S. during this storm. With the exception of the Moss Landing station in California, all sites generally provide calculated peak GIC within ~ 20% agreement to observed peak GIC values (References AP3-1 and AP3-4).

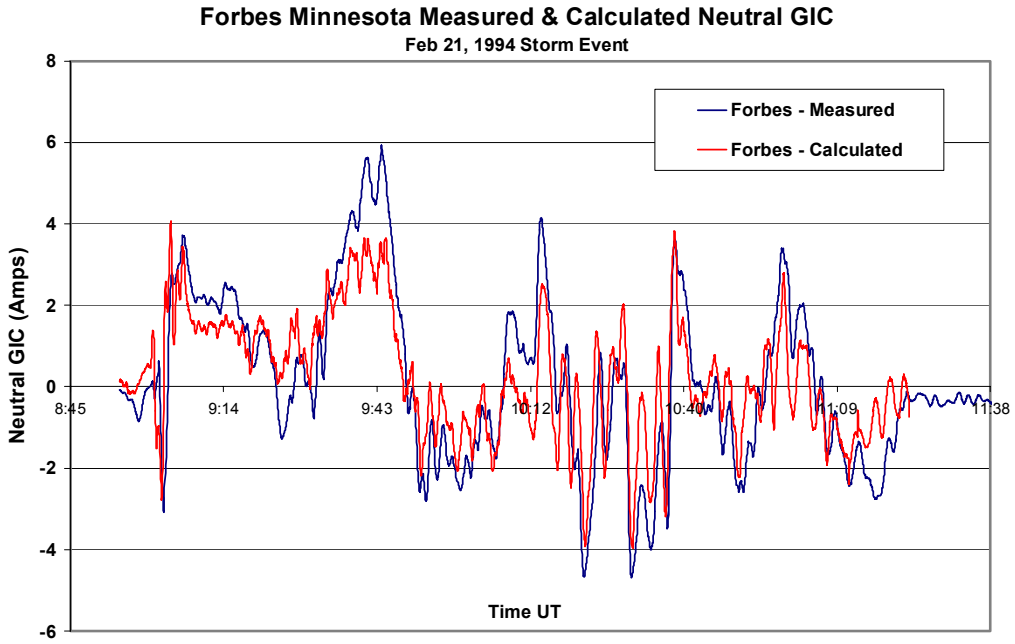

Figure A3-8. Observed GIC and calculated GIC for Forbes on Feb 21, 1994.

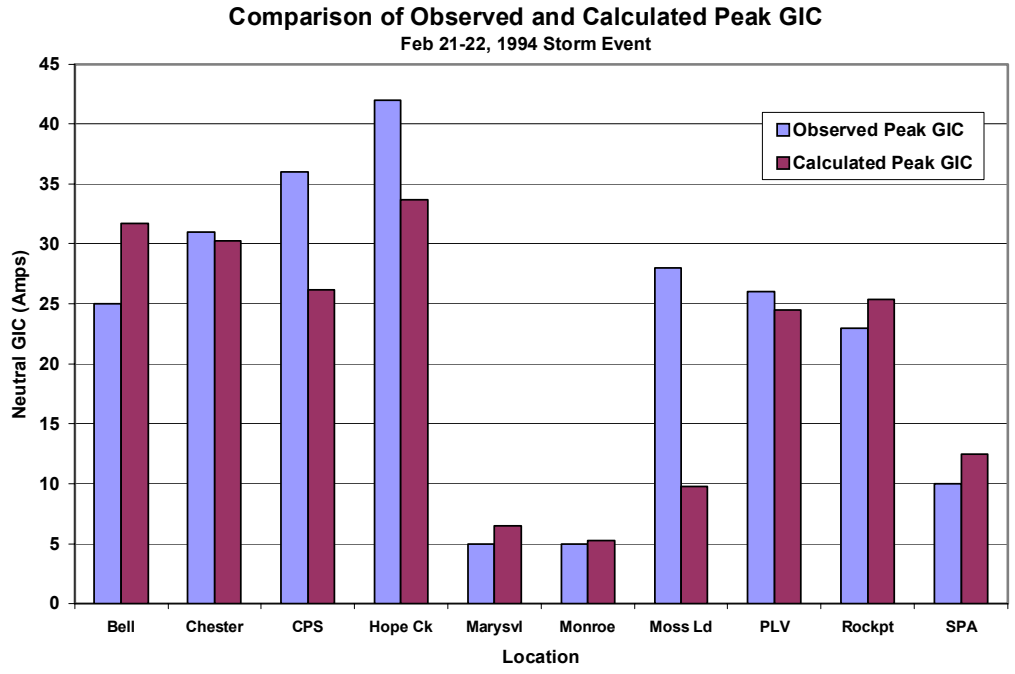

Figure A3-9. Observed GIC and calculated GIC peaks at various locations on Feb 21, 1994.

A3.2 Benchmarking the U.S. Grid Model – Oct 28, 1991 Storm

The Oct 28, 1991 storm also provides a good opportunity to validate the accuracy of the U.S. Power Grid Model. This storm is more energetic than the Feb 21, 1994 storm and also has a sudden and very severe onset condition. This onset, while relatively small in magnitude, mimics in smaller scale the severe disturbance environments that could occur for an E3 environment or a large impulsive electrojet disturbance from a 1-in-100 year storm scenario. Because this was a more energetic storm event, larger levels of GIC have been observed compared to the prior storm. Figure A3-10 provides a summary of the geomagnetic disturbance intensity (in units of nT/min). At around 15:39 UT, a large impulsive disturbance is observed. Figure A3-11 provides a detailed map of the ground-level geomagnetic disturbance conditions at 15:39 UT. As shown, the intense portion of the disturbance is located over a large mid-latitude portion of the eastern U.S. The GIC flow was observed during this storm at a number of eastern U.S. monitoring sites, as detailed in Figure A3-12. The South Canton 765kV station in Ohio provides a model validation opportunity for this storm. Shown in Figure A3-13 is the observed GIC and the calculated GIC at this location during the most intense portion of the geomagnetic storm (Reference AP3-3). Overall good agreement on wave shape and magnitudes of the GIC are confirmed at this location. Observations at other sites are summarized in Figure A3-14. These observations include two locations in Maine, a location at Pleasant Valley in the lower Hudson River Valley in New York, and also a location in Virginia (Reference AP3-4). These comparisons between observed and calculated again indicate general agreement being within approximately 20%.

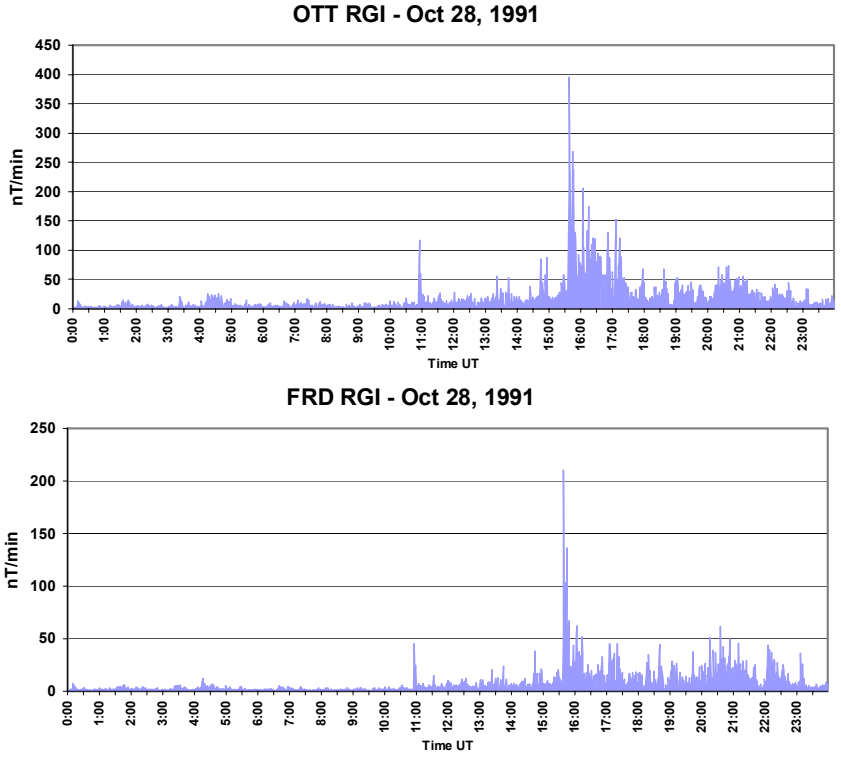

Figure A3-10. Intensity of geomagnetic storm in nT/min on Feb 21,1994, as measured at Ottawa (top) and Fredericksburg (bottom).

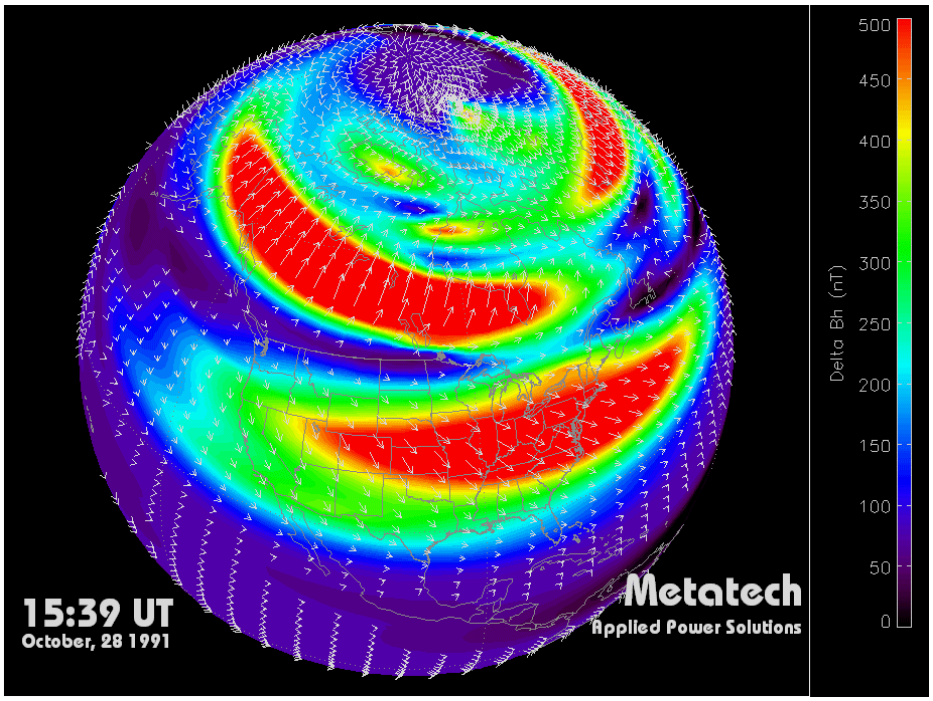

Figure A3-11. Geomagnetic disturbance conditions at 15:39 UT on Oct 28, 1991.

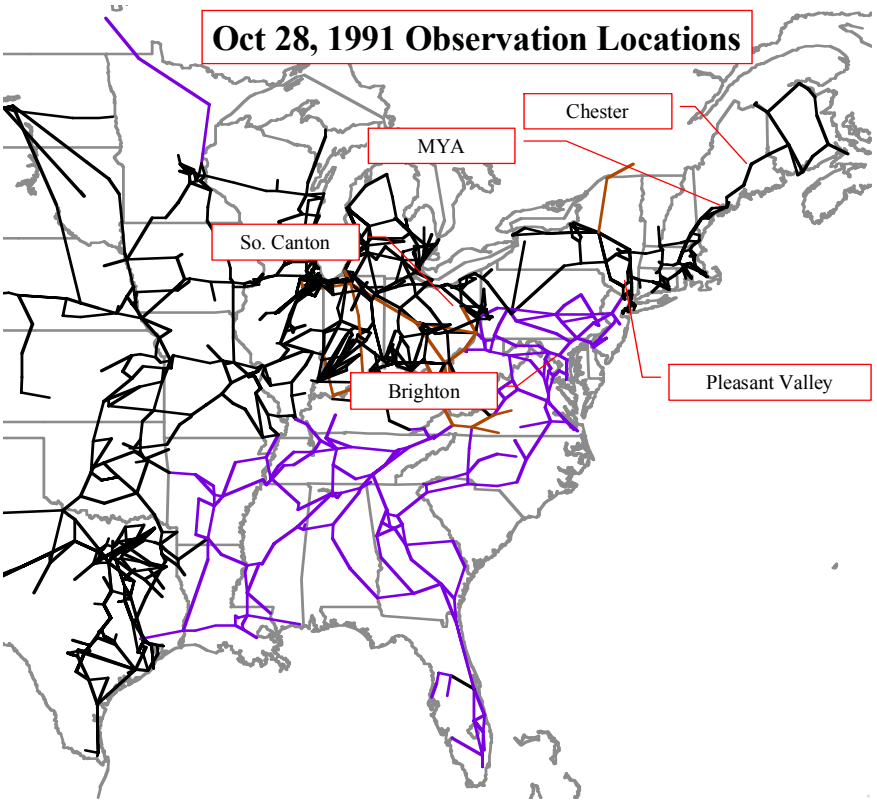

Figure A3-12. Locations of reported GIC observations on Oct 28, 1991.

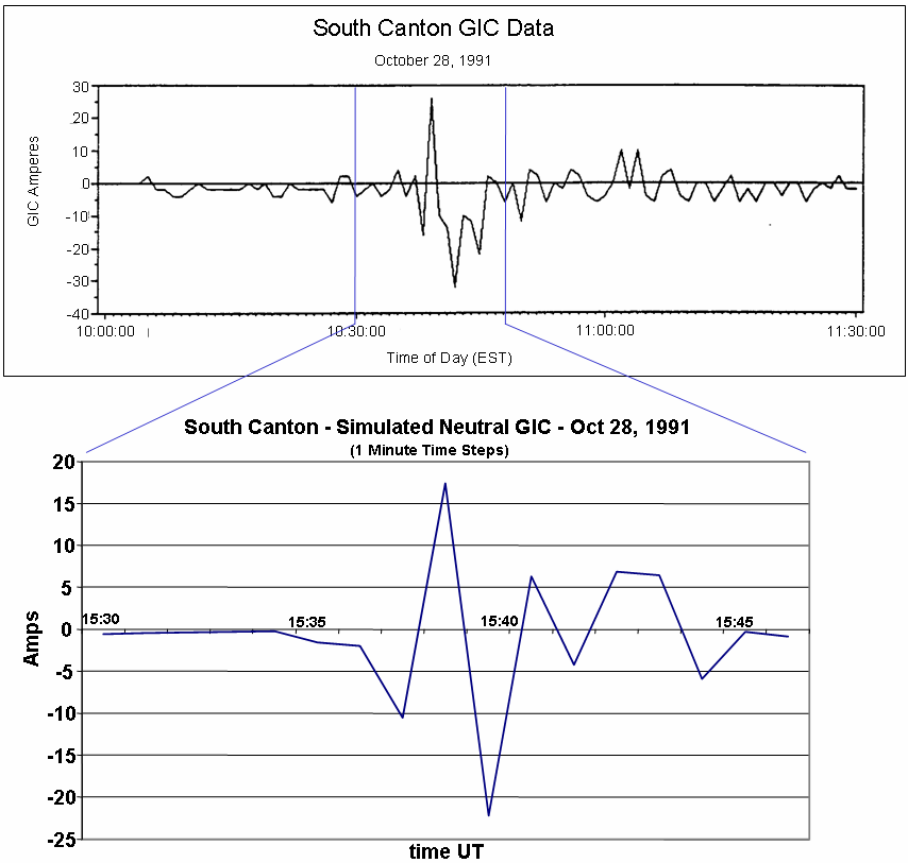

Figure A3-13. Observed GIC (top) and calculated GIC (bottom) at South Canton on Oct 28, 1991.

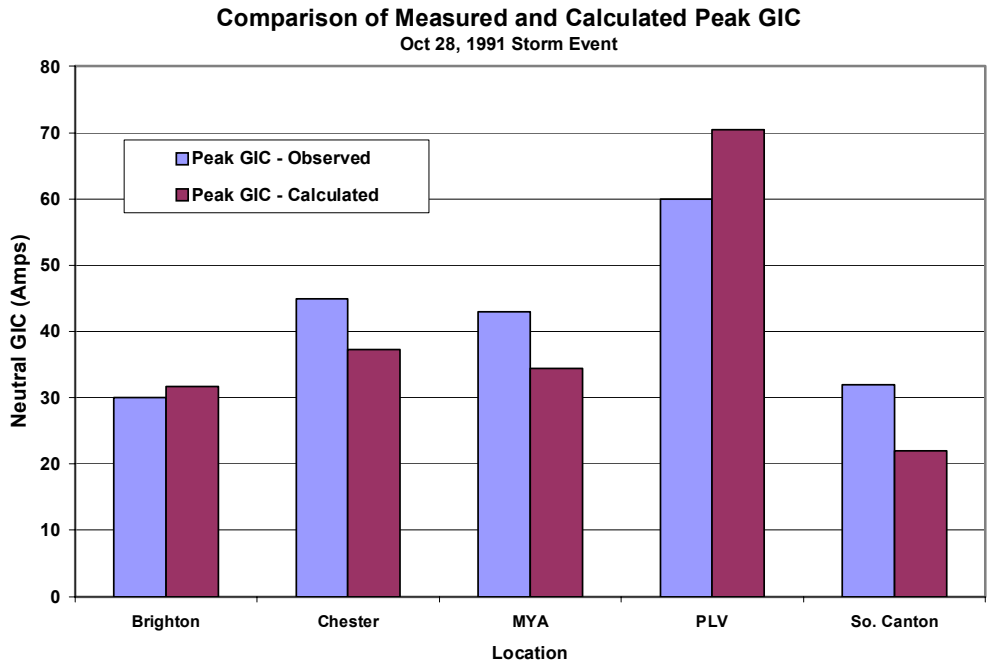

Figure A3-14. Comparison of observed and calculated peak GIC at various locations on Oct 28, 1991.

A3.3 Benchmarking the U.S. Grid Model – May 10, 1992 Storm

The storm on May 10, 1992 was a storm of moderate intensity and duration. The peak intensities of the storm reached levels of approximately 350 nT/min, as observed at the Ottawa observatory, but remained less than 80 nT/min at the Fredericksburg,Virginia observatory. This storm event also provides an opportunity to validate the performance of the model at a number of locations distributed North to South along the power grid in the Eastern U.S. These sites cover the NEPOOL, NYISO, PJM, ECAR and SERC power pool regions. Figures A3-15 and A3-16 provide details of the geomagnetic field disturbance at 9:10 UT and 9:43 UT. As indicated, the most intense portions of the storm event are generally located along the U.S./Canada border throughout the storm duration. Figure A3-17 provides a comparison of peak observed and calculated GICs at eight different locations from the New England through mid-Atlantic regions of the eastern U.S. (Reference AP3-4). These results also confirm general agreement between observed and calculated, with accuracies within ~20%. Figure A3-18 provides a time plot of the observed GIC at these locations, to indicate the relative coherence in GIC intensification that occurs over this large region.

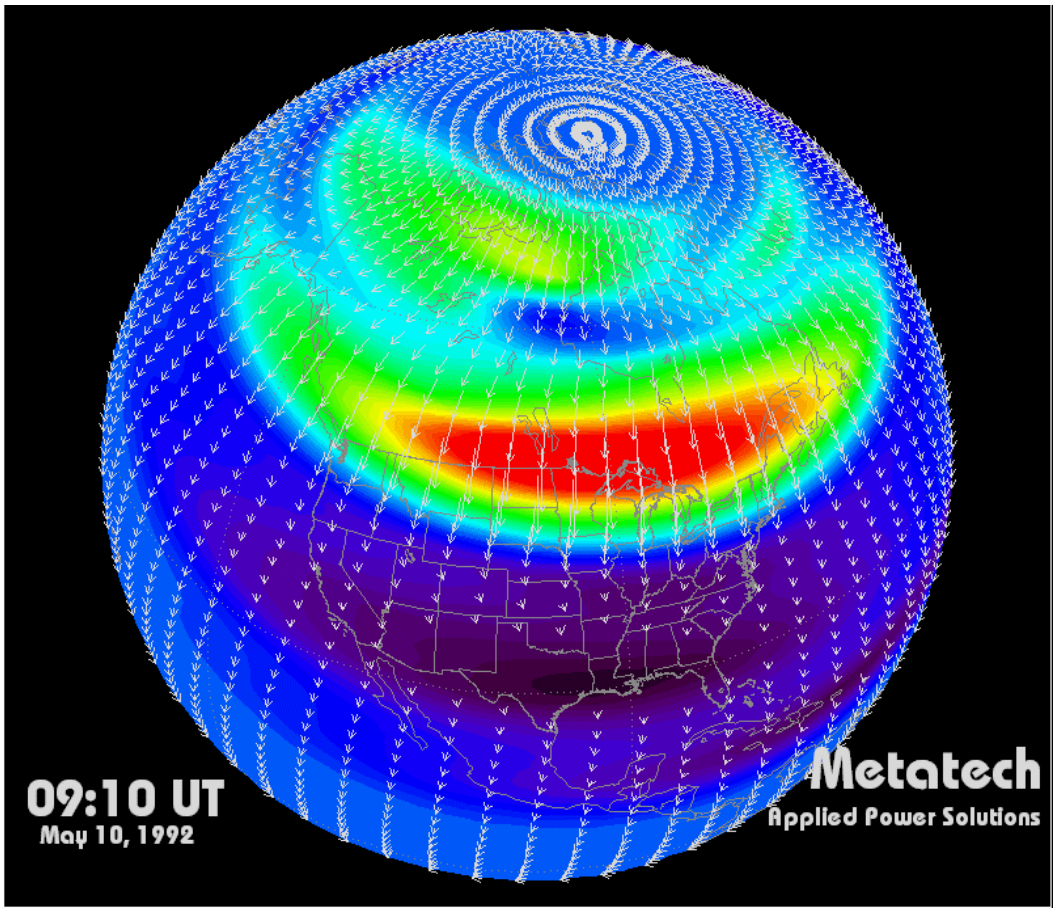

Figure A3-15. Geomagnetic disturbance conditions at 9:10 UT on May 10, 1992.

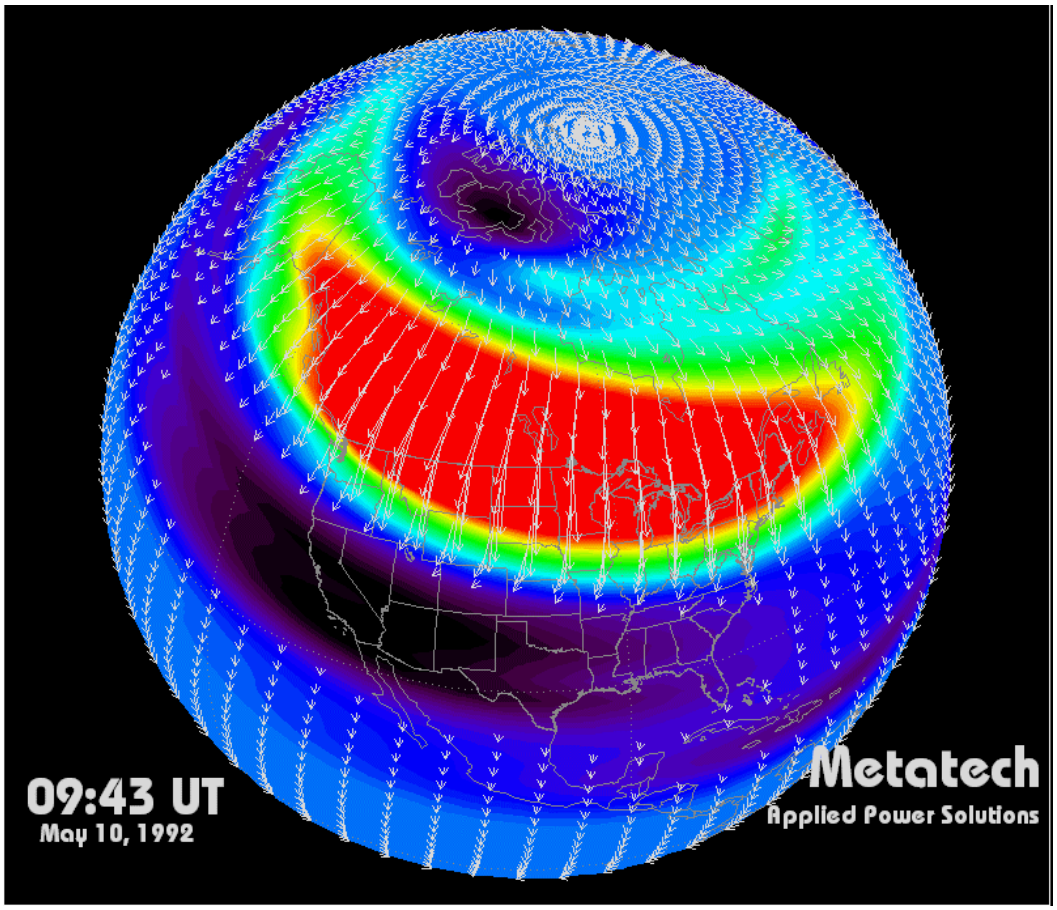

Figure A3-16. Geomagnetic disturbance conditions at 9:43 UT on May 10, 1992.

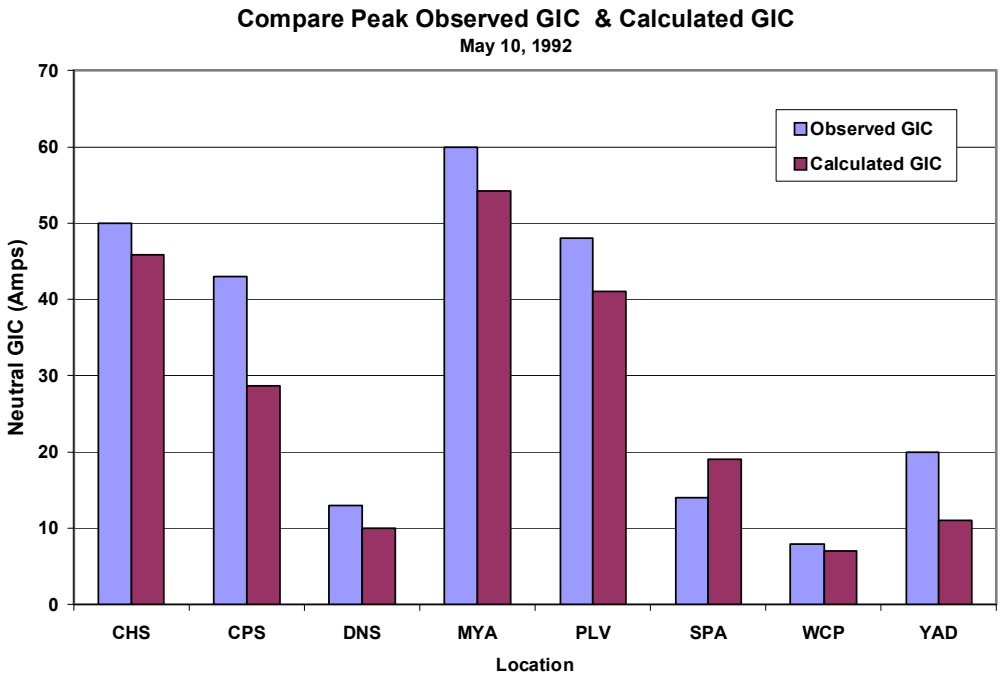

Figure A3-17. Comparison of observed and calculated GIC at various locations on May 10, 1992.

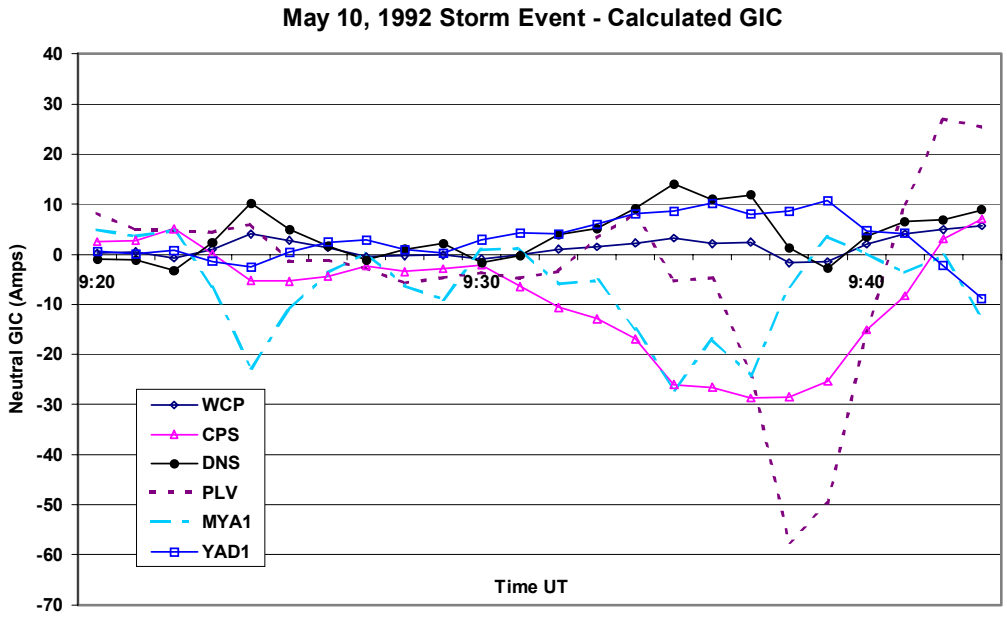

Figure A3-18. Plot of calculated GIC at several locations on May 10, 1992.

A3.4 Benchmarking the U.S. Grid Model – March 24, 1991 SSC Event

The storm event of interest on March 24, 1991 was a sudden storm commencement. This particular geomagnetic disturbance mimics, at a much lower intensity, many of the characteristics of an E3 threat. Therefore, the SSC event allows for the testing of the Grid Model for higher spectral content conditions, as the SSC presents an environment that also closely duplicates the spectral content of the late-time HEMP threat. Because of the rapid onset and rate of change of the geomagnetic field, a higher cadence of magnetometer observation is needed to represent the fast transients. For this disturbance, several sites with 2-second cadence are available (electrojet disturbances are simulated using one-minute cadence). Figure A3-19 provides a plot of the observed geomagnetic field disturbance at Tuckerton, New Jersey during this brief SSC event. SSCs present a less spatially complex disturbance environment. Figure A3-20 provides an observation of simultaneous observations at Point Arena in California, Victoria British Columbia, Ottawa Ontario, and Tuckerton New Jersey. This data, along with studies of many other SSC events, indicated that a plane-wave type disturbance developed over mid-latitude portions of North America. Since the benchmark region of interest is also very close in proximity to the Tuckerton location, this approach is used for simulation of the disturbance environment.

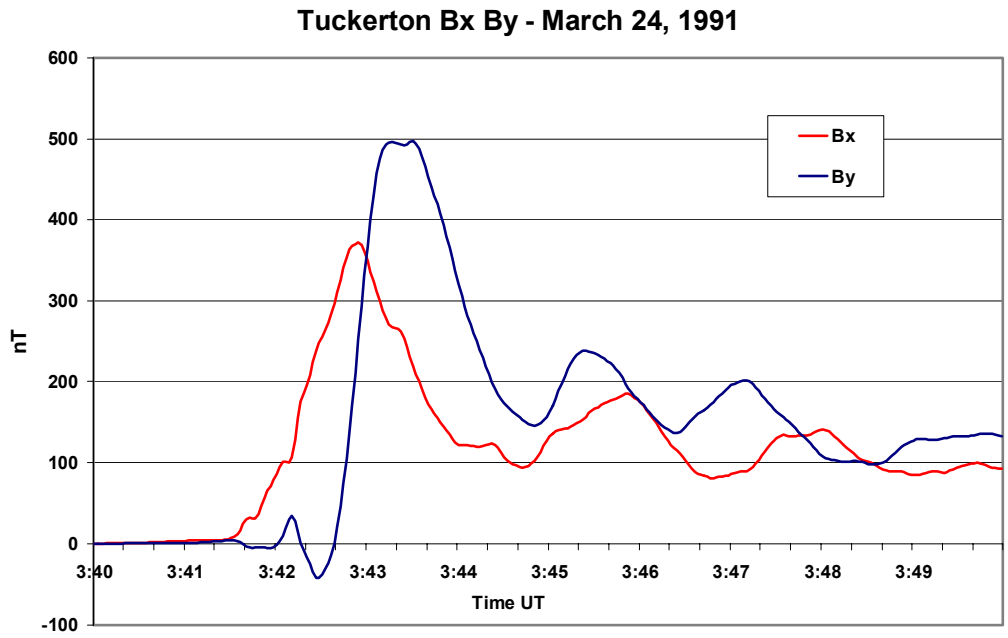

Figure A3-19. Tuckerton, New Jersey geomagnetic observatory data of SSC event on March 24, 1991.

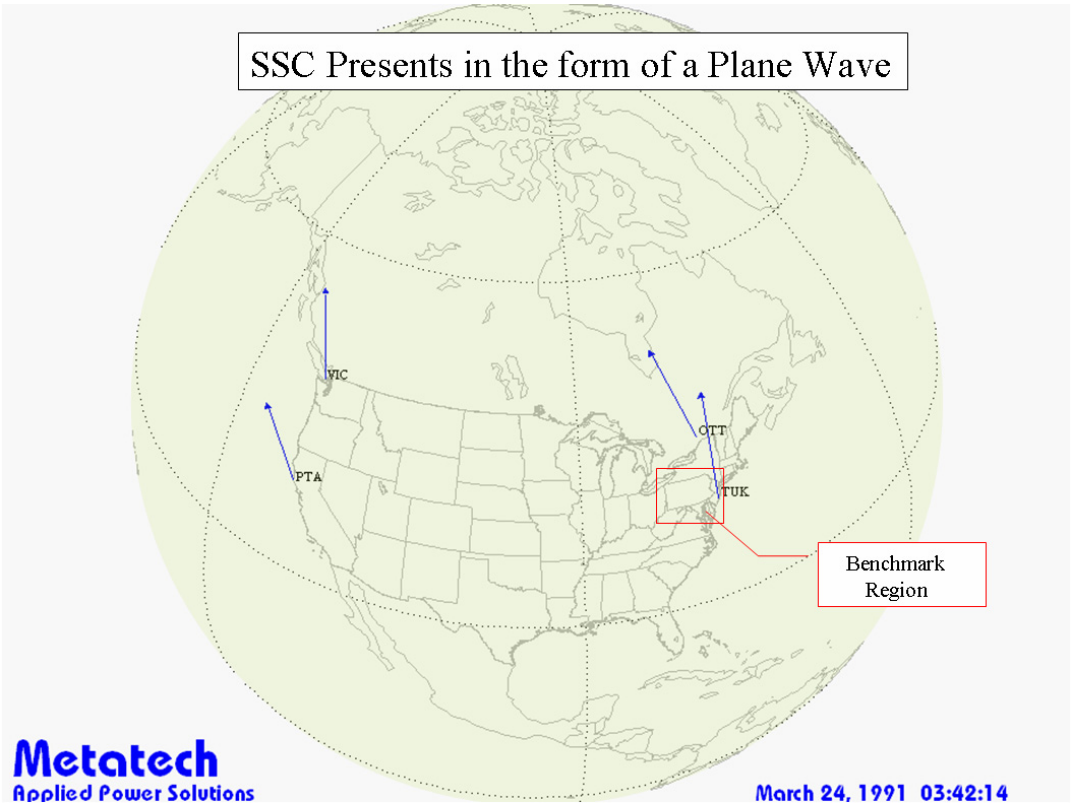

Figure A3-20. Limited high cadence geomagnetic observatory data from March 24, 1991 indicates large plane wave.

Again, a number of measurements of power grid observations were captured during this March 24, 1991 brief disturbance, to indicate the importance of the power system reaction to the disturbance. Figure A3-21 is a paper strip chart record of both GIC and AC observations made at the Limerick nuclear plant transformers near Philadelphia, Pennsylvania (Reference AP3-5). These recordings indicate a very large full-scale spike of GIC observed, as well as a large spike in AC neutral current flow in the Limerick transformer at the time of the SSC event. This confirms that the SSC and, in general, fast geomagnetic disturbances, can produce proportionately large geo-electric field and GIC responses, and also that even these brief GICs will cause near immediate and severe half-cycle saturation response in exposed transformers. Digital measurements were also available from one of the 500kV transformers at the Meadowbrook station in Virginia, though the sampling was only at a 20 second cadence, which limits spectral resolution of the fastest portion of the event (Reference AP3-6). Figure A3-22 provides a comparison of the observed GIC and the calculated GIC for this disturbance. The comparison illustrates that there is relatively good overall agreement, and very good agreement with regard to large-scale magnitude and timescale features, between observed and calculated. The calculation was performed using a 2 second cadence. This likely explains some of the small-scale spectral content differences. Figure A3-23 shows the observation of GIC and transformer AC 3rd harmonic neutral current response at the Pleasant Valley, New York station during the March 24, 1991 SSC event (Reference AP3-4). The very large spike of GIC and observed AC harmonic at the very beginning of the plot are time-coincident with the SSC event. This observation also confirms that large GICs and rapid transformer reaction will occur for these brief events. Figure A3-24 provides a benchmark of the calculated GIC during the SSC at the Pleasant Valley station. This again confirms generally good overall agreement between the model and observations. Figure A3-25 provides a comparison of observed and calculated Peak GICs at 11 different sites extending across Ohio, Pennsylvania, New York, and Virginia. The model and simulation results again indicate very good overall agreement with the observed GICs event, with the higher spectral resolution simulations that are being performed.

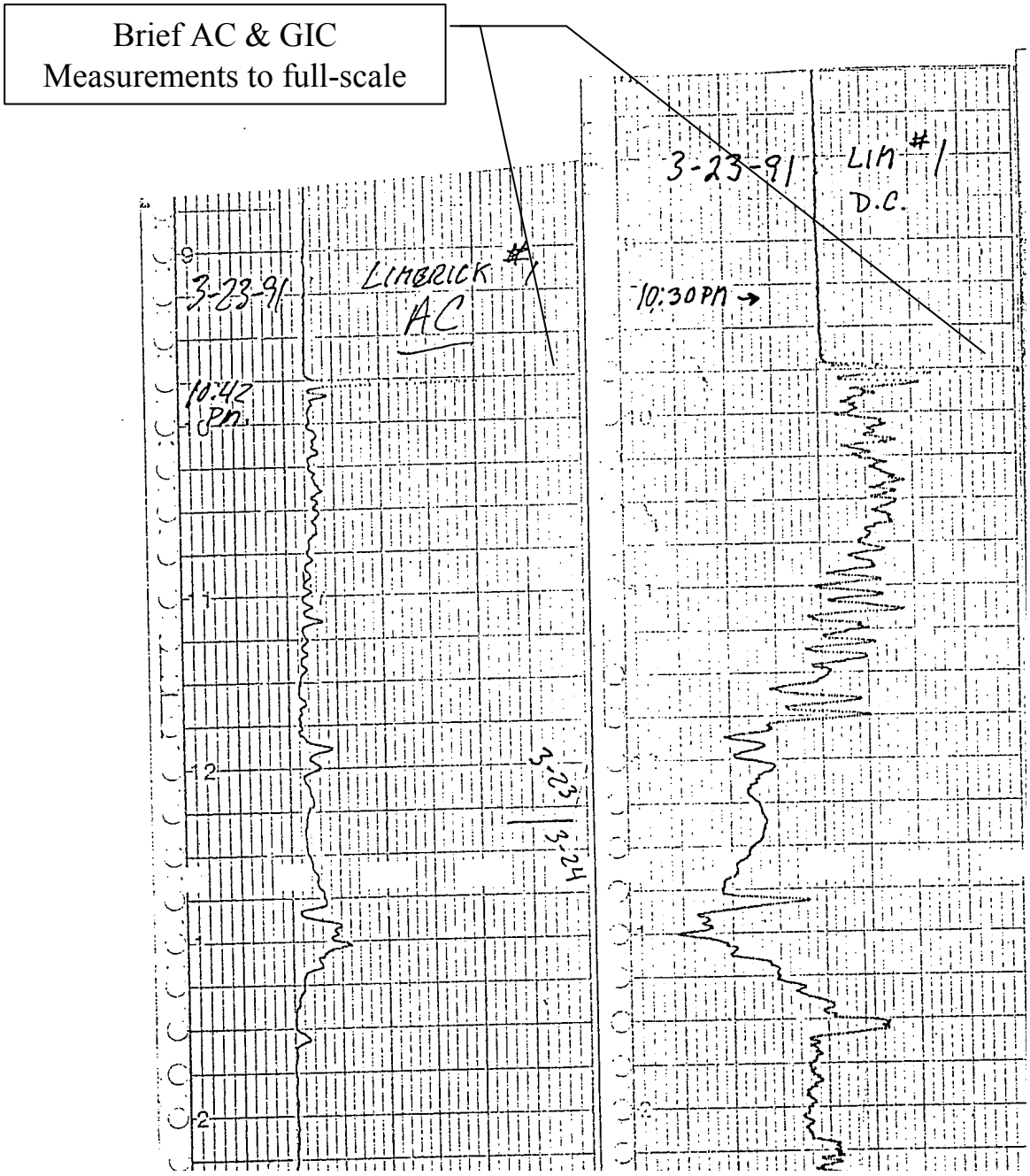

Figure A3-21. Observed GIC and neutral AC current at Limerick on March 24, 1991 (times above are EST, not UT).

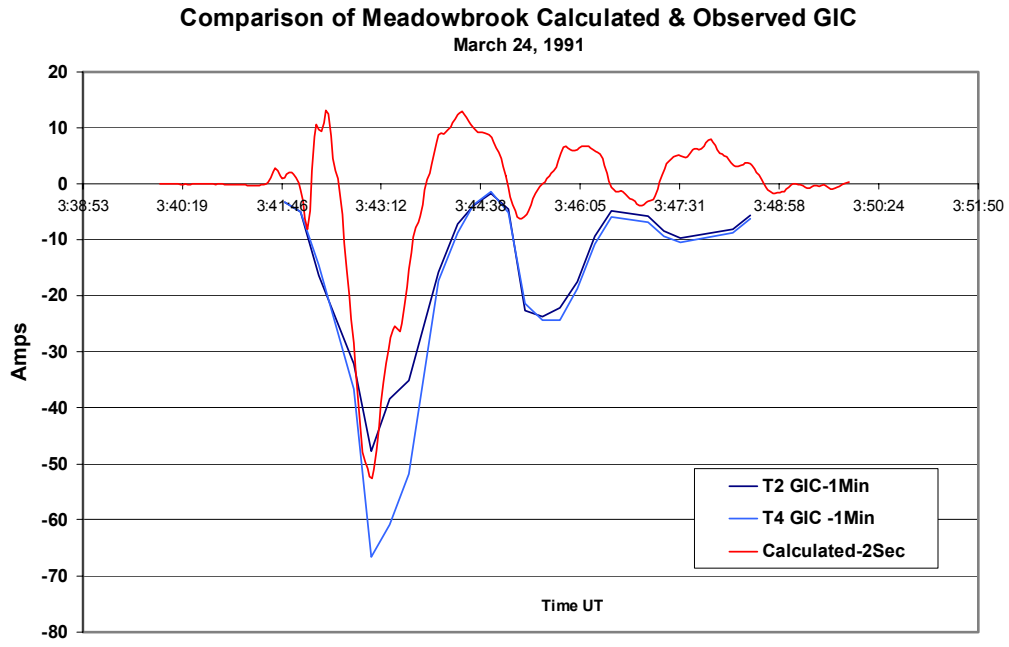

Figure A3-22. Meadowbrook GIC observed and calculated on March 24, 1991.

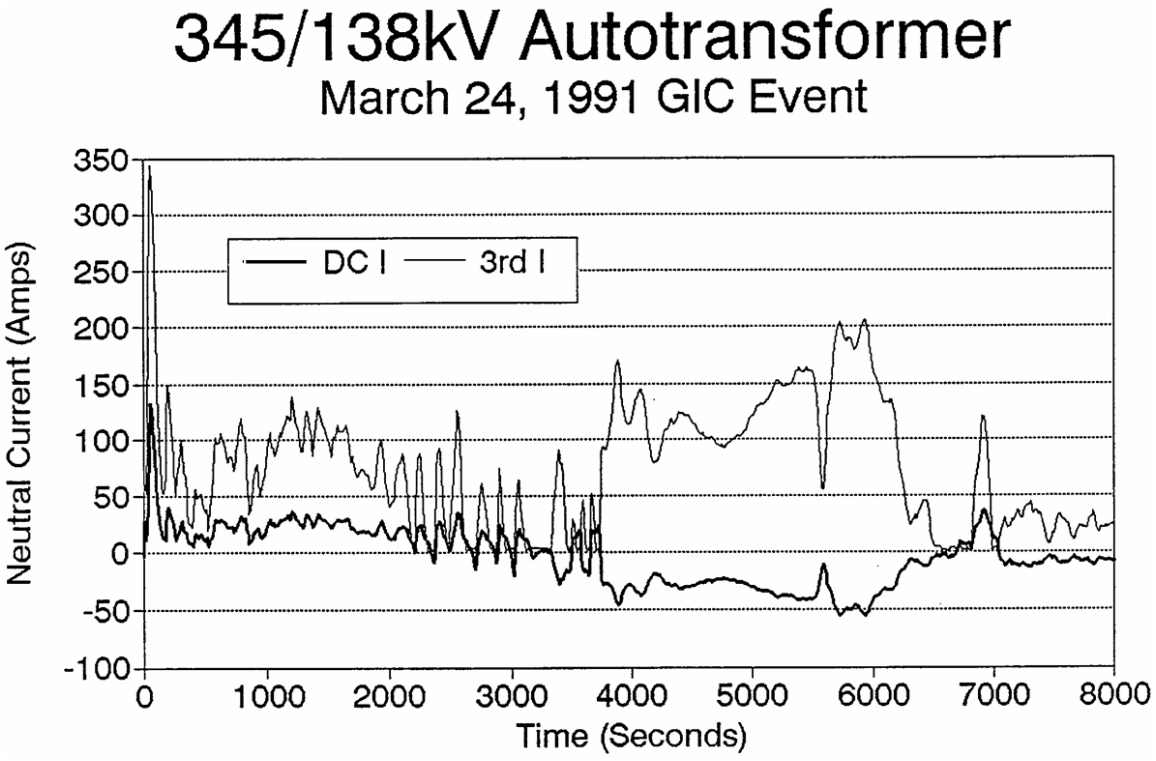

Figure A3-23. Neutral GIC and 3rd harmonic current observed at Pleasant Valley on March 24, 1991.

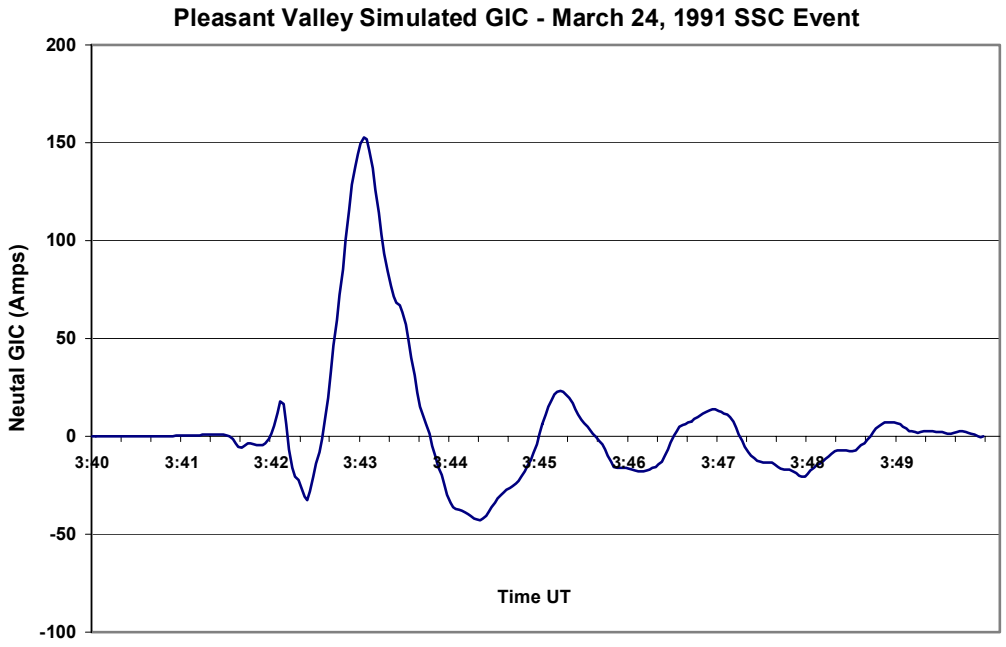

Figure A3-24. Calculated GIC at Pleasant Valley on March 24, 1991.

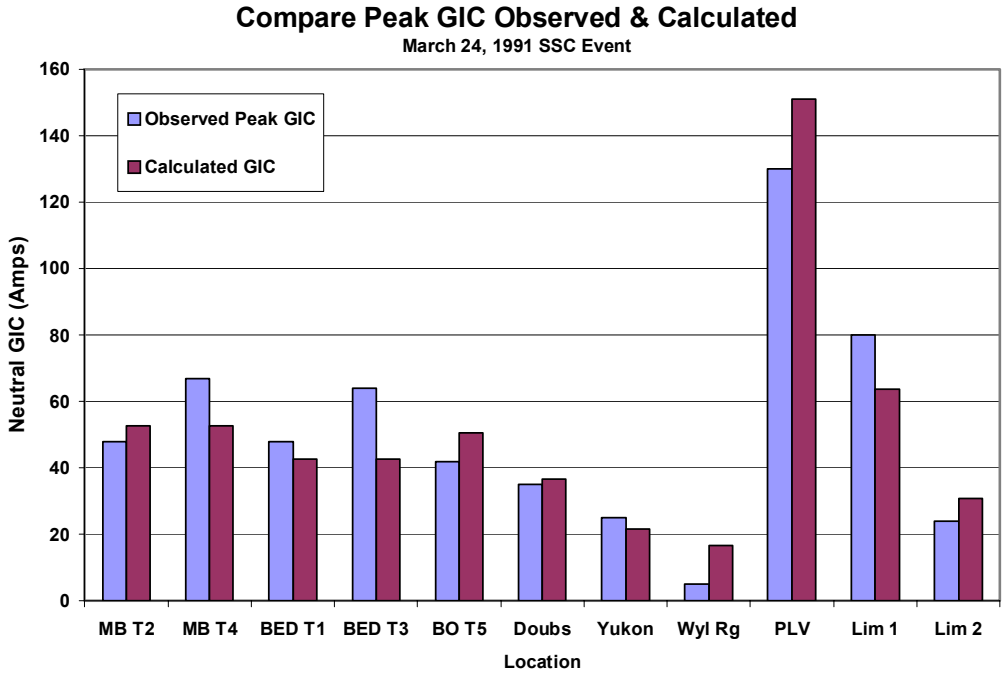

Figure A3-25. Comparison of observed and calculated peak GIC levels at various locations on March 24, 1991.

While these benchmarks have provided opportunities to rigorously evaluate the accuracy of the U.S. Power Grid Model over broad areas, there are some regions that opportunities for model validation are very limited or essentially unavailable using these direct simulation methods. This is particularly true in the southern tier of states, though there have been verified power system impacts due to prior geomagnetic storm in many of these areas as well. For example, during the March 13-14, 1989 superstorm, voltage regulation and large AC neutral current flows were confirmed in the transmission network in and around the Los Angeles area. During the Oct 28, 1991 storm, a DC transmission interconnection between the ERCOT and WECC pools tripped co-incident with the sudden onset of the storm. Impacts were also observed in the TVA transmission network throughout their transmission areas of Tennessee, Mississippi, Alabama, and Georgia. TVA also confirmed the trip of several high-voltage capacitor banks during the SSC event, and also during the main phase of a geomagnetic storm on July 15, 2000. Some of these events occurred as far south as central Mississippi. In this case, TVA was able to provide GPS accurate timestamps, which verify the coincidence of these device failures to specific time stamps of geomagnetic disturbance intensifications (Reference AP3-7). While these events are verified, in most respects they also lack the special measurements of GIC flows, etc., that are most useful for model benchmarking purposes. While the accuracy of these regions is not strictly available for verification, the same methodology was applied in developing the models for these regions as was used for the regions that have been rigorously benchmarked.

A3.5: Quebec Transmission Network Model Benchmark

Because an analysis was performed for the conditions that caused the collapse of the Hydro Quebec power grid during the March 13-14, 1989 superstorm, it was desired to perform a model validation of this network as well. The Quebec system operates asynchronously from the U.S. and other Canadian power grids and is only tied via several DC interconnection points. For purposes of GIC threat assessment, this system can be modeled as a separate network. Very little information has been made publicly available on GIC measurements that would allow for independent validation of the network model. In January 2000, the TransÉnergie Corp (the successor company to Hydro Quebec, responsible for operation of the transmission network) provided a report to the NPCC power pool, discussing the actions they have taken to prepare for geomagnetic storms during the present solar cycle 23 (Reference AP3-8). This report mentioned the estimate of peak system-wide reactive demands during a small storm on Oct 22, 1999. They acknowledge, “There is not sufficient information available to calculate exactly the quantity of reactive power which the network had to provide to compensate for the saturation of power transformer. One can however roughly estimate it as about 700 MVARs”. They also indicate that voltage at several locations on their 735kV transmission network dropped about 2% from normal voltage levels. They further note that the peak of activity occurred around 2:40 EDT or 6:40 UT. Using this limited information, a simulation of the Quebec transmission model was undertaken during this time interval, and an evaluation was made of transmission-wide reactive demand increases that would have occurred on the network. Figure A3-26 provides a plot of the

simulated reactive demand on the network for this storm event. Because this model validation includes all model components (the magnetic storm environment, ground model, Power Grid Model and transformer AC model), this provides an end-to-end validation. As shown, the results indicate a peak reactive demand of approximately 1200 MVARs, which is higher but still within the factor of 2 goal that was sought. This analysis also needs to take into consideration the stated uncertainties on the part of the report authors. The validation also confirmed that the time of peak intensity was 6:40 UT. In relative terms, this model provides useful insights, as comparisons between various storm events will ultimately provide a delta change of stress of one storm event where the system survived compared to other storm events where system collapse occurred. These comparisons would tend to remove any underlying model bias that may be present.

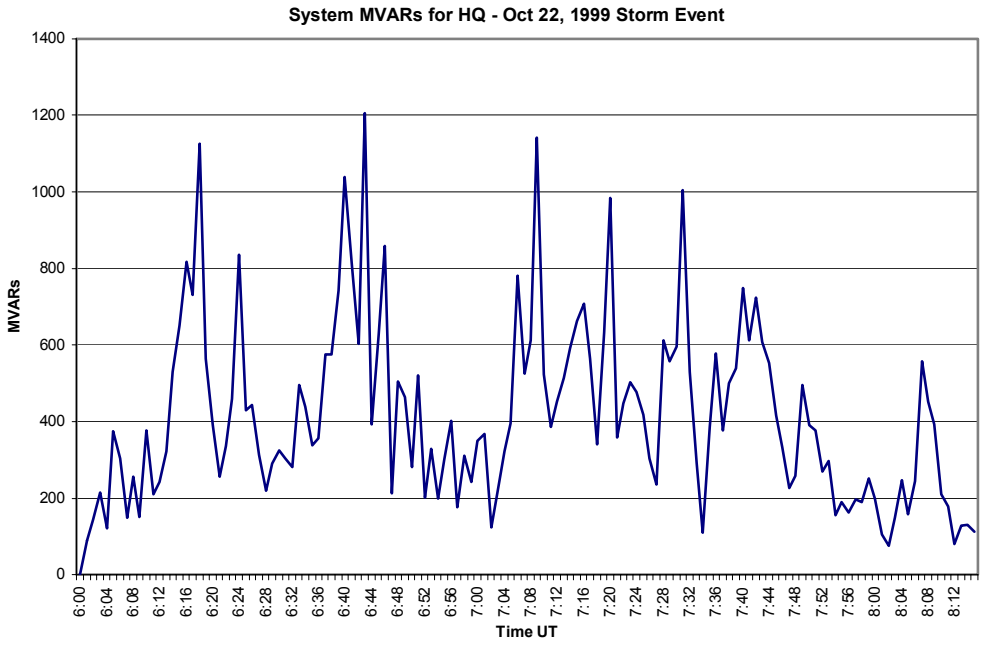

Figure A3-26. Calculated system MVARs in Quebec grid on Oct 2, 1999.

Appendix 3 References

AP3-1 NERC Electric Supply and Demand Database Software – Year 2001 Edition.

AP3-2 E.E. Wilcox, "AEP's GIC Monitoring Experience", Report to EEI, 179th Meeting, Electrical System & Equipment Committee, Cleveland , Ohio, May 17, 1994.

AP3-3 J.G. Kappenman, W.A. Radasky, J.L. Gilbert, I.A. Erinmez, "Advanced Geomagnetic Storm Forecasting: A Risk Management Tool for Electric Power Operations", IEEE Transactions on Plasma Science, Special Issue on Space Plasmas, Vol 28, No 6, December 2000, pp2114-2121.

AP3-4 Electric Research & Management Inc, "SUNBURST GIC Network – Phase II Progress Report", December 1995.

AP3-5 Plot distributed by Don Fagan, Philadelphia Electric.

AP3-6 Report from Phil Gattens Allegheny Electric to EEI, "The Effects of Solar Magnetic Disturbances on the Allegheny Power System".

AP3-7 Email from Fred Elmendorf, TVA, December 2000.

AP3-8 Antonio Dutil, Impact of Geomagnetic Storms on TransÉnergie Transmission System – Situation at the Dawn of the Year 2000, Report to NPCC, January 2000.

Appendix 4
Validation of Transformer and Power System Impact Modeling for GIC

A4.1 Transformer Modeling Background and Validations

A transformer with half-cycle saturation makes a rich source of even and odd harmonics and draws significant inductive VARs from the power system. This potentially could create a variety of problems in the power system. It is very important to estimate and evaluate the effect of GIC on transformers and the power system. The modeling of the power system includes this aspect of transformer behavior under geomagnetic storm or other comparable threat conditions from HEMP E3 environments, in order to provide an accurate assessment of system impacts. GIC monitoring of various levels of sophistication has been in operation in North American. More importantly, detailed staged tests have been performed to closely study the harmonics and reactive power consumption during transformer saturation. Several simulation methods have been developed to calculate harmonic currents and reactive power intake of transformers resulting from GIC. These include the FEM based models (Reference AP4-1), and the magnetic circuit models (Reference AP4-2).

Transformer core configuration is one of the primary design factors when considering the behavior of a transformer in the presence of GIC, and also needs to be incorporated into models as well. It is less complicated to estimate harmonic currents for the single-phase transformer since it involves only one common main flux path that can be represented by the non-linear inductance (or the no-load *V-I* curve of the transformer). An iteration algorithm can be used to obtain harmonic currents with a given value of GIC. Once the harmonics currents are available, it is straightforward to calculate the reactive power. For three-phase transformers, the key problem is in the construction of the equivalent non-linear magnetizing curve for the entire transformer.

As shown in the following case validations, the models for transformer half-cycle saturation generally produce results within a range of +/-15% over the range of GIC values tested.

A4.2 Simulation Results

A series of cases were developed, simulating each of the transformer models. An extensive literature research was also undertaken to find specific cases of test examples for each design. Models were then developed for each specific case, and the calculated results were compared with the measurement results to verify the feasibility of the method.

Case 1: single-phase, core form transformer bank (Reference AP4-3, Table 1)

Figure A4-1 shows the measured current waveform and the frequency spectrum for a GIC of 11.5 amp/phase (Reference AP4-3). The calculations for the exciting current waveform and the frequency spectrum are the same, as seen in Figure A4-2.

Table 1. Characteristics of each single-phase unit of Transformer T4

MVA 160/320/400
Type ONAN/ONAF/OFAF
Single-phase 2-legged core-form
HV 512500 GRD Y/295900
LV 242000 GRD Y/139715
Tertiary Voltage 12600
Interleaved Disc winding
Tertiary Exciting Current = 10.2 A
Tertiary Core Loss = 86 kW
Tertiary Magnetising Current = 7.58 A
500 kV Magnetising Current =

$$7.58\ \text{A} \cdot \frac{12.6\ \text{kV}}{512.5/\sqrt{3}\ \text{kV}} = 0.32\ \text{A}$$

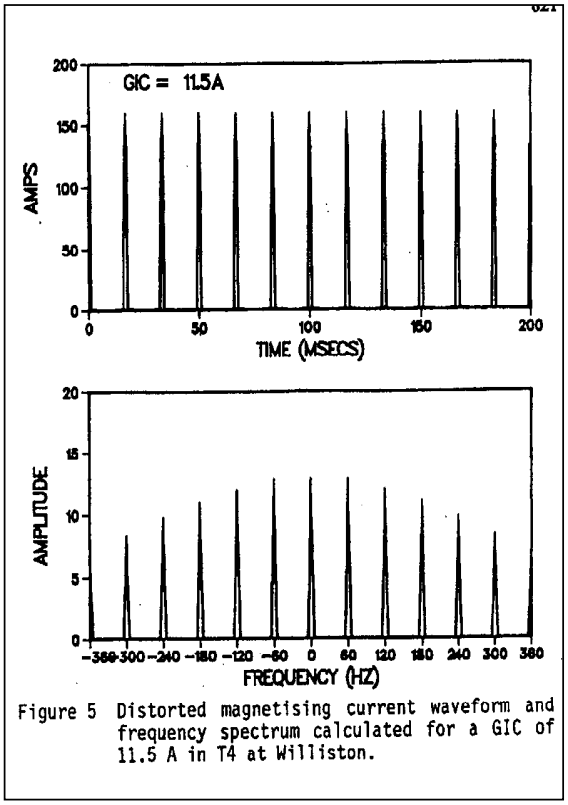

Figure 5 Distorted magnetising current waveform and frequency spectrum calculated for a GIC of 11.5 A in T4 at Williston.

Figure A4-1. The measured current results (512.5/242 kV, from core form, single-phase).

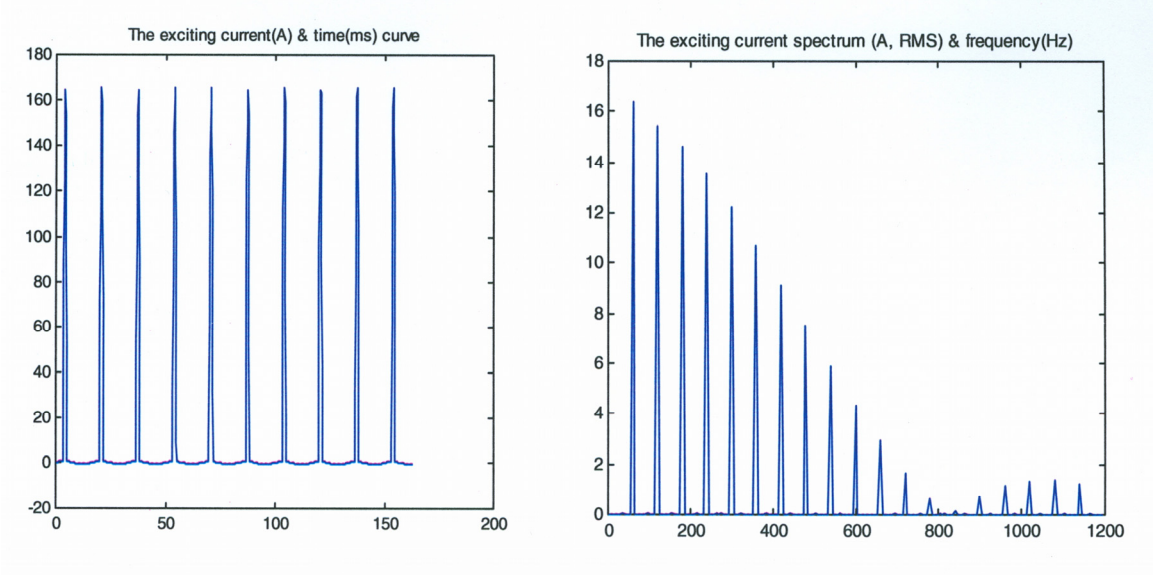

Figure A4-2. The exciting current waveform and frequency spectrum calculated for a GIC of 11.5 amp/phase (512/242 kV single-phase transformer).

Case 2: 500/230kV, 360 MVA single phase shell form auto transformer (Reference AP4-4)

Figure A4-3 shows the exciting current waveform and the frequency spectrum for a GIC of 75A in the neutral. The peak of the fundamental frequency exciting current is 49.7A, and the peak of the exciting current is ~ 300A. Compared with the test result in Figure A4-4, the measured fundamental frequency exciting current is about 47A (Reference.3, Figure 5-3), the deviation is 5.7%. The measured peak of the exciting current is about 300 A.

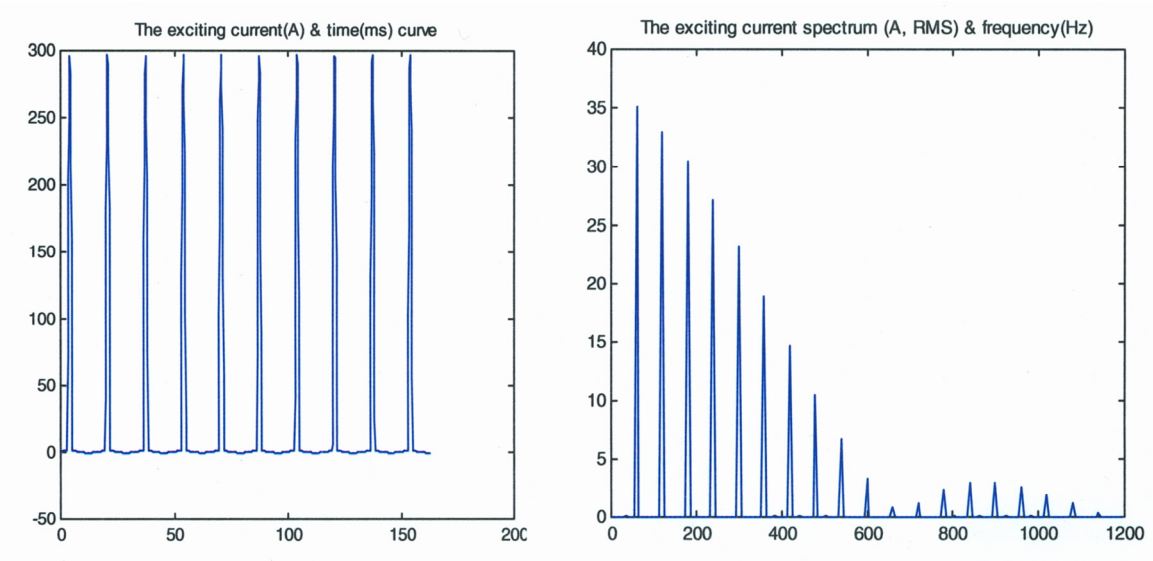

Figure A4-3. Exciting current waveform and frequency spectrum calculated for a GIC of 75A in neutral (500/230 kV single-phase shell form auto-transformer).

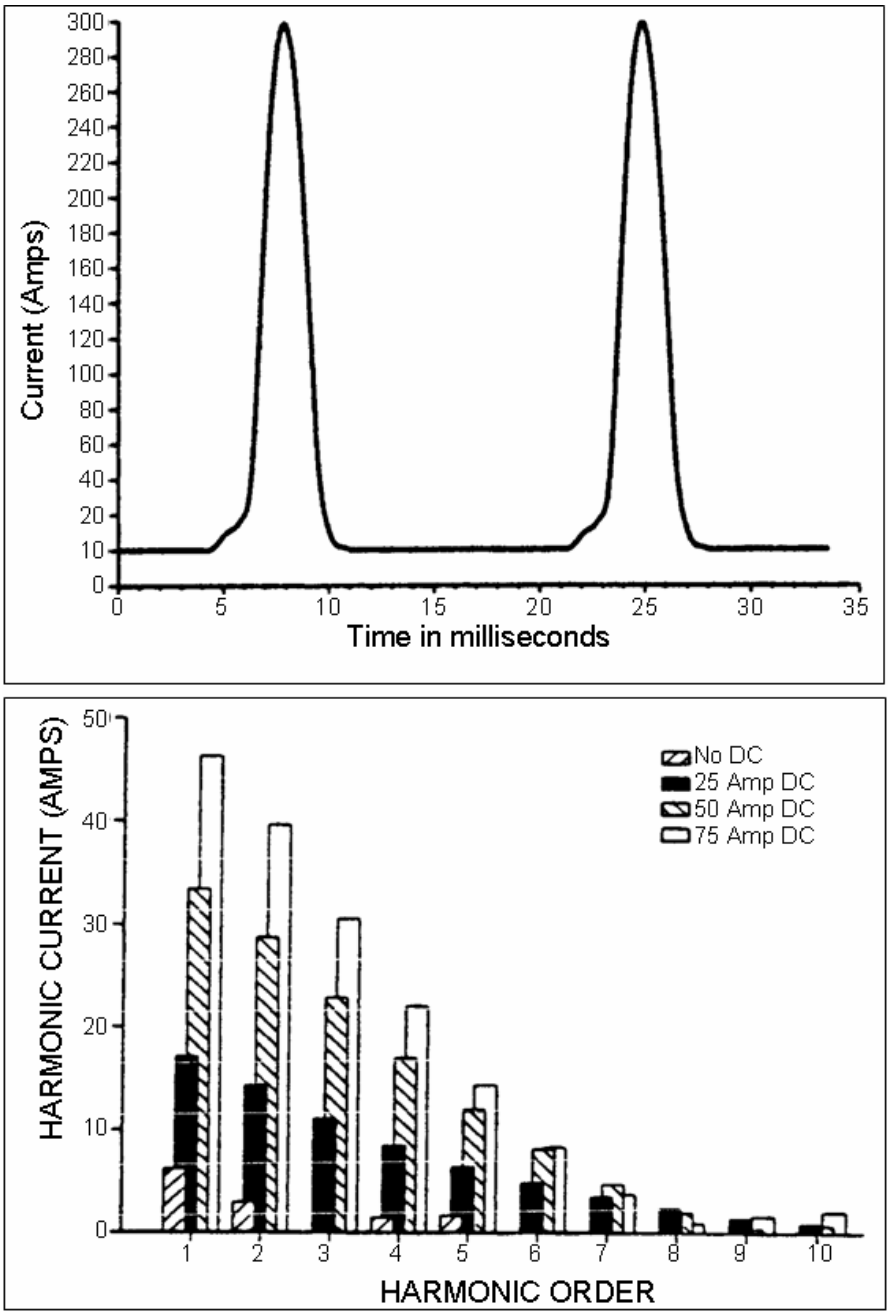

Figure A4-4. The test result (500/230 kV, shell form, single-phase, auto-transformer).

Case 3: 230/115 kV 200 MVA, 3-phase, 3-legged core form auto-transformer (Reference AP4-4)

Figure A4-5 shows the exciting current waveform and the frequency spectrum for a GIC of 75A in the neutral. The calculated reactive power is 3.27 MVAR, the second harmonic current is 7.0A RMS, and the peak exciting current is 92A. Compared with the test results in Figure A4-6, the measured second harmonic current is about 6.72A RMS

(the deviation is 4.2%) and the measured reactive power is 5 MVAR. The simulated RMS value of second harmonics is 10.5A with GIC of 100A in neutral. The simulated reactive power is 4.59 MVAR, the test result is 10.6A RMS, the deviation is 1%, and the measured reactive power is 8 MVAR.

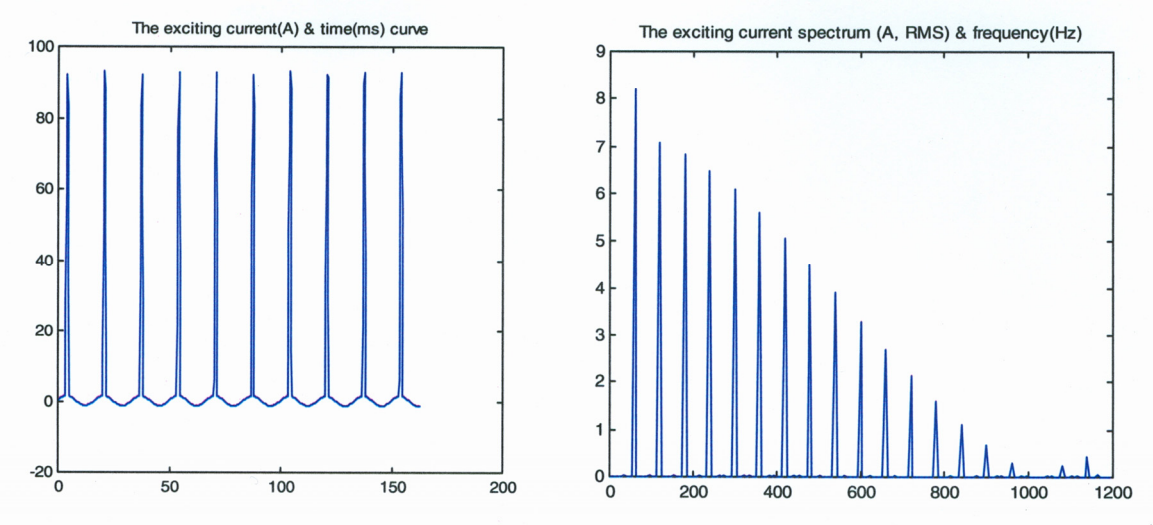

Figure A4-5. The exciting current waveform and frequency spectrum calculated for a GIC of 75 amps in neutral (230/115 kV, 3-legged, 3-phase core form auto-transformer).

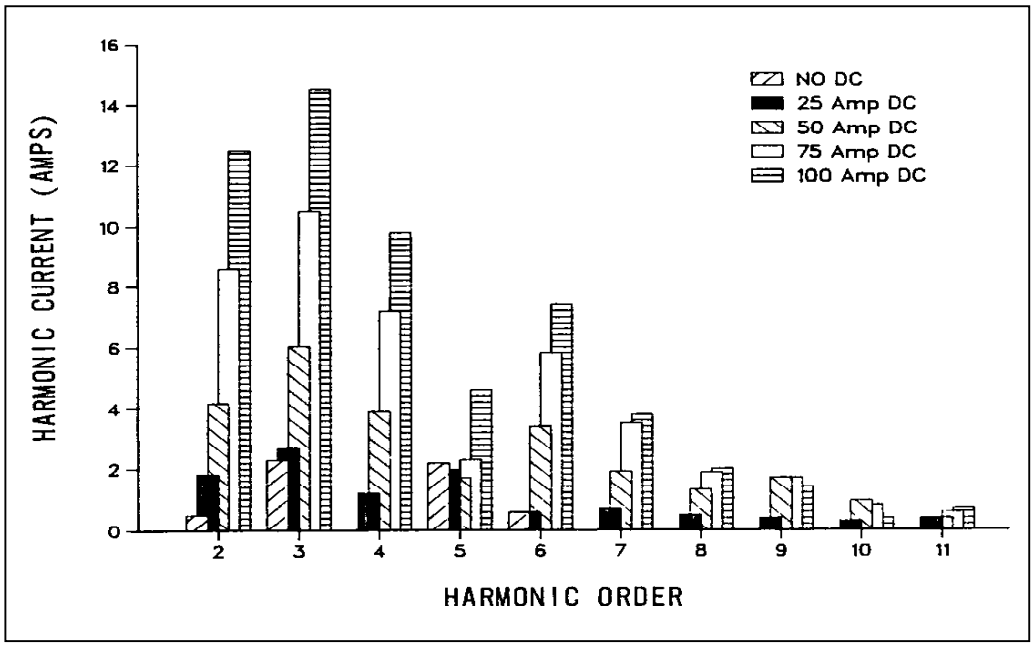

Figure A4-6. The test results (230/115 kV, 3-legged, 3-phase core form auto-transformer).

Case 4: 230/115 kV 200 MVA, 3-phase, shell form auto-transformer (Reference AP4-4)

Figure A4-7 shows the calculated exciting current waveform and the frequency spectrum for a GIC of 75A in the neutral. The reactive power is 4.67 MVA and the second harmonic current is 9.5A, and the maximum of the exciting current is 60.0A. Compared with the test results in Figure A4-8, the measured second harmonic current is about 10.0A, and the deviation is 5%. The simulated RMS value of second harmonics is 12.0A with a GIC of 100A in neutral. The test result is 11A, and the deviation is 9.1%.

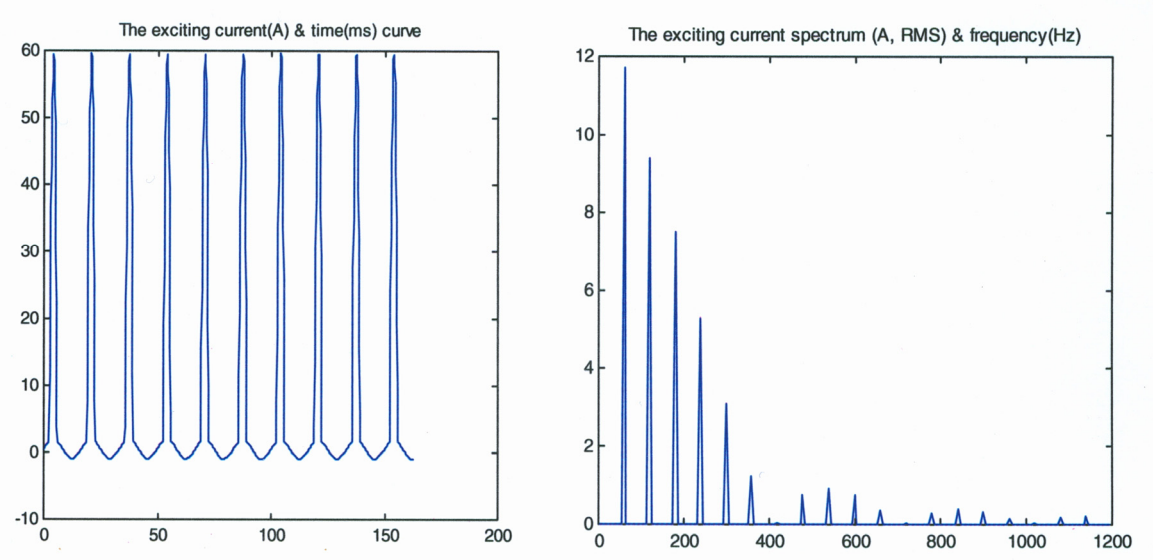

Figure A4-7. The exciting current waveform and frequency spectrum calculated for a GIC of 75 amps in neutral (230/115 kV, 3-phase, shell form auto-transformer).

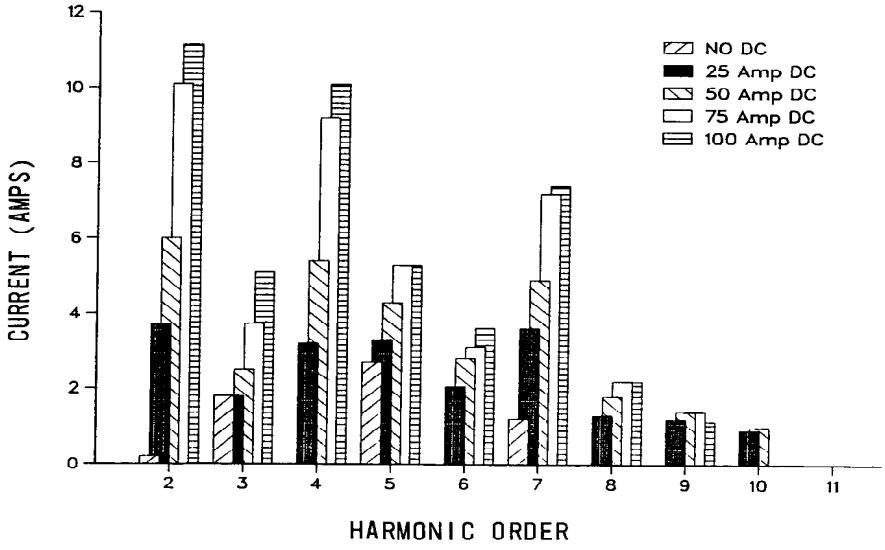

Figure A4-8. The test results (230/115 kV, 3-phase, shell form auto-transformer).

Case 5: 400 kV, 400 MVA, 5-legged, three-phase, core form, Y-Y transformer (Reference AP4-6)

Figure A4-9a shows the excitation current waveform and the frequency spectrum for a GIC from tests with 200A in the neutral from Finngrid tests. Figure A4-9b provides a replication of B phase (or center phase) excitation current for this 5-legged core form transformer. Good agreement is achieved on overall waveform and magnitudes of the excitation current. Figure A4-10a provides a comparison of observed and calculated reactive demand increases (MVARs) for various levels of DC current from 0 to 200 amps. Figure A4-10b provides a chart of the observed harmonics from the 5-legged core form transformer with 200 amps of GIC, while Figure A4-10c provides a comparison of observed and calculated harmonics for the same transformer. In all cases deviations between observed and measured MVARs and harmonics are small.

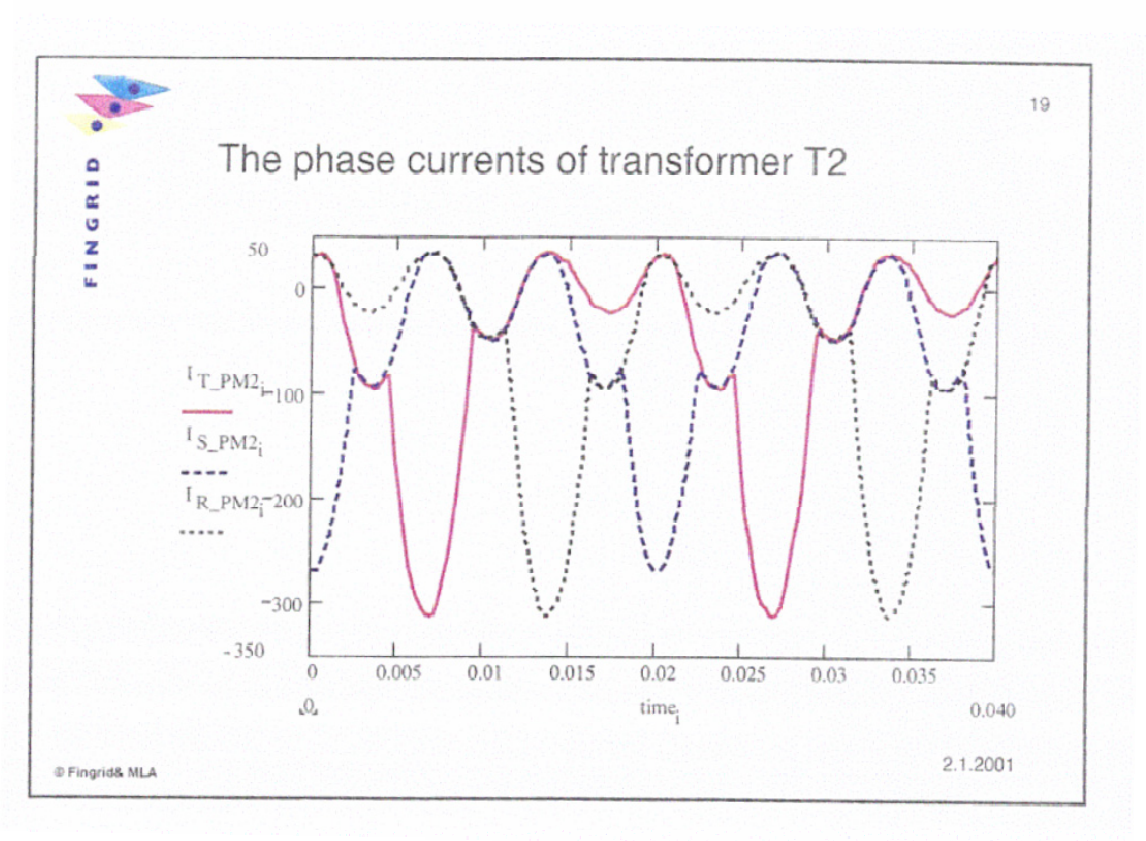

Figure A4-9a. Measured transformer excitation current with 200 amps in transformer neutral on 5-legged core form transformer.

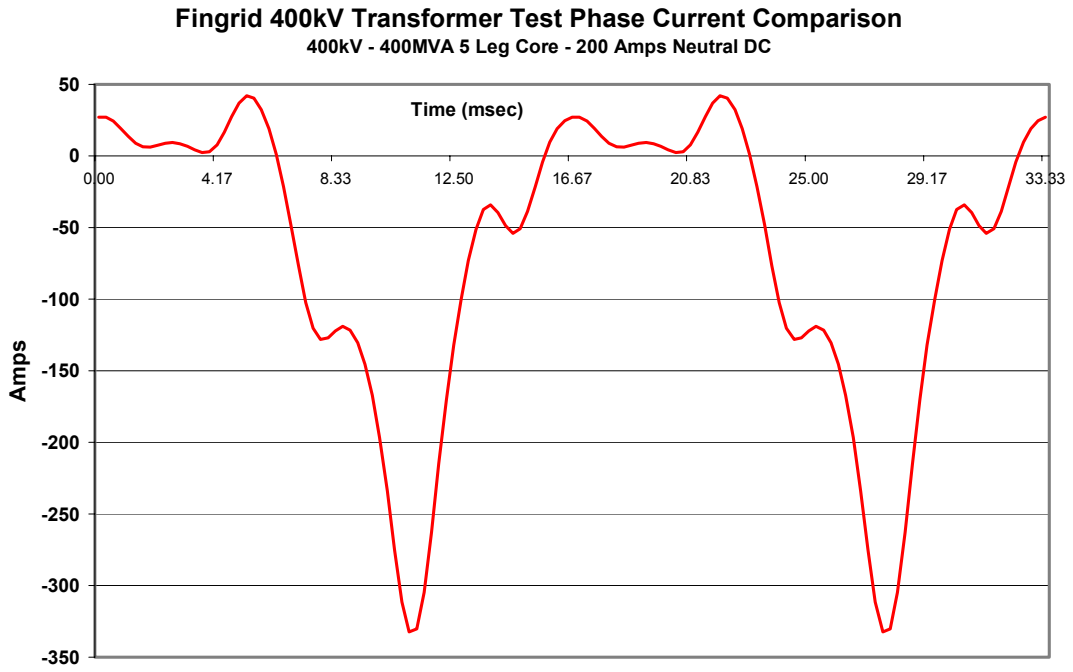

Figure A4-9b. Calculated B phase (center phase) excitation current of 5-legged core form transformer.

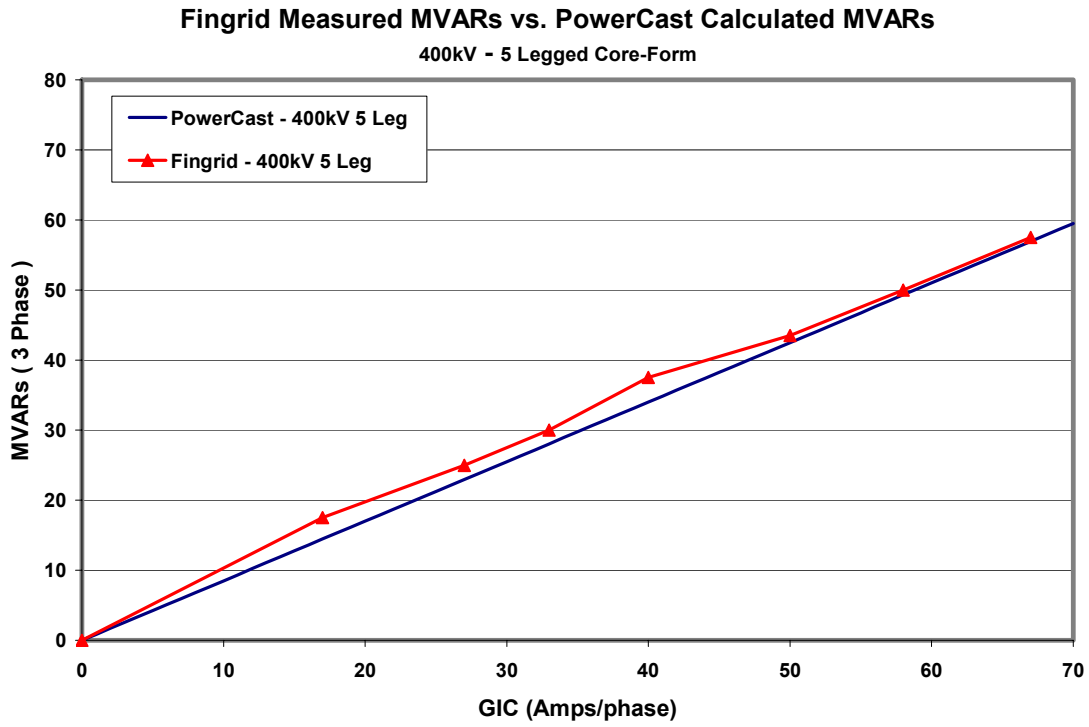

Figure A4-10a. Observed and calculated MVAR increases versus GIC for 5-legged core form transformer.

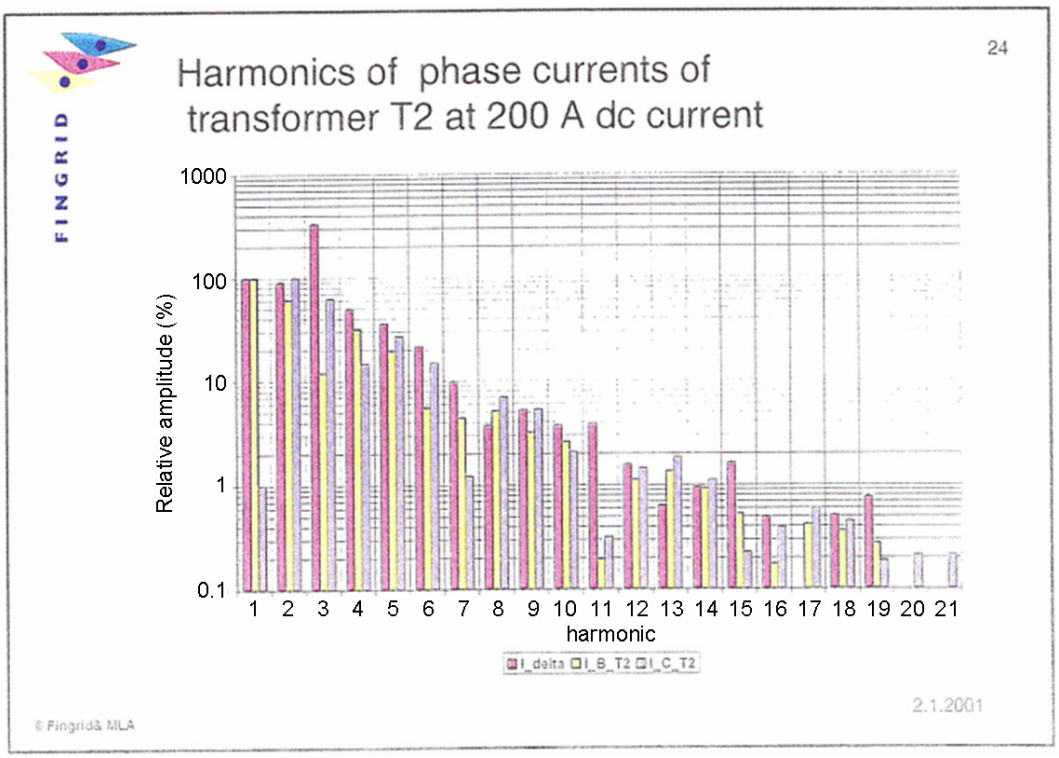

Figure A4-10b. Observed harmonics at 200 amps GIC for 5-legged core form transformer.

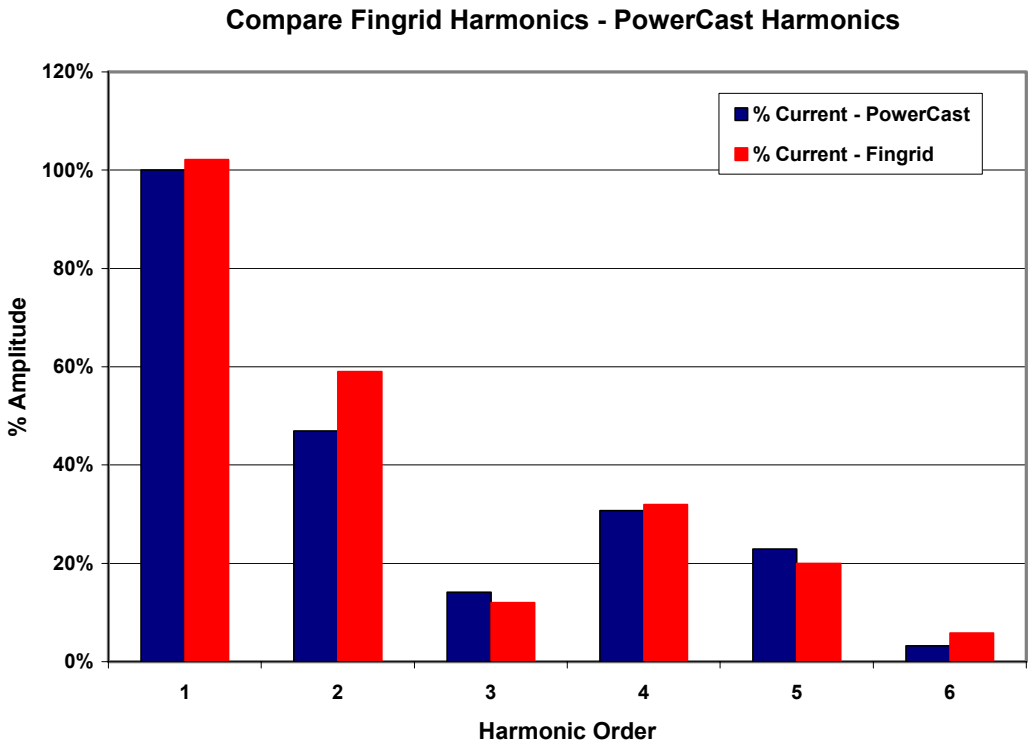

Figure A4-10c. Comparison of observed and calculated AC harmonics for 5-legged core form transformer.

A4.3 Field Tests of Large Power Transformer Performance under DC Excitation

Extensive tests were performed on the operation of large power transformers in the presence of GIC at Minnesota Power in the 1980's and early 1990's (Reference AP4-4). These tests provided much of the data and observation information needed to develop accurate models of transformer behavior in the presence of GIC. The tests were important because they established some of the principle behavior patterns of transformers that are due to differing magnetic core type construction. These tests were performed on the major U.S. transformer core types of single phase, 3-phase, 3-legged, and three-phase shell-form transformers. Prior to these tests, it had been widely modeled and assumed that the 3-phase, 3-legged core type would be immune to GIC currents. Testing, however, determined these core types would readily saturate. These tests were also essential to determine the degree of behavior of the other transformers in the presence of GIC, attributes that were essentially un-quantified before these tests were carried out. These tests were also important in that they tested the behavior of large power transformers in their intended in-situ environment of the power grid, rather than tests in a laboratory environment. This natural environment allowed the transformers to be operated at full high voltage, high power conditions. This also allowed the ability to observe and test the response of the network as a whole to these conditions.

These and other tests performed were primarily conducted for the purpose of understanding performance concerns due to naturally occurring GIC from geomagnetic storms. The extremes of this environment had not at this time been well established. As a result, the test levels for field tests were typically only conducted to GIC levels that were about 10% of rated current levels on most transformer designs, while extreme geomagnetic storms, as well as HEMP E3 threats, will likely cause much higher GIC levels. In some cases, these levels of GIC can easily exceed the rated AC currents of the exposed transformers, levels that have not been tested (with the exception of small-scale low-voltage tests – Reference AP4-2). The test data and models have been extended to estimate performance levels at these higher exposure levels, though some increase in uncertainty of model performance exists at these extreme exposure levels than at lower levels of GIC exposure. Some of the field tests waveform observations are summarized to illustrate the degree of agreement that exists with models used in the U.S. Power Grid analysis at higher relative exposure levels of GIC.

Figure A4-11 shows the high-side current on a 230/115kV 200MVA 3-phase 3-legged core form transformer with 33.3 amps/phase of GIC. This level of GIC is only 6.5% of the rated AC current of the high-side windings of this transformer. The blue waveform shows the normal load current flowing in the transformer, while the red waveform shows the same load current and the current distortions due to the saturation from the relatively small flow of GIC. The distortion, caused by the saturation, is evident near the zero crossing as the excitation current lags the load current by 90 degrees in the sine wave. For this test condition, the transformer has an excitation current waveform as shown in Figure A4-12.

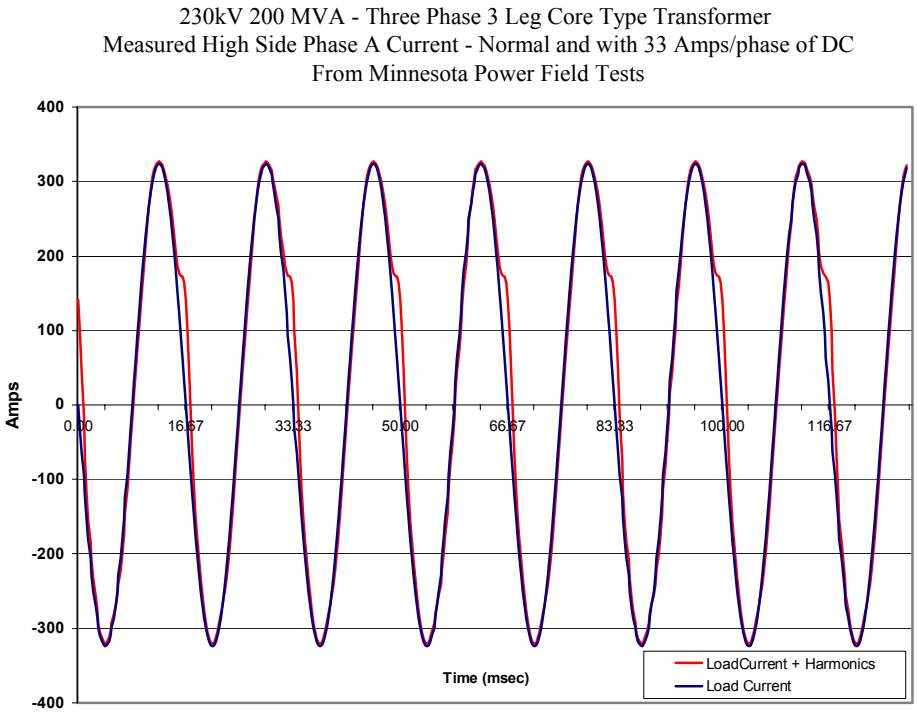

Figure A4-11. Normal and distorted AC current in 230kV 3-phase, 3-legged transformer with and without GIC present.

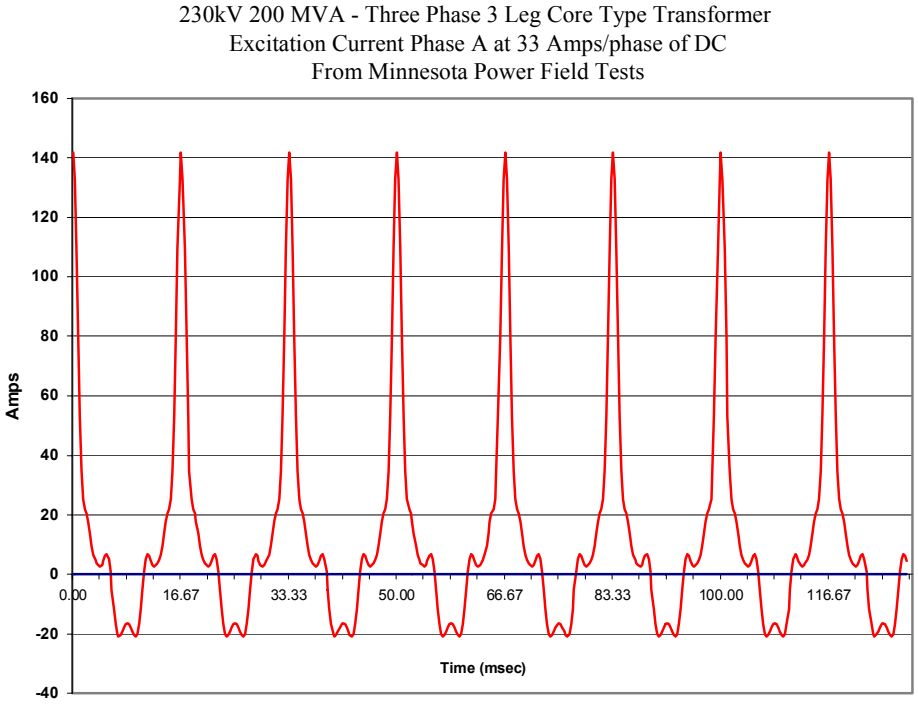

Figure A4-12. Estimated excitation current in 230kV 3-phase, 3-legged transformer with GIC present from Figure A4-11.

The excitation current from a field test of 33.3 amps of GIC per phase on a 230/115kV 200 MVA 3-phase shell form transformer is shown in Figure A4-13. As shown, the exciting current distortion for this transformer type is similar to that produced by the 3-legged core form transformer with identical ratings. This indicates that both of these transformers will saturate at similar levels in the presence of GIC.

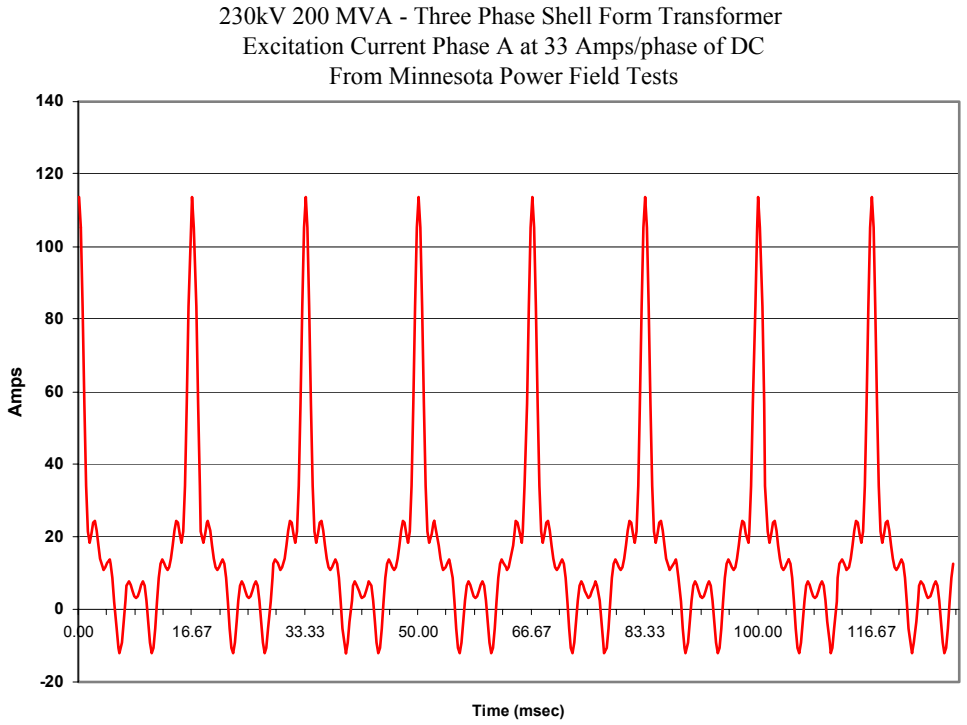

Figure A4-13. Excitation current from 230kV 3-phase shell form transformer with GIC present.

A harmonic analysis of the excitation currents from these two transformer core types is shown in Figure A4-14. There is an overall trend of decreasing amplitude as the harmonic order increases. However, for the triplen harmonics (particularly 3rd, 6th, and 9th), there are larger differences in the amplitudes of these constituents between the two core designs. In a 3-phase balanced system, the triplen harmonics are zero sequence (or in phase rather than separated in phase by 120 degrees, as is the normal case at the fundamental frequency) and would add to higher magnitudes as a result. Since these staged tests were only instrumented to fully analyze one phase and the neutral current quantities, an examination of the neutral currents is needed to further review the degree of phase imbalance that is occurring in the different core types.

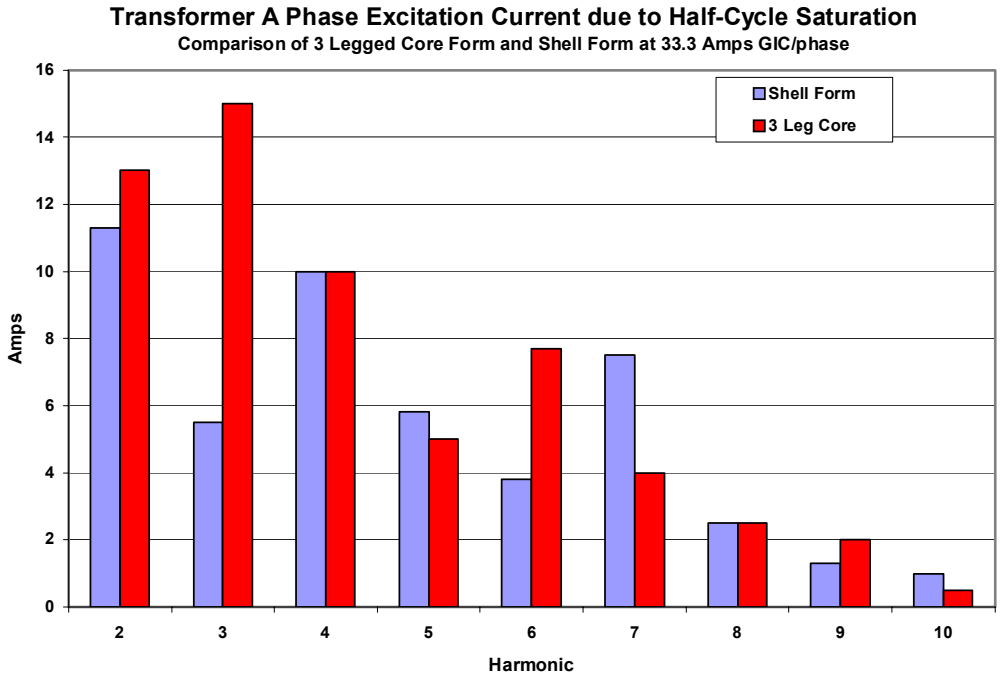

Figure A4-14. Comparison of AC harmonics in transformer excitation currents for 3-phase, 3-legged core form and 3-phase shell form 230kV transformers with GIC present.

The Figures A4-15 and A4-16 show the AC neutral current for the 3-legged core form and 3-phase shell form transformer under conditions with a DC excitation of 33.3 amps/phase. Simple inspection shows that the two neutral currents differ markedly in harmonic spectrum and amplitude. As shown for the neutral current from the 3-legged core form transformer, this is predominantly made up of triplen harmonic constituents, an expected outcome for a transformer that is experiencing balanced saturation on all three phases in the presence of the DC current. The neutral current for the shell form transformer, for identical DC excitation conditions, has a different mix of fundamental and harmonic constituents present. This indicates a phase imbalance in the level of half-cycle saturation on each phase of the 3-phase transformer.

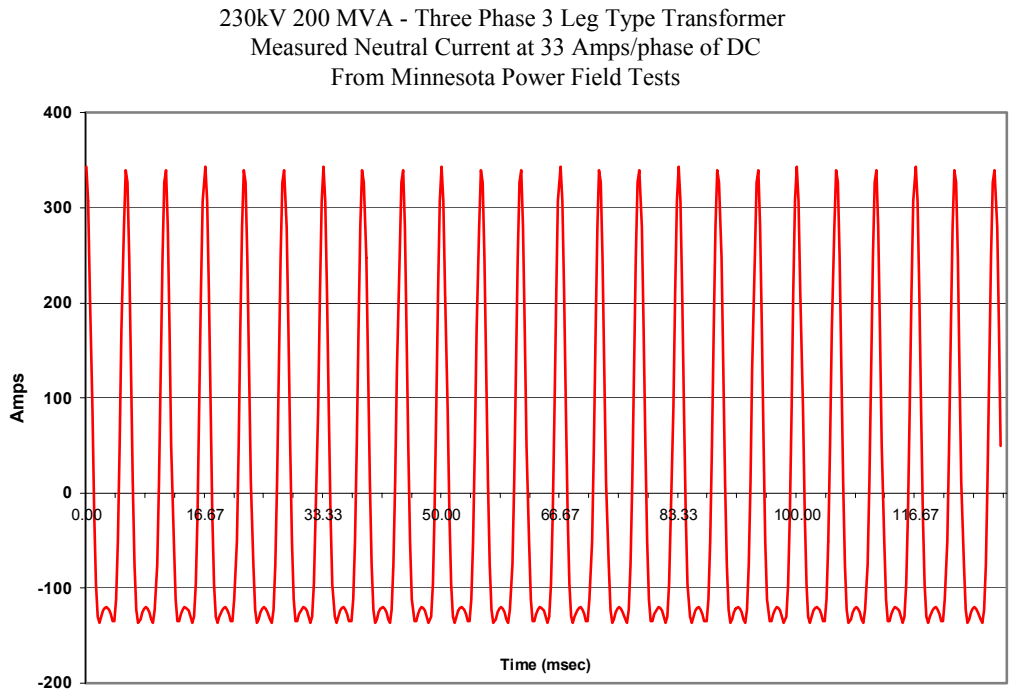

Figure A4-15. Measured neutral current for 3-phase, 3-legged core form transformer with GIC present.

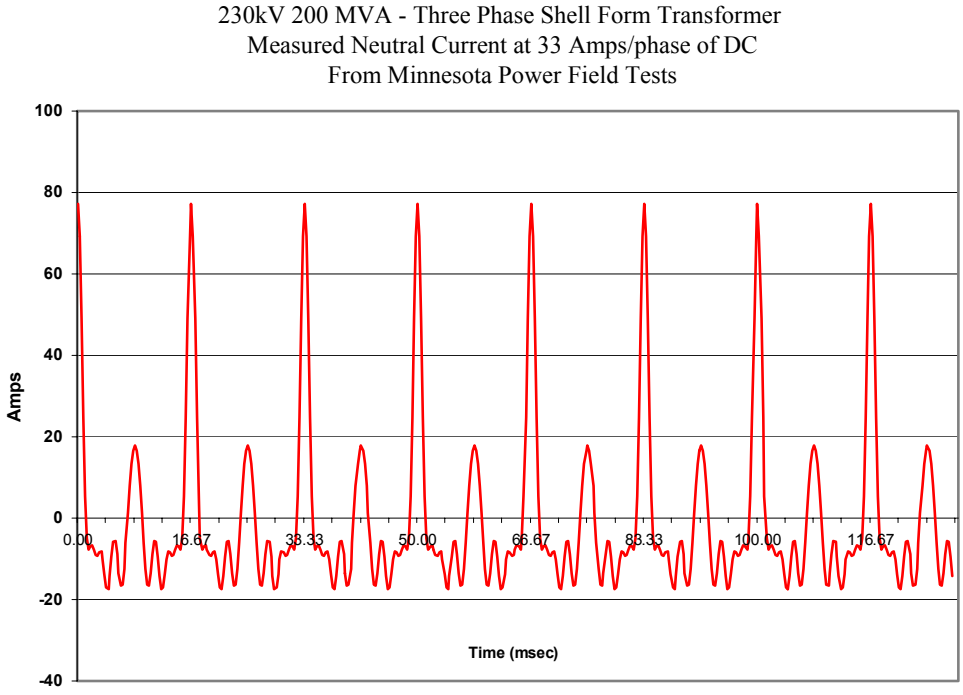

Figure A4-16. Measured neutral current for 3-phase shell form transformer with GIC present.

Figure A4-17 shows the spectrum analysis of the two transformer neutral currents. As shown, for the 3-legged core form, the neutral current consists only of triplen harmonics, while the neutral current for the shell form transformer has harmonic components at all frequencies.

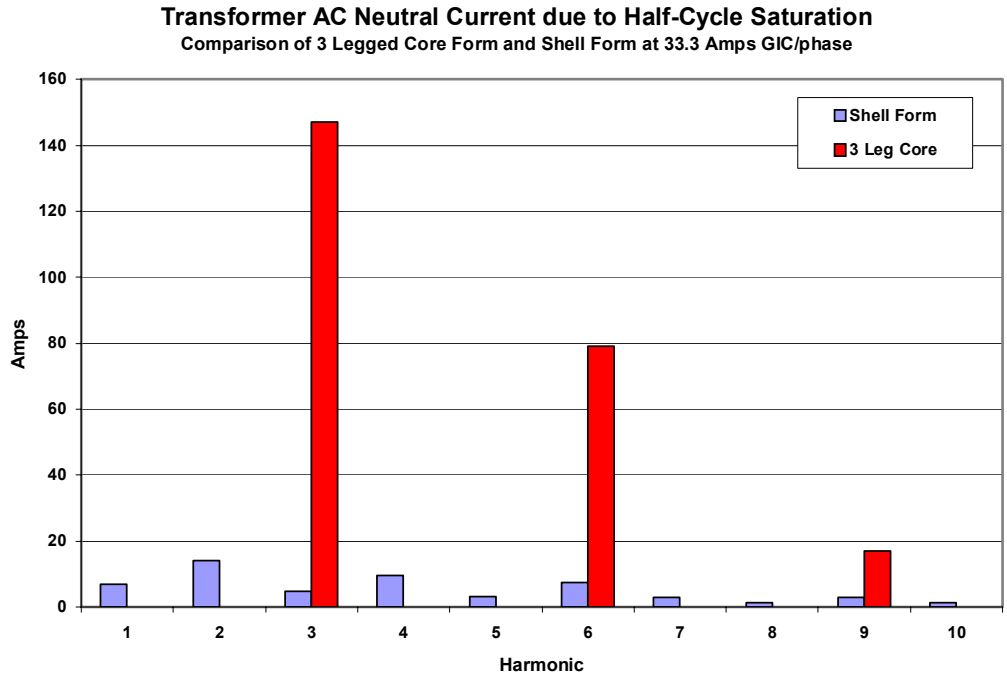

Figure A4-17. Comparison of AC harmonics in transformer neutral currents for 3-legged core form and shell form transformers.

The excitation currents for a series of DC excitation tests on a bank of 500kV single-phase transformers are shown (Figures A4-18, A4-19, and A4-20). The excitation currents for DC excitations of 16.7 amps/phase, 25 amps/phase, and 33.3 amps/phase are equivalent to AC transformer currents that are 4%, 6%, and 8% respectively of rated. As would be expected, these excitation currents exhibit higher degrees of distortion with growth in amplitudes in levels of DC excitation.

500kV 360 MVA – Single Phase Shell Form Transformer
Measured Phase A Excitation Current at 16.7 Amps/phase of DC
From Minnesota Power Field Tests

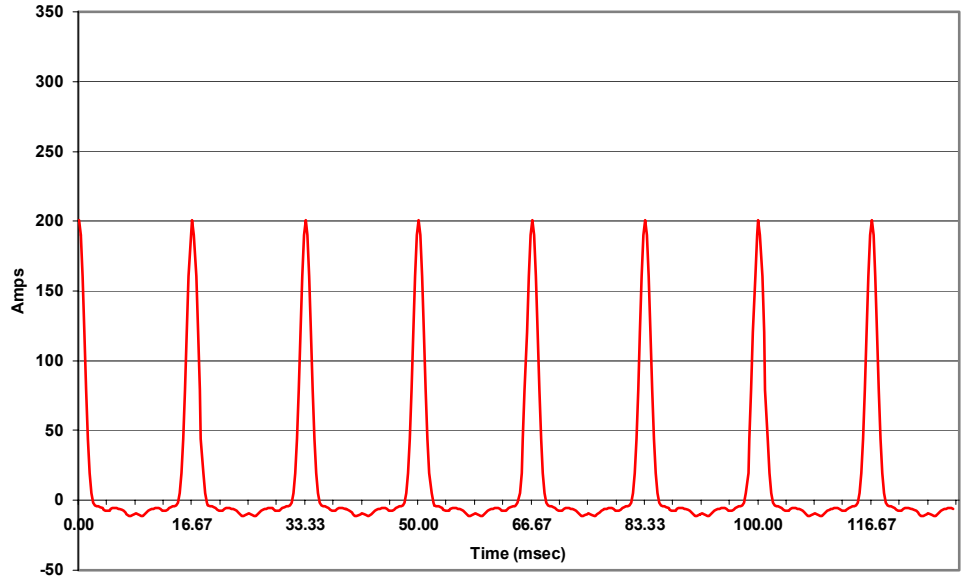

Figure A4-18. Excitation current for 500kV single-phase transformer
with 16.7 amps/phase of DC current present.

500kV 360 MVA – Single Phase Shell Form Transformer
Measured Phase A Excitation Current at 25 Amps/phase of DC
From Minnesota Power Field Tests

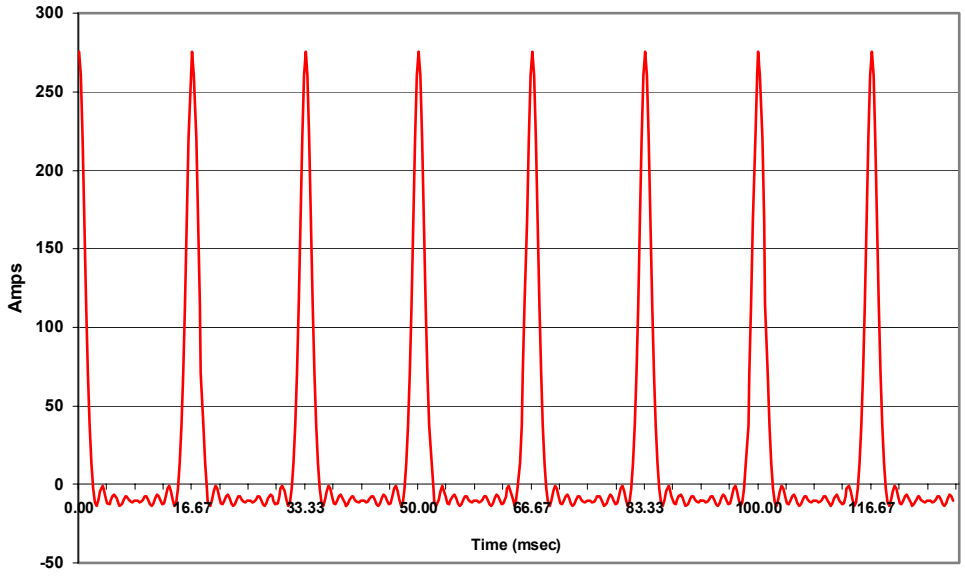

Figure A4-19. Excitation current for 500kV single-phase transformer
with 25 amps/phase of DC current present.

500kV 360 MVA – Single Phase Shell Form Transformer
Measured Phase A Excitation Current at 33.3 Amps/phase of DC
From Minnesota Power Field Tests

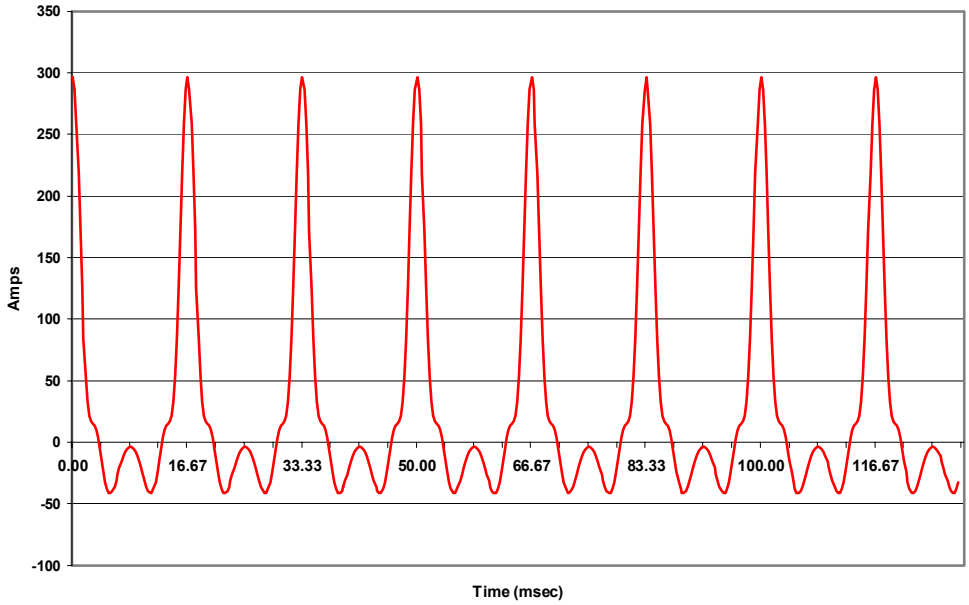

Figure A4-20. Excitation current for 500kV single-phase transformer
with 33.3 amps/phase of DC current present.

A spectrum analysis of the three excitation currents for the 500 kV transformer are shown on the bar chart of Figure A4-21. In all cases of increasing levels of DC excitation, the fundamental and 2nd harmonic components experience a monotonic increase in magnitude for increasing levels of DC excitation. At higher harmonic orders and higher DC excitation levels, more variation in harmonic current constituencies is evident. This fits well with the behavior patterns also projected in the transformer models.

In addition to measured distortions of current and power consumption on individual transformers, measurements were also made on the current flow in a major 500kV interconnection in Northern Minnesota during these staged field tests. As shown in Figure A4-22, the 500kV interconnection current was highly distorted, due to the test condition where 25 amps/phase was injected into one of several 500kV transformers that were connected to this transmission line. In addition to the normal fundamental frequency load current flowing on the line, a substantial amount of 3rd and 5th harmonic currents also flowed on the line, causing the distortions observed. This is no longer recognizable as a 60 Hz waveform, due to the severe harmonic distortion present. The total harmonic distortion (THD) for this condition is an extremely large 141.5%. In contrast, the IEEE-519 guideline for maximum harmonic distortion is only 3% on a high voltage transmission line.

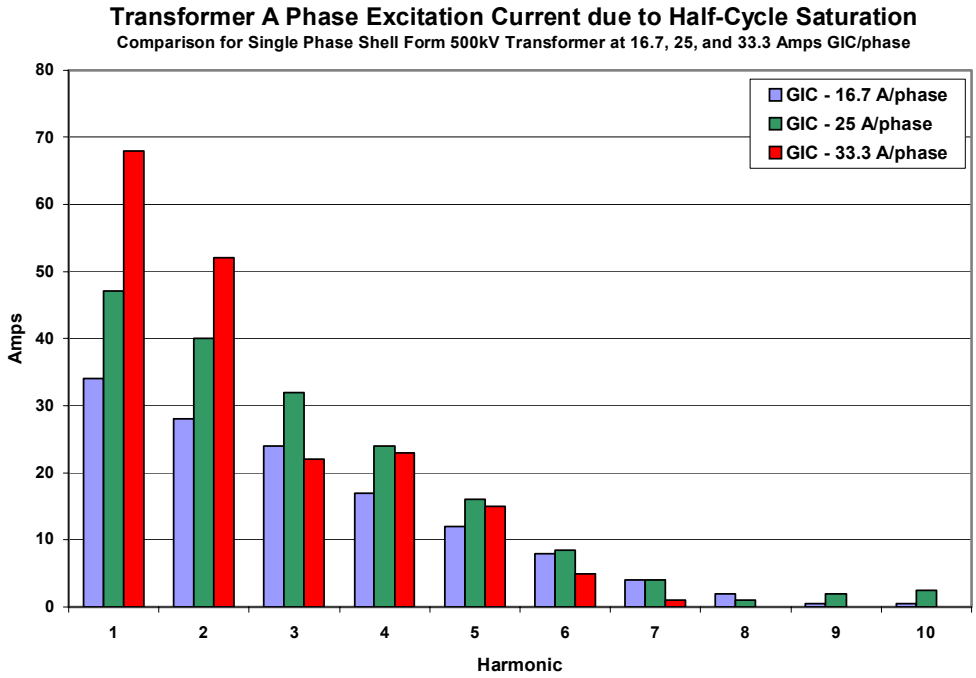

Figure A4-21. Comparison of AC harmonics in excitation current of 500kV single-phase transformer for various levels of DC excitation.

500kV 360 MVA – Single Phase Shell Form Transformer
Measured 500kV Line Current - Phase A Current at 25 Amps/phase of DC
From Minnesota Power Field Tests

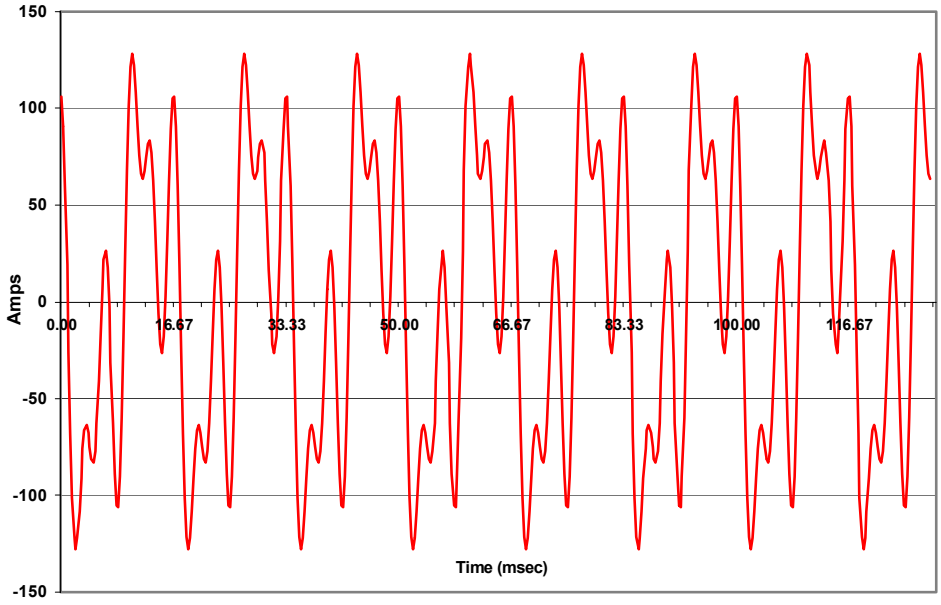

Figure A4-22. Distorted AC current on adjacent 500kV transmission line due to DC excitation of 500kv single-phase transformer.

For perspective, this is a significant degree of distortion occurring in a major high voltage, high power facility due to the saturation from relatively low-levels of GIC-caused saturation in just one of many transformers connected to the network. Under a true geomagnetic storm scenario, it is likely that many large transformers throughout the exposed region will experience this level, or substantially higher levels of GIC and GIC-caused half-cycle saturation simultaneously. This would be likely to result in significantly higher levels of distortion than illustrated in this limited observation. As mentioned in the beginning of this section, these tests were performed at very low levels of DC excitation compared to those that are expected to be possible due to the HEMP E3 threat environments or severe geomagnetic storm conditions to transformers in the U.S. power grid. Though GIC levels up to 33.3 amp/phase were used, in relative terms, these DC excitation levels only approach about 8% of rated AC current for these various 500kV and 230kV transformers. The levels of total GIC per phase are expected to be as much as, or even more than, 100% of the rated current for a number of transformers.

In the calculation of reactive power demand, the most important component of increased reactive power demand in a transformer due to the presence of GIC is from the increase in excitation current during half-cycle saturation. There can be a contribution to increased reactive power due to increased I^2X losses. However, this is usually ignored because it is a minor component and falls within the uncertainty of the model for transformer behavior. In the case of large GICs from either an E3 threat or very large geomagnetic disturbance, the component of losses due to I^2X is less certain. Therefore, an effort was undertaken to analyze this further. Figure A4-23 provides an example of the levels of GIC flow that could result from both a SSC event geomagnetic disturbance and that from a late-time or E3 HEMP in the same transformer. As shown, the peak GIC for the SSC event is ~50 amps/phase while the GIC from the E3 threat is nearly 800 amps/phase. Using the data from the Forbes 500 kV transformer, an estimate can be made of the reactive demand increases due to half-cycle saturation from these two GIC levels, taking into account estimates of the I^2X component of losses.

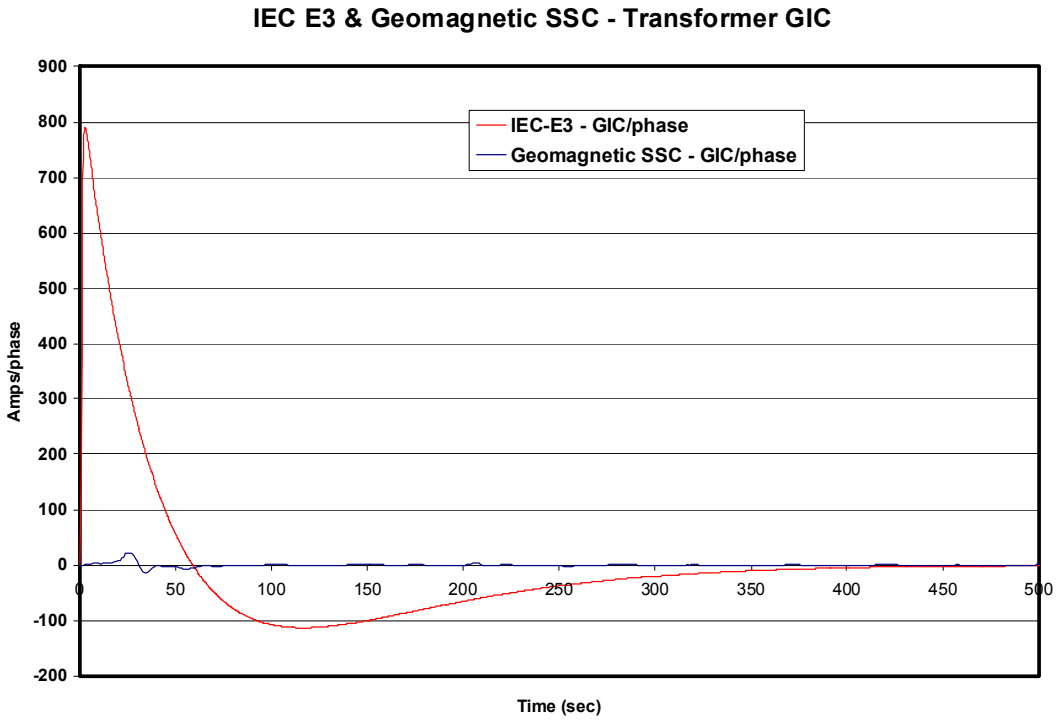

Figure A4-23. GIC per phase in transformer from SSC and E3 threat.

A4.4 Transformer Reactive Power Modeling for Severe GIC Environments

To further analyze the behavior of transformers during this unusual half-cycle saturation mode of operation, it is helpful to develop an equivalent circuit representation of the transformer, as shown in Figure A4-24. In this circuit, the excitation characteristics and the impedance characteristics of the transformer are shown as lumped elements on the high-voltage winding. The impedance values shown are also those of the Forbes 500kV transformer.

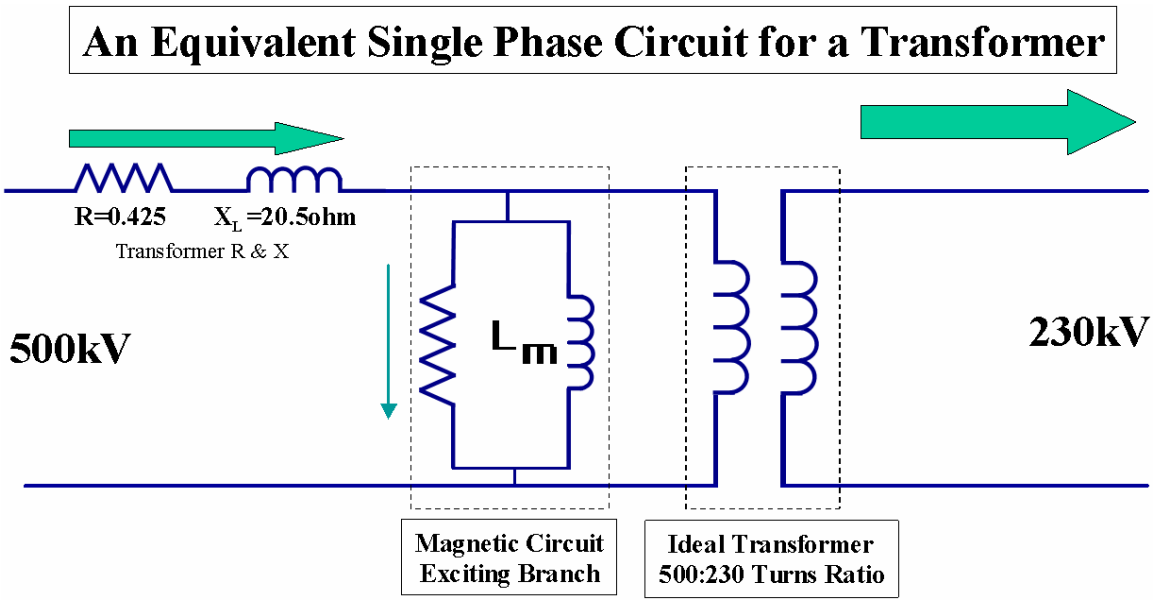

Figure A4-24. Simple equivalent one-line diagram of 500/230kV transformer model.

In this example, we are further simplifying by assuming that all increased AC current flows in the transformer from half-cycle saturation due to GIC are supplied from the primary input and that normal primary AC load current is 1000 amps. We will also assume that transformer saturation onset due to GIC is instantaneous and that system voltage remains at 100%. As shown above, the flow of current is from the high voltage winding to the low-voltage winding, with the magnitude of current modified by the turns ration of the transformer and internal losses such as those of the excitation branch. Under normal conditions, the current flow through the excitation branch is very small (less than 1 amp in this case), but increases substantially under half-cycle saturation. Reactive power increases arise from the (V)x(Iexc) product of increased excitation current flows in the transformer. Increases in I^2X losses also result from increased excitation current flows through the lumped impedance of the transformer as well. The total reactive power losses for the SSC event, along with the fraction of losses due to increased excitation current and I^2X, are shown in Figure A4-25. As shown, the total reactive power increase due to the GIC from the SSC event was ~ 43 MVARs in this transformer. Of this 43 MVARs total, approximately 85% was due to (V)x(Iexc) from increased excitation current, while only ~15% was due to I^2X losses.

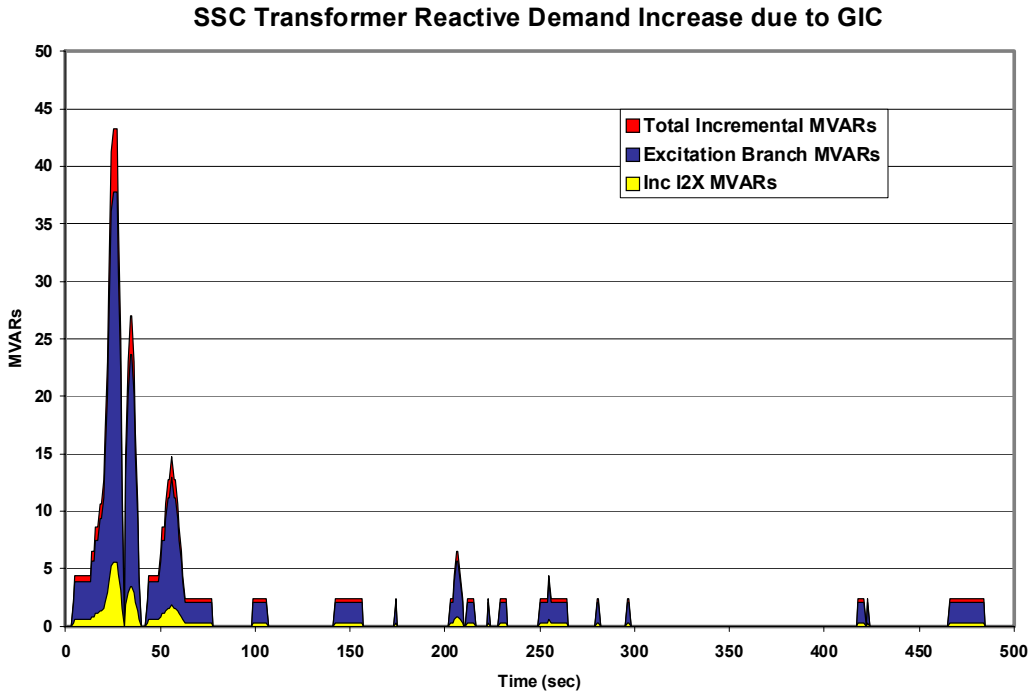

Figure A4-25. Transformer reactive power loss versus time estimates due to low level GIC from SSC event.

Figure A4-26 shows the same transformer reactive power demand increases for the conditions with the large E3 GIC event. For this event, the reactive power losses in the transformer are projected to increase to a level of ~1600 MVARs (it should be noted that system limiting factors and assumptions such as constant 100% voltage are not likely in real network scenarios at these extraordinarily high GIC levels). As previously noted, models of transformer over-excitation due to GIC have only been experimentally verified for large power transformers for GIC levels up to about 25% of maximum rated AC current. These levels of GIC far exceed previous experience. In addition, due to extremely high reactive demand at this transformer and many other exposed transformers from HEMP E3 events, power grid voltage collapse is likely before these levels are reached. While these totals have some uncertainty, the components due to increased excitation current and I^2X reactive power losses continue to illustrate that ~75% of total losses will be due to the effects of increased excitation current and (V)x(Iexc) product. Voltage collapse in most power grids will typically occur between 80-90% of normal voltage. Therefore, MVAR levels this high are not likely to actually occur before onset of system collapse. For the reactive power calculations of Figure A4-26, the normal AC primary current was 1000 amps, while for lower AC current flows an exponential reduction will occur in the I^2X component of losses. Using an AC current flow of 300 amps, the losses can be re-calculated. In this case, this portion of losses due to I^2X reduces to ~15% of total increased MVARs, while losses due to Iexc are nominally unchanged. Since AC current levels are usually quite variable and uncertain and tend to be a minor component of total losses, the I^2X affects have not been included in analysis results.

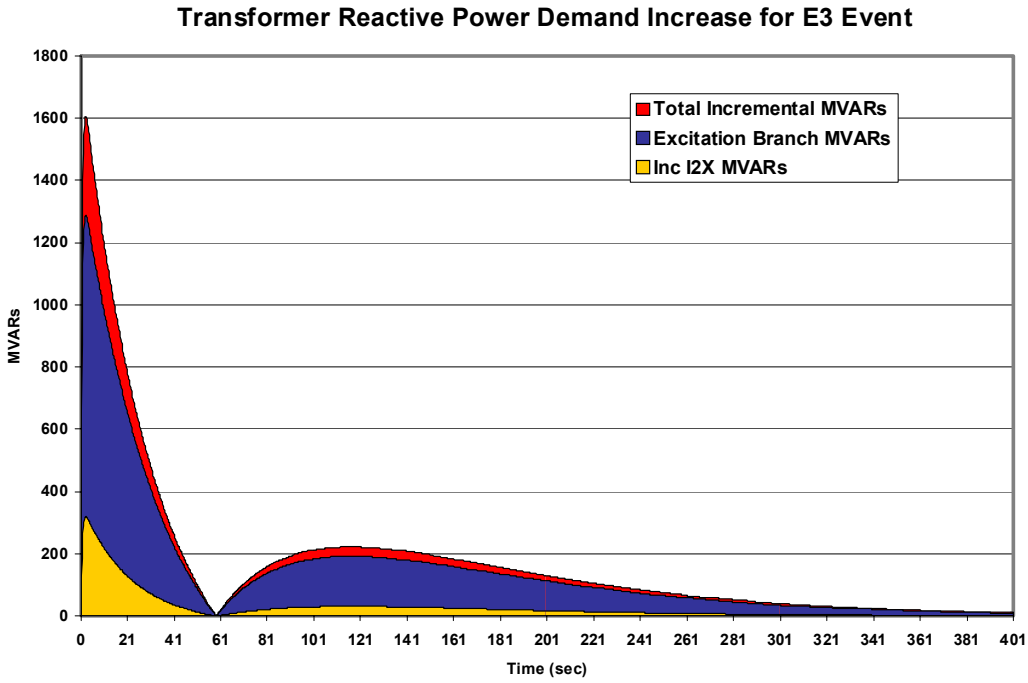

Figure A4-26. Transformer Reactive Power Loss versus time estimates due to large GIC from E3 event.

Appendix 4 References

AP4-1 P. Price, "Geomagnetically Induced Current Effects on Transformers", IEEE Trans on Power Delivery, 2000 Winter Power Meeting.

AP4-2 R.A. Walling, A.H.Khan, "Characteristics of transformer exciting-current during geomagnetic disturbances", IEEE Trans. on Power Delivery, vol. 6, no. 4, 1991, pp.1707-1714 .

AP4-3 W. Xu, T.G. Martinich, J.H. Sawada, Y. Mansour, "Harmonics from SVC transformer saturation with direct current offset", IEEE PES Summer Meeting, 404-4 PWRD, 1993, pp.1-7.

AP4-4 John G. Kappenman, "Transformer DC excitation field test & results", IEEE Special Panel Session Report, IEEE PES Summer Meeting, July 12, 1989, Long Beach, California, USA, pp.14-22.

AP4-5 Xuzhu Dong, Yilu Liu, John G. Kappenman, "Comparative Analysis of Exciting Current Harmonics and Reactive Power Consumption from GIC Saturated Transformers", IEEE Trans on Power Delivery, 2000 Winter Power Meeting.

AP4-6 M. Lahtien, J. Elovaara: "GIC occurrences and GIC test for 400 kV system transformer", IEEE Trans on Power Delivery, vol17, no 2, April 2002, p555-561.